JOURNAL OF

METALS

May 1955

IN 2 SECTIONS—SECTION 1

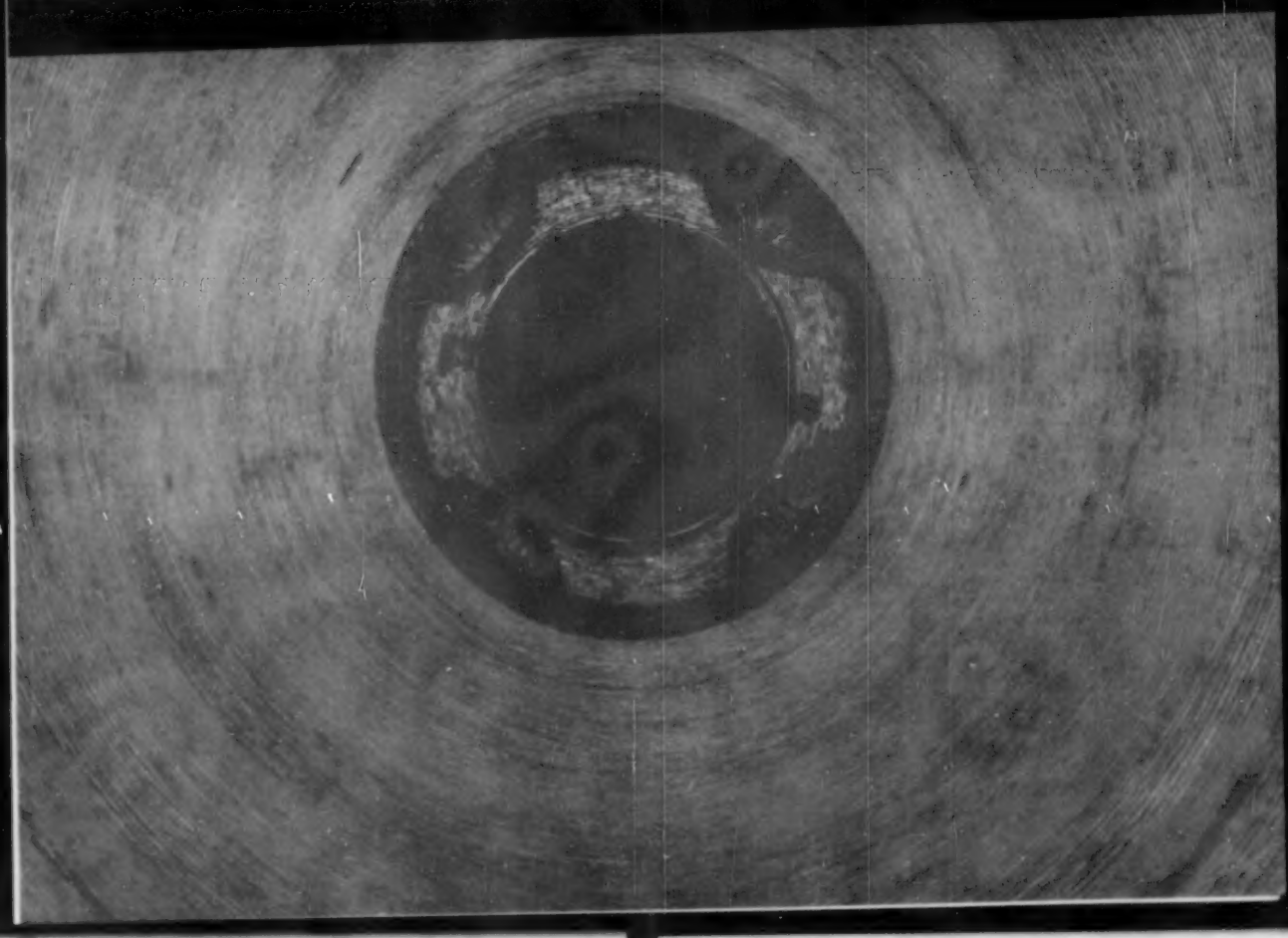

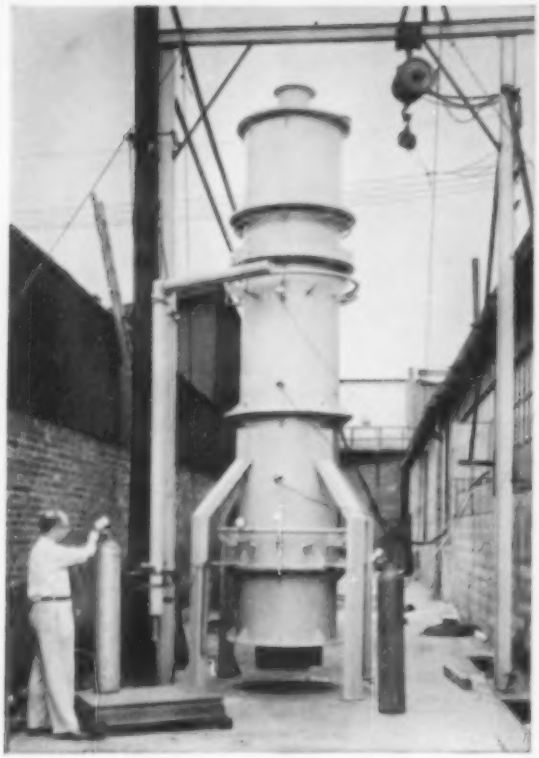

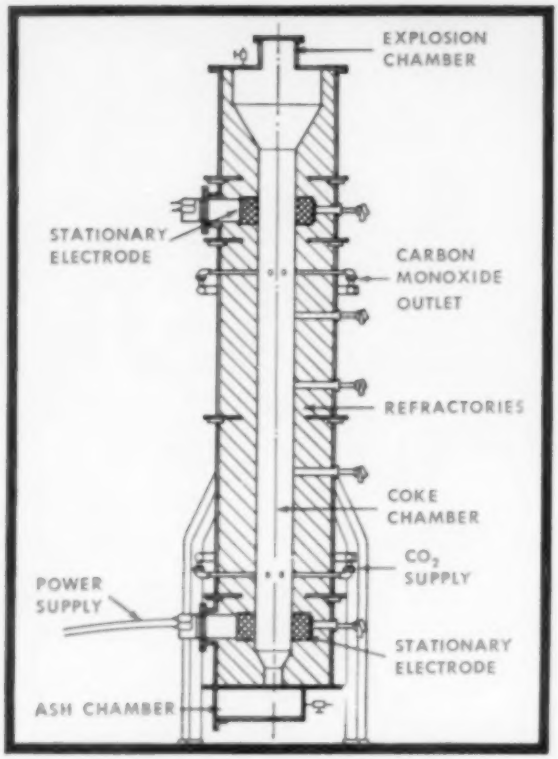

CAN YOU USE SOMETHING LIKE THIS?

...for gaseous reactions using a conducting medium

This Lectromelt* Reactor was built for converting carbon dioxide to carbon monoxide continuously, on a pilot basis. The CO_2 is fed into the manifold near the bottom; it passes up through a column of heated coke where it is transformed into CO. This is taken off through the upper manifold.

This reactor offers these advantages over previous similar equipment: The ring electrodes should last for many months, since they are always under an atmosphere of dead gas. Because this vessel is gas-tight, it can be used on a batch basis for processes requiring pressure.

Where can you use it?

Carbonaceous reduction, calcining, chlorinating of titanium—these are a few of the applications suggested for this reactor. You give us your ideas. Lectromelt engineers have been dealing for years in problems of electrothermic reduction. Describe your problem and they'll help you solve it.

Whether you're expanding accepted processes or developing something new, we'll be interested in talking with you. Outline your thinking to Pittsburgh Lectromelt Furnace Corporation, 326 32nd Street, Pittsburgh 30, Pennsylvania.

Manufactured in ... GERMANY: Friedrich Kocks GMBH, Dusseldorf ... ENGLAND: Birlec, Ltd., Birmingham ... FRANCE: Stein et Roubaix, Paris ... BELGIUM: S. A. Belge Stein et Roubaix, Bressoux-Liege ... SPAIN: General Electrica Espanola, Bilbao ... ITALY: Forni Stein, Genoa. JAPAN: Daido Steel Co., Ltd., Nagoya

*REG. T. M. U. S. PAT. OFF.

MOORE RAPID

WHEN YOU MELT... *Lectromelt*

50 K.V.A. TO 50,000 K.V.A.

JOURNAL OF

METALS

Published to provide a continuing, authoritative, and up-to-date record of technological, engineering, and economic progress in all branches of the metals industry by the
Metals Branch
American Institute of Mining and Metallurgical Engineers, Inc.
29 West 39th Street, New York 18

• • •

ALVIN S. COHAN
Manager of Publications
Editor, JOURNAL OF METALS
EDWIN M. WEISS
Associate Editor

• • •

M. A. MATZKIN M. SNEDEKER
G. M. ZILL
Assistant Editors
GRACE PUGSLEY Production Manager
W. J. SEWING Asst. Prod. Mgr

• • •

METALS BRANCH COUNCIL

J. H. Scaff — Chairman
E. O. Kirkendall — Secretary
J. S. Smart, Jr. — IMD Chairman
A. W. Thornton — ISD Chairman
A. W. Schlechten — EMD Chairman
P. T. Stroup — M. E. Volin
J. S. Marsh — D. S. Eppelsheimer

EDITORIAL ADVISORY COMMITTEE

J. S. Smart, Jr. — Chairman
W. A. Dean — Evan Just
J. C. Kinnear, Jr. — John Marsh
T. D. Jones — M. Tenenbaum

TECHNICAL PUBLICATIONS COMMITTEES

Robert Aborn — AIME Chairman
M. A. Jones — ISD Chairman
S. J. Dickinson — EMD Chairman
W. R. Hibbard, Jr. — IMD Chairman
E. J. Kennedy, Jr. — Secretary

• • •

WARREN V. SMITH
Eastern Advertising Manager
BOB WILSON
Western Advertising Manager
84 E. Randolph St., Chicago

• • •

The AIME Publishes:
Journal of Metals
Mining Engineering
Journal of Petroleum Technology

VOL. 7, NO. 5 MAY, 1955

COVER

Refractory brick designs are the theme of this month's cover by Harry Brocke. Articles on refractories start on pp. 601 and 612.

NEWS

Employment Service	580	Trends	594
Books for Engineers	584	Drift of Things	596
Industrial Notes	588	Reporter	599
Coming Events	588	AIME News	651
Personals	653		

TECHNICAL FEATURES

Super Refractories Give Operators Unique Range of Properties — B. M. Johnson, A. A. Turner, H. S. Schroeder — 601
Methods Developed at Armco For Decreasing Scrap Charging Time — W. W. Bergmann — 608
New Refractory Uses For Silicon Nitride Reported — J. F. Collins, R. W. Gerby — 612
Sintering Practice at Rouge Plant Utilizes Low Grade Hematite — R. L. Cleveland — 616

TRANSACTIONS

Impact of Magnetism Upon Metallurgy — C. Zener — 619
Experimental Production of Al-Si Alloys in a Three-Phase Furnace — L. H. Banning, W. F. Hergert — 630
Hydrometallurgy of Copper-Zinc Concentrates. Kosaka Smelter, The Dowa Mining Co., Japan — H. Kuroshima, S. Tsunoda — 634
Topochemical Aspects of Iron Ore Reduction — G. Bitsianes, T. L. Joseph — 639
Integration of Metallurgical Engineering Education — R. Schuhmann, Jr. — 647

TECHNICAL NOTE

Oxidation of Oxygen-Saturated Titanium — M. Simnad, A. Spilners, O. Katz — 645

This issue of JOURNAL OF METALS is in two Sections:
Section 1—Magazine Section 2—Transactions Section

Published the first day of each month by the American Institute of Mining and Metallurgical Engineers, Inc., 29 West 39th Street, New York 18, N. Y. Telephone: PEnnsylvania 6-9220. Subscription $8 per year for non-AIME members in United States and North, South and Central America; $10, foreign; $6 for AIME members, or $4 additional in combination with a subscription to "Mining Engineering" or "Journal of Petroleum Technology." Single copies, 75 cents; single copies foreign, $1.00; special issues, $1.50 . . . The AIME is not responsible for any statement made or opinion expressed in its publications . . . Copyright 1955 by the American Institute of Mining and Metallurgical Engineers, Inc. . . . Registered cable address, AIME New York . . . Indexed in Engineering Index, Industrial Arts Index and Chemical Abstracts . . . Reentered as second-class matter Sept. 21, 1949, at the post office at New York, N. Y., under the Act of March 3, 1879. Additional entry established at Manchester, N. H.

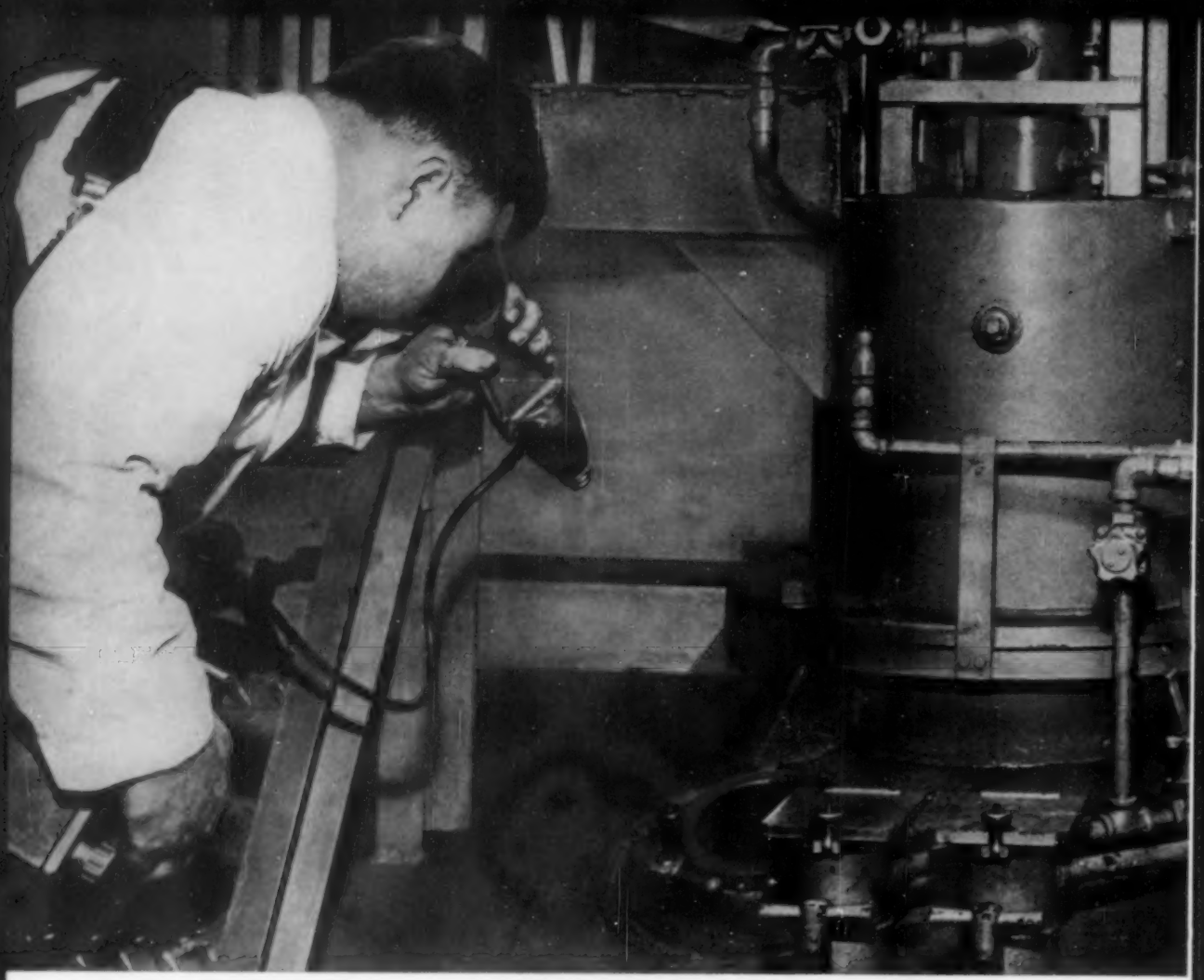

Operator at Thompson Products, Inc., Cleveland, Ohio, uses optical pyrometer to make a supplementary check on melt temperature in Stokes high-vacuum furnace.

THE COMPLETE LINE OF STOKES

Stokes manufactures a complete line of vacuum pumping equipment. This includes mechanical vacuum pumps, diffusion and booster pumps, vacuum valves and gages, and complete vacuum instrumentation. In engineered high vacuum equipment, Stokes builds vacuum metallizers, vacuum furnaces and other vacuum processing equipment.

Stokes has for many years been active in vacuum research. Vacuum experience among our engineers covers the range from laboratory equipment to some of the largest vacuum equipment in service. This experience is available to help solve your vacuum problems.

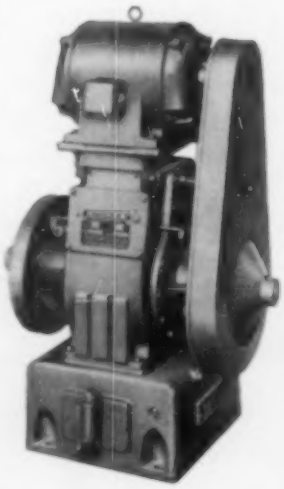

STOKES MECHANICAL VACUUM PUMPS

For vacuum processing systems and for maintaining low forepressures in high-vacuum systems, the Stokes Microvac pump provides efficient, economical operation. Designed with fully automatic lubrication and a long-lasting exhaust valve assembly, every Microvac pump is assured of smooth, trouble-free operation. Six sizes give capacities from 15 to 500 cfm. Send for catalog listed at right.

Thompson Products Uses
STOKES *Vacuum Furnace in Metals Research*

Thompson Products, Inc., of Cleveland, Ohio, one of the country's largest suppliers to the automotive and aircraft industries, carries on an extensive research and development program. To aid in the investigation of high-purity metals, Thompson has installed a Stokes high-vacuum furnace.

Thompson's vacuum furnace is currently rated at 200 pounds melt capacity: however, the unit is capable of 1000-pound production with only minor modifications, an important advantage should full-scale vacuum metal production be initiated.

Stokes is the leading supplier of production vacuum furnaces for industry. Outstanding features are a vacuum lock, which permits multiple melts and melt manipulation *without breaking vacuum;* high-capacity vacuum pumping systems, utilizing the new, high-speed Stokes Ring-Jet Booster pumps and the dependable Microvac forepump; and grouped controls for convenient operation. Stokes has many basic furnace designs – any of which can be modified to meet your particular needs.

If you are interested in high-purity metals, you'll want to know more about Stokes high-vacuum furnaces for both laboratory and full scale production. Write for your free copy of Stokes Catalog No. 790, "High-Vacuum Furnaces."

F. J. Stokes Machine Company
5502 Tabor Road
Philadelphia 20, Pa.

SEND FOR TECHNICAL LITERATURE:

- Microvac Pumps—Catalog 750
- Diffusion and Booster Pump Specification sheets and performance curves
- The Story of the Ring-Jet Pump
- Complete Vacuum Processing Systems—Catalog 730
- How to Care for Your Vacuum Pump—Booklet 755
- Vacuum Impregnation—Catalog 760
- Vacuum Drying—Catalog 720
- Vacuum Furnaces—Catalog 790
- Vacuum Metallizing—Catalog 780
- Vacuum Calculator Slide Rule

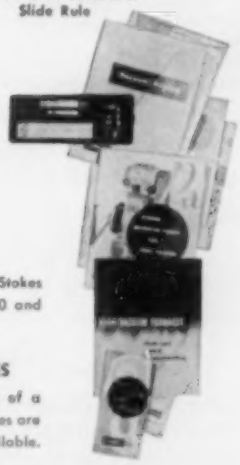

VACUUM EQUIPMENT

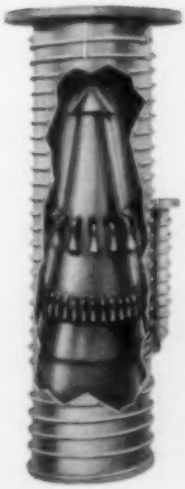

STOKES RING-JET DIFFUSION AND BOOSTER PUMPS

The new Stokes Ring-Jet Pumps embody a new concept of the diffusion principle. Size for size, they have pumping speeds of 10% to more than 100% above any other diffusion pump for a given heat input. Ring-Jet Diffusion Pumps are available in sizes of 4, 6, 10, 14 and 16 inches; Booster Pumps in sizes of 4, 6, 10 and 16 inches. Send for information listed.

STOKES VACUUM VALVES

To control vacuum safely and surely, Stokes vacuum valves are available in 4, 6, 10 and 16-inch standard flange sizes.

STOKES-McLEOD VACUUM GAGES

For measuring vacuums from fractions of a micron up to 50 mm, Stokes-McLeod gages are the standard of reference. Four sizes available.

STOKES

OFFICES IN PRINCIPAL CITIES, REPRESENTATIVES THROUGHOUT THE WORLD

—Personnel Service—

THE following employment items are made available to AIME members on a non-profit basis by the Engineering Societies Personnel Service Inc., operating in cooperation with the Four Founder Societies. Local offices of the Personnel Service are at 8 W. 40th St., **New York 18**; 100 Farnsworth Ave., **Detroit**; 57 Post St., **San Francisco**; 84 E. Randolph St., **Chicago 1**. Applicants should address all mail to the proper key numbers in care of the New York office and include 6c in stamps for forwarding and returning application. The applicant agrees, if placed in a position by means of the Service, to pay the placement fee listed by the Service. AIME members may secure a weekly bulletin of positions available for $3.50 a quarter, $12 a year.

——POSITIONS OPEN——

Assistant Professor of Metallurgy, with good training in physical metallurgy; also some metals physics. Will teach undergraduate courses, but should also be able to give post graduate instruction in thermodynamics as it applies to metallurgy, X-ray diffraction techniques, and kinetics of relations in solids. Location, northern New Jersey. W1291.

Assistant Professor, Ph.D. in physical metallurgy, to teach graduate and undergraduate courses in physical metallurgy. Salary, $5400 or more a year. Location, East. W1214.

Metallurgical or Mechanical Engineer, who majored in metallurgical engineering, Ph.D. or M.S. degree. Work involves primarily metallurgical work with no supervisory responsibility. Some traveling. Should be interested in contact work. Salary open. Location, South. W1257b.

Research Metallurgists. (a) Metallurgists, from recent graduates desiring graduate work leading to M.S. or D.Sc. in metallurgy, to applicants with Ph.D., to do fundamental research in thermodynamics, crystal mechanics, general physical metallurgy and solid state technology with distinct future possibility for entering research field of own choice. Salaries: full time research assistantships, $3000 to $4500 a year plus tuition; research associateships for qualified Ph.D., commensurate with experience. (b) Graduate assistant-

METALLURGIST

Graduate mechanical or metallurgical engineer with minimum 7 years' experience in analyzing and resolving metallurgical problems relating to ferrous and nonferrous metals. To render technical service to operating departments and serve as a staff consultant in the company's overseas operation located in Saudi Arabia.

Must be thoroughly familiar with metallography laboratory techniques and be capable of establishing laboratory procedures and the training of technicians. He should have complete knowledge of alloys suitable for refinery processing and be capable of investigating failures possibly due to improper materials or operating procedures and recommending remedial action.

PLANT AND EQUIPMENT INSPECTOR

Graduate engineer with minimum 10 years' experience in design or inspection of petroleum processing plants and equipment of which 5 years must have been in inspection work entailing general knowledge of all facilities. Thorough knowledge of A.P.I. and A.S.M.E. codes for fired and unfired pressure vessels and piping is required.

To develop inspection methods, supervise and conduct inspections and advise operations in connection with codes, equipment limitations, etc., in a major oil installation.

Salaries commensurate with experience and training. Write giving full particulars regarding personal history and work experience. Please include telephone number.

Recruiting Supervisor, Box 53

ARABIAN AMERICAN OIL COMPANY
505 PARK AVENUE NEW YORK 22, NEW YORK

METALLURGICAL ENGINEER—BS Degree plus one to three years experience for research and process development in special alloys having atomic energy application. Location Ohio. Please include complete description of work experience, present salary, etc., in reply.

Box C-8M AIME
29 W. 39th St., New York 18

METALLURGICAL AND MECHANICAL ENGINEER: Work involves all experimental fabrication operations for metallic fuel elements of interest to the AEC, such as rolling, swaging, forging, extruding, etc. Specific familiarity with these operations is not necessary, although an interest in mechanical and metallurgical factors is required. All problems are attacked both theoretically and practically.

The experience required is very flexible ranging from a recent college graduate to a man with several years experience in metal working or related fields.

Original thinking and ability to carry several experimental projects with little supervision as well as ability to work under considerable pressure with frequent changes in program are important.

Box E-16M AIME
29 West 39th St., New York 18

METALLURGIST

Large Growth Corporation In New York State Has Unusual Opportunity For Exceptional Metallurgist To Head Research Group On Development of Metal Alloys For Nuclear Reactors.

— **Salary Open** —

QUALIFICATIONS: Age under 36, Ph.D. in Metallurgy with two years experience, or B.S. in Metallurgy with five years experience in nonferrous alloy development.

REPLY TO:
Box E-15M AIME
29 W. 39th St., New York 18

METALLURGISTS

Alloy Development—composition development for high temperature and magnetic alloys, phase diagrams, creep, precipitation hardening, vacuum melting and other techniques. Development experience in powder metallurgy, physical metallurgy or alloy systems, background in theoretical physical metallurgy and knowledge of solid state physics useful; M.S. or Ph.D. in Metallurgical Engineering, desirable but not required.

Metals Application—guidance of design and manufacturing engineers in the selection and processing of ferrous or nonferrous metals.

Metallography—experienced metallographer to evaluate structures of ferrous and nonferrous commercial and experimental alloys.

Pilot Plant—follow process, development of casting, working and heat-treatment on specialized high temperature and magnetic alloys.

Send complete resume, including salary expectations, to:

S. A. ROSECRANS
Materials Engineering Dept.
WESTINGHOUSE ELECTRIC CORP.
East Pittsburgh, Pa.

ship for men interested in pursuing graduate work. Tuition remission plus stipend for 10 months and a possibility for part time summer employment in research laboratory. Positions available Sept. 1, 1955. Location, New York metropolitan area. W1246.

Metallurgist, recent graduate. No previous industrial experience required, to work in materials control laboratory of automotive company on product control and material specifications. Salary, $4800 a year. Location, Michigan. W1220.

Junior Metallurgist, graduate, for testing and processing of copper and aluminum wire and strip products. Salary, $4200 to $4700 a year. Location, central New York State. W1218(a).

Metallurgical Engineer, graduate in metallurgy, with ore concentration experience preferably including operation, design, construction and research (ore testing) for research and development. $6000 to $7200 a year. Location, Colorado. S718.

METALLURGIST

. . . . . needed as Process Metallurgist in brass mill manufacturing beryllium-copper, phosphor-bronze and nickel-silver in the form of strip, wire and rod.

Excellent position offering advancement and many benefits.

Reply fully giving age, experience and salary desired to: Personnel Department, The Riverside Metal Company, Div. of H. K. Porter Company, Inc., Riverside, New Jersey.

PROCESS METALLURGIST

Process Metallurgist under 40 with 5 to 10 years experience in ore flotation field. For responsible position in separation and concentration of ores. Southeast U. S. Your reply will be held confidential. Include age, education, experience, and salary requirement.

Box D-13M AIME
29 West 39 St., New York 18

METALLURGICAL ENGINEER—BS Degree plus one to three years experience with interest in welding application and development of welding materials and processes in special alloys including titanium, zirconium, etc. Location Ohio. Please include complete description of work experience, present salary, etc., in reply.

Box C-7M AIME
29 W. 39th St., New York 18

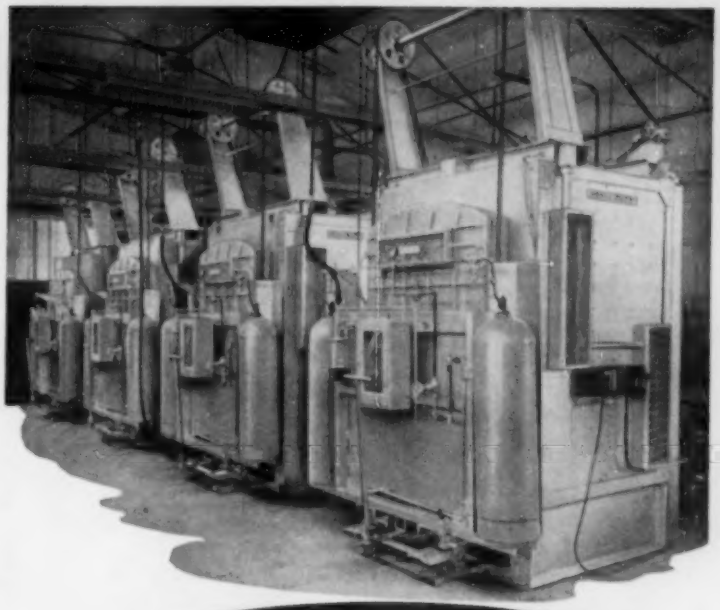

FOR INCREASED PRODUCTION OF NITRIDED PARTS USE A HEVI DUTY CAR BOTTOM NITRIDING FURNACE

Manufacturers producing nitrided parts for aircraft, engines, and heavy machinery items have found that more production is possible at a saving in cost when they use the Hevi Duty Car Bottom Nitriding Furnace. The furnace car, complete with sealed retort and ammonia dissociation equipment can be removed from the furnace for cooling and a second car with a cold load can be inserted immediately for a minimum loss of time between heats.

Write for Bulletin HD-664

HEVI DUTY ELECTRIC COMPANY

HEAT TREATING FURNACES HEVI-DUTY ELECTRIC EXCLUSIVELY
DRY TYPE TRANSFORMERS — CONSTANT CURRENT REGULATORS
MILWAUKEE 1, WISCONSIN

Norelco Announces Availability...

either

PROPORTIONAL OR SCINTILLATION DETECTORS

...with counting rates in excess of 100,000 cps, designed to extend range of existing equipment

The Norelco Proportional Detector is designed with a side window to provide a homegeneous field for obtaining true distribution of pulse energies while maintaining the same efficiency as the Geiger Counter at all wavelengths. *It is the only high speed detector suitable for soft x-radiation to wavelengths below 3 A°.* It will maintain a very high counting rate with linear response—in excess of 100,000 counts per second.

The Scintillation Detector possesses *a relatively uniform response at all wavelengths shorter than 3 A°.* Carefully selected scintillation crystals transform X-ray quanta to light which strikes a photomultiplier tube. Overall efficiency is high; the thin crystal absorbs almost 100% over the entire X-ray spectrum up to 100 KV.

Illustrating maximum utility, either of these detectors may be easily interchanged with Geiger tubes. Norelco electronics are available to amplify voltage level of pulses. The speed of these detectors provide high accuracies and short reading times. Because of the *linearity* of the amplifier used, the addition of a pulse height analyzer permits the detectors to be used as a secondary monochromator to increase signal-to-noise ratio, thus, discriminating against radiations other than the wavelength selected by the crystal or specimen.

A Norelco PRODUCT NORTH AMERICAN

Serving Science and Industry

PHILIPS COMPANY, INC.

750 South Fulton Avenue, Mount Vernon, N. Y.

In Canada: Rogers Majestic Electronics Ltd., 11-19 Brentcliffe Road, Leaside, Toronto 17, Ontario

Heroult ELECTRIC MELTING FURNACES

TOPS FOR PRODUCTION OF HIGH GRADE STAINLESS, ALLOY AND RIMMING STEELS

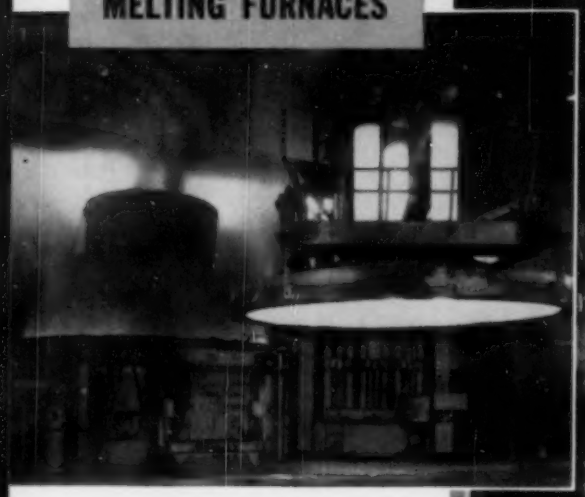

World's Largest Electric Furnaces

. . . now in operation!

INSTALLED in the ultra-modern mill of McLouth Steel Corporation, in Detroit, these giant *200-Ton* Heroults are the largest electric melting furnaces ever built. With an inside shell diameter of 24'6", they have a rated charge capacity of 400,000 pounds, and each is designed for efficient operation on 25,000 to 33,000 KVA transformer capacity. Featuring a swing-type roof, these furnaces are equipped with the finest, most up-to-date mechanism and electrical controls available.

McLouth's adoption of electric furnaces of this size sets a precedent. It is a "first" which should conclusively prove that, in addition to closer control, higher uniformity, better performance, and greater safety, large capacity Heroult Electric Furnaces are an economically sound investment—even for high tonnage steel-making.

We welcome an opportunity to help you select and install the furnace best suited to your particular requirements.

ASK FOR NEW CATALOGUE. *Contains latest information on modern electric furnaces—types, sizes, capacities, rating, etc. Write Pittsburgh Office for free copy.*

AMERICAN BRIDGE DIVISION, UNITED STATES STEEL CORPORATION
GENERAL OFFICES: 525 WILLIAM PENN PLACE, PITTSBURGH, PA.

Contracting Offices in New York, Philadelphia, Chicago, San Francisco and other principal cities.
United States Steel Export Company, New York

USS

UNITED STATES STEEL

Books for Engineers

ORDER YOUR BOOKS THROUGH AIME—Address Irene K. Sharp, Book Department. Ten per cent discount given whenever possible. Order Government publications direct from the agency concerned.

Steam, Its Generation and Use, 37th edition. *The Babcock & Wilcox Co.* $10.00, 22 chapters, 1955—The first edition of this book appeared in 1879. All material of the current edition was prepared and edited by engineers and specialists of the Babcock & Wilcox Co. It is intended primarily for mechanical engineers and mechanical engineering students in the applied thermo field.

Principles of Emulsion Technology, by Paul Becher. *Reinhold Publishing Corp.*, $2.95, 149 pp., 1955—This book is for those who have studied chemistry and want to learn more about both theoretical and applied emulsions than the passing note given them in physical chemistry courses. While the discussion is largely physiochemical, those without formal training in the subject should be able to follow the presentation. The worker in the field will find little new in the portions of the book dealing with applied problems. What has been attempted is the enunciation of general principles in terms of the practical.

PROFESSIONAL SERVICES

Limited to AIME members, or to companies that have at least one AIME member on their staffs. Rates $40 per year per inch.

DR. B. EGEBERG
Metallurgical Consultant
Reg. Prof. Engr.
Steel & Metals
Operations — Research
Meriden, Conn.

LEDOUX & COMPANY
Chemists Assayers Spectroscopists
SHIPPERS REPRESENTATIVES
Mine Examination Analyses
359 Alfred Ave. Teaneck, New Jersey

MAX STERN
Consulting Engineer
Expert for Scrap Recovery and Shipwrecking — Modernization of Plants and Yards for Ferrous and Nonferrous Metal Scrap
149 Broadway New York 6, N. Y.

H. L. TALBOT
Consulting Metallurgical Engineer
Extraction and Refining of Base Metals
Specializing in Cobalt and Copper
Room 331, 84 State St., Boston 9, Mass.

Electrons, Atoms, Metals, and Alloys, by William Hume-Rothery. *Philosophical Library*, $10.00, 387 pp., 1955—The book was first published in 1948, but has been revised and reprinted. Book is aimed at those who find the ordinary textbook treatment of the application of the electron theory to the structure and properties of metals and alloys, unattractive. It is divided into four parts dealing with the structure of atoms, metals, alloys, and other atomic nuclei, and is presented in the form of a dialogue between an older metallurgist and a young scientist.

The Fatigue of Metals and Structures, by H. J. Grover, S. A. Gordon, and L. R. Jackson. *Bureau of Aeronautics, Dept. of the Navy*, $2.50, 394 pp., 1954—The book is directed particularly to the designer or engineer with some knowledge of but limited practical experience in fatigue problems. It provides a summary of present-day information on the most important items in the aircraft industry.It is recognized that in a number of instances present-day knowledge is incomplete. Thus the information offered can only be considered a guide and starting point toward solution of specific problems. The book is obtainable from the Superintendent of Documents, U. S. Goverment Printing Office, Washington 25, D. C.

Abstracts of the Literature on Semiconducting and Luminescent Materials and Their Applications, compiled by Battelle Memorial Institute. *John Wiley & Sons, Inc.*, $5.00, 169 pp., 1955—Because of the many and somewhat distantly related types of scientific and engineering efforts which are employed in developing and utilizing electronic processes in solids, publications are appearing in more than 50 periodicals throughout the world. This publication attempts to meet the need for an organized collection of abstracts in this field. For the purpose of this bibliography materials are made the keynote. Listing of materials is, roughly, with important semiconductors first.

Electroplating Engineering Handbook, edited by A. Kenneth Graham, assisted by H. L. Pinkerton. *Reinhold Publishing Corp.*, $10.00, 650 pp., 1955—Book contains most recent information on processing techniques and engineering factors involved in constructing and installing plating equipment. Full chapters cover design of parts to be plated, standards and specifications, processing sequences, testing of deposits, waste treatment, plating machinery, rinsing and drying, maintenance, and all other engineering and operating considerations.

Die Metallurgie Der Ferrolegierungen, edited by R. Durrer and G. Volkert (German). *Springer-Verlag*, 409 pp., 1953—A treatise on the metallurgy of ferroalloys for engineers and metallurgists, covering theoretical aspects as well as the technology of production methods. Separate sections deal with the general metallurgy of ferroalloys and the electric furnace and electrodes. More than half the book is devoted to special metallurgy, treating the various ferroalloys individually.

Advances in Electronics and Electron Physics, Vol. VI, edited by L. Marton. *Academic Press, Inc.*, $11.80, 538 pp., 1954—Title of this year's volume has been changed from *Advances in Electronics* in order to express the coverage of the series more clearly. As in previous years, the present volume includes critical reviews of developments in a variety of fields. They are: Metallic conduction at high frequencies and low temperatures; relaxation processes in ferromagnetism; physical properties of ferrites; space charge limited currents; traveling wave tubes; comparison of analogous semiconductor and gaseous electronics devices; the electron microscope; and paramagnetism.

Materials of Construction, 6th edition, by Adelbert P. Mills, Harrison W. Hayward, and Lloyd F. Rader. *John Wiley & Sons, Inc.*, $7.50, 650 pp., 1955—Mr. Rader is responsible for the sixth edition, which incorporates some 15 pct more material, and has been thoroughly revised to reflect the latest data. The early part of the book deals with fundamentals, followed by a treatment of materials of construction. Among the new material is a discussion on the metallography and constitution of metals.

S. S. Ocean Vulcan S. S. Clan Alpine Structural Trials. Report No. R.12. *Admiralty Ship Welding Committee*, $5.75, 73 pp., 1954—The Admiralty Ship Welding Committee sponsored full-scale experiments on the structure of actual ships as part of an investigation of problems arising from the extended use of welding in shipbuilding.

Protective Coatings for Metals, 2nd edition. by R. M. Burns and W. W. Bradley. *Reinhold Publishing Corp.*, $12.00, 643 pp., 1955—In this new edition expanded sections can be found on the evaluation of organic coatings; completely new chapters on corrosion inhibitors; chemical conversion coatings; sprayed metal coatings; full explanations of such newly experienced troublesome phenomena as silver migration and metallic whiskers; latest practices in metal cleaning, coating application, and testing; and other material.

UNITED STATES STEEL

Reynolds Metals Company's La Quinta Alumina Plant Corpus Christi, Texas

Engineered Economy

IN EXTRACTIVE METALLURGY

This forty-million dollar ore-processing plant recovers pure alumina — 365,000 tons a year — from Jamaican bauxite. By advances in engineering and design, the operation makes possible the economic processing of a new type ore.

Evaluation of the economics of such operations, the engineering and construction of the complete plants, like the one shown above — these are important parts of Braun's services to the mining, metallurgical, and chemical industries.

Braun
engineers

C F BRAUN & CO ALHAMBRA CALIFORNIA · *NEW YORK · HOUSTON · SAN FRANCISCO*
CHICAGO · TULSA · C F BRAUN OF CANADA LTD · BRAUN TRANSWORLD CORPORATION

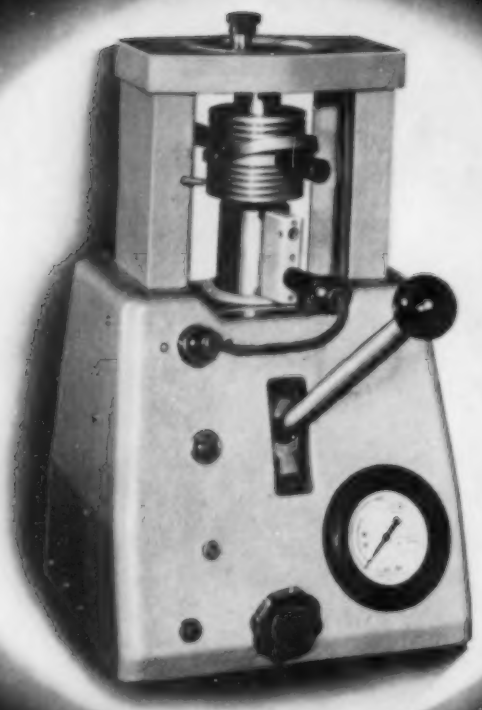

CENTERMET PRESS

Latest design in Press equipment for processing Bakelite and Transoptic mounted micro samples is now offered to the Metallographic Laboratory.

This new Press provides practical center ejection of 1" or 1¼" mounted specimens. The heating unit is controlled by thermostat and need not be removed from the press structure. The cooling block rigidly encloses and holds the mold assembly.

Minimum amount of handling molding accessories, speed and ease of sample ejection, practical and economical operation of molding tools were paramount in the development of this new AB Centermet Press.

Buehler Ltd.

METALLURGICAL APPARATUS

2120 GREENWOOD at Hartrey Ave., EVANSTON, ILL., U. S. A.

32 pages; 92 pictures and sketches

You belong in this picture

An evening with this interesting booklet will bring you the fascinating story of alloys and what they do for today's better steels and irons. For your copy of "Hot-Metal Magic," write to Electro Metallurgical Company, a Division of Union Carbide and Carbon Corporation, Room 350, 30 East 42nd Street, New York 17, N. Y. In Canada: Electro Metallurgical Company, Division of Union Carbide Canada Limited, Welland, Ontario.

Can your testing machines

Industrial Notes

• Mallory-Sharon Titanium Corp., Niles, Ohio, announced the quantity production of two new titanium alloys. First of the two in production is the 6 aluminum-4 vanadium (MST 6Al-4V) developed by Armour Research Foundation under contract to Watertown Arsenal Laboratory. The second alloy is termed the 3 manganese complex alloy, and is composed of 3 pct Mn, 1 pct Cr, 1 pct Mo, 1 pct Va, 1 pct Fe, the balance Ti.

• Engineering evaluation of a nuclear power plant system using liquid metal as fuel is underway at the Atomic Energy Commission's Brookhaven National Laboratory. The evaluation is being made by a group of 14 industrial and 3 other organizations, it was announced jointly by the Babcock & Wilcox Co., responsible for the work, and the laboratory. The system is intended to generate electric power, breed new fuel for itself, deliver by-products to waste tanks, all in continuous process. It would provide the first usage of a liquid metal alloy, in this case uranium-bismuth, as fuel stream to interconnect continuous processes.

• The Laboratory of Electron Microscopy in the dept. of engineering physics, College of Engineering, Cornell University, will again give the summer lab course in Technique and Applications of the Electron Microscope. The course will run from June 13 to 25 under the direction of Prof. Benjamin M. Siegel. Guest lecturers this year will be Prof. C. E. Hall of MIT, and Prof. R. C. Williams of the University of California.

• The world's largest slab heating furnaces have been erected at the Weirton Steel Co. plant, Weirton, W. Va., by Surface Combustion Corp., Toledo, Ohio. Each of the three furnaces will have a normal capacity to reheat 200 tons of steel slabs to rolling temperature per hour. The furnaces are about 118 ft long, and wide enough to take 26 ft long slabs.

• A new cold mechanical pipe expander is in operation at the No. 3 seamless pipe mill at U. S. Steel Corp., National Div., Lorain Works, Lorain, Ohio. Designed to produce pipe for high pressure gas and oil transmission lines, the installation will produce cold-expanded pipe from 16 in. min to 26 in. max, OD, with wall thicknesses to ½ in. Pipe is made of medium-carbon killed steel. Billets up to 12½ in. diam and weighing between 1½ to 3 tons are pierced in a Mannesmann-type mill. They are then expanded in a rotary rolling mill. After trimming pipe goes to the cold expander. A 60 ft ram of 14-in. seamless pipe is positioned at one end of the pipe. An expander plug is fitted on the bar cap and the ram, under 300,000 lb of pressure, forces the plug through the pipe. A set of five plugs are used in sequence, permitting uninterrupted operations and cooling of plugs between use.

• The George P. Reintjes Co. has issued a brochure covering sand seal castings for soaking pit covers. It covers the Reintjes inverted V principle for forming a double seal to level the sand lengthwise. The copy discusses some problems in successful pit cover design and operation.

• Among the expenditures in Armco Steel Corp.'s $60 million expansion program will be $25 million for a new 56-in. hot strip mill and other projects at the Butler Pa., plant. Another $18 million will be spent for two 275-ton open earth furnaces at Middletown, Ohio. A $15 million expenditure at the Ashland, Ky. Works will include addition of a second reversing cold mill and extensive building operations. Armco has spent some $275 million for expansion since World War II.

• May 5th is the day set for the inauguration of what has been termed "America's mightiest forging operation" when a combination of 50,000 and 35,000 ton presses start operation at the Air Force heavy press plant at Cleveland. Aluminum Co. of America will operate the plant located adjacent to its casting and forging works. Air Force Secretary Harold E. Talbot will give the signal that is to start the $40 million facility.

• Kaiser Steel Co. purchased the plant and facilities of Union Steel Co., a major steel fabrication and erection firm in east Los Angeles. According to Jack L. Ashby, Kaiser vice president and general manager, the move is another step in the company's expansion and diversification program. Another Kaiser news note is the exercise of options by the chemicals div. of Kaiser Aluminum & Chemical Corp., on 160 acres at Columbiana, Ohio for its new $4 million basic refractory brick plant. The property is being purchased from A. W. Andrich, C. R. Hollenshead and the Roller family.

AJAX Engineering Corporation, Trenton, N. J., wishes to correct a temperature figure which was given in their April advertisement in the JOURNAL OF METALS. The statement was made that the temperature of the melt is held at 870°F. This should have been 1170°F.

Coming Events

May 1-4, American Institute of Chemical Engineers, Shamrock Hotel, Houston, Texas.

May 1-5, Electrochemical Society, Inc., Sheraton-Gibson Hotel, Cincinnati, Ohio.

May 2-6, Electrochemical Society, Sheraton-Gibson Hotel, Cincinnati, Ohio.

May 4-7, National Screw Machine Products Assn., annual convention, Statler Hotel, Buffalo, N. Y.

May 6, American Assn. of Spectrographers, annual conference, Chicago, Ill.

May 8-11, National Industrial Advertisers Assn., national convention, Sheraton-Park Hotel, Washington, D. C.

May 9-11, Metal Treating Institute, annual spring meeting, Ambassador Hotel, Los Angeles, Calif.

May 10-12, Metal Powder Assn., Bellevue-Stratford Hotel, Philadelphia, Pa.

May 12-13, Michigan State College, symposium, Automation-Engineering for Tomorrow, East Lansing, Mich.

May 14-22, Chemical Engineering & Equipment Exhibition, Frankfort-am-Main, Germany.

May 16-19, American Mining Congress, coal convention and exposition, Public Auditorium, Cleveland, Ohio.

May 18-20, Porcelain Enamel Institute, mid-year div. conference, Edgewater Beach Hotel, Chicago, Ill.

May 19, AIME, Utah Local Section and University of Utah Student Chapter, joint meeting.

May 21, AIME, Columbia Section Student Meeting, State College of Washington, Pullman, Wash. Student papers program, baseball game, dinner.

May 30-June 1, Chemical Institute of Canada, annual conference, Quebec, Canada.

May 31, World Power Conference, International Executive Committee, Paris, France.

June 1-10, Joint Metallurgical Societies, European meeting.

June 7-10, American Welding Society, national spring meeting, Muehlebach Hotel, Kansas City, Mo.

June 8-18, International Organization for Standardization, general assembly meeting, Stockholm, Sweden.

June 13-25, Cornell University, summer laboratory course, Techniques and Applications of Electron Microscope, Ithaca, N. Y.

June 14-16, Conference on Magnetism and Magnetic Materials, AIEE, AIME, American Physical Society, Carnegie Institute of Technology, William Penn Hotel, Pittsburgh, Pa.

June 17, AIME, Spokane Subsection, Desert Hotel, Spokane, Wash.

June 19-23, ASME, semi-annual meeting, Statler Hotel, Boston, Mass.

June 20-23, Industrial Finishing Exposition, Cleveland Public Auditorium, Cleveland, Ohio.

June 20-24, American Society for Engineering Education, annual meeting, Pennsylvania State University, State College, Pa.

June 26-July 1, ASTM, annual meeting, Chalfonte-Haddon Hall, Atlantic City, N. J.

June 28-July 9, International Electrochemical Commission, London.

Sept. 6-16, Metal Show, Chicago Coliseum, Chicago, Ill.

Sept. 14-16, Porcelain Enamel Institute, annual shop practice forum, Deshler-Hilton Hotel and Ohio State University, Columbus, Ohio.

Sept. 25-28, American Institute of Chemical Engineers, Lake Placid Club, Lake Placid, N. Y.

Oct. 9-13, Electrochemical Society, William Penn Hotel, Pittsburgh, Pa.

Oct. 17-19, AIME, IMD, fall meeting, Adelphia Hotel, Philadelphia, Pa.

Nov. 4, AIME, NOHC, Pittsburgh Local Sections, annual off-the-record meeting, Pittsburgh, Pa.

Can your testing machines pass this "aptitude test"?

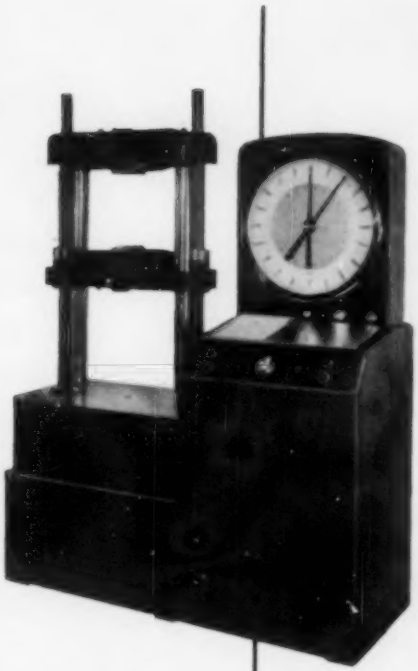

(Check box for each "no" answer. If "yes," leave blank.)

	No		No
Does my present equipment have infinitely variable speed control?	☐	Can it obtain high magnification stress-strain recordings?	☐
Can it control rate of loading?	☐	Does it have unlimited testing stroke over the complete distance between upper crosshead and weighing table?	☐
Can it control rate of strain?	☐	Can it handle off-center loads?	☐
Can it hold a stress or strain in the elastic range indefinitely?	☐	Can it unload as accurately as it loads?	☐
Can it utilize automatic load holding attachments?	☐	Does it have simple controls?	☐
Is its drive smooth enough not to affect the indicating system?	☐	Is its accuracy independent of the operator's skill?	☐

Are you proud of the appearance of your testing equipment? ☐

If your machines rate more than 4 "no" answers, they may be inadequate for today's conditions. Better clip this list and mail to us. Without obligation, we'll be glad to give full information on what you could accomplish with machines that do have the features checked. Also check here for Catalog RG-14-55 describing Riehle's complete line of modern testing equipment. ☐

FIRM NAME

ADDRESS

CITY ZONE STATE

ATTENTION MR.

Mail to: **RIEHLE TESTING MACHINES**
Division of American Machine and Metals, Inc., Dept. JM-555, East Moline, Illinois

Just how well are your present machines suited to modern testing procedures? Many machines now in use are, by today's standards, limited in versatility and convenience — and may be of questionable accuracy.

Here's an easy way to find out if your equipment is doing as complete a job as you could accomplish with up-to-date machines. Simply ask yourself the questions on the check list and determine how your equipment measures up to modern Riehle machines.

This check list also provides a chance to learn the full implications of the features referred to in the questions. Simply check off these features that are lacking in your present equipment. Clip and mail the list now so you'll have the information in your files. No obligation.

RIEHLE *TESTING MACHINES*

"One test is worth a thousand expert opinions"

Division of
American Machine and Metals, Inc.
EAST MOLINE, ILLINOIS

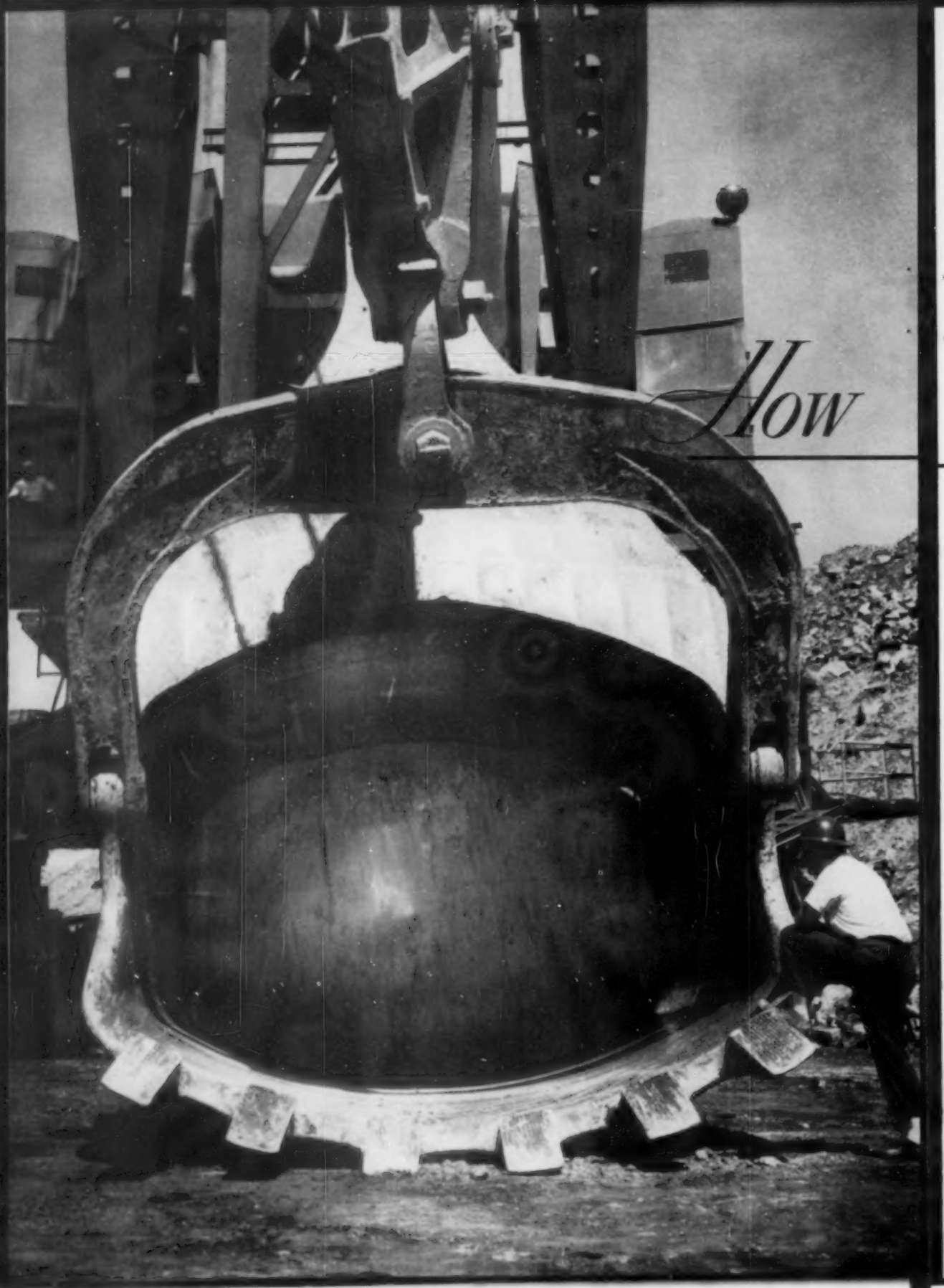
How

The entire shell of the bucket on this 50-cu. yd. power shovel is fabricated from ¾" to 6½" "T-1" Steel Plate. Liner plates are made of 1½" "T-1" Steel. "T-1" Steel Plate only 6½" thick has replaced large castings a foot thick in the lip of the bucket. Lighter weight construction with "T-1" Steel made it possible to increase the cubic capacity of the bucket by 10 cubic yards.

USS "T1" STEEL

in big machines

cuts weight, cuts cost, increases service life

Hanna Coal Company just can't afford to have this giant 50-cu. yd. shovel break down. This machine can move 2,280,000 tons of material a month, and it must operate continuously—24 hours a day, 7 days a week—to pay off.

Strong, weldable "T-1" Steel has improved the performance of this incredibly rugged machine, and it also has cut cost and weight. It enables the designers to use *fabricated* parts in place of larger, heavier, more expensive castings. And these lower-cost fabricated parts *last longer* than castings. As a result, Hanna Coal Company has standardized on "T-1" Steel for the vital parts of much of its heaviest-duty equipment.

Write for complete information on new USS "T-1" Steel. It has application in pressure vessels, rotating machinery, structural steel towers, steel mill equipment, big trucks, mine cars, and elsewhere.

USE "T-1" AT HIGH TEMPERATURES. New USS "T-1" Steel has good creep rupture strength up to 900° F. It is being used in heavy-duty parts that operate at high temperatures.

USE "T-1" AT LOW TEMPERATURES. This same steel is amazingly tough at sub-zero temperatures. In pressure vessels, it has survived impacts of 2,000,000 ft. lbs. at 38 degrees below zero F.

USE "T-1" TO CUT FABRICATING COSTS. You have a yield strength of 90,000 psi. in "T-1" yet you can weld or flame cut this steel without pre- or post-heating. Your welds will develop the full 90,000 psi. And you can fabricate parts either in the shop or the field—wherever it is more convenient and less costly.

Visit the U. S. Steel Booth at the
AMERICAN MINING CONGRESS AND COAL SHOW
MAY 16-19, 1955 · CLEVELAND, OHIO

UNITED STATES STEEL CORPORATION, PITTSBURGH · COLUMBIA-GENEVA STEEL DIVISION, SAN FRANCISCO
TENNESSEE COAL & IRON DIVISION, FAIRFIELD, ALA.
UNITED STATES STEEL SUPPLY DIVISION, WAREHOUSE DISTRIBUTORS, COAST-TO-COAST
UNITED STATES STEEL EXPORT COMPANY, NEW YORK

USS "T1" CONSTRUCTIONAL ALLOY STEEL

USS

5-476

UNITED STATES STEEL

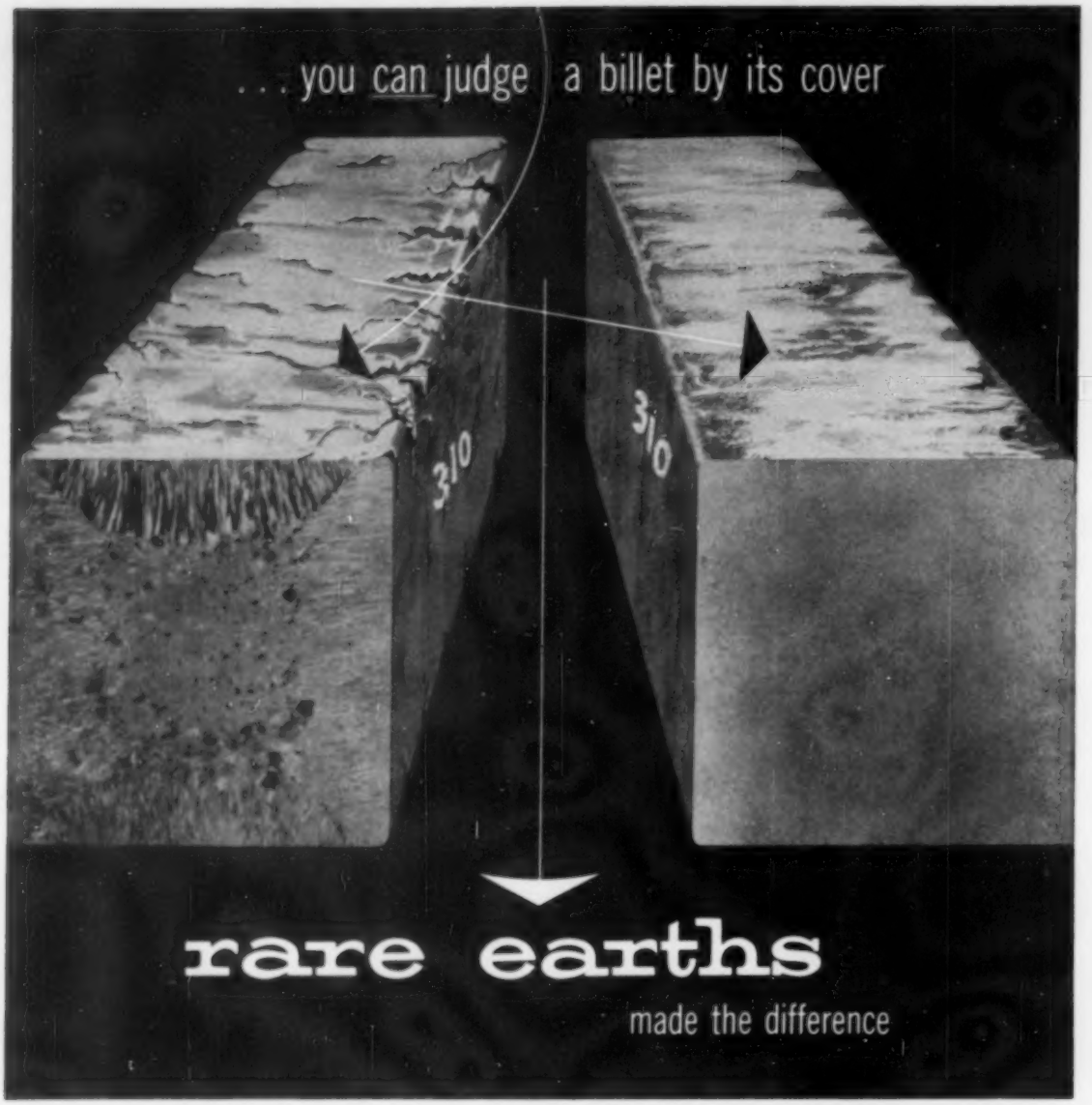

The two billets shown were produced by a prominent manufacturer of 310 stainless steel. Before rare earth additions, the billet on the left shows a coarse columnar structure, with frequent corner cracks. Heavy cogging was necessary to permit rolling with a minimum of hot tearing; after rolling a grinding loss from the edges incurred additional production time and expense.

Consider the billet on the right, and the great improvement made by a small economical addition of **MCA RareMeT Compound.** The fine primary crystal pattern shown in the sectional view is taken from an unretouched, unmagnified photograph. This steel was rolled without intermittent heating cycles from ingot to billet, and frequently to final size, all with a minimum of hot tearing.

MCA's RareMeT Compound is currently being used successfully in A.I.S.I. grades **309, 310, 316, 317,** and other stainless steel by many progressive producers. *Write today for further information.*

MOLYBDENUM

Grant Building CORPORATION OF AMERICA **Pittsburgh 19, Pa.**

Offices: Pittsburgh, Chicago, Detroit, Los Angeles, New York, San Francisco
Sales Representatives: Edgar L. Pink, Detroit; Brumley-Donaldson Co., Los Angeles, San Francisco
Subsidiary: Cleveland Tungsten, Inc., Cleveland Plants: Washington, Pa., York, Pa.

MCA

AS PARTNERS IN YOUR PROGRESS

...we have great confidence in you – our customers!

It is because we have this confidence in you that we substantially increased the production capacity of our Niagara Falls, N. Y. and Morganton, N. C. plants.

It is because of this confidence that we are constantly engaged in far-reaching research and developmental activities to insure your steadily increasing acceptance of our products in the years to come.

And it is because of this confidence in you that we look forward to still greater rewards from our partnership in your progress — to the degree that they are merited through the dependability of our products and the alertness of our service.

ELECTRODE GLC DIVISION

Great Lakes Carbon Corporation

GRAPHITE ELECTRODES. ANODES. MOLDS and SPECIALTIES

ADMINISTRATIVE OFFICE: 18 East 48th Street, New York 17, N. Y.
PLANTS: Niagara Falls, N. Y., Morganton, N. C.
OTHER OFFICES: Niagara Falls, N. Y., Oak Park, Ill., Pittsburgh, Pa.

Sales Agents in Other Countries: Great Northern Carbon & Chemical Co., Ltd., Montreal; Overseas Carbon & Coke Company, Inc., Geneva; Great Eastern Carbon & Chemical Co., Inc., Chiyoda-Ku, Tokyo.

Journal of Metals

THIS is something that could happen to any engineer, almost any day in his professional life. He sits before a typewriter, staring at it, occasionally fiddling with the keys, sometimes even punching out a few words. Sheet after sheet of paper finds its way into the wastebasket. He sits there, two steps away from an idea, but still too far to reach out and grasp it. The engineer may be aware that the things so clear in his own brain must be transmitted to paper in such a manner that they will leap from the page into the reader's conscious without effort. But how can he possibly take years of work and condense it down to the confines of a few sheets of paper? It may be a report to management, or a technical paper, or a speech. The problem remains the same.

Communication has become so important in the corporate world that many firms have people whose job it is to expedite the flow of information, as there are people responsible for sales, engineering, operation and other functions. It has become a complicated field, filled with filing cabinets, electronic brains, books on writing and speaking, millions of miles of wire, and much deep thinking. Underlying it all is a basic need for the understanding of the necessity for directness and simplicity. In recognition of this need the American Society of Mechanical Engineers devoted its 75th Anniversary Meeting to communications.

The general session was devoted to *The Engineer and His Communications*, with Col. Willard T. Chevalier presiding over a panel composed of Edgar Kobak, president of the Advertising Research Foundation; James G. Lyne, president of the Simmons-Boardman Publishing Co.; Ormand J. Drake, assistant secretary of New York University; and E. W. Engstrom, executive vice president, research and engineering, Radio Corp. of America. Colonel Chevalier delineated the problem at the start by saying: "One of the interesting developments of the time we are living in is the strange and sometimes new importance that is being attached to words. We hear ordinary, everyday words that we always thought we understood and we find them in strange contexts. We find that special meanings and significances are being attached to words that we always looked upon as old familiars. The word communications is one of these. . . . The battle for men's minds, as it is called today, is primarily a matter of communications, and I am afraid that one of the difficulties in dealing with this matter of communications between people is that too much of the communication consists of words and not enough of ideas."

Edgar Kobak recounted his early days as a technical magazine editor, when one of the major problems was to get engineers to exchange ideas. Since then things have improved, largely because of the educational job that has been done. "I find that engineers are much better qualified and better able to express themselves today than they were in those years."

Mr. Kobak feels that the herd instinct is too strong amongst engineers—mechanicals in one group, electrical in another, and so on. Even here he finds a gradual change taking place. He wants engineers to get out and take part in the community affairs of the world. Engineers, he says, are bashful and in fear of not being understood. In speaking of the current upsurge in the public utterances of pure scientists, Mr. Kobak had this to say:

"I do not say that scientists do not have the right to comment on . . . things, but they have got to give the matter thought and know what they are talking about and have ideas."

James Lyne pointed to the "ample and constantly widening external facilities for communicating with other engineers." But because of the magnitude of the ways of communicating, merit alone in the communication is not enough to win an audience. "Some engineers as well as other scientists seem to believe that the art of getting attention is somehow unworthy of their attention. Also, there has been, not on the part of engineers but on the part of other scientists certainly, a thought that if they can only get what they dreamed up into the archives whether it has any practical application or not, they have won the battle."

Ormand J. Drake, entered into the discussion by starting his talk with an object example of the application of one of his theories of speech. "I knew in the time that I had that I could not possibly speak on this subject, the whole thing, and have anybody take home what I wanted him to take with him, so I limited it."

Mr. Drake pointed out that written or spoken communication is designed not for the speaker or writer, but the audience. His "single condemnation" about those who make technical speeches, about most technical speaking, is that it is not human. He has no designs on making great orators out of engineers. The aim is two-fold—having people interested in the engineer's remarks from the platform on a technical subject; and through that interest, understand.

"A good technical paper is seldom . . . if ever a good speech . . . a good technical paper is never a good speech; and curiously enough, the better it is as a technical paper, the worse it can be as a speech."

Narrowing the subject down was emphasized by Mr. Drake as of primary importance as soon as the audience is known. "Do not try to tell the whole story in any given speech. Do not even try to tell a big part of the story. You cannot do it. This is because of the difference between that moving word and that nailed-down written word."

Mr. Drake also advises that the speaker determine exactly what he wishes to do in terms of the particular audience. Then, "find the most important parts from the listener's point of view." It's also a good idea, according to Mr. Drake, to tell the listener where you are going by stating the subject. Another rule is to arrange ideas so that the listener sees his relationship to the subject early. The final proposition offered by Mr. Drake is the use of simple language. "A speech is a short cut to reality, but sometimes it looks like a circuitous route rather than a short cut."

E. W. Engstrom emphasized the engineer's growing importance in the field of communication in view of the tremendous growth of means. He traced the past, present, and possible future of communi-

cation methods. He saw a need for the scientist-engineer relationship to broaden to include "the arts, the humanities, and politics." These will be the needs of the future in order that the scientist and engineer may discharge with competence their growing responsibilities.

◆◆◆◆◆◆

THERE is every possibility that Soviet scientists will be playing around with an American atomic energy reactor this summer. It will all be on the up-and-up and the Russians won't learn much that will help them make bigger and better bombs. The occasion will be the August meeting of the United Nations at Geneva for the purpose of exploring means for the peaceful employment of the atom.

The Atomic Energy Commission plans to install a swimming pool reactor for exhibition at the conference, and "Qualified scientists and technicians will be allowed to operate the machine using the controls to start, maintain, and stop a nuclear chain reaction," the AEC announced. Invitations to the meeting have been sent to 84 nations and it is expected that the Soviet and its nine satellites will come. President Eisenhower, in line with his atoms-for-peace program, wants Soviet participation. The Russians at least seem to be willing to play.

The swimming pool reactor will be sunk in a 10 ft sq, 20 ft deep pool. The reactor is similar to one at Oak Ridge and others of its type are being built by Pennsylvania State and Michigan Universities.

It's quite suited to the needs of a nation just beginning an atomic energy program under the U. S. partnership proposal. The reactor works on a weak mixture of uranium the U. S. is willing to supply for peaceful purposes. The fuel is unusable for weapons manufacture, but will perform experiments with neutrons and gamma rays, and produce radio-isotopes. The Geneva project will be handled by Oak Ridge, operated for the AEC by Carbide & Carbon Chemicals Corp., a subsidiary of Union Carbide & Carbon Corp. Reactor cost is estimated at $350,000.

◆◆◆◆◆◆

U.S. IRON ore imports were the greatest in its history in 1954, with 17.7 million tons entering the country, 60 pct of the total coming from U. S. developed properties in Venezuela, Canada, and Liberia.

Dept. of Commerce records indicate that the new high is 42 pct greater than the previous record set in 1953. Venezuela supplied 5.8 million tons, a 250 pct jump over the previous year. Another 4 million came from Canadian fields, or 90 pct more than in the previous year. Strangely enough, Canada last year imported 2,935,237 net tons of iron ore from the U. S. in 1954. Ore exchange between the U. S. and Canada is largely based on mine-to-plant location. Liberian shipments to the U. S. were 857,000 tons, up 6 pct over 1953.

Peru sent 945,000 tons of ore to the U. S. in 1953, and nearly 2.2 million tons last year. Chile and Sweden, long standing shippers to the U. S., sent significantly less ore to this country in 1954. Chile, the largest exporter of ore to the U. S. in 1953, fell to fourth place, while Sweden dropped from second to fifth.

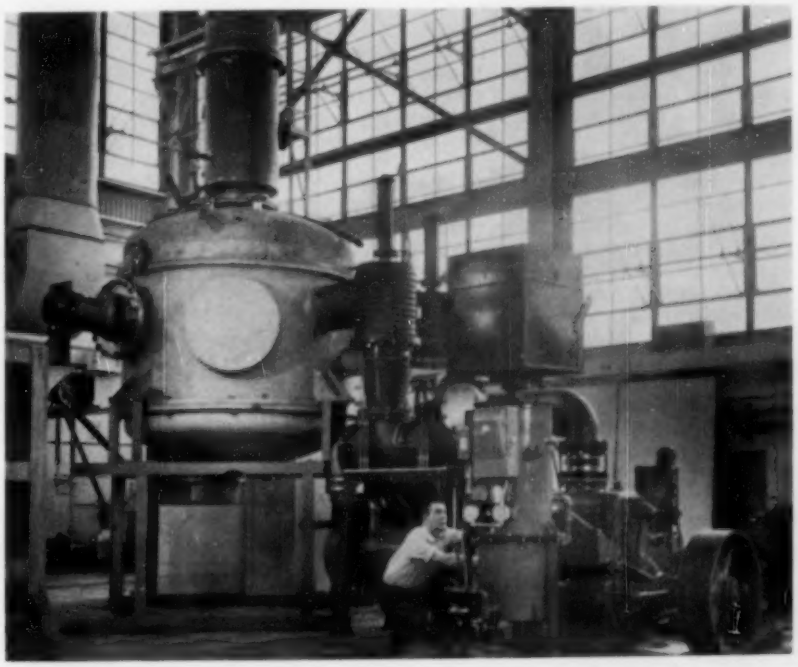

This is the first modular type 1000-lb high vacuum furnace. It's going through final tests in the Rochester plant of Consolidated Vacuum Corp. The unit is being installed at the metallurgical development laboratory of Westinghouse Electric Corp., Blairsville, Pa.

Drift of Things

THE American male in his most recent attempt to show that pioneer blood still courses through his veins, i.e., the Do-It-Yourself movement, may be unwittingly undermining the very system which has given birth to the cult's basic weapon—the ¼ in. drill. Whether ego, economic, or recreational motivations are behind the desire to do-it-yourself, financial writers are saying that the cult is endangering the principle of division of labor.

If, they warn, the trend continues and painters, plumbers, carpenters, masons, etc., are bypassed in favor of one's own inner resources—one may find oneself stuck with one's own little talents. People will start doing their own advertising campaigns, do-it-yourself kits will furnish everything needed to make I beams, and so on. At the recent Do-It-Yourself Show in New York City, one enterprising bank took exhibit space and emphasized How-To-Finance purchase of equipment and materials, and general home improvements—without so much as driving one nail. Doing-It-Yourself can be fun, save money, and give a man a sense of achievement—and it can also drive him down to a 98 lb weakling.

But, we claim no tried and true solution. The simplest way may be to look carefully to make sure that the local artisans are off fishing—or better, safely in bed—and then paint, replace the washer, or hammer like mad. (M.A.M.)

IN the 30 years that the Bayonne research laboratories of International Nickel Co., have been in existence, there has never been a cut back in operations or in personnel. Considering that this period encompassed some mighty bad times it is an indication of the value of research to the company. An important innovation has just been made that will please the research staff and probably extend the scope of the work done—staff members will be permitted to spend a portion of their time on projects of their own personal choice.

This information came to light during a visit to the Bayonne research laboratories last month. The purpose of our trip was to see the new plating laboratory, and to witness demonstrations of a new corrosion resistant alloy for the chemical industry, a new welding electrode for the welding of dissimilar metals, and a new improved Inconel welding rod.

The plating laboratory is concerned with the evaluation of new plating processes and coatings, research aimed at new uses for nickel, and research to improve the properties of nickel coatings. It is a research center in itself, designed to handle all work projects from bench scale to a pilot plant that approximates the operations of an actual industrial plating plant. This pilot plant, considered to be the world's only fully automatic pilot plating plant, has great flexibility. It encompasses an area 145x65 ft and has provision for 13 different stages of plating and/or cleaning. The machine is completely automatic except for loading and unloading, and can handle work up to 3 ft in cross-section. It can be operated entirely from a control panel board where time, current and voltage for each stage of a cycle can be observed and controlled. Also included in the plating laboratory is a manual plating line of 18 stations.

The new high nickel alloy, called Nionel, contains approx 40 pct Ni, 21 pct Cr, 3 pct Mo, 1.75 pct Cu, 31 pct Fe, and small amounts of Mn, Si, and C. The relatively high nickel content plus molybdenum and copper make the alloy considerably more resistant to hot sulphuric, sulphurous, and phosphoric acid solutions than any of the common stainless steels. The chromium content is sufficient so that when fortified with nickel, the alloy resists a wide variety of oxidizing chemicals. It is expected that Nionel will find major applications in the sulphuric acid pickling of iron, steel, and copper base alloys; in petroleum refineries, synthetic detergent plants, rayon manufacture, ore processing plants, handling combustion gases and condensate from sulphur-bearing fuels, in the pulp and paper industries, and in the wet process for producing phosphoric acid from phosphate rock. The good resistance of Nionel to pitting attack in sea water and also to stress-corrosion cracking in chloride solutions should lead to applications in tubular heat exchangers. The alloy is strong and weldable, with mechanical properties on the same order as those of Inconel. It is produced in all standard mill forms including plate, rod, seamless condenser tubing, pipe and extruded tubing.

To fulfill the long existing need for a welding rod capable of making strong, ductile joints between a large number of metals of substantially different compositions, the research laboratory announced the development of Inco-Rod A. The area of its greatest usefulness is expected to be in the joining of so-called ferritic materials, like mild steel, to the austenitic or stainless steel compositions. In addition, either group of alloys can be successfully joined to high nickel alloys such as Monel and Inconel. Pilot plant lots of Inco-Rod A have been made and tested in 20 dissimilar metal combinations: Mild steel to 304 stainless, mild steel to 405 stainless, Croloy to 347 stainless, mild steel to 330 stainless, 405 stainless to 316 stainless, mild steel to 316 stainless, mild steel to 310 stainless, 304 stainless to 410 stainless, mild steel to 347 stainless, Croloy to 304 stainless, 405 stainless to 304 stainless, 405 stainless to 310 stainless, 405 stainless to 347 stainless, 405 stainless to 330 stainless, mild steel to Croloy, mild steel to 410 stainless, Hastelloy C to 316 stainless, Monel to 410 stainless, Inconel to 347 stainless, and Inconel to 405 stainless. In all combinations the welds were ductile and crack free and the joint strength was sufficient to force failure in the base metal in tensile tests. In most cases, the corrosion properties of the weld deposit were superior to the parent metals involved.

For the welding of Inconel to itself, the Inconel 132 electrode represents a substantial improvement. The new electrode has a highly durable coating, and it is no longer necessary for the user to rebake the electrode to insure top quality weld deposits.

A. S. Cohan

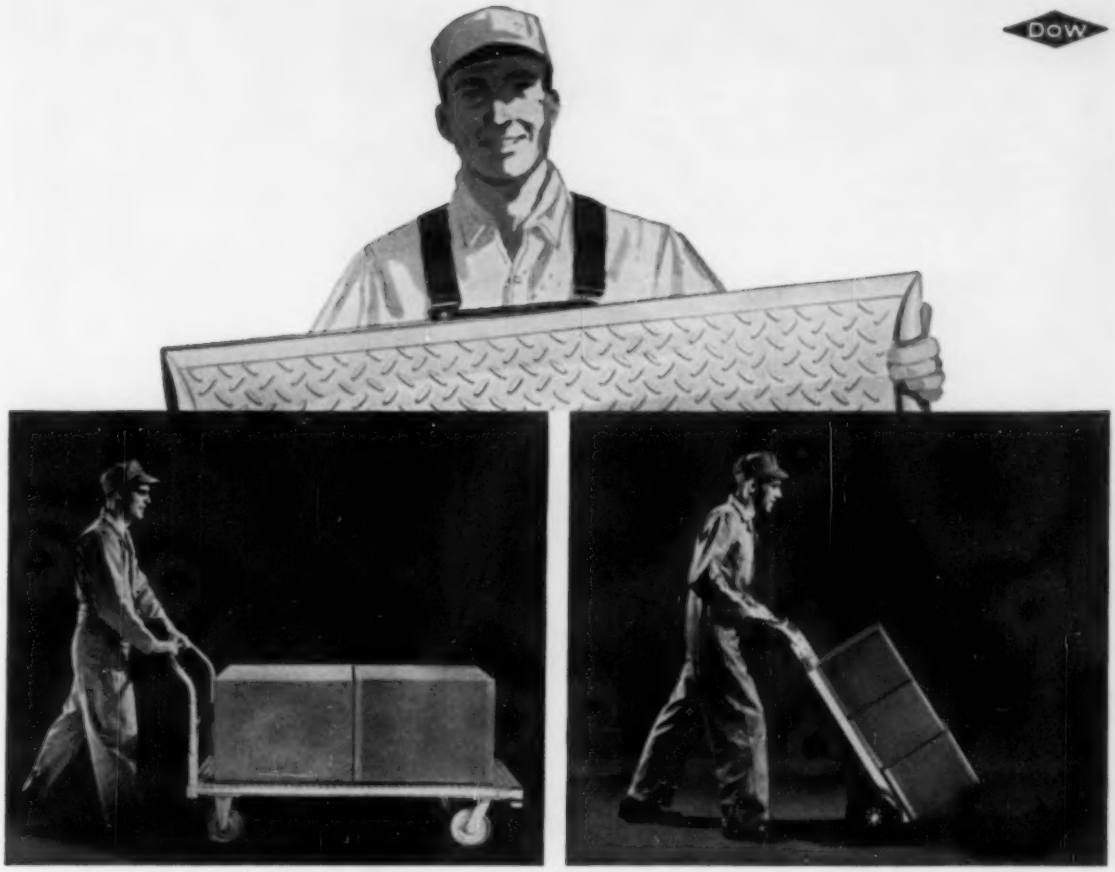

MAGNESIUM

Lightness in equipment saves manpower when materials are on the move

That's why magnesium is being used more and more to build lightweight but rugged materials handling equipment —to save manpower. Dockboards, platform trucks and hand trucks are just a few of the many applications where magnesium's light weight has increased efficiency and saved money.

One fourth the weight of steel, one third lighter than aluminum, magnesium has simplified design problems while maintaining maximum strength required. Fabrication is also made easier by the excellent weldability, forming, drawing and machining characteristics of magnesium.

To the equipment purchaser, "Made of Magnesium" assures peak efficiency in operation. To the equipment manufacturer, magnesium has become the key to more useful products, greater volume and complete customer satisfaction.

For further information about magnesium, call your nearest Dow sales office, or write to THE DOW CHEMICAL COMPANY, Midland, Michigan, Dept. MA 317H.

you can depend on DOW MAGNESIUM

DOW

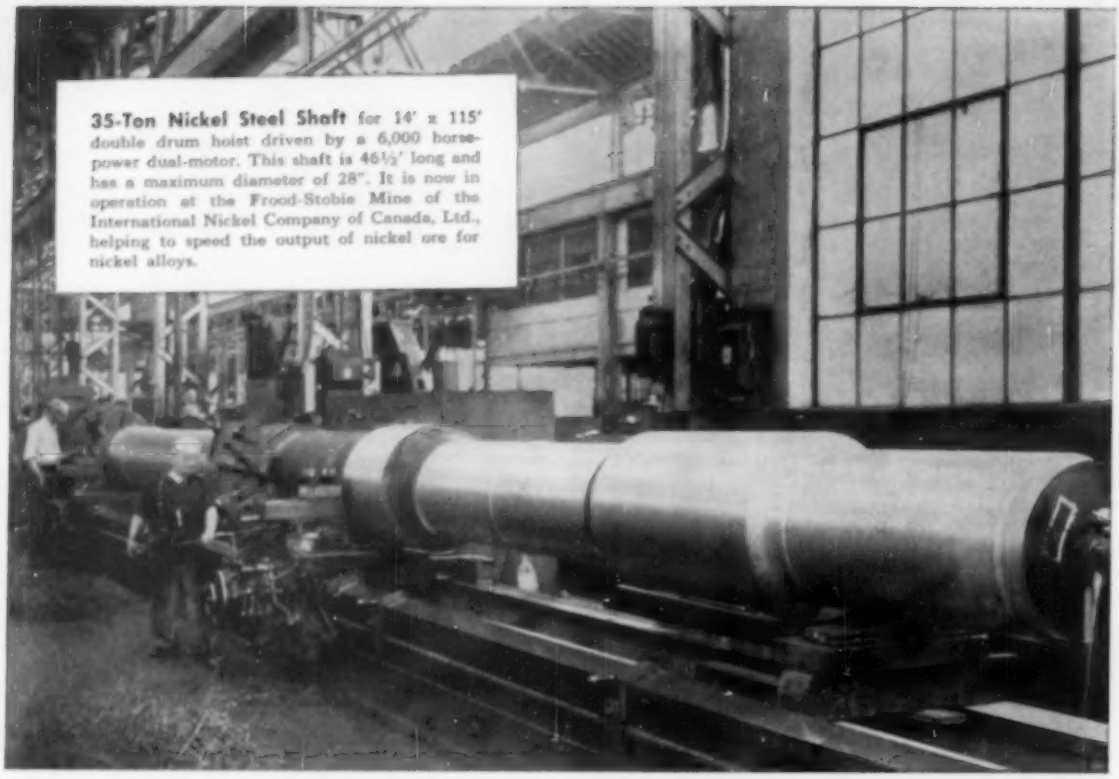

35-Ton Nickel Steel Shaft for 14' x 115' double drum hoist driven by a 6,000 horsepower dual-motor. This shaft is 46½' long and has a maximum diameter of 28". It is now in operation at the Frood-Stobie Mine of the International Nickel Company of Canada, Ltd., helping to speed the output of nickel ore for nickel alloys.

How nickel strengthened the shaft for

Canada's highest powered mine hoist

IN LARGE FORGINGS such as this giant shaft, high tensile and elastic properties do not come easily.

Liquid quenching of heavy forgings is usually impractical. Even when the shape is such that this treatment may be safely applied, the section sizes involved often restrict cooling to rates which render the quench ineffective.

Increased strength, hardness, toughness and other mechanical properties in a large forging depend to a great extent upon selection of alloy content.

Accordingly, to attain maximum strength and toughness in the shaft of Canada's highest powered mine hoist, at our own Frood-Stobie mine, we specified a shaft forged of 3½% nickel steel . . .

Because nickel, either alone or in combination with other alloying elements, provides a number of advantages.

For one thing, it has a strengthening effect on ferrite . . . independent of carbon content or heat treatment of the steel.

For another, it lowers the rate and temperature of the upper transformation, thus inducing better response to the necessarily milder heat treatments used. And it reduces grain growth.

Whenever you face a metal problem, let us help you make a selection that will meet your particular fabricating and service requirements. Send us details of your applications, for our suggestions.

INCO
TRADE MARK

Double Drum Hoist for the Frood-Stobie Mine, during course of shop erection by the builder, The John Bertram & Sons Co., Ltd., Dundas, Ontario. Spiders that support the steel shell of the hoisting drum were cast in an iron containing 1½% nickel . . . to assure adequate strength in the 74,600-pound drum-spider assembly. This hoist, operated by push button control from a station far underground, can lift skips containing 15 tons of nickel-copper ore, at an average rate of 14,000 tons daily.

THE INTERNATIONAL NICKEL COMPANY, INC.

67 WALL STREET
NEW YORK 5, N.Y.

International Nickel Co., has finally officially unveiled the details of its oxygen flash smelting process for the extraction of copper from ore concentrate. Inco is now using the method exclusively for treating all its copper sulphide concentrates. The process has completed a full year of successful operation, according to C. E. Young, who reported to the annual meeting of the Canadian Institute of Mining and Metallurgy. JOURNAL OF METALS, April 1954, carried some details of the process and the complete story will appear in June 1955. It eliminates the fuel normally required for smelting and permits production of by-product liquid sulphur dioxide.

A closed die forging press of 100,000 tons may not be too far in the future, according to Erwin Loewy, of Loewy Construction Co. Mr. Loewy stated that the plans for such a press have been presented to the U. S. Air Force. A 35,000 ton press has been operating since March 8 at the Wyman-Gordon USAF plant. Heinrich Albers, Loewy chief engineer, feels that "the law of diminishing returns" on closed die presses will not be reached until 500,000 tons of pressure have been attained.

Secret testimony disclosed by the House Appropriations Committee indicates that life of the atomic reactor aboard the Navy submarine Nautilus is from two to three times greater than expected. The original life estimate for the reactor is still a closely guarded secret.

Nickel for civilian use is expected to be scarcer in the second quarter, despite 3 million lb from stockpile that will go into industrial use during the period. The Business and Defense Services Administration blames an increase in priority defense orders for nickel-bearing steels in April. Overall supply for defense and non-defense uses during the second quarter will be about the same as the first.

Foster Wheeler Corp. announced that it can build an atomic power plant for much less than has been estimated up to now. The combustion equipment manufacturer states that it is ready to build a nuclear power plant with a 100,000 kw capacity for $21 million - a cost competitive with some present power station costs. Generally accepted estimate for the size plant quoted by Foster Wheeler is around $25 million.

Bell Telephone Laboratories announced that the efficiency of its solar battery has been practically doubled in the year since its introduction. Efficiency has been raised from 6 to 11 pct. It compares with the best gasoline engines and is more than 20 times higher than that of the best photovoltaic devices.

Ten tons of heavy water were sold to the Government of India by the U. S. for use in a research reactor near Bombay. The sale was in accord with the U. S. program for developing arrangements with friendly nations to promote peaceful use of atomic energy.

New G-E Accessories

contribute greater accuracy and versatility to

X-Ray Diffraction

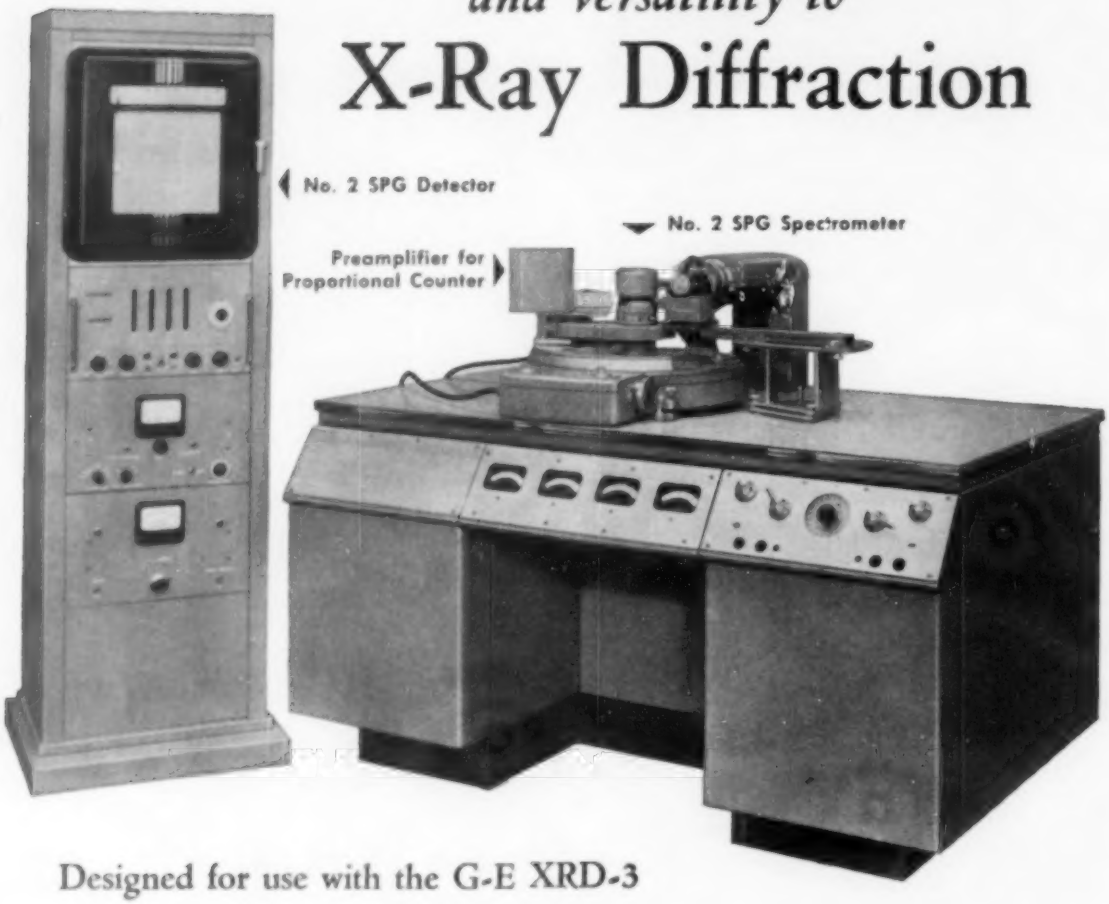

Designed for use with the G-E XRD-3

The G-E XRD-3 x-ray diffraction unit is widely used for physical and chemical analysis of many kinds of materials. To extend this unit's working range — and to make it even more accurate — we offer the following new accessories:

1. No. 2 SPG Detector. Unit features scaler of extended range with resolving time of one micro-second . . . with provision for both counting for preset time and timing for preset count . . . with automatic recording counter . . . with precisely adjustable long wavelength pulse discriminator to complement proportional counter. Also featured is ratemeter with both linear and logarithmic response by selector switch. Linear response contributes convenience in measuring relative intensities. Logarithmic response provides uniform measurability of widely differing intensities.

2. No. 2 SPG Preamplifier for proportional counters is designed to work with the No. 2 SPG Detector. Gas-filled proportional counter is generally preferred because of the semi-monochromating effect of the selective absorption characteristics of the gas in nearly all x-ray diffraction procedures.

3. No. 2 SPG Spectrometer uses a reflecting crystal to measure x-ray spectra of small atomic number elements in helium atmosphere. Offers vast improvement of intensities for all elements in air.

Get complete details from your General Electric x-ray representative. Call him today . . . or write X-Ray Department, General Electric Company, Milwaukee 1, Wisconsin, for Pub. AY-45.

Progress Is Our Most Important Product

GENERAL ELECTRIC

Super Refractories Give Operators Unique Range of Properties

by B. M. Johnson, A. A. Turner and H. S. Schroeder

THE phrase *super refractories* encompasses a unique class of materials, both in composition and properties. In this category are bonded refractories of silicon carbide, fused alumina, and fused mullite—all products of the electric furnace, and as a consequence relatively expensive. Impact of their cost on those hearing it for the first time invariably produces the appellation *gold brick*. Super refractories usage, nevertheless, is broad in scope and is quite essential to nonferrous metallurgy, usually proving to be *gold* brick from the standpoint of value received.

Each product constitutes a group or family of many varieties. One manufacturer claims over 50 standard compositions of silicon carbide refractories developed through bond modifications, changes in grit sizes and/or different production methods. Individual group members retain to a major extent the properties of their principal constituent. Often one or two properties can be further enhanced by scientific control of the variables mentioned, thereby increasing product suitability for a specific job. Concurrently, material selection for an installation becomes increasingly difficult and emphasizes the need for full cooperation between refractories producer and user.

Added to these three families of products is another group, essentially fused alumina, but so different in structure, properties, and application as to justify separate classification. This group has been called *fusion-cast refractories*. The raw materials used in their making are melted, cast into molds, cooled and then annealed; all steps simulating those followed in producing cast metal parts. Conversely, screen sized grains and spheres of silicon carbide, fused alumina and fused mullite may be readily bonded, formed by several methods into shapes, dried, and fired.

Refractory Properties

Table I lists four groups of super refractory materials and shows chemical compositions and physical properties of specific, widely used varieties of each type. It will be noted that high thermal conductivity, excellent wear and spalling resistance, low porosity, and high hot strength distinguish the silicon carbide group. In the fused alumina group, purity and heat conductivity are the main attributes of the low silica type, whereas the lightweight product is characterized by its light weight, high porosity and low rate of heat transfer. This latter material is made from hollow spheres or *bubbles* of alumina. The mullite refractories exhibit high load-carrying strength at elevated temperatures, ability to withstand metallic oxides and no excess or free silica. Corrosion resistance, purity, and dense homogeneous structure highlight the fusion-cast materials property-wise.

Common to all super refractories is the faculty of resisting high temperatures which, while of major import, can also be deceptive. Many kilns, furnaces and processing equipment, functioning at room to moderate temperatures, employ these materials for some unique property or properties other than that of heat resistance. Super refractories are seldom selected simply because they stand at the upper end of the temperature scale.

Considered on the basis of Pyrometric Cone Equivalent values, super refractories rate Cones 37 to 40 compared with Cones 31 to 33 for some high duty firebrick and Cones 33 to 34 for superduty brick. This narrow spread suggests the second way in which this property of refractories can deceive. Under heat, fireclay materials begin to soften several hundred degrees below the temperatures indicated by their PCE values so that much of their usefulness is lost long before theoretical limits are reached. Super refractories, on the other hand, retain strength and rigidity at temperatures much closer to their PCE values with great increase of serviceability.

Illustrating this point is the comparison shown by Fig. 1. These four brick, commonly used to resist high temperatures, were held at 3000°F for 5 hr. Only one, marked M, is a super refractory and it alone is untouched by the heat.

High temperature, Ni-Cr alloys also can be included in this comparison. For example, 25-12 Cr-Ni steel melts at 2575°F. It can be used under conditions up to 2000°F but strength drops rapidly above 1500°F.

Uses in Roasting and Smelting

Multiple-hearth roasters usually develop relatively mild conditions that refractories, other than those mentioned, usually satisfy. Some work, however, has been done with a muffled-type unit as

B. M. JOHNSON, A. A. TURNER and H. S. SCHROEDER are respectively General Manager, Technical Manager, and Senior Engineer, Refractories Div., The Carborundum Co., Perth Amboy, N. J.
This paper was presented at the AIME Annual Meeting, Chicago, Feb. 14 to 19, 1955.

Table I. Typical Chemical Analysis And Physical Properties of Bonded And Fused-Cast Refractories Made From Electric Furnace Products

Properties	Silicon Carbide		Fused Alumina			Electric Furnace Mullite		Fusion-Cast	
	Grade A*	Special	Low Silica	Regular	Light-weight	Grade W	Grade C	Beta Alumina	Alpha-Beta Aalmina
Ignition	1.37	—	nil	0.15	nil	nil	nil	0.18	0.07
SiC	89.16	—	—	—	—	—	—	—	—
Al_2O_3	0.35	—	96.89	92.03	81.02	75.57	78.10	93.90	94.56
SiO_2	7.72	—	0.50	6.75	16.80	23.47	18.10	0.04	0.80
Fe_2O_3	0.87	—	0.13	0.27	0.09	0.27	1.96	0.11	0.12
CaO	<0.10	—	nil	0.10	tr	<0.10	0.04	<0.10	0.23
MgO	—	—	tr	0.10	0.10	<0.10	0.35	<0.10	<0.10
Na_2O	—	—	0.37	0.53	1.59	0.40	0.10	5.62	4.07
TiO_2	—	—	0.01	0.07	0.40	0.09	1.80	<0.05	<0.05
Cr_2O_3	—	—	—	—	—	—	—	—	—
Pyrometric Cone Equivalent	39	—	39 to 40	38 to 39	38 to 39	38 to 39	39	39 to 40	39 to 40
Wt of 9x4½x2½ in. straight, lb	9.25	10.3	10.4	10.3	4.8	9.0	9.0	10.2	11.6
Avg bulk density, cgs	2.57	2.87	2.90	2.87	1.30	2.43	2.54	2.80	3.20
Porosity, pct	13.2	7.9	21.9	22.6	66.6	23.7	21.25	7.5	2.5
Mean sp ht 0° to 1400°C	0.255	—	—	0.330	0.320	0.230	0.230	—	—
Mean coef of expansion per °C, 25° to 1400°C	4.4×10^{-6}	4.4×10^{-6}	7.4×10^{-6}	7.4×10^{-6}	8.6×10^{-6}	4.6×10^{-6}	4.6×10^{-6}	8.6×10^{-6}	8.2×10^{-6}
Thermal cond at 2200°F, Btu	109	113.5	24	24	7	15	15	24	31
Modulus of rupture at 1350°C	2000	5040	200	658	63	433	267	—	—
1500°C load test at 25 psi, contraction: cold, pct	nil	0.0	0.50	0.35	0.65**	0.15	0.29	nil	nil
Abrasion resistance	excellent	excellent	fair	fair	poor	fair	fair	fair	good
Relative resistance to spalling	high	very high	good	good	good	very good	good	fair	low

* This covers a variety in common use. Where required, higher silicon carbide content varieties can be supplied.
** At 12.5 psi.

shown in Fig. 2. Mullite hearths, essentially inert, resist reaction with the charge and withstand mechanical wear. The high thermal conductivity of silicon carbide arches leads to their use to obtain rapid, uniform heat flow to the ore. Strength of both materials has proven more than adequate in operation even in self-supporting units exceeding 20 ft diam.

Of passing interest in connection with the multihearth roaster are the silicon carbide rabble blades used where heat, corrosion, and abrasion are a combination much too severe for metal. Fig. 3 gives a comparative picture of steel and silicon carbide blades following six months service in the same furnace. However, three important factors must be considered with respect to refractory blade usage: A—Whether a suitable metal fixture or holder for the refractory blade can be devised; B—Size range of ore, for large lumps tend to crack the refractory due to impact; and C—Approximate tensile stresses developed in actual service. Silicon carbide refractories have high compressive strength but like other refractory materials, tensile strength is much lower than that of various metals.

Reduction

The continuous, vertical retort method of reducing zinc ore provides one of the most striking illustrations of the value of *gold* brick in nonferrous metallurgy. The high heat conductivity and high load-bearing strength of silicon carbide brick account for the economic practicability of the process. Internal cross-section of the indirectly heated retort shown in Fig. 4 is about 6x1 ft and its 4½ in.

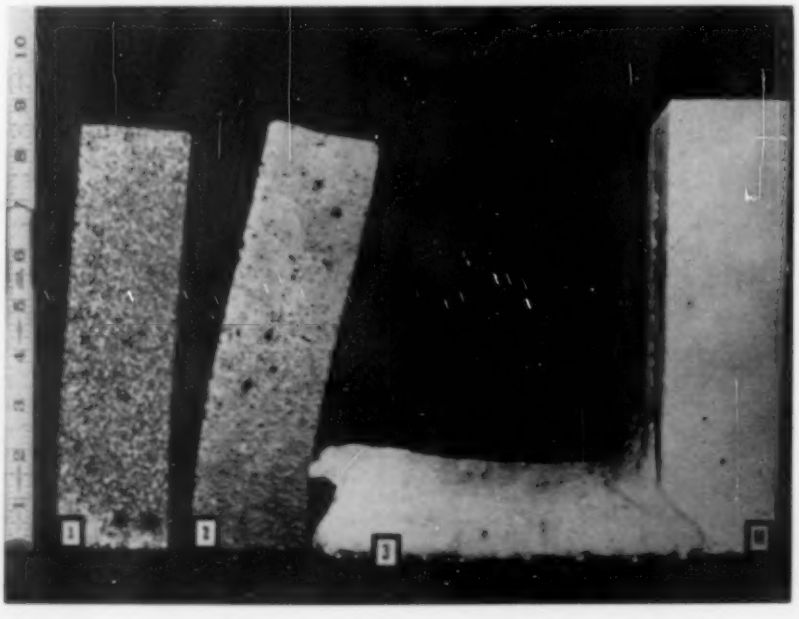

Fig. 1—Four brick commonly used to resist high temperatures were held at 3000°F for 5 hr. Brick marked M is super refractory and it alone is untouched by heat.

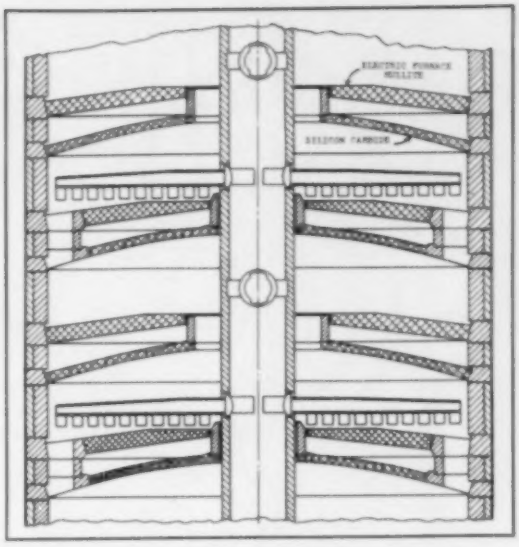

Fig. 2—Silicon carbide has been used on muffled-type multiple-hearth roasters to obtain rapid uniform heat flow to the ore.

thick walls tower 25 ft high. Entrance end or top of the retort is shown in Fig. 5 and may give a somewhat better idea of the construction.

A temperature of 2000°F is required within the retort through which briquetted oxide and carbon move continuously to reach a capacity of about 12 tons daily. Roughly, 5 million Btu's must be transmitted to the charge for each ton of zinc produced. As the metal is evolved in vapor form, retort walls must be kept tight during useful life that ranges from three to five years. Essential tightness is attained by means of spring compression applied externally to the brickwork.

Silicon carbide retorts are also used for treatment of other ores. A process for calcination of briquettes consisting of a metallic ore, carbon and a binder, for example, utilizes a unit of similar design shown in Fig. 6 with dimensions inside the shaft of 6x1 ft and 12 ft of heated height. Heat flow through the walls in bringing the charge to 1500°F in 4 hr is

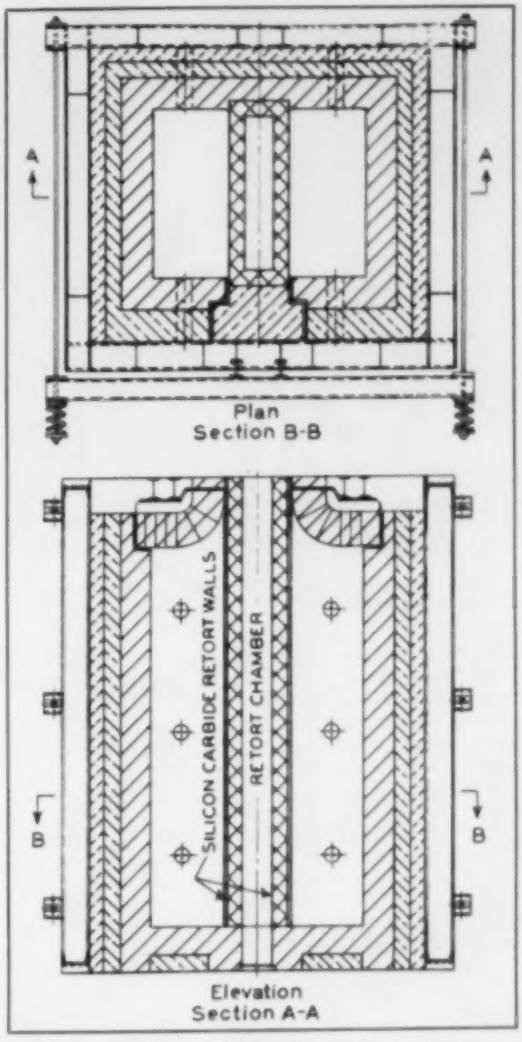

Fig. 4—Continuous vertical retort showing use of silicon carbide has a 6x1 ft cross section and is 25 ft high.

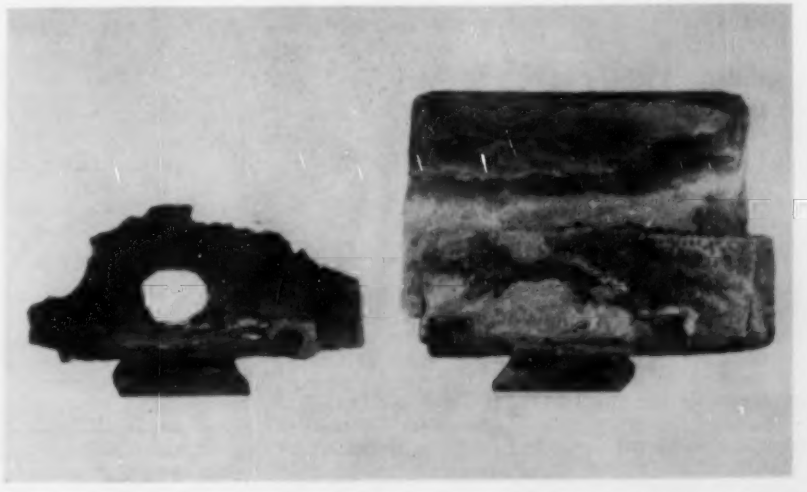

Fig. 3—Comparative picture of steel and silicon carbide rabble blades shows wear after six months service in the same furnace.

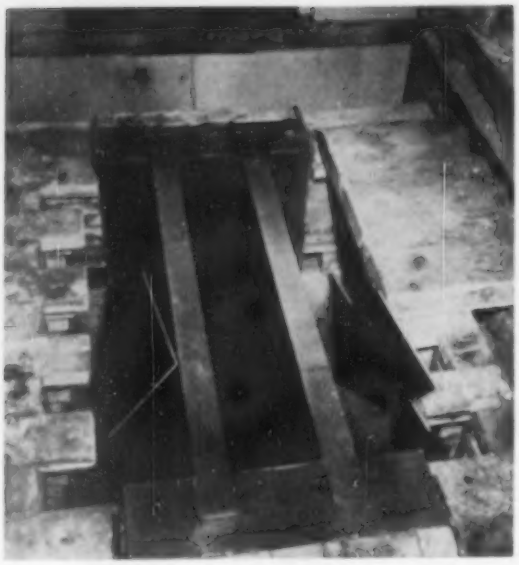

Fig. 5—Entrance or top end of continuous vertical retort shows construction features.

5400 Btu per hr per sq ft. Temperatures outside the retort are 2100°F at the bottom, dropping progressively to 1500°F at the top.

In a process for obtaining cobalt metal, small cylinders of cobalt oxide and carbon move downward inside a silicon carbide retort that is subjected to a temperature of 2400°F. This unit is much smaller than the retorts already described. It is built of 9x12x2 in. silicon carbide tile, tongued and grooved on four edges, to give structural stability and avoid leakage. The same properties of heat conductivity, hot strength, low permeability, and wear resistance are as beneficial here as in the larger retort structures.

Silicon carbide grain mixed with plastic fireclay is used to make horizontal retorts for the Belgian process of zinc ore reduction. Compared with the all-fireclay retort, this mixture increases life some four to six times, reduces zinc vapor losses, lowers fuel consumption, and expands productivity by faster heating of the retorts.

The electrothermic process of zinc ore reduction uses two furnaces, 69 in. IDx37 ft high and 96 in. x 37 ft high, as shown in Fig. 7. Silicon carbide brick and shapes provide the density or low permeability, hot strength and inertness to zinc vapors and molten zinc required in the vapor ring, distribution feeder arch, tapping well and condenser. The refractories' high thermal conductivity also plays an important role although used in reverse. Huge amounts of heat must be dissipated through the lining and the metal shell to obtain rapid cooling of the zinc vapors.

In producing ferromolybdenum, a bottomless steel shell, lined with a 4½ in. thick silicon carbide brick, is placed on a bed of sand. A thoroughly mixed charge, ignited by means of a starting fuse made from sodium peroxide and aluminum, completes reaction in 15 to 20 min. During this time a temperature of about 3500°F is developed but, because of fast heat dissipation and high slag corrosion resistance at such temperature, these brick give several hundred melts before replacement is

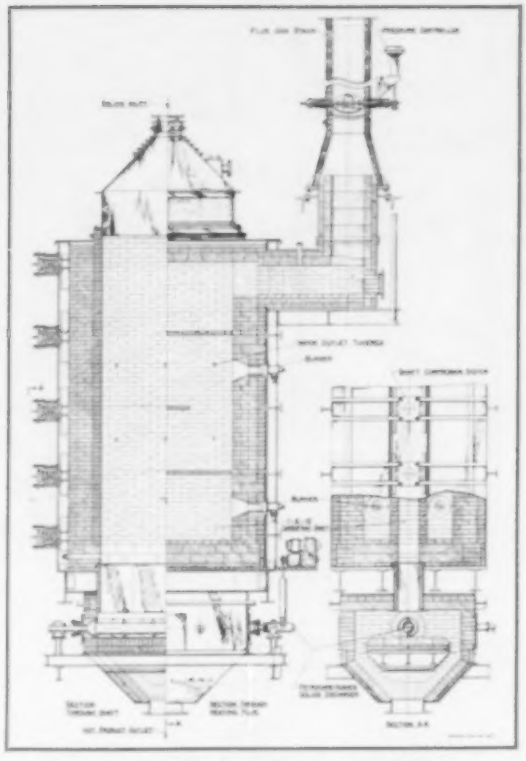

Fig. 6—Silicon carbide retorts are used for calcination of briquettes consisting of a metallic ore, carbon, and a binder. Diagram furnished by Petrocarb Equipment, Inc.

needed. Uniform thermal flow through the brick largely eliminates spalling from the heat shock experienced. The fireclay brick lined pot to the left in Fig. 8 has had two heats as opposed to 60 heats for silicon carbide brick in the crucible to the right.

A different type of application involves the electrolytic cells used in the Dow process for extracting

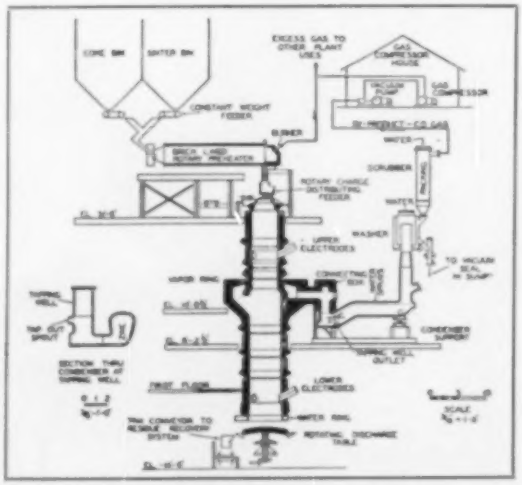

Fig. 7—Electrothermic process of zinc ore reduction uses two furnaces, 69 in. IDx37 ft high and 96 in. x 37 ft high.[1]

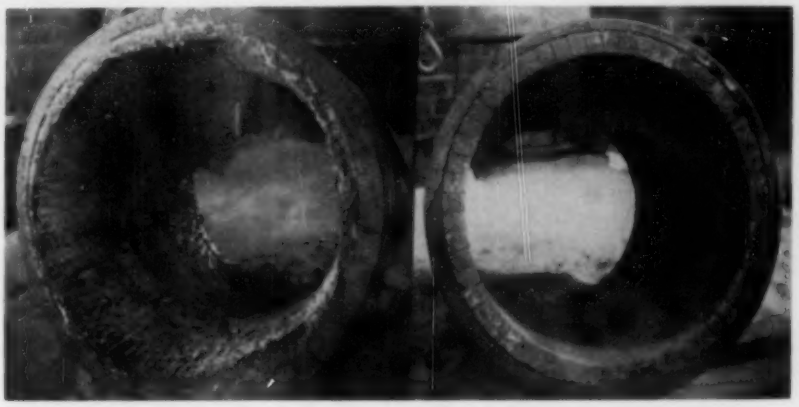

Fig. 8—Fireclay brick lined pot to left has had two heats in contrast to 60 heats for silicon carbide brick in crucible to right.

magnesium from sea water. The cell, 5x6x16 ft long, contains an electrolyte composed of approximately 25 pct $MgCl_2$, 15 pct $CaCl_2$, and 60 pct NaCl held at a temperature of roughly 1300° to 1400°F. Because of the extremely corrosive conditions, fusion-cast alumina blocks are placed in the upper cell walls. The dense, impervious nature of this material makes it a suitable container.

Refining

Apparatus used in refining zinc continuously by distillation is shown in Fig. 9. Each column consists of refractory enclosed silicon carbide trays, 18x27x7 in. deep or larger, each with a bottom outlet of its own. When stacked, the openings in succeeding trays are alternated so that the molten zinc travels the full length of individual trays as it cascades from top to bottom of the column.

Zinc and cadmium are distilled in the left hand fractionating column leaving a lead residue, whereas cadmium is distilled in the other column with a high grade zinc residue collected in the pot. In both instances, carefully controlled external heat is applied to the trays. It is closely maintained and evenly transferred to the metal through the silicon carbide trays. The strength of this super refractory is much greater than required by the imposed load. This quality permits consideration of larger trays for the distillation process.

Efforts to produce oxygen free copper in a reverberatory type furnace without poling have been successful by installing an arch of relatively thin silicon carbide interlocked shapes over the metal bath. Combustion occurs above the arch and radiant heat alone is applied to the metal. Gas leakage is reported practically nil and fuel consumption is lower than might be anticipated.

Another muffle-type furnace, shown in Fig. 10, is used to recover metallic zinc and zinc oxide from zinc base, die cast scrap. Melting takes place in chamber A and the molten metal flows to vaporizing chamber C above which a silicon carbide arch separates combustion gases and zinc vapors. In this distillation area temperatures must be controlled closely and gas leakage in either direction cannot be tolerated. Economical life of the furnace is determined by the heat transfer efficiency of the arch.[9] Although heat transfer is reduced by accretions of zinc oxide accumulated beneath the arch and slag build-up on top of the arch, more than two years service is normal before major repairs are needed. Tin-lead alloy, aluminum and copper are recovered from the residual metal tapped from chamber C.

Fig. 11 shows a typical reverberatory type aluminum melting furnace. A special grade of silicon carbide brick lines the sidewalls below the metal line as well as the bottom. Unusually high density silicon carbide brick, installed in the charging area floor, better resist the wear when heavy ingots are pushed into the furnace. Upper sidewalls and arch are built of fused alumina *bubble* brick to: A—resist fluxes, B—avoid stalactite formations that become a source of inclusions, and C—eliminate oxide formations on the brickwork of the structure above the bath. Electric furnace mullite brick and shapes are used for the tap, drain and burner blocks to furnish heat shock and erosion resistance.

Casting, Rolling, Fabricating and Finishing

Personal preferences and prejudices play principal roles in furnace selection and refractories employed. There are, of course, more furnace types than there are casting, rolling, fabricating, and finishing operations.

Possibly the simplest furnaces are the stationary and tilting types found in nonferrous foundries and equipped with from one to four burners and a crucible in which melting occurs. These furnaces are lined with cement rammed into place or with prefired shapes backed up with refractory insulation.

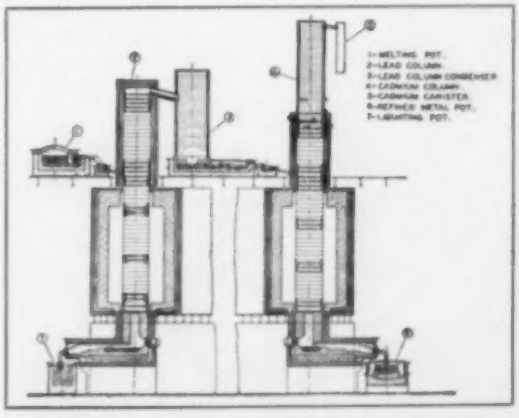

Fig. 9—Each column in apparatus used in refining zinc continuously consists of refractory enclosed silicon carbide trays each with a bottom outlet.[1]

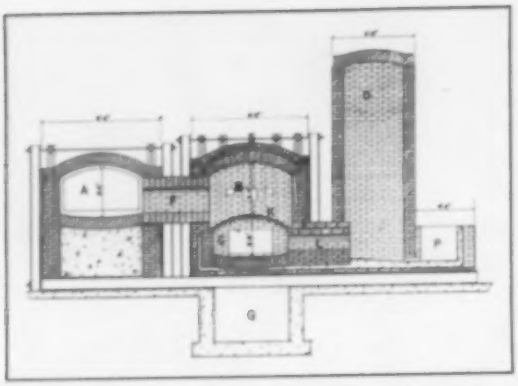

Fig. 10—Muffle-type furnace used to recover metallic zinc and zinc oxide from zinc base, die cast scrap utilizes silicon carbide refractories.

Most of the ramming cements are composed of clay and silicon carbide running upwards of 30 pct SiC, although high grade silicon carbide cements are required with some alloys. Prefired linings are formed of silicon carbide brick, tile segments, rings or one piece shapes in back of which are installed fireclay and/or refractory insulating brick, crushed firebrick or castable cements. A 1½ in. thick silicon carbide ring lining backed up with a castable cement prepared from alumina *bubbles* for insulation is growing in popularity because it can be installed in less than 2 hr. This results in a low heat capacity furnace that can be worked faster and is long lasting in spite of rigorous service.

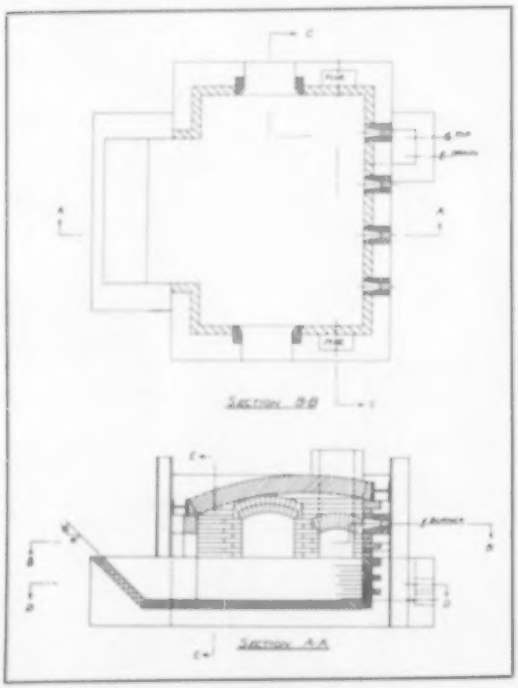

Fig. 11—Special grade of silicon carbide brick lines sidewalls below metal line as well as bottom in reverberatory type aluminum melting furnace.

In the electric arc furnace common practice is to use a lining of heavy Sillimanite blocks even though they evidently create installation and performance problems. An operator handling nonferrous metals for extrusion, in cooperation with a super refractories manufacturer, changed to rammed linings of electric furnace mullite cement. Average lining life of 300 heats from Sillimanite increased to 1800 heats; metal qualities improved; operating troubles, particularly with slag build up, largely disappeared; and refractories cost per pound of metal was lowered. All indications point to similar possibilities in other plants using this type of furnace providing installation instructions are followed.

Against bearing metals produced in a smaller version of the gray iron cupola, it is found that a

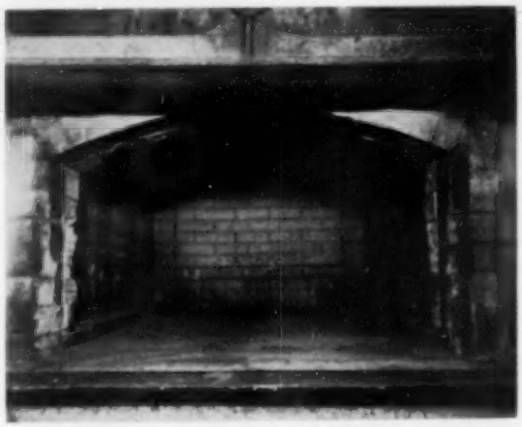

Fig. 12—Aluminum-bronze castings weighing up to 700 lb are heat treated in an under fired furnace equipped with a silicon carbide tile hearth. Life of furnace exceeds three years as contrasted with one year from fireclay hearths.

4½ in. thick lining of silicon carbide arch brick is more serviceable than other refractory linings. Downtime for repairs or replacement of the lining is less frequent and it is easier to hold the metal characteristics desired.

A marked difference of opinion about refractories usage prevails in die casting shops operating either small or large furnaces, particularly those in which aluminum is melted. It can be reported, however, that silicon carbide brick and/or shapes have given creditable performance when used both above and below the metal line. Inclusions, with attendant difficulties, are virtually eliminated due to the material's spall resistance.

In aluminum die cast furnaces that were shut down silicon carbide brick, in a few instances, acted in a phenomenal manner when exposed to the atmosphere for a period of time. Decomposition seemed to take place and what once was a brick lining became a mound of sand having a strong odor of hydrocarbon gas. This reaction does not occur if the furnace is kept heated. In fact, brick examined soon after operation is stopped show little or no deterioration. A possible way of expressing the chemical reaction is: $Al_4C_3 + 6H_2O = 2Al_2O_3 + 3CH_4$.

In an extrusion mill furnace, used for heating brass billets 6¾ and 8 in. diam in lengths up to 22 ft, five rows of billets are pushed end to end over 37 ft of silicon carbide troughs or skid rails. These required no attention for over three years at which time they were replaced. Alloy skids in the cool

section of the furnace warped badly and chrome-refractory hot zone hearths wore rapidly so that repairs had to be made every two to three weeks and complete replacements averaged five week intervals.

Aluminum-bronze castings weighing up to 700 lb are heat treated in the under fired furnace equipped with a silicon carbide tile hearth shown in Fig. 12. Its rapid heat transmission from combustion to work chamber is responsible for uniform heating of the castings with a reduction in fuel costs. Wear by the large castings primarily is forestalled by the abrasion resistance of this super refractory and life exceeds three years which compares with less than one from fireclay hearths.

Steel Industry Use

A recent development, conceived and nourished in the steel industry, is attaining a stature sufficient to command attention wherever severe wear poses problems. It is no surprise that silicon carbide should be suitable for combating wear whether by rubbing or by sliding. The hardness factor that makes silicon carbide grinding wheels such an excellent abrasive, imparts to super refractories the same or even better resistance to wear. Lack of consideration until now probably can be traced to the absence of heat or a temperature so low that a refractory material appeared unnecessary. But regardless of the reason, these same *gold* brick currently are demonstrating their worth in dust collectors, blast furnace downcomers, hot blast mains, coke chutes and wharves, bin throats, etc.

The hardness of silicon carbide falls between 9 and 10 on Moh's scale.[5] By Knoop's diamond indentation method the rating is 2480 which compares with 2800 for boron carbide and 8000 to 8500 for diamond. Boron carbide and silicon carbide are the hardest of man-made minerals but of the two, silicon carbide is the only practical material for commercial size equipment.[4, 5]

New Super Refractory

A new super refractory silicon-nitride bonded silicon carbide whose physical characteristics appear in column 2 of Table I deserves mention even though its possibilities are just being explored. Of particular significance are its metal-like qualities and the intricate, thin section shapes into which it can be formed for use up to and sometimes above 3000°F. Because it is not wet by aluminum and because of its dimensional stability, the material offers real potentialities for the die casting industry.[6] Use as fixtures in continuous brazing operations

Table II. Physical Properties of Zirconium Boride

Apparent Density	5.2 to 5.4 g per cu cm	
Melting Point	5400°F	
Hardness	88 to 91 Rc A	
Ultimate Tensile Strength (at 1800°F)	35,000 to 40,000 psi	
Transverse Rupture Strength (2 in. span)	60°F	68,000 psi
	1800°F	63,000 psi
	2200°F	55,000 psi
Stress to Rupture Strength (at 1800°F)	100 hr	18,500 psi
	1000 hr	14,000 psi
Electrical Resistivity	60°F	17.3 microhm-cm² per cm
	1800°F	249.6 microhm-cm² per cm
Thermal Shock Resistance	Good — passed NACA type test	
Thermal Conductivity	110°F	15.9 Btu per ft per hr per ft² per °F
Expansion Coefficient	75° to 1000°F	2.7×10^{-6} per °F
	75° to 2200°F	3.2×10^{-6} per °F

Table III. Corrosion Resistance of Zirconium Boride to Molten Metals*

Metal	Test Temp °F	Test Duration Hr	Boron and Zirconium Content of Metal	
			Before Test	After Test
Aluminum	1470	115	No B, no Zr	Trace B and Zr
Tin	730	100	No B, no Zr	No B, no Zr
Brass 90/10	2010	144	0.080 pct B, no Zr	0.097 pct B, no Zr
Brass 85/15	2010	116	None	0.037 pct B, no Zr
Brass 80/20	2010	100	Trace B, no Zr	0.037 pct B, no Zr
Lead	730	104	No B, no Zr	No B, no Zr
Copper	2010	100	No B, no Zr	No B, no Zr

* Tests were conducted by melting the metals in zirconium boride crucibles. No wetting of crucibles was evident.

proves this new super refractory capable of making many more trips without any attention whatsoever than is possible with even the best alloy whose initial cost normally is much higher. Brazed parts are dimensionally accurate to close tolerances as the fixture undergoes virtually no change in size; warpage seldom develops.

Other super refractories that more properly might be called refractory hard metals made from carbides, borides, silicides, and aluminides are still in laboratory stages. Typifying this product group, however, are the physical properties of zirconium boride given in Table II. Table III shows the material's corrosion resistance to various molten metals.

A ceramic fiber having, among other notable properties, a devitrification point above 2300°F, is now also supplied in various sizes of blocks. Textiles, roving, blankets, etc., produced from this fiber appear close to achievement so that a whole new vista is dawning, which will undoubtedly be felt in nonferrous metallurgy.

Conclusion

Four points are worthy of emphasis despite possible repetition: A—Super refractories usage most often is the result of their unique properties other than temperature resistance; B—Because super refractories are practically custom made, thorough cooperation with the manufacturer is imperative for best results; C—Super refractories complement rather than replace other refractory materials; and D—*Gold* brick return in value far more than their original investment.

References

[1] C. R. Hayward: *An Outline of Metallurgical Practice*. (1952) 3rd Ed. D. Van Nostrand Co. Inc., New York.

[2] G. E. Johnson: Development of Muffle Furnaces for the Production of Zinc Oxide and Zinc. *Trans.* AIME (1949) **185**.

[3] R. E. Wolfensperger: Practical Aspects of Silicon Carbide Wear-Resistant Linings. *Blast Furnace and Steel Plant* (March 1955).

[4] K. A. Baab and H. M. Kranef: Investigation of Abrasion Resistance of Various Refractories. *Journal* American Ceramic Society (1948) **31**.

[5] F. C. Roe and H. S. Schroeder: Abrasion Resistant Refractory Materials As Applied to Blast Furnace Operations. *Blast Furnace and Steel Plant* (April 1952).

[6] W. L. Wroten: Specially Bonded Silicon Carbide. *Materials and Methods* (November 1954).

Fig. 1—General view of north runway showing miscellaneous No. 2 sheet scrap in the foreground.

Methods Developed at Armco For Decreasing Scrap Charging Time

by W. W. Bergmann

A CONCENTRATED effort was made in 1954 to increase the density of scrap per pan in the stockyard of No. 1 open hearth, Middletown Works, Armco Steel Corp. Loading by cranemen and leveling by stockers proved to be the key to greater efficiency. These operations were improved by on the job training by stockyard foremen. This, together with improved preparation of the different grades of scrap in the mill and scrap preparation yard, resulted in decreasing the average charging time per heat by 30 min.

No. 1 open hearth consists of four 170-ton and four 190-ton furnaces operating through 1954 on a 57 pct hot metal practice. The transportation and charging facilities consist of the following: A—three 15-ton cranes in scrapyard, B—two 70-ton locomotives, C—one stockyard scale equipped with Streeter-Amet weighing device, D—140 buggies with automatic couplers and 20.5 cu ft pans, and E—three 5-ton charging machines.

All scrap is delivered to the furnaces over an elevated track to the charging floor lean-to building. It is switched to the furnace charging buggy track over a single cross-over located in the center of the shop. Empty buggies are removed from one end of the charging floor and returned to the stockyard over the same tracks used for delivery.

W. W. BERGMANN is Superintendent, No. 1 Open Hearth, Middletown Works, Armco Steel Corp., Middletown, Ohio. This paper was presented at the AIME National Open Hearth Conference, Philadelphia, Apr. 18 to 20, 1955.

Scrap Classification and Preparation Yard

All inbound cars of foreign scrap are delivered to the receiving yard where they are inspected and

classified by the scrap inspector working out of the purchasing dept. It is the responsibility of this inspector to determine whether the scrap meets specifications as to quality, size or usability. Inspecting cars in this yard before placement to various points of use eliminated transportation of rejected cars.

It is the responsibility of the scrap inspector to keep the open hearth stockyard supplied with the various kinds of foreign scrap required for current melting schedules, and also to keep scrap piles in the stockyards filled.

A scrap preparation yard became necessary to relieve the congestion in the open hearth stockyard which was too small to prepare foreign scrap. Therefore, the yard was erected adjacent to the plant to reshear domestic and foreign scrap. The scrap preparation yard covers an area of 15 acres and the department consists of two crane runways, each 825 ft in length. Two 7½-ton overhead cranes are on the north runway and three 7½-ton overhead cranes on the south runway. Under these runways there are placed 16 alligator shears and a Harris hydraulic baler. The shear capacities are as follows: four No. 4 shears, four No. 3 shears, and eight No. 2 shears.

A 25-ton dinkey locomotive is used to transfer cars of scrap iron on the numerous tracks required for storage of both prepared and unprepared scrap. A 40-ton diesel crane is used to load and unload scrap iron in yard outside of crane runways.

Fig. 1 is a general view of the north runway. Miscellaneous No. 2 sheet scrap is seen in the foreground. This scrap is received in trucks and cars which are unloaded with the overhead crane and sorted as to heavy and light gage. The scrap iron that is too heavy for bundling is put on a separate pile, resheared or burned to charging pan size. The light gage No. 2 sheet scrap is also put on a separate pile, and when a carload is accumulated it is sent to open hearth to be bundled. A carload of enameled scrap is shown in right foreground. This scrap is sheared on two No. 2 shears in this runway. In the background there are four No. 2 shears for shearing heavy scrap and pipe. These shears are located in the middle of the runway due to the necessity of the scrap being handled with a crane.

Fig. 2 shows scrapped pipe being prepared for shearing. A carload of scrapped pipe is unloaded by a crane under the runway. Enough pipe is distributed on the ground by means of a crane to keep work ahead of the burners. All pipe is cut to approximately 6-ft lengths. It is necessary to split all pipe over 6 in. in diam into two or more pieces in order to get it under the shear blade. Shearmen pick up the split pipe and put it on the gravity conveyer ahead of the shear. Pipe is sheared to 18 in. or under in order to get heavier weight per open hearth charging pan.

Fig. 3—General view of south runway shows the Harris bundler building and the clip stock in the foreground.

Fig. 3 shows the general view of the south runway. The Harris bundler building and clip stock are in the foreground. Four No. 3 shears and six No. 2 shears are operated under this runway. Miscellaneous prepared scrap iron is received in trucks and unloaded in this yard with a crane. When a carload of scrap is accumulated it is loaded and sent to the stockyard.

Unprepared scrap iron is sheared on the No. 3 shears under the south runway. It is sorted as much as possible when unloaded by a magnet. The scrap iron which is too heavy for shearing is sent to the area in the center of the runway where it is cut with a burner to charging pan size. Space is reserved under this runway for preparing current heavy material. Miscellaneous unprepared scrap is stocked ahead of shears with a crane. The shearman

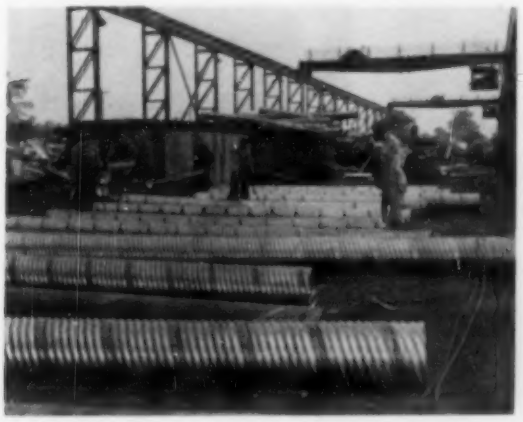

Fig. 2—Scrap pipe is sheared to 18 in. or under in order to get heavier weight per open hearth charging pan.

Fig. 4—Coil ends of cobbles are sheared on No. 3 shear. There are four No. 3 shears in the yard.

Fig. 5—Finished bundles from the Harris baler measure 14x18x22 in. and weigh approximately 300 lb.

sorts out the undesirable nonferrous metals, cast iron, and light gage scrap. It is necessary for the shearman to handle every piece of scrap iron. Only a portion of this scrap has to be sheared to charging pan size.

Fig. 4 shows coil ends of cobbles being sheared on No. 3 shear, and Fig. 5 shows finished bundles from the Harris baler. The bundles are 14x18x22 in. and weigh approximately 300 lb. The baler produces bundles at the rate of 5 tons per hr. Very light gage scrap iron, such as clips, used autos, etc., is charged into baler with a crane. Bundles are also loaded into cars with a magnet.

Fifty-seven men are required to operate the scrap preparation yard, one 8-hr turn 5 days per week. Approximately 6300 net tons of scrap are burned, sheared, pressed, or sorted for the mill each month. An average of 1.59 man hr are required to prepare each ton of scrap.

Uniform Scrap Distribution

Proper and uniform scrap distribution is a function of close scheduling between the scrap inspector,

Table I. Comparison of Prepared and Unprepared Scrap Efficiency

Grade of Scrap	Weight Per Pan, Lb		No. Pans Required to Charge 10 Tons Scrap	
	Unprepared	Prepared	Unprepared	Prepared
Loose clips	500	—	40	—
Hydraulic bundles	—	1150	—	17.4
Mechanical bundles	—	2500	—	8.0
Loose sheet scrap	1000	—	20	—
Bundled sheet scrap	—	3000	—	6.6
Cut pipe	600	—	30	—
Pipe sheared	—	910	—	21.9
Turnings	800	—	25	—
Turnings admixed in mechanical bundles	—	3000	—	6.6

Table II. Weight of Scrap Charged, Lb

Scrap	Wt Per Cu Ft	Wt Per Pan
Mixed steel	55.6	1140
Hydraulic bundles	54.5	1117
Turnings	51.0	1045
Coils and thin bars	158.8	3255
Bar crops	205.5	4212
Shear bundles	119.6	2452

scrap preparation foreman, and the foremen of each of the open hearth scrap yards. Segregation of various grades of scrap is required to meet anticipated melting schedules in each shop. Every effort is made by the open hearth stockyard foreman to distribute heavy melt, thin bar, and bar crops over all heats uniformly. These efforts pay dividends in keeping shop operational schedules uniform. In this manner, charging time, for example, is fairly consistent from furnace to furnace, and as a result, the timing of all the sequences from the stockyard through the pit can be quite accurately predicted and controlled.

Scheduling and movement of prepared scrap delivery has been improved through extensive use of communication systems. Interplant telephones, locomotive radios, and telautographs play a vital role in speeding delivery to the proper locations.

Home Scrap Preparation

The domestic scrap originating in the plant consists of bar crops, coil ends, and sheet scrap, side and end shearings. The bar crops are extremely good scrap, but the other types of scrap must be prepared at the source or compressed into bundles.

Domestic scrap, not subject to compressing, is packed and strapped in forms at the source and delivered to the stockyard as shown in Fig. 6. These bundles are 18x24x72 in. and average 3000 lb. Bundled sheet scrap is loaded into interplant trucks and sent to the stockyard. The bundles are loaded on piling blocks and spaced about 6-in. apart to avoid breakage when unloading with magnet in stockyard. Bundles are loaded into pans on buggies with a magnet as illustrated in Figs. 7 and 8.

Sheet scrap bundled at source increased a four-pan buggy weight from 4000 to 12,000 lb. A large mechanical bundler was installed in 1916 to bundle light scrap. Bundle size is 24x24x72 in.

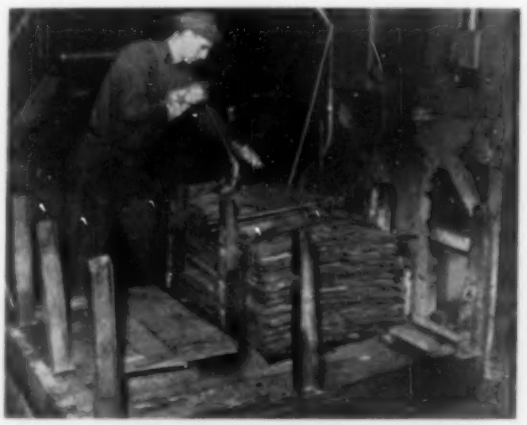

Fig. 6—Domestic scrap is packed in bundles measuring 18x24x72 in. and average 3000 lb.

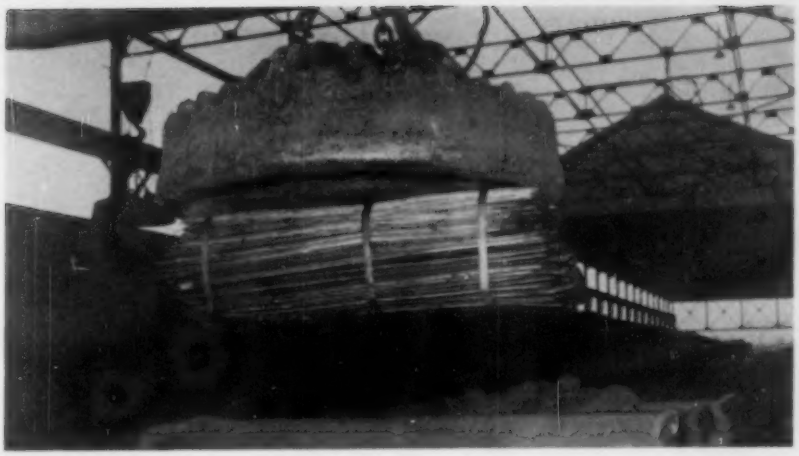

Fig. 7—Scrap bundles are loaded into pans on buggies with a magnet. Pans have a 20.5 cu ft capacity.

Table III. Pertinent Scrap Charging Data

Charging Data	1953	1954	Pct Increase or Decrease
Scrap avg lb per cu ft	84.4	95.8	13.5 Inc.
Scrap avg wt per four pan buggy	6924	7859	13.5 Inc.
Pans avg No. per heat	118.74	105.63	11.1 Dec.
Scrap charging time hr per heat	2.07	1.58	23.7 Dec.
Pct hot metal	55.3	57.2	3.4 Inc.

Cars of domestic scrap from the mill are sent directly to the bundler. A 15-ton overhead crane with a 65-in. magnet picks up the scrap from the car and deposits it in the bundler. The bundles are delivered directly into special charging pans from the machine. If the sheet scrap were bundled loose, it would be necessary to load 50 more pans of scrap per heat at 500 lb per pan. It would require approximately five charging pans to handle the same amount of loose scrap as is compressed into one bundle. This means faster charging and less interference on charging floor. Approximately 0.25 man hr per ton are required to operate the mechanical bundler.

Miscellaneous domestic scrap, such as pit runner scrap and ingot butts are shipped directly to the stockyards. Scrap too bulky to charge, of course, is first prepared in the scrap preparation dept. Steel

Fig. 8—Transportation and charging facilities at No. 1 open hearth include 140 buggies with automatic couplers.

buttons are cut to size at a button cutting station located in the scrap preparation yard. The burner is set up on a small trolley which operates on a 5 ft high runway. The burner travels in any direction. Cutting speeds average from 1 to 3 ipm, depending on the thickness and the cleanliness of the steel being cut. Buttons are cut up to 40 in. thick.

Maintenance of Charging Buggies

Charging buggies are of four and five pan design. The original buggies were cast bodies with friction type bearings having links and pins for coupling. In recent years a revamping program on all buggies included replacement of friction with roller bearings and the links and pins with automatic couplers.

Roller bearings and automatic couplers require continual inspection and preventive maintenance. A buggy bearing lubrication man, assigned from the round house, lubricates all buggies at least once a month. As a result, there are very few bearing failures and few buggies out of service. Two repairmen from the car shop inspect and repair automatic couplers and buggy bodies one turn per week. On the day assigned, as many drags of buggies as possible are set out for this service. Buggies found in need of major repair because of body cracks are taken out of service and repaired at the round house.

Since the stockyard has been equipped with the Streeter-Amet automatic weighing device to weigh cars in motion from 1 to 3 mph, maintenance on buggies has been sharply reduced. This eliminates the need for a complete stop of each buggy on the scale and the damage resulting from impact loads on all bodies and couplers.

Results

Table I shows a comparison of weight per pan of prepared and unprepared scrap and also the number of pans required to charge 10 tons of scrap. Since each pan eliminated saves approximately 54 sec of furnace charging time, the advantages of good scrap preparation can easily be justified.

Table II shows the weight of six grades of scrap per cu ft and weight per pan, and Table III gives other pertinent charging data. The average charging time per heat in 1954 was 1.58 hr, which was a decrease of 23.7 pct over the previous year when the charging time averaged 2.07 hr. The improved charging time was due to increased weight of scrap per cu ft along with increased amount of home scrap prepared in the mill.

New Refractory Uses For Silicon Nitride Reported

by J. F. Collins and R. W. Gerby

IN the commercial production of silicon nitride, silicon is placed in a nitrogen-atmosphere furnace which is then heated to approximately 2372°F (1300°C).[1] After a suitable holding period at this temperature, the furnace is cooled to room temperature and the resulting silicon nitride removed from the furnace.

The process of forming silicon nitride appears to be one of diffusion of nitrogen into silicon. Pieces of silicon metal 20x40 mesh-size were held in the nitriding temperature range for only a short period of time; hence, nitriding was not complete. From photomicrographs it can be readily assumed that there is a practical limit to the size of the silicon nitride piece that can be completely nitrided, and laboratory studies indicate this to be about 150 mesh. Therefore, the coarsest grade of silicon nitride powder, commercially available, is 150 mesh. Silicon nitride powder as fine as 1 micron has also been produced, but only −10 micron powder is commercially available.

This does not mean that silicon nitride can be supplied in powder form only. Silicon nitride is also available in slip-cast, pressed, and extruded shapes with the size of the shapes being limited only by the internal dimensions of the nitriding furnace. Pressed shapes of silicon nitride are made by pressing silicon metal powder, 150 mesh or finer, into the desired, finished form. This porous silicon metal shape is then subjected to the nitriding cycle. The voids that exist between the individual silicon particles provide paths for the nitrogen to come into intimate contact with each silicon particle. In this way, the entire silicon article is transformed to silicon nitride, and the resulting shape is all silicon nitride with no foreign bonding agent which would represent a source of potential mechanical and chemical weakness.

The pressing technique described above is ideal for simple, straight-lined solid bodies. Long, thin-walled tubes present an extremely difficult pressing problem but can be easily fabricated by other techniques. One such technique is slip-casting—an old fabricational process well developed in the pottery field. In this process, extremely fine silicon powder is made into a water slip which is then poured into a hollowed out, plaster mold having a contour exactly the same as that desired in the finished shape. As the plaster absorbs moisture from the slip, particles of silicon are deposited on the inner surface of the plaster mold. With the passage of time the number of silicon particles being deposited increases. Hence, the thickness of the so-called *green ware* depends upon the time the slip is permitted to remain in the plaster mold. After removing the green ware from the plaster mold, it is placed in a nitriding furnace and converted to silicon nitride. Although solid articles may be produced by this process, it is most applicable to hollow shapes.

Extrusion techniques can also be applied to silicon nitride shapes, particularly when thick-walled or solid bars and rounds are desired. In this process, fine silicon is used as a thick paste which is extruded into the desired shape. By placing the extruded article into a nitrogen-atmosphere furnace, the silicon is converted to silicon nitride.

This brief description of fabrication techniques indicates the variety of articles that can be made from this material. The fabrication technique used will depend on the shape as well as the quantity desired. There is no significant difference in the mechanical characteristics of shapes fabricated by any of the above techniques.

Sections as thin as 1/16 in. have been slip-cast from silicon and then nitrided, while articles having a 3-in. thick wall have been pressed and nitrided. There is no limitation on the size of section that can be nitrided as long as the individual particles of silicon metal are no larger than 150 mesh. The ability of slip-cast silicon to hold dimensional tolerances during nitriding is excellent. While there is a slight contraction of the green silicon ware away from the plaster mold, there is a corresponding small expansion during nitriding; thus, the finished shape will be within ±0.005 in. per in. of the dimensions of the pattern used to make the plaster mold. Many ceramic materials cannot be made in long, tubular or strip sections without being carefully supported during the firing cycle because of their tendency to sag as the maximum temperature of the firing cycle is approached. This difficulty is not experienced in the nitriding of slip-cast silicon parts. Thin-walled, silicon nitride thermocouple protection tubes are consistently cast to a center line tolerance of ±0.01 in. per ft.

Regardless of the fabrication technique used, the resulting articles have a density that is approximately 72 pct of the theoretical. While silicon nitride shapes are not of maximum density, they are not pervious. One standard production test is an internal 50 psi, compressed-air-pressure test applied to a thin-walled tube submerged in water. Appearance of air bubbles is cause for tube rejection.

Silicon Nitride Properties

The physical properties of silicon nitride are compared with some other well known materials in Table I. Silicon nitride (Si_3N_4) does not have a true

J. F. COLLINS is a Metallurgical Engineer, Technical Service and Development Dept., Electro Metallurgical Co., Niagara Falls, N. Y., and R. W. GERBY is a Metallurgical Engineer, Engineering Research Group, Metals Research Laboratories, Niagara Falls, N. Y. This paper was presented at the AIME Annual Meeting, Chicago, Feb. 14 to 17, 1955.

melting point, a characteristic shared with other refractories, but decomposes by sublimation at approximately 3450°F (1900°C). This material has been successfully used in neutral or reducing atmospheres at temperatures up to 3400°F (1871°C). Silicon nitride has a sublimation point considerably higher than the melting point of conventional steels and high temperature alloys.

The theoretical density of silicon nitride it 3.44 g per cu cm. However, as was mentioned previously, fabricated shapes of silicon nitride have a density of approximately 2.5 g per cu cm or about 72 pct of the theoretical density. Silicon nitride has a unit volume weight about 30 pct greater than graphite; approximately equal to silicon carbide but less than half the density of cast iron and steels.

Using a diamond-pointed hardness indentor, Eberbach readings have been obtained on individual grains of silicon nitride. The values were in the range of 2400 to 4300. On individual particles of aluminum oxide and silicon carbide values of 1900 and 2400 to 3200, respectively, were obtained. Both silicon nitride and silicon carbide give a reading of 9+ on the Moh's scale which is not sensitive enough to distinguish between the two materials. These hardness values were on individual grains of silicon nitride. Much lower hardness values were obtained on silicon nitride shapes. For example, slip-cast silicon nitride articles have a Rc A hardness value of about 99. This lower hardness is probably due to the less-than-theoretical density of silicon nitride shapes. Aluminum oxide and silicon carbide shapes usually have Rc A hardness values in the range of 60 to 70, respectively. Of course, these figures are subject to wide variation depending upon the type of binder used to hold the individual grains together.

Because there is no standard strength test for evaluating silicon nitride, a bend test frequently applied to refractory materials was used to evaluate the strength of silicon nitride. In this test, a ½-in. square bar of silicon nitride was placed on hardened steel knife edges 3 in. apart. A load was applied midway between this 3-in. span by means of a hardened steel knife edge having a width of more than ½ in. The results of these tests are summarized in Table I. Silicon nitride shapes have a modulus of rupture of 16,000 to 20,000 psi which is about midway between the modulus of rupture of aluminum oxide (37,700 psi) and of silicon carbide (4000 to 6500 psi). The modulus of rupture of silicon carbide is dependent upon the binder used to hold the individual grains together.

Relatively little information is available on the modulus of rupture of silicon nitride at elevated temperatures. Using the test equipment described above, the modulus of rupture of a ½ in. square, slip-cast silicon nitride bar was 16,000 psi at 1830°F (999°C). This modulus of rupture value is within the range that would be obtained at room temperature. Field observations, made at temperatures up to 2000°F (1093°C), have confirmed that silicon nitride shapes lose little if any strength at elevated temperatures.

The compressive strength of silicon nitride was measured on a section of the ½-in. square bars used to determine the bend strength. After the bend test was complete, a ½ in. thick slice was taken from the square bar, polished to a 1.2 cm cube, and subjected to a compressive load until failure occurred.[11] A compressive strength in the range of 72,000 to 90,000 psi was obtained at room temperature.

Silicon nitride articles have no ductility as measured by standard metal tensile specimens, but have an impact resistance similar to aluminum oxide. Normal shop handling accorded to thin-sectioned, gray iron casting would be satisfactory for handling silicon nitride shapes. However, the best rule to follow in handling silicon nitride is to treat this material as any other refractory, and no difficulty will be experienced due to mechanical failure because of the lack of ductility.

No absolute thermal shock test has been developed for ceramic materials. Many thermal shock tests have been devised, but their results cannot be accurately correlated. Hence, it is necessary to describe some conditions under which a material has been used to obtain a practical answer to its relative thermal shock resistance. Thin-walled silicon nitride thermocouple protection tubes have been removed from a furnace at temperatures up to 3400°F (1871°C) and cooled to room temperature in still air with no thermal shock failures. Whereas, in similar tests, aluminum oxide tubes failed. It has usually been possible to quench the silicon nitride tubes from this temperature into water at least once, but on the second immersion, the tubes usually fail. While it is not necessary to preheat silicon nitride tubes before placing in furnaces or metal and salt baths operating at elevated temperatures, longer operating life would be expected if the tubes are preheated. From these results, it appears that silicon nitride is less sensitive to thermal shock than many ceramic tubes.

Electrical and Thermal Properties

Silicon nitride has properties characteristic of a

Table I. Properties of Silicon Nitride as Compared With Other Materials

Property	Silicon Nitride	Aluminum Oxide	Silicon Carbide	Graphite	Cast Iron	316 Stainless Steel
Melting Point						
Centigrade	1900°[1]	2050°[2]	2600°[2]	3652°[2]	1120 to 1371°[3]	1371 to 1399°[4]
Fahrenheit	3452°	3722°	4712°	6382°	2046 to 2500°	2500 to 2550°
Density						
G per cu cm	3.44[5]	3.9[5]	3.3[5]	2.25[5]	7.0 to 7.7[5]	7.96[5]
Lb per cu in.	0.124	0.140	0.12	0.081	0.26 to 0.29	0.29
Hardness						
Eberbach	2400 to 4300	1900	2400 to 3200	—	—	—
Rc A	99	60	70	—	60.5-[6]	48.5 to 52.5[6]
Modulus of Rupture						
Room temp. psi	16,000 to 20,000	37,700[5]	4000 to 6500[5]	1800[7]	—	—
Electrical Resistivity						
Ohm-cm at room temp	1.436×10^{5}	10^{14}[1]	50[5]	0.8 to 1.3×10^{-3}[7]	98.6 to 114×10^{-6}[8]	74×10^{-6}[4]
Thermal Conductivity						
Btu-in. per ft² per hr per °F (400° to 2400°F)	10.83	18.5 to 30[5]	21 to 81[5]	7.3 to 2.5[5]	310.1[5]	112.8 to 140.8[4] (212° to 932°F)
Linear Thermal Expansion						
Micro in. per in. per °C (20° to 1000°C)	2.46	7.7[5]	4.38[10]	2.2[5]	10.8 to 12[5]	11.1[4]

Table II. Corrodents to Which Silicon Nitride Is Resistant

20 pct HCl, boiling
65 pct HNO_3, boiling
HNO_3 fuming, boiling
10 pct H_2SO_4 at 158°F (70°C), air-free
77 pct H_2SO_4
85 pct H_2SO_4
HPO_3
$H_4P_2O_7$
25 pct NaOH
Cl gas, wet, at 68°F (20°C)
Cl gas, at 1652°F (900°C)
H_2S gas, at 1832°F (1000°C)
H_2SO_4, boiling, conc + $CuSO_4$ + $KHSO_4$
$NaNO_3$ + $NaNO_2$, salt bath at 662°F (350°C)
NaCl + KCl, salt bath at 1454°F (790°C)

semiresistor. Its electrical resistivity is 1.426 x 10^6 ohm-cm at room temperature. Graphite, an excellent conductor, has approximately 10^{-4} ohm-cm resistance, and aluminum oxide, an excellent resistor, has 10^{14} ohm-cm resistance at room temperature. Incomplete tests indicate that the resistivity of silicon nitride decreases with increasing temperature and in this way silicon nitride is similar to most materials.

Silicon nitride has an extremely low coefficient of thermal conductivity, being one half that of aluminum oxide, one fifth of silicon carbide and one tenth that of steel. The thermal conductivity of silicon nitride between 400° and 2400°F (204° and 1315°C) is 10.83 Btu-in. per ft² per hr per °F.

Silicon nitride has a linear thermal expansion coefficient of 2.46 micro in. per in. per °C. This is about half that of silicon carbide, one third that of aluminum oxide, and about one fifth of that of most steels. One theory of thermal shock failures is that they are related to temperature gradients which exist between different parts of a given piece resulting in the expansion or contraction of individual areas of the shape. It is the expansions and contractions which set up stresses. If the stresses are greater than the strength of the material, failure of the section will occur. While silicon nitride has a strength comparable to other ceramic materials, it has a much lower thermal expansion characteristic; thus, it is not likely that marked contractions and expansions will be set up in this material on heating and cooling. Therefore, it would be expected that silicon nitride would have better thermal shock resistance than most ceramic materials, and this is the case.

Chemical Properties

One of the most attractive properties of silicon nitride is excellent chemical stability. Silicon nitride is resistant to the attack of most acids. Compacts of silicon nitride have been suspended in various concentrations of hydrochloric, nitric, sulphuric, and phosphoric acid solutions for minimum times of 500 hr with no indication of attack. The silicon nitride compacts were porous; consequently, it was not possible to make a weight-loss measurement as some of the specimens actually showed a weight gain due to the pickup of the corrodent in the pores of the test piece. However, careful visual and petrographic examinations showed that the silicon nitride had not been attacked during the test period.

Table III. Corrodents That Attack Silicon Nitride

Corrodent	Test Duration in Hr*
30 pct NaOH, boiling	115
NaOH, molten at 842°F (450°C)	5
48 pct HF at 158°F (70°C)	3
1 pct HF + 10 pct HNO_3 at 158°F (70°C)	116
NaCl + KCl, salt bath at 1652°F (900°C)	164
$NaB(SiO_3)_2$ + V_2O_5 at 2012°F (1100°C)	4
NaF + ZrF, at 1472°F (800°C)	100

* These tests were discontinued at the times indicated and represent the time at which corrosion was first observed.

Silicon nitride is not attacked by chlorine or hydrogen sulphide gases but is attacked by solutions of sodium hydroxide stronger than 25 pct. For example, specimens treated in boiling 50 pct caustic showed indications of attack after 115 hr. Molten caustic soda at 842°F (450°C) attacked silicon nitride in 5 hr. Various concentrations of hydrofluoric acid also attacked silicon nitride.

With the exception of hydrofluoric acid, silicon nitride is resistant to the more common inorganic acids of various concentrations at a variety of temperatures. However, silicon nitride is subject to the attack of strong caustic solutions and, therefore, is not recommended for this use. Tables II and III give data on the chemical properties of silicon nitride.

Molten Metals

Another outstanding characteristic of silicon nitride is its extreme resistance to attack by most nonferrous metals. As a matter of fact, this resistance to attack is so pronounced, it actually appears silicon nitride is not even wetted by these metals.

Table IV. Resistance of Silicon Nitride to Attack of Molten Metals

Metal	°F	°C	Holding Time Hrs	Remarks
Aluminum	1472	800	950	No attack
Aluminum	1832	1000	100	No attack
Lead	752	400	144	No attack
Tin	572	300	144	No attack
Zinc	1022	550	500	No attack
Magnesium	1382	750	20	Slightly attacked
Copper	2120	1150	7	Badly attacked

In laboratory tests, already confirmed by field trials, 50 ml slip-cast silicon nitride crucibles were filled with metal and heated to various temperatures above the melting point of the metals being evaluated. Periodically, crucibles were removed from the furnace and examined visually and microscopically. The results of these tests are summarized in Table IV.

Since these initial tests were run, additional laboratory work has been done to determine the time required for the attack of aluminum on silicon nitride to be observed. These tests, at 1800°F (932°C), have been in progress for over 3000 hr, and there has been no indication that the molten aluminum will ever attack the silicon nitride.

Similar results were obtained with lead, tin, and zinc. The results of the magnesium tests were inconclusive since failure occurred at the slag-metal interface; however, there was no indication of attack by the molten magnesium metal. To prevent the molten magnesium from oxidizing, a chloride-fluoride flux was placed on the surface of the heat; it is possible the flux attacked the silicon nitride.

Oxidation Resistance

Standard techniques for measuring oxidation resistance have not yet been developed, but the work of Crandall and associates,[3] at Alfred University, is of fundamental interest. Their apparatus is designed to give a continuous record of the weight gain or loss of a specimen during the time it is in the furnace. The oxidation resistance of silicon

nitride as compared with other ceramic materials, using this apparatus, is shown in Table V. Silicon nitride has an oxidation resistance at 2192°F (1200°C) that is considerably better than titanium diboride or titanium carbide but not quite so good as silicon carbide bonded with silicon nitride.

Relatively simple oxidation tests were also conducted in Electro's laboratories. In these tests, 3 in. square plates, ⅛ in. thick, were placed in air-atmosphere furnaces that were heated to various temperatures in the range of 1500° to 3000°F (815° to 1649°C). The silicon nitride plates were held in these furnaces for 10 hr and then removed. The difference in weight was taken as an indication of oxidation resistance. The results of these tests showed that silicon nitride exhibited no weight gain up to 2200°F (1204°C) and only a slight weight gain in the range of 2200° to 2550°F (1204° to 1399°C). Above 2550°F (1399°C) silicon nitride showed a rapid increase in weight and, in some cases, even crumbled due to extreme oxidation. As a result of these tests, it is suggested that silicon nitride can be used continuously in an oxidizing atmosphere up to 2200°F (1204°C) but for only limited exposure to an oxidizing atmosphere in the range of 2200° to 2550°F (1204° to 1399°C). In a neutral or reducing atmosphere, silicon nitride can be used up to 3400°F (1871°C).

Applications

The resistance of silicon nitride to the attack of many molten nonferrous metals, and to the attack of molten steel and cast iron for lesser periods of time, has suggested that this material can be used as a mold wash. One formulation that has shown promise for this application is given in Table VI.

In this mixture, the Mogul acts as an excellent binder, while Methocel is the suspending agent. Such a formulation, when vigorously stirred, at least once during the working day, will keep the silicon nitride in suspension for 24 hr. This silicon nitride wash can be applied to metal or ceramic surfaces at room temperature or upward to 300°F (149°C). The advantage of preheating the surfaces, prior to applying the wash, is more rapid drying of the wash. One pound of silicon nitride or five lb of the formulation will cover approximately 50 sq ft of a metal surface, such as an ingot mold. The surface area of a refractory that can be covered will depend largely upon the porosity of the surface.

Because of good thermal shock resistance and high temperature stability, silicon nitride has shown promise as a material of construction for aspirator thermocouple assemblies used to measure the temperature of combustion gases in the checker system of open hearth furnaces. In this application, thin-walled, slip-cast silicon nitride sections of the aspirator thermocouple are inserted through the side wall of the checker system into the combustion gas stream. The thermocouple and silicon nitride parts of the aspirator reach the operating temperature of the combustion gases, which is approximately 2500°F (1371°C) in 10 sec. After a temperature reading is obtained, the aspirator thermocouple is removed from the inside of the checker system and cooled to room temperature before the cycle is repeated. Silicon nitride thermocouple protection tubes have withstood as many as 50 cycles in the checker system and have averaged 45 cycles in one large open hearth shop. A maximum of 24 cycles was obtained with aluminum oxide protection tubes with an average of 10 to 12 cycles.

The ability to produce silicon nitride in thin-walled, long tubes, and the resistance of this material to the attack of molten aluminum have resulted in the use of silicon nitride thermocouple protection tubes in the aluminum industry. These tubes have been used at varying temperatures up to 1800°F (932°C) with no indication of attack in 3000 hr and have proved to be particularly suitable for use in hard to reach and, thereby, difficult to service areas.

Table V. Oxidation Resistance of Some Ceramic Materials At 2192°F (1200°C)[10]

Ceramic	Wt Gained, Mg Per Sq Cm Original Area in 2 Hr
Silicon Carbide bonded with Silicon Nitride	2.5
Silicon Nitride	5.0*
Titanium Diboride	10.0
Hot-pressed Titanium Carbide	42.5

* There was no additional weight increase of the silicon nitride sample after 50 hr at 2192°F (1200°C).

Table VI. Formula for Mold Wash

Material	Pct by Weight
Silicon Nitride Powder 150 M x D	20
Mogul*	1
Methocel HG**	1
Water	78

* Trade name of Corn Products Refining Co., New York, N. Y.
** Trade name of Dow Chemical Co., Midland, Mich.

Acknowledgments

The permission of S. M. Norwood and G. A. Sands to publish this paper is appreciated. The assistance of C. R. Allenbach, F. H. Buttner, A. L. Cerda and J. W. Szymaszek in preparing the data for publication is gratefully acknowledged.

References

[1] G. R. Regby: The Thin Section Mineralogy of Ceramic Materials. (1948) Brit. Refrac. Research Assn.
[2] *Handbook of Chemistry and Physics.* (1953 to 1954) 35 Ed. Chemical Rubber Publishing Co.
[3] *Metals Handbook.* (1948) ASM Cleveland, Ohio.
[4] *Steel Products Manual.* (1950) Stainless and Heat Resisting Steels Section 24, AISI.
[5] P. Lebeau and F. Trombe: *Les Hautes Temperatures Et Leurs Utilisations En Chimie.* (1950) Masson & Co.
[6] K. C. Nicholson: Carbide, Boride, Nitride and Silicide Refractories and Hard Bodies. (1953) Paper presented at October Ceramic Meeting, Oak Ridge National Laboratories, Oak Ridge, Tenn.
[7] *Industrial Carbon and Graphite Products.* (1951) National Carbon Co., Div. of Union Carbide & Carbon Corp., New York.
[8] Mellor: *A Comprehensive Treatise on Inorganic and Theoretical Chemistry.* (1925) **5**, p. 882.
[9] F. H. Norton: *Refractories.* (1942) McGraw-Hill, Book Co., New York.
[10] *International Critical Tables of Numerical Data, Physics, Chemistry, and Technology.* (1926) McGraw-Hill Book Co., New York.
[11] E. Ryshkewitch: Journal of American Ceramic Society (1953) **36**, p. 65.
[12] R. Muller: *Analytical Chemistry.* (1949) **21**, No. 5, p. 25A.
[13] Private communication from J. R. Tinklepaugh, New York State College of Ceramics, Alfred, N. Y.

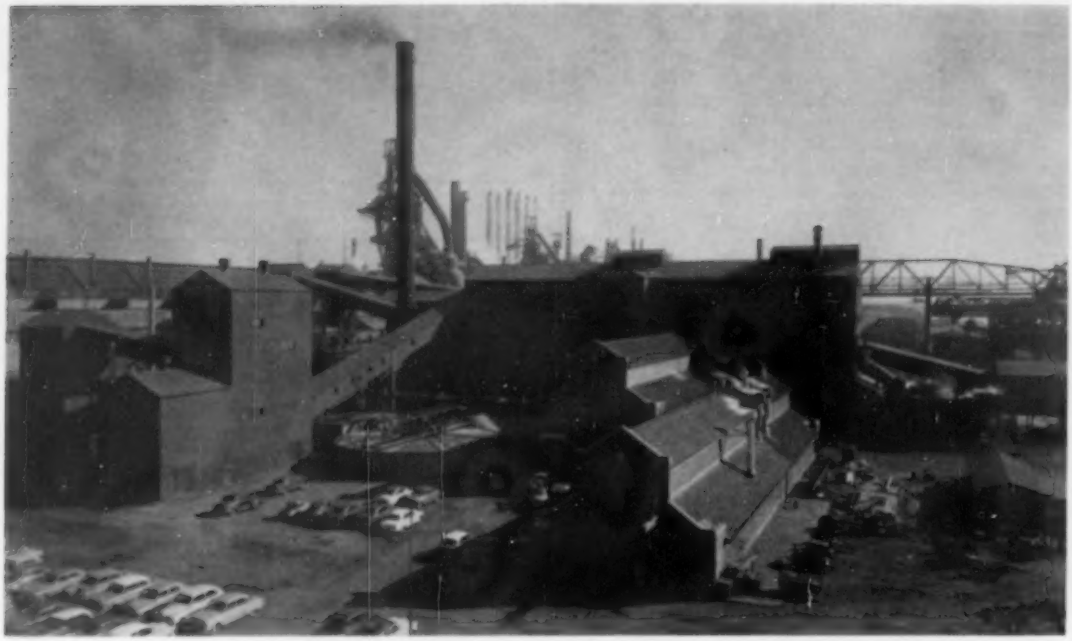

Fig. 1—North sinter plant of the Ford Motor Co. was completed in 1953. Plant utilizes iron concentrates produced from low grade hematite deposits at Humboldt in northern Michigan.

Sintering Practice at Rouge Plant Utilizes Low Grade Hematite

by Robert L. Cleveland

FORD Motor Co. has been producing sinter for blast furnaces since 1946. Two separate plants are in operation at Rouge. The south plant is a six windbox Dwight-Lloyd machine 72 in. wide equipped with 59 pallets and producing 500 tons per day on a 215 sq ft grate area. This plant is unusually compact in that it occupies an area only 100x70 ft but is seven stories high.

Raw material is delivered to the swinging spout feeder on the machine from standard feeder tables and through the single fluffer by means of seven conveyor belts and a bucket elevator with a 100 ft lift. The finished sinter is dumped directly from the machine into railroad cars.

The north plant, completed in 1953, is a 16 windbox Dwight-Lloyd machine 72 in. wide and 96 ft long equipped with 119 pallets with a production of 1500 net tons on 576 sq ft grate area. This plant was constructed by A. G. McKee Co. and based on a previous plant for Oliver Iron Mining Co. at Virginia, Minn.

Fig. 1 shows the general arrangement of the plant. In the left foreground is the ore screening plant. The 65 ft Dorr thickener, which receives the underflow from the gas washer water at the furnaces, is in the center and the sintering plant is in the background.

In Fig. 2 the ore screening building is in the background at the extreme lower right. The two conveyors in the foreground carry the sinter from the cooler to the high-line storage bin. The conveyor to the left discharges the sinter onto a vibrating grizzly screen set $-\frac{1}{2}$ in. At this junction point screened sinter can be bypassed into storage yard or sent over conveyor, to the right, into high-line storage bin. This elevated storage bin has a capacity of

R. L. CLEVELAND is a Technical Assistant, Blast Furnaces, Rouge Works, Ford Motor Co., Dearborn, Mich. This paper was presented at the AIME Blast Furnace, Coke Oven and Raw Materials Conference, Philadelphia, Apr. 18 to 20, 1955.

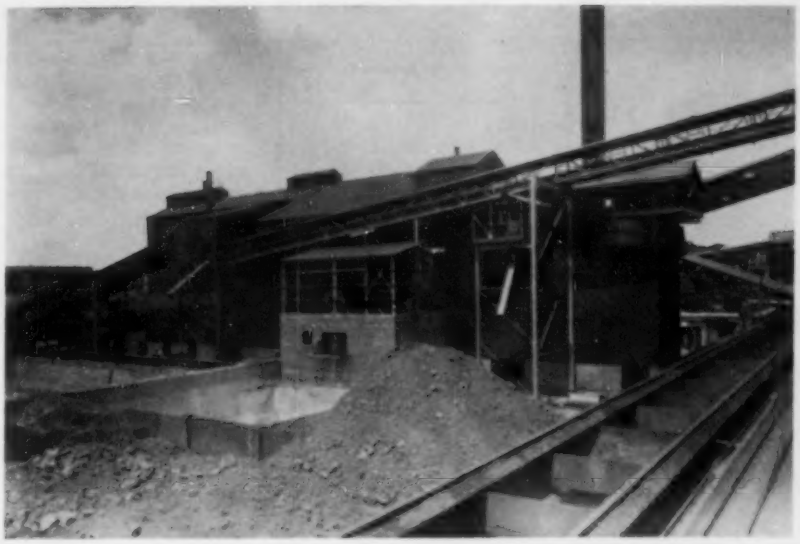

Fig. 2—Another view of the sinter plant shows the stockpiles and the sinter conveyors. The conveyor to the left discharges the sinter onto a grizzly screen set $-\frac{1}{2}$ in.

250 net tons and is equipped with two quadrant gates for loading into the blast furnace transfer car. An adjacent stock bin for the furnace is filled directly from the storage bin. All of the screened material used in the plant is stocked in the various storage bins using a reversible shuttle conveyor.

Fig. 3 shows the ignition burners on the sintering machine developed at Ford and used at both plants, consisting of two sets of $\frac{3}{4}$ in. diam pipes supplied with coke oven gas through a 4 in. diam manifold. At front of the burner is the fluffer employed to prevent segregation of the feed after it leaves the swinging spout. The discharge end of the machine with water sprays and dust collecting hood is illustrated in Fig. 4.

The sinter is discharged onto a rotary cooler shown in Fig. 5. The conveyor in the center of the picture goes to the storage bins, stockpile, or open hearth railroad cars. Operation of all equipment in the sinter plant, including the cooler, is controlled from a main control panel.

Fig. 6 diagrams the flow of the six raw materials normally fed to the machine plus recirculation of hot return fines from the discharge end of the machine and cold return fines screened $-\frac{1}{2}$ in. before the storage bins.

Sinter Production

All raw material is screened before going to the storage bins. The ore is dumped by transfer cars into the high-line feeder bins through 1x2 ft grizzlies and screened with +4 in. and $+\frac{5}{8}$ in. oversizes returned separately to the furnaces. Minus $\frac{5}{8}$ in. travels over a shuttle conveyor either to the feeder tables or to the yard stockpile for use in the other plant.

Flue dust, mill scale, grinding mud, and coke breeze is scalped over a -1 in. screen before storage. Weightometers are used to record the amount of material screened and the sinter produced.

With the exception of the Humboldt concentrates, all feed materials are conventional. The Humboldt concentrate is an old material in a new form produced through the joint effort of Cleveland-Cliffs Iron Co. and Ford Motor Co. from the Humboldt mine near Ishpeming, Mich. The open pit mine and the concentration mill is operated by Cleveland-Cliffs. The specular hematite in this area, containing about 33 pct Fe and a combination of iron oxides plus silica ranging about 98.5 pct is mined from the massive jasper formation, trucked to the crushing plant and after crushing and grinding is reduced to a -65 mesh feed for the flotation mill. At

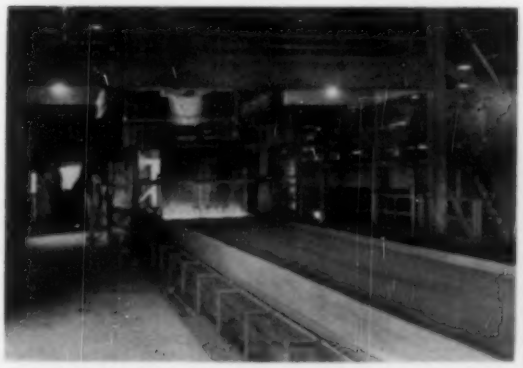

Fig. 3—Ignition burners developed at Ford consist of two sets of $\frac{3}{4}$-in. diam pipes supplied with coke oven gas.

Fig. 4—Discharge end of the sinter machine is equipped with water sprays and a dust collecting hood.

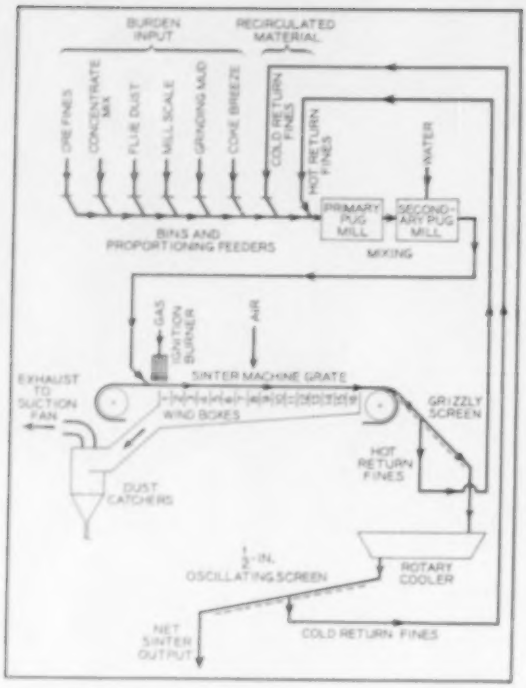

Fig. 5—The sinter is discharged into a rotary cooler. Conveyor in center goes to storage bins, stockpile, and open hearth railroad cars.

the mill the product of a closed circuit system of rod mill, rake classifier and ball mill is aerated through a series of roughers, cleaners, and recleaners which floats the concentrates. After thickening, the filtered concentrates contain about 62 pct Fe, dry basis, 6 pct H_2O and 8 pct SiO_2 with 95 pct −100 mesh and 40 pct −325 mesh.

While the Humboldt concentrates of Michigan are often confused with the taconite concentrates of Minnesota there are basic differences. The Humboldt being a hematite formation cannot be recovered by magnetic separation and has less tendency to coalesce when sintered. This later property tends to limit the percent of Humboldt in the sinter machine burden. This difference is pronounced when two samples of the concentrates are heated in an open pan; the heat compacts the taconite pile and crumbles the Humboldt concentrate.

The first shipments of Humboldt were blended 75 pct to 25 pct with a carrier ore to eliminate any danger of cargo shifting due to the almost micaceous structure of the concentrates. Experiments continue to revise this ratio upward. The Humboldt mine and mill began operation in February 1954, and during the 1954 shipping season 150,000 gross tons of concentrates were shipped to Dearborn with this year's shipments estimated at 250,000 gross tons.

Testing Concentrates

The plant at the Rouge was designed to sinter blast furnace flue dust, consisting of 20 pct pugged dust catcher flue dust and filtered sludge cake, 70 pct screened ore −½ in. and 10 pct roll scale. The amount of carbon required to produce 1500 net tons of sinter per day based on this mix was estimated to be approximately 136 lb per net ton of sinter produced. Under normal operating conditions a good quality sinter was produced at a rate of 1500 net tons per day which is equivalent to 2.6 net tons per sq ft of effective grate area with normal operating conditions as follows: A—speed of sintering machine, 60 to 65 ipm; B—thickness of material bed, 14 in.; C—vacuum under the bed, 24 to 26 in. and at the fan inlet, 28 to 30 in; and D—temperature of exhaust gas at the 13th wind-box 650° to 750°F.

Table I. Chemical Analysis of Sinter

Material	Pct	Material	Pct
SiO_2	8.30	TiO_2	0.10
MnO	0.57	FeO	15.61
CaO	1.20	Fe_2O_3	69.58
Al_2O_3	1.25	C	0.33
MgO	2.50	P	0.084

A series of tests were run to determine the maximum percentage of concentrates that could be used under normal operating conditions and the production rate that might be anticipated with these percentages in the ore mix.

The bed was reduced to 10½ in. at the beginning of the tests to avoid a bed that would be too compact. With the 10½ in. bed various percentages of concentrates and return fines were used, and in each case when normal conditions were obtained effort was made to increase the speed of the chain. Over a range of 9¼ to 11 in. of bed it was found that best control of the operation was obtained with a 9½ or 10 in. bed and a chain speed of 66 to 72 in. Every attempt so far to exceed this speed resulted in higher vacuum, lower wind-box temperatures and reduced tonnage.

The results of this test to date indicate that with approximately 30 pct pure Humboldt concentrates in the ore mix a sinter of good quality can be produced with a 10 in. bed at a rate of 55 net tons per hr. This is equivalent to 1320 tons per day or approximately 2.3 tons per sq ft of effective grate area. Chemical analyses of the sinter is given in Table I.

The final test of sinter is always made in the blast furnace. Addition of concentrate sinter to the furnace burden had no appreciable affect on the working of the furnace. However, increased tonnage resulted from the higher iron content in the charge.

Fig. 6—Diagram shows flow of the six raw materials normally fed to machine plus cold and hot returned fines.

being zero for electrons with antiparallel spins

Impact of Magnetism Upon Metallurgy

by C. Zener

THE present paper has its origin in an attempt by the author, extending over the last several years, to understand the influence of the magnetic properties of the constituent atoms upon the various properties of metals and alloys. During this study the author has been impressed by the important role which magnetism plays in the many facets of metallurgy. In writing this paper he has attempted to convey to his colleagues some concept as to the role magnetism will play in the future development of metallurgy. In some of the subjects herein discussed, such as the influence of magnetism upon phase boundaries and upon mechanical properties, only general thermodynamical properties associated with ferromagnetism are introduced. For these subjects, it is not anticipated that any serious differences of opinion will be encountered. A discussion of the other subjects requires the adoption of a quite specific model of the magnetic structure of the metal. This model is discussed under "Magnetic Shells and Their Interactions." The simple model adopted in this paper has been criticized[1] as being mathematically inconsistent. This criticism has been ably silenced by Dr. W. J. Carr[2] of this laboratory. The simple model adopted in this paper has been criticized as being inconsistent with observations on magnetic structure using neutron diffraction. This apparent discrepancy has been resolved by Bader[3] who has shown that the finite velocity of neutrons prevents neutron beams from detecting the antiferromagnetic structure of the type predicted by the simple model adopted in this paper.

Magnetic Shells and Their Interactions

An electronic shell of an atom is specified by two symbols.[4] The first symbol is a number and denotes the total quantum number of the shell. The second symbol is a letter and denotes the orbital angular momentum of each electron within the shell. The letters s, p, d, f are used to denote an orbital angular momentum of 0, 1, 2, 3, respectively, in units of $h/2\pi$, where h is Planck's constant. As we pass from scandium to nickel in the first transition period, we gradually fill the 3d shell. This shell is responsible for ferromagnetism and hence may be called the *magnetic* shell. The component of the orbital angular momentum along some specified direction must be an integral multiple of $h/2\pi$. Thus, for a d electron this component can have any one of the values -2, -1, 0, 1, 2 times $h/2\pi$. In addition to its orbital angular momentum, each electron has an intrinsic angular momentum, hereafter called *spin*, due to a rotation about its own axis. This spin can have either of two components $+\frac{1}{2}$ $(h/2\pi)$ or $-\frac{1}{2}$ $(h/2\pi)$ along the specified direction. A fundamental principle of atomic structure, known as *Pauli's exclusion principle*, is that no two electrons in a given shell may have identical components of orbital angular momentum simultaneous with identical components of spin. The 3d shell thus may have at most ten electrons. Since an intrinsic angular momentum of a charged particle is necessarily associated with a magnetic moment, the *spin* of an electron may be thought of as referring to either this angular momentum or to the associated magnetic moment.

Table I. Outer Shells of Isolated Atoms of the First Transition Row

K	Ca	Sc	Ti	V	Cr	Mn	Fe	Co	Ni	Cu
$4s$	$4s^2$	$3d4s^2$	$3d^24s^2$	$3d^34s^2$	$3d^54s$	$3d^54s^2$	$3d^64s^2$	$3d^74s^2$	$3d^84s^2$	$3d^{10}4s$

The electron configuration of the ground state of the isolated atoms in the first transition row is reproduced in Table I. The superscript represents the number of electrons in each shell.

For the purpose of this paper, the most important principle of atomic structure relates to the manner in which electrons are added to a shell as the atomic number is increased. This principle, commonly known as the *principle of highest multiplicity* or more simply as *Hund's rule*, states that within a given shell the maximum number of electrons have spins pointing in the same direction as is consistent with Pauli's exclusion principle. An application of this principle to the d shell is illustrated in Fig. 1, where the spin structure is given for shells containing from 1 to 10 electrons.

The physical basis of Hund's rule is the *exchange energy* discussed first by Heisenberg in 1928. This is a coupling between electrons with parallel spins (spins pointing in the same direction), the coupling

C. ZENER, Member AIME, is Associate Director, Research Laboratories, Westinghouse Electric Corp., East Pittsburgh, Pa.

TP 4016E. Manuscript, Feb. 16, 1955. Chicago Meeting, February 1955.

The Transactions papers appearing in the Journal of Metals during 1955 will subsequently appear in AIME Transactions Volume 203, and may be permanently referenced to that volume.

of the transition metals and in view of the argu-

alloying elements upon the γ field as simply reflect-

being zero for electrons with antiparallel spins (spins pointing in opposite directions). This exchange energy is negative for electrons in the same atom and hence leads to a minimum energy when the maximum possible number of spins are parallel. The value of this exchange energy in specific shells of specific atoms may be deduced from the tables in ref. 5. For the *d* shells, this exchange energy is about −0.6 ev per pair of parallel spins. Thus 2.5 ev are required to reverse one of the five parallel spins in the *d* shell of chromium. An apparent anomaly in Table I may be explained by this exchange coupling. Following potassium, all atoms have two electrons in the 4*s* shell, save chromium and copper. If chromium were to have two electrons in the 4*s* shell, its *d* shell would have four electrons with parallel spins. In order to take advantage of the exchange coupling with these four electrons, one of the two 4*s* electrons is *demoted* from the 4*s* shell into the 3*d* shell. A similar demotion occurs in copper in order to take advantage of an exchange coupling with four electrons with parallel spins in the *d* shell.

The foregoing interpretation of the anomaly in chromium and in copper may be described more vividly as a tendency to form closed half *d* shells. A closed half *d* shell refers to five electrons in a *d* shell, all five electrons having parallel spins and therefore all five permissible values of orbital angular momentum components. A tendency to form closed half shells implies a reluctance to start a new half shell. This reluctance is, in fact, quite real; the energy required to demote one of the two 4*s* electrons into the first half *d* shell decreases from 2.5 ev in calcium to 0.3 ev in vanadium and again, to demote one of the two 4*s* electrons into the second half *d* shell, decreases from 2.1 ev in manganese to 0.02 ev in nickel.[5]

The charge distribution within the *d* shell of Cu^+ has been calculated fairly accurately[6] and is reproduced in Fig. 2. The ordinate in this figure, the radial charge density ρ, is defined such that $\rho\delta r$ is the charge lying between r and $r + \delta r$. In order to illustrate the small overlap of the *d* shells in a metal, we show in this figure the radius of a copper atom, the radius being defined as half the closest distance between atoms in the metal. As we pass to the left from copper along the first transition row, the effective charge in which each *d* electron moves decreases and hence the radial charge density of the *d* shell expands. Since the direct interaction between neighboring *d* shells is proportional to the amount of overlap of the *d* shells, we are particularly interested in the manner in which the radial charge density decreases with radius at values of the radius comparable to that of the metal atoms. Toward this end, a second plot of the radial charge density is given in Fig. 3, this time on a semilogarithmic scale. We see that, in the region of interest, the radial charge density decreases exponentially with radius.

Fig. 1—In the diagram, the spin structure is given for *d* shells containing from 1 to 10 electrons.

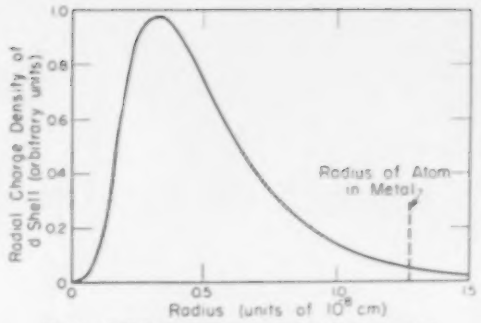

Fig. 2—Radial charge density of Cu^+ is represented.

The calculation of the radial charge density presents a formidable mathematical task. The calculation of the interaction between two adjacent *d* shells is an order of magnitude still more difficult. A significant insight into this interaction may be gained, however, from certain qualitative observations. This interaction between any two shells of adjacent atoms is represented as the sum of two parts. The first part, called the *Coulomb* interaction, is just the interaction which would be computed classically. It gives rise to an attraction coming from the penetration of the negative charge of each shell into the positive potential within the other shell. This Coulomb interaction is independent of the spin structure of the two shells. The second part, the *exchange* interaction, represents a coupling between the spins of electrons in neighboring shells. It was first discussed by Heitler and London in their quantum mechanical interpretation of the chemical bond.[7] Strictly speaking, this exchange coupling exists only between electrons having spins pointing in the same direction. If it were not for the fact that this exchange energy has for the last 25 years been incorrectly taken as the origin of ferromagnetic coupling, we could merely state without discussion that this exchange energy is positive.

In the early days of quantum mechanics, it was reasonably assumed that the coupling which aligned the *d* shell spins in iron, cobalt, and nickel arose directly from the exchange interaction between the *d* shells of adjacent atoms. But such a ferromagnetic coupling was possible only if the exchange interaction were attractive. Since Heitler and London had pointed out that the very existence of a chemical bond depended upon the exchange interaction being repulsive, it was assumed that the exchange integral becomes attractive only when the overlap of the *d* shells is very small, as is the case in iron, cobalt, and nickel. A large literature has been built upon this concept of a change in sign of the exchange integral with amount of *d* shell overlap. Several years ago, however, it was recognized that the ferromagnetic coupling arises from an indirect exchange via the conduction electrons,[8-11] an exchange which does not require an overlap of adjacent *d* shells. The necessity for the assumption of a change in sign of the exchange integral with decreasing amount of overlap thereby was eliminated.

In view of the importance of the exchange interaction between adjacent *d* shells to the metallurgy

of the transition metals and in view of the arguments between theorists even as to the sign of this interaction, it is fortunate that a fairly direct experimental approach to this problem may be adopted. In this approach, one used extensively[33-34] in studies of diffusion mechanisms, we utilize the information furnished by the elastic constants of the metal crystals. Now if the energy of a face-centered-cubic or body-centered-cubic crystal could be expressed solely as a sum of central force interaction between pairs of atoms, the Cauchy relation[35, 36]

$$C_{12} = C_{44}$$

would be satisfied. In crystals such as nickel and copper, C_{44} is more than twice C_{12}. The physical origin of this discrepancy lies, no doubt, in the energy of the conduction electrons, an energy which essentially is dependent only on the volume. Our approach consists of expressing the energy of the crystal in the form

$$\Sigma_{ij} \cdot V(r_{ij}) + \phi(\theta)$$

where, corresponding to the exponential decrease in radial charge density previously discussed

$$V(r) = A\, e^{-\beta(r - r_0)/r_0}$$

r_0 being the distance between nearest neighbors under equilibrium conditions, and where ϕ is some function of the dilation θ. The two constants A and β are completely determined by the two shear elastic coefficients C_{44} and $(C_{11} - C_{12})/2$. When this calculation is carried out for nickel and copper, the coefficient A is found to be positive. But a positive A corresponds to a repulsion between the atoms and hence to a repulsive exchange interaction.

Influence of Magnetism Upon the Phase Boundaries of Binary Iron Alloys

Alloying elements in iron may be classified into two groups, those which close the γ field and those which open the γ field. The elements in the first group, namely those forming γ loops, are found in two regions of the periodic table, as indicated in Table II.

There is a temptation to interpret the effect of alloying elements upon the γ field as simply reflecting the difference in the standard free energy of the alloying elements in the two phases. If this free energy is lower in the α phase, this phase will be favored by the alloying element, thereby leading to a closed γ field. If this free energy is lower in the γ phase, this phase will be favored by the alloying element, thereby leading to an open γ field. Several writers, including the present author, in fact have discussed the details of the binary iron diagrams from this point of view.[37-39]

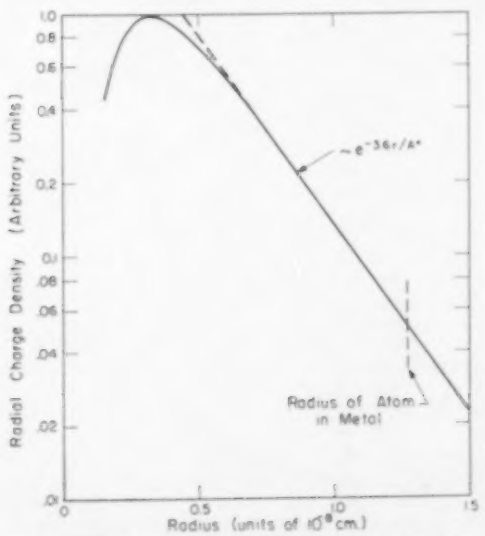

Fig. 3—Radial charge density of Cu^+, given in Fig. 2, has been plotted on a semilogarithmic scale.

Table II. Elements which Close the γ Field

Ti	V Cb Ta	Cr Mo W	Be	B*	Al	Si Ge Sn	P As Sb

* Loop would be closed if not stopped by intermetallic compound.

At least for those elements in the vanadium and chromium columns, the foregoing naive interpretation is in direct conflict with observations as to the effect of these elements upon the M_s temperature. If the standard free energy of molybdenum, for example, is lower in the α than in the γ phase, then we would expect molybdenum to raise the M_s temperature; whereas, in fact, it lowers this temperature. Of course, one could dismiss this discrepancy with the observation that martensite does not form reversibly and, hence, equilibrium requirements should not be considered. The present writer prefers not to adopt this negative approach. The M_d temperature, the highest temperature at which martensite may be induced by plastic deformation, may, in fact, be regarded as that temperature at which the γ and the α phase of the same composition are in equilibrium with one another. The M_d temperature lies above the M_s temperature by an amount which is nearly independent of composition, namely, about 200°C. We therefore expect that changes in the M_s temperature induced by alloying elements will reflect, in fact, a like change in the true equilibrium temperature for a transition involving no change in composition.

The observations upon the effect of the vanadium and chromium column elements upon the γ field and upon the M_s temperature can both be interpreted only if we assume that the standard free energy difference of these elements in these two phases changes with temperature, at low temperatures being lower in the γ phase, at higher temperatures being lower in the α phase. Now the heat absorption with the loss of magnetization in the neighborhood of the Curie temperature is many times larger than the heat absorbed in the α-γ transformation at 910°C in pure iron. We therefore anticipate that the influence of the alloying elements upon the magnetic properties of α iron may play a dominant role in the difference in standard free energy of these elements in the two phases of iron. In particular, we hope that through their influence upon the magnetic characteristics we may understand the temperature dependence of the standard free energy difference.

In order to understand the influence of the alloying elements upon the magnetic characteristics, we shall study in detail the differences in free energy between the α and the γ phase of pure iron. We shall denote by G^α and G^γ the (Gibbs') free energy per mol in pure iron of the α and γ phases, respectively. The difference $G^\alpha - G^\gamma$ has been computed

by Johansson[22] for the entire temperature range up to the melting point of iron. His data are plotted in Figs. 4 and 8 for temperatures above 100°C. The relation of the $G^\alpha - G^\gamma$ vs T curve to the phase diagrams may be expressed most succinctly through equiconcentration curves. The usual curves in a phase boundary give the concentration of two phases which are in complete equilibrium with one another, both with respect to a transfer of solute and of solvent atoms. The equiconcentration curves give the concentration at which two phases are in equilibrium with one another, the constraint being imposed that the two phases are to be at the same concentration. Thus a plot of M_s vs concentration would form an equiconcentration curve. These curves always lie within the two-phase region of a true equilibrium diagram. Now suppose that we add to one mol of pure iron C mols of a solute, where C is small compared with unity. Let us further suppose that the attendant increase in free energy of the system is greater when the system is in the α than in the γ phase and that this increase is independent of temperature and is proportional to C. The constant of proportionality then will be the one parameter which completely characterizes the alloying element. The effect of the solute addition upon the $G^\alpha - G^\gamma$ vs T curve is then as represented in Fig. 5. The $G^\alpha - G^\gamma$ curve is displaced horizontally to the right by an amount proportional to C. The intercepts of the new $G^\alpha - G^\gamma$ curves with the vertical axis give the new temperatures at which the α and γ phases are in equilibrium, both at the concentration C. A plot of these new intercepts vs C thus gives us the equiconcentration curves. Actually the equiconcentration curves are identical, apart from the scale of the horizontal axis, to the $G^\alpha - G^\gamma$ vs T curve for pure iron outside the temperature interval from 910° to 1400°C, since according to our assumption $G^\alpha - G^\gamma$ is displaced horizontally by an amount proportional to C. Similarly, in the case where the attendant increase in the free energy of the γ phase is greater than that of the α phase,

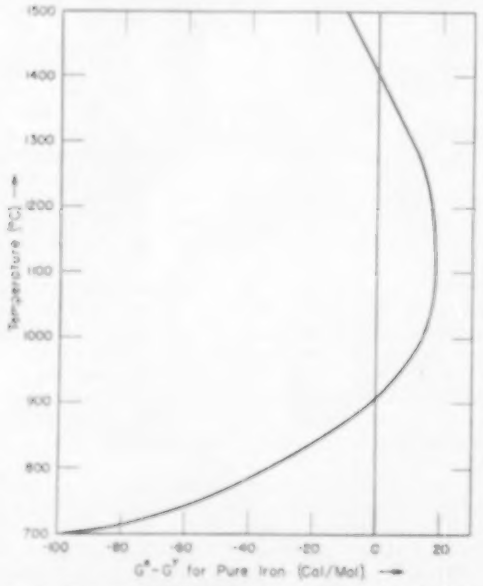

Fig. 4—Free energy difference between α and γ iron is plotted from the data of Johansson.[22]

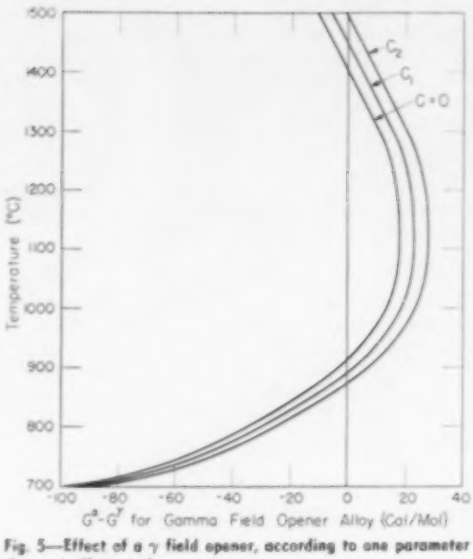

Fig. 5—Effect of a γ field opener, according to one parameter theory, is illustrated.

the $G^\alpha - G^\gamma$ vs T curve is displaced horizontally to the left, as illustrated in Fig. 6, and the equiconcentration curve with a closed loop is identical, apart from the scale of the horizontal axis, to the $G^\alpha - G^\gamma$ vs T curve for pure iron within the temperature interval from 910° to 1400°C. We review in Fig. 7 the equiconcentration curves of binary iron alloys as derived according to the simple one parameter theory that alloying elements add to $G^\alpha - G^\gamma$ an increment which is independent of temperature.

We have previously seen that the effect of elements of the vanadium and chromium columns upon the $G^\alpha - G^\gamma$ curve cannot be represented merely by a horizontal shift of this curve. Such a shift would automatically associate a raising of the M_s temperature with the addition of an element that closed the γ field. In order to find how we can represent more appropriately the effect of alloying elements upon

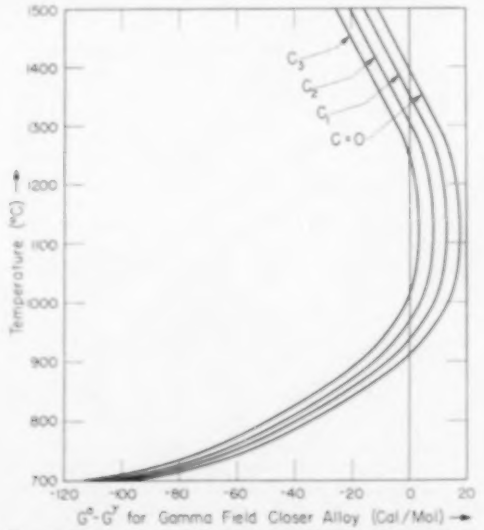

Fig. 6—Effect of a γ field closer, according to one parameter theory, is illustrated.

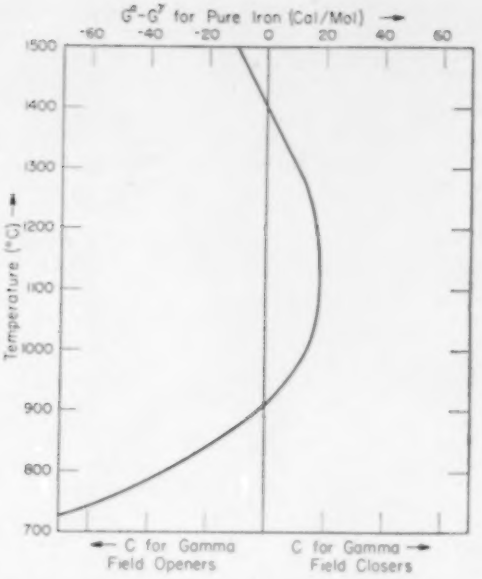

Fig. 7—Relation of equiconcentration curves to G^α-G^γ for pure iron according to simple one parameter theory is reviewed in this figure.

the $G^\alpha - G^\gamma$ curve and, in particular, how we can most appropriately introduce a second parameter, we must understand the general characteristics of the $G^\alpha - G^\gamma$ curve itself.

From 100° to 500°C, the $G^\alpha - G^\gamma$ curve is essentially a straight line. Beyond 500°C this curve gradually acquires a negative second derivative which gradually reaches a maximum in the neighborhood of the Curie temperature at 760°C. It is just because of this curvature that the $G^\alpha - G^\gamma$ curve reverses its direction with increasing temperature, crossing the vertical axis a second time, and thereby giving rise to the γ-α transition at 1400°C. Now the slope $d(G^\alpha - G^\gamma)/dT$ is $-(S^\alpha - S^\gamma)$, where S^α and S^γ are the entropies per mol of the α and γ phases, respectively. The second derivative $d^2(G^\alpha - G^\gamma)/dT^2$ is $-(C^\alpha - C^\gamma)/T$; C^α and C^γ are the thermal capacities per mol of the α and γ phases, respectively. A negative curvature therefore implies either an anomalously low thermal capacity of the γ phase or an anomalously high thermal capacity of the α phase. Since anomalously low thermal capacities are not to be expected at these temperatures, the negative curvature must be due to an unusually high thermal capacity of the α phase. Since the negative second derivative has a maximum at the Curie temperature, we are led to ask whether all the curvature above 500°C may be blamed upon the uncoupling of the magnetic moments of the individual iron atoms from one another. The slope of the $G^\alpha - G^\gamma$ curve between 100° and 500°C is 1.41; the slope at the melting temperature is −0.06 cal per mol °C. The negative of the total change in slope from 500°C to the melting point, which is just the increase in $S^\alpha - S^\gamma$ from 500°C to the melting point, is therefore 1.47 cal per mol °C. Now the increase in entropy associated with a complete uncoupling of the magnetic moments of the individual iron atoms from one another is $R \ln W$ per mol. Here R is the gas constant, 2 cal per mol °C, and W is the ratio of the statistical weights associated with a completely uncoupled and a completely coupled atomic moment. Since the individual atomic moments arise from the parallel coupling of two electron spins, W is the ratio of 3 to 1. We thereby obtain for $R \ln W$ the value of 2.2 cal per mol °C. The potential change in entropy associated with magnetic uncoupling is thus more than enough to explain the observed change in $S^\alpha - S^\gamma$ between 500°C and the melting temperature. From the observed change in entropy we must surmise, in fact, that even at the melting temperature a large amount of magnetic order persists.*

* An analysis of the thermodynamic functions of iron more recent than that of Johannson has been given by L. S. Darken and R. P. Smith, *Industrial and Engineering Chemistry* (1951) 43, p. 1815. Darken has informed the writer that the change in the slope of the G^α—G^γ vs T curve between 100°C and the melting point of iron is 2.1 cal per mol °C, rather than the value 1.47 reported previously. We therefore conclude that only a very slight magnetic order persists to the melting point.

A somewhat similar interpretation of the phase change in iron, and of the effect of alloying elements thereon, has previously been proposed by Smoluchowski.[10] In his theory Smoluchowski correctly interpreted the behavior of $G^\alpha - G^\gamma$ as arising from differences in the electronic specific heats of the α and γ phases but failed to recognize the relation of this difference to the magnetic uncoupling in the α phase.

The realization that the curvature of the $G^\alpha - G^\gamma$ curve arises essentially only from the magnetic uncoupling in the α phase encourages us to investigate the potentialities of representing $G^\alpha - G^\gamma$ as the sum of two parts, a nonmagnetic and a magnetic part, as in Fig. 8. The nonmagnetic part represents what $G^\alpha - G^\gamma$ would be if the magnetic moments of the individual atoms remained coupled to one another. It is given by the straight line

$$(G^\alpha - G^\gamma)_{NM} = 1.41\ (T - 740) \text{ cal per mol.}$$

The magnetic part $(G^\alpha - G^\gamma)_{MAG}$ arises solely from the absorption of heat associated with the gradual uncoupling of the magnetic moments. It is zero below 500°C.

This separation of $G^\alpha - G^\gamma$ into two physically significant parts suggests that we may be able to describe adequately the effect of each alloying element by means of only two parameters characteristic of each element. One parameter will be taken to correspond to a horizontal shift of $(G^\alpha - G^\gamma)_{NM}$ by an amount proportional to the concentration C of

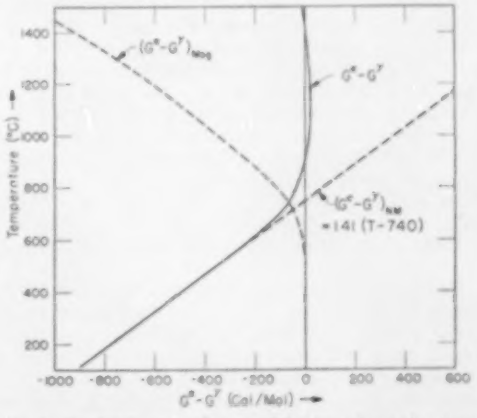

Fig. 8—Resolution of free energy difference of α and γ iron (after Johansson[10]) into magnetic and nonmagnetic components is illustrated.

age of alloying element. Our value of −19°C for

regards the binding in metals as similar to the bind-

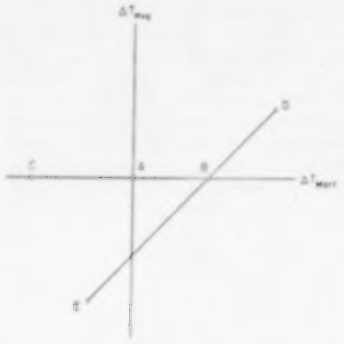

Fig. 9—Effect of alloying elements is represented parametrically.

the alloying element. Now a horizontal shift of a straight line is identical to a vertical shift. Such a vertical shift must, of course, be identified with the change in M_s associated with the introduction of the alloying element. The vertical shift of $(G^\alpha - G^\gamma)_{T_M}$ will thus be taken as $\Delta T_{Mn\gamma}\, C$. The change $\Delta T_{Mn\gamma}$ in M_s associated with unit concentration C thereby will be taken as one parameter characteristic of each alloying element.

In choosing the second parameter we must ask ourselves what is the major influence of an alloying element upon $(G^\alpha - G^\gamma)_{M_{s0}}$. One important way in which an alloying addition affects the magnetic transition is to change the temperature range in which the magnetic uncoupling occurs. A simplified way of representing this effect is by a vertical shift of $(G^\alpha - G^\gamma)_{M_{s0}}$ by an amount proportional to C. The constant of proportionality will be denoted by $\Delta T_{M\alpha}$ and will be taken as our second parameter.

A general survey of the effect of the two parameters $\Delta T_{Mn\gamma}$ and $\Delta T_{M\alpha}$ upon the equiconcentration diagrams may best be portrayed by means of a diagram in which $\Delta T_{Mn\gamma}$ is the abscissa and $\Delta T_{M\alpha}$ the ordinate, as depicted in Fig. 9. Point A at the origin will give equiconcentration boundaries as horizontal straight lines. A point on the positive horizontal axis, such as B, will give a closed γ loop. The equiconcentration boundary will be of precisely the shape shown in the left half of Fig. 7, again the horizontal scale being dependent upon $\Delta T_{Mn\gamma}$. The effect of going off the horizontal axis may be most succinctly described by proceeding along a line having a 45° slope, as from B to D. Along such a line, $\Delta T_{Mn\gamma}$ and $\Delta T_{M\alpha}$ are undergoing identical increments. Now a simultaneous change in $\Delta T_{Mn\gamma}$ and in $\Delta T_{M\alpha}$ by equal amounts results in vertical shift in $G^\alpha - G^\gamma$ and hence also in identical shifts in the equiconcentration boundaries, the amount of the shift being proportional to C. But a vertical shift in a phase diagram, the amount of the shift being proportional to C, may alternately be described as a simple shear parallel to the vertical axis. The shear will be upward for a point in the $\Delta T_{Mn\gamma}$ — $\Delta T_{M\alpha}$ diagram above the horizontal axis, such as D, and downward for a point below the horizontal axis, such as E.

The foregoing general discussion will now be followed by an analytical treatment for the case of a closed γ field. This analysis leads to equations by means of which we may directly determine the parameters $\Delta T_{Mn\gamma}$ and $\Delta T_{M\alpha}$ from the equiconcentration diagram, or vice versa. The two assumptions introduced previously lead to the following equation as an expression of the condition that along an equiconcentration line a transformation from the γ to the α phase leads to no change in the free energy of the system:

$$(G^\alpha - G^\gamma)_{T_M}\{T - \Delta T_{Mn\gamma}\, C\} + (G^\alpha - G^\gamma)_{M_{s0}}\{T - \Delta T_{M\alpha}\, C\} = 0$$

where the quantity in a bracket is the argument of the preceding term. We shall find it advantageous to rewrite this equation in the following form

$$s(\Delta T_{Mn\gamma} - \Delta T_{M\alpha})C = (G^\alpha - G^\gamma)\{T - \Delta T_{M\alpha}\, C\} \qquad [1]$$

where $s = d(G^\alpha - G^\gamma)_{T_M}/dT = 1.41$ cal per mol °C.

In the case of a closed γ loop, Eq. 1 may be expressed as

$$C = C_{M\alpha}\frac{(G^\alpha - G^\gamma)\{T - \Delta T_{M\alpha}\, C\}}{(G^\alpha - G^\gamma)_{M\alpha}}. \qquad [2]$$

Thus, apart from a change of scale and apart from a shear along the T axis, a plot of C vs T is identical with a plot of $G^\alpha - G^\gamma$ vs T. This similarity is illustrated in Fig. 10 for the case of chromium. Here, curve A is a plot of $G^\alpha - G^\gamma$ for pure iron as a function of T. Corresponding to the experimental observation that the γ loop extends to a C of 13 wt pct, the C scale, placed on the bottom horizontal axis, has been adjusted so that the maximum extent of the loop occurs at 13. From Eq. 1 we find

$$\Delta T_{Mn\gamma} - \Delta T_{M\alpha} = (G^\alpha - G^\gamma)_{M\alpha}/s\, C_{M\alpha}. \qquad [3]$$

Upon taking for $(G^\alpha - G^\gamma)_{M\alpha}$, s, and $C_{M\alpha}$, the values 18.5 cal per mol, 1.41 cal per mol °C, and 13 wt pct,[m] respectively, we obtain for our particular case

$$\Delta T_{Mn\gamma} - \Delta T_{M\alpha} = 1.0°\text{C per wt pct.} \qquad [4]$$

Thus for this case, point B in Fig. 9 lies at a distance of 1.0°C per wt pct to the right of the origin.

The argument of $G^\alpha - G^\gamma$ in Eq. 2 is $T - \Delta T_{M\alpha}\, C$. The plot of C vs T thus corresponds to curve A sheared parallel to the T axis, the coefficient of shearing being just $\Delta T_{M\alpha}$. The observed γ loop of chromium has a minimum at 815°C. In order that curve A acquire such a minimum, it is necessary that it suffer the shear −20°C, thereby being distorted into curve B. We thus obtain

$$\Delta T_{M\alpha} = -20°\text{C per wt pct}$$

and hence from Eq. 4

$$\Delta T_{Mn\gamma} = -19°\text{C per wt pct.}$$

In terms of our Fig. 9, this shear corresponds to our moving from B toward E, a distance corresponding to a vertical drop of 20°C per wt pct.

Table III. ΔT Parameters for Elements which Close the γ Field

	°C per Wt Pct		°C per Atomic Pct	
	$\Delta T_{Mn\gamma}$	$\Delta T_{M\alpha}$	$\Delta T_{Mn\gamma}$	$\Delta T_{M\alpha}$
Chromium	−19	−20	−18	−19
Molybdenum	−10	−15	−17	−26
Tungsten	−5	−8	−17	−26
Vanadium	−33	−48	−32	−44
Silicon	0	−6	0	−3
Aluminum	30	17	15	8

* After Hollomon and Jaffe.[m]

A crucial test may now be made as to how well our analysis corresponds to reality. If our method of representing the effect of an alloying element in terms of the two parameters $\Delta T_{Mn\gamma}$ and $\Delta T_{M\alpha}$ is essentially correct, we should be able to correlate these parameters with other types of experimental data. The first parameter $\Delta T_{Mn\gamma}$ is directly comparable with experiments on the lowering of the martensite transformation temperature per percent-

age of alloying element. Our value of −19°C for chromium is in excellent agreement with the experimental value[8] of −20°C. Unfortunately the second parameter $\Delta T_{M_{eq}}$ is not subject to such direct experimental verification. The effect of alloying elements upon the magnetic transformation cannot be represented precisely by a mere shift because alloying elements tend to smear out the temperature range over which the transformation extends. A precise description of the effect of alloying elements upon the magnetic transformation would thus certainly require more than one parameter.

Only for the element chromium can we obtain both parameters $\Delta T_{M_{art}}$ and $\Delta T_{M_{eq}}$ solely by use of the equiconcentration diagram. The other γ field closers have γ loops which extend an order of magnitude less than in the case of chromium. Their γ loops are correspondingly less sensitive than that of chromium to a shear. In these cases we must take $\Delta T_{M_{art}}$ as given by experiments on martensite transformation and then calculate $\Delta T_{M_{eq}}$ from the difference $\Delta T_{M_{art}} - \Delta T_{M_{eq}}$ as given by the breadth of the γ loop, according to Eq. 3. In estimating the breadth of the γ loop, we consider the equiconcentration boundary to lie in the center of the two-phase region. Values of $\Delta T_{M_{art}}$ and $\Delta T_{M_{eq}}$ so obtained are listed in Table III.

The estimated values of $\Delta T_{M_{eq}}$ for aluminum and for vanadium appear contradictory to experience. Since additions of aluminum up to 10 atomic pct have a small but definite effect in lowering the Curie temperature, it would appear that a positive $\Delta T_{M_{eq}}$ is inconsistent with experiment. Now $\Delta T_{M_{eq}}$ is estimated from the experimental data on the width of the γ loop and on $\Delta T_{M_{art}}$. The value of the latter is taken from Hollomon and Jaffe,[8] who in turn take it from Klier and Troiano,[10] who in turn take it from Zyuzin, Sadovski, and Baranchuk.[11] The present writer suspects that the value of $\Delta T_{M_{art}}$ first reported by the latter authors is much too high, a value under 13°C per wt pct being required to render $\Delta T_{M_{eq}}$ negative.

According to Table II, vanadium has a marked effect in lowering the temperature range in which the magnetic transformation occurs, 20 wt pct lowering this range by as much as 700°C. The Curie temperature, however, remains essentially unchanged by the addition of this amount of vanadium. We must conclude that the addition of vanadium has a marked effect in lowering the temperature at which the magnetic moments of the iron atoms begin to uncouple from one another, which effect would be manifested both by a lowering of the region in which the thermal capacity of the α phase is anomalously high, as well as by a premature onset of the lowering of the saturation magnetization with increasing temperature.

Whereas satisfaction may be found in having a system which reproduces the observed binary diagrams, the real value to metallurgy of the foregoing described system lies in its ability to predict the location of the phase boundaries of steels having more than one alloying element.

Role of Magnetic Shells in Binding Energy

Scientists are not unanimous as to the most fitting approach to the problem of the binding energy of metals. The approach first formulated by Wigner and Seitz[12] is adopted by most physicists. In this approach, one emphasizes the band character of the conduction electron. In the second approach, pursued primarily by Pauling and his students,[13] one regards the binding in metals as similar to the binding in molecules, namely, as covalent bonds, or more correctly, as resonating valence bonds.

The present author believes the band description of the conduction electrons to be closer to reality than the resonating valence bond description, and therefore he will adopt this viewpoint in the present paper. For the purposes of this paper, the following somewhat oversimplified presentation of the band description is sufficient: Each conduction electron contributes two terms to the energy. The first term is negative, representing a binding, and may be thought of as a potential energy, E_p. This potential energy is the same for all the conduction electrons. The second term is positive, representing a repulsion, and may be thought of as a kinetic energy, E_z. The kinetic energy is quantized and hence forms an energy band. Now, according to Pauli's exclusion principle, only two electrons, one of positive and one of negative spin, may occupy the same quantum state. The first conduction electrons which we add lie at the bottom of the kinetic energy band. As more electrons are added, they occupy successively higher states in this kinetic energy band. When the density of conduction electrons becomes sufficiently great, the positive kinetic energy of the last electron added more than compensates for its negative potential energy. In such circumstances, the addition of further conduction electrons results in a decrease in binding energy.

The kinetic energy band is customarily represented through a plot of density of states vs E_z. The density of states N_z is defined such that $N_z(E_z)d\,E_z$ is the number of conduction electrons which may have a kinetic energy lying between E_z and $E_z + d\,E_z$. Such a plot is given in Fig. 11.

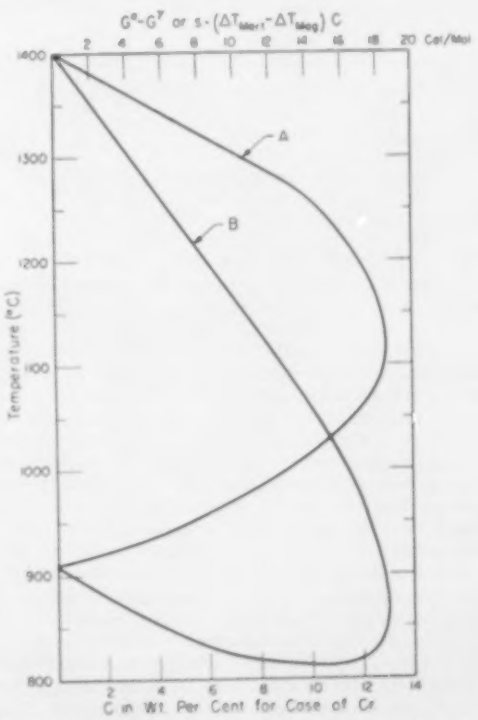

Fig. 10—Graph demonstrates how γ loop of chromium is obtained from G°-G^γ for pure iron.

We are now in a position to understand why the binding is drastically decreased as we add one more conduction electron per atom in passing from copper to zinc, from silver to cadmium, and from gold to mercury. The kinetic energy of these added electrons is so high as to overcompensate for their negative potential energy.

In copper, silver, and gold, and in the elements lying to their right in the periodic table, the *d* shells play a passive role in binding. The mere fact that they are completely filled means that the number of conduction electrons is fixed, namely, one in copper, silver, gold, two in zinc, cadmium, mercury, etc. In the elements lying to the left of copper, silver, and gold, the *d* shells play an active role. The incomplete filling of the *d* shells in these elements allows electrons to be transferred from the conduction band into the *d* shell. Such electrons are said to be demoted. The flexibility introduced by this process of demotion allows these elements to have the optimum number of conduction electrons for maximum binding. If no demotion occurred in nickel, its magnetic saturation would correspond to one Bohr magneton (μ_B) per atom. Since actually nickel has a magnetic saturation of only 0.6 μ_B per atom, we must conclude that 0.4 conduction electrons per atom have been demoted into the *d* shell. In Table IV are presented the data for the binding energies of copper, silver, gold, and the elements lying immediately to their right and to their left in the periodic table. The increased binding of nickel, palladium, and platinum over copper, silver, and gold may be interpreted solely in terms of the demotion possible in the first three elements, but impossible in the latter three. We have previously interpreted the low binding energies of zinc, cadmium, and mercury as arising from the excessive kinetic energy associated with their two conduction electrons.

Table IV. Heat of Formation at 25°C,[m] Cal per Mol

Nickel 101,000	**Copper** 81,000	**Zinc** 31,000
Palladium 93,000	**Silver** 69,000	**Cadmium** 37,000
Platinum 122,000	**Gold** 82,000	**Mercury** 15,000

As mentioned in the opening paragraphs of this paper, the model of isolated *d* shells can be taken as close to reality only for the first transition period where the radius of the outer *d* shell is very small compared with the radii of the atoms. It will be instructive therefore to pursue the correlation between demotion and binding energy only for this first period. Table V presents the data for the first period from vanadium to copper. We note as we pass to the left from copper that nickel, cobalt, and iron have almost identical binding energies. From Table I we see that they all three have two outer *s* electrons in the isolated atomic state, together with a partially filled half *d* shell. When the nickel or cobalt or iron atoms coalesce to form a solid, these partially filled half *d* shells act as reservoirs into which are demoted such a number of conduction (or 4*s*) electrons as will maximize the binding energy.

When we now proceed to the left in Table IV, we note that manganese has an anomalously low binding energy. As explained in the introduction, an electron which starts a new half shell is unfavorably situated in that it has no exchange with other electrons in the same shell. Table VI is presented in confirmation of this expectation. We see that in demoting one of the two electrons in the 4*s* shell to the 3*d* shell in an isolated atom, much more energy is required in the case of manganese than in the case of the elements on either side of manganese in the periodic table. The anomalously low boiling temperature and the anomalously high vapor pressure of manganese are, of course, direct consequences of its low binding energy and hence may ultimately be traced to the *d* shell structure of the isolated manganese atom.

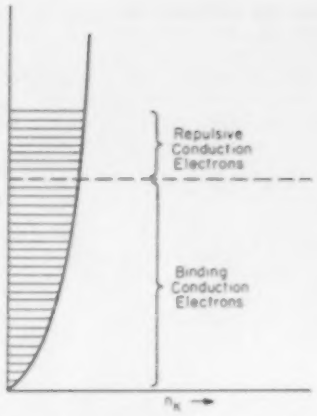

Fig. 11—Kinetic energy band is illustrated. The shaded region represents that portion of the band which is filled with conduction electrons.

Inspection of Table V shows that chromium also has a comparatively low binding energy, 20,000 cal per mol lower than iron, cobalt, and nickel. Its binding energy is, in fact, almost identical with that of copper. This essential identity in binding energy in chromium and in copper may be interpreted as a reflection of similar demotion difficulties. Each atom has, in the isolated state, one 4*s* electron. The metal copper has a complete *d* shell. Any demotion of its one conduction electron per atom therefore is debarred. The metal chromium has a complete half shell. Any demotion of its one conduction electron per atom therefore would involve starting a new half shell. It is doubtful therefore if any appreciable demotion occurs. Independent evidence of the extreme difficulty in starting a new half shell is seen in the fact that more energy is required to demote the one 4*s* electron in chromium than the two 4*s* electrons in iron or cobalt or nickel.[8] Independent evidence that no demotion occurs is given by the electronic specific heat. The electronic specific heat may be most readily interpreted in terms of the band model. According to this model, this specific heat is proportional to the density of states at the top of the Fermi distribution. As may be seen from Table VII, chromium and copper are anomalous in the first transition period in having very low elec-

Table V. Heats of Sublimation at 0°K of Elements in First Transition Period

	Cal per Mol
Vanadium	122,000[n]
Chromium	80,000[n]
Manganese	68,050[n]
Iron	99,200[n]
Cobalt	101,600[n]
Nickel	101,100[n]
Copper	80,300[n]

tronic specific heats, indicating that in both of these metals no partially filled half shells are present.

As in the case of manganese, the anomalously low boiling point and high vapor pressure of chromium may be traced to its anomalously low binding energy and hence ultimately to the *d* shell structure of the isolated chromium atoms.

Relation between Magnetism, Thermal Expansion, and Crystal Structure

The best known example of a material with an anomalous thermal expansion is Invar, an Fe-Ni alloy with about 40 pct Ni. The upper limit of the temperature range in which the thermal expansion of Invar is anomalously low coincides with the temperature at which ferromagnetism disappears. This coincidence led the early workers in the field to the belief that the anomalous thermal expansion of Invar is in some way related to ferromagnetism. In this section we shall examine this relation in some detail. This examination leads not only to a natural interpretation of the low thermal expansion coefficient of Invar, but also to a natural interpretation of the anomalously high thermal expansion coefficient of manganese-rich Mn-Cu alloys, and finally to an interpretation of the face-centered-tetragonal structure of these alloys and to an interpretation of the body-centered-cubic structure of chromium and vanadium.

Table VI. Energy Required to Promote a 4s Electron to the 3d Shell in Isolated Atoms, the Initial State Having Two 4s Electrons*

	Cal per Mol
Chromium	−23,000
Manganese	48,000
Iron	21,000

* Data from ref. 4.

For our present purpose, two properties of *d* shells discussed under "Magnetic Shells and Their Interactions" are pertinent. The first property is that the exchange interaction between shells in adjacent atoms is positive, and hence represents a repulsion and that this repulsion is greatest when the spins of the two atoms are parallel. When we heat a ferromagnetic material through its Curie temperature and thereby change the spins from a parallel arrangement to a random orientation, the repulsive exchange interaction thus will be reduced. The resulting contraction will at least partially counteract the normal thermal expansion arising from atomic vibrations, thereby giving rise to an anomalously low net thermal expansion.

The second pertinent property of the *d* shells is their contraction as we pass to the right along a row in the periodic table. Thus, of the elements in the first transition period, nickel has the smallest *d* shell. The overlap of the *d* shells in nickel thus will be very small, and the anomaly in thermal expansion coefficient will be correspondingly small. Actually in nickel a rise in temperature through the Curie point results in a slight excess thermal expansion. Such an excess thermal expansion is what would be expected if the overlap of adjacent *d* shells was negligible. The writer[2] had previously pointed out that the ferromagnetic coupling which tends to align the *d* shell spin of adjacent atoms is an indirect coupling which takes place through the conduction electrons. This ferromagnetic coupling does not require an overlap of the *d* shells themselves, only an overlap of the conduction electrons with the *d* shells. Now this indirect ferromagnetic coupling represents an attraction, and this attraction overshadows the direct exchange repulsion when the overlap of adjacent *d* shells is sufficiently small. The disappearance of this indirect ferromagnetic coupling as we pass through the Curie point in nickel thus is associated with a slight expansion.

From the foregoing discussion, we expect the thermal expansion associated with the loss of ferromagnetic coupling to increase as we pass from nickel through cobalt to iron. Data are not available for making such a comparison for the pure metals. Thermal expansion data for cobalt are not available. A comparison of iron with nickel should be made only for similar crystal structures, but the face-centered-cubic phase of iron is not ferromagnetic. In the absence of data for pure metals, recourse will be taken to a study of the thermal expansion of Fe-Ni alloys for compositions lying in the face-centered-cubic phase. We plot in Fig. 12 the magnetic dilation θ_{Mag} for these alloys. The magnetic dilation is defined as that dilation associated with the magnetic configuration changing to a complete alignment of the atomic spins from a completely random orientation. In Fig. 12, two sets of data are plotted. One set[20] is from thermal expansion measurements, from which an estimate is made of the difference between the actual thermal expansion from 0°K up to the Curie temperature, and the corresponding estimated thermal expansion which would have arisen in the absence of ferromagnetic uncoupling. The second set of data is from the measurements of Patrick[20] on the effect of pressure upon the Curie temperature. If one considers the spin entropy S to be a function of only the pressure and temperature and if one assumes $(dT/dP)_s$ to be independent of temperature, one obtains from simple thermodynamic arguments that

$$\theta_{Mag} = -(dT/dP)_s \Delta S$$

where ΔS is the change in the spin entropy per unit volume associated with passing from complete alignment to a complete random orientation of the spins. The coefficient $(dT/dP)_s$ has been measured by Patrick. The entropy ΔS is computed by assigning the value of R ln 3 to one mol of iron atoms, the value of 0.6 R ln 2 to one mol of nickel atoms, corresponding to every iron atom having a spin multiplicity of 3 associated with a magnetic moment of 2 Bohr magnetons, and to 60 pct Ni atom having a multiplicity of 2 associated with a spin of one Bohr magneton. We see that, in Fig. 12 as we approach high iron concentration, the magnetic dilation as obtained from pressure measurements becomes considerably larger than that obtained from thermal expansion data. We infer from this discrepancy that at the higher iron concentration the atomic spins do not become completely randomized upon passing through the Curie temperature. This inference is consistent with our interpretation of the $\alpha \rightarrow \gamma \rightarrow \delta$ transformation in iron, where we had to assume that the spins in the α phase become only partly randomized at the Curie temperature.

Table VII. Coefficient of $T(\gamma)$ Electronic Specific Heats*

	Cal per Mol						
Metal	V	Cr	Mn	Fe	Co	Ni	Cu
$\gamma \times 10^3$	14	2.7	42	12	12	17.4	1.80

* After Stoner.[21]

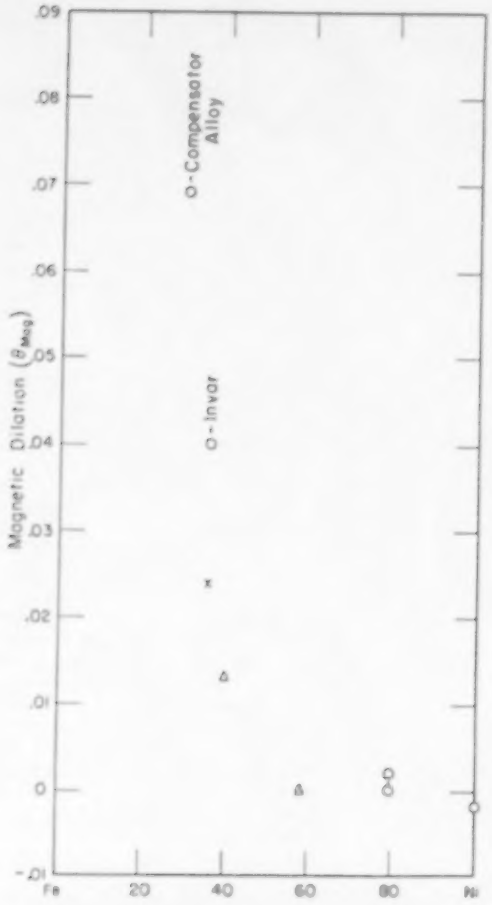

Fig. 12—Magnetic dilation in face-centered-cubic Fe-Ni alloys is shown. Circle represents data of Patrick;[28] triangle, Scott;[29] and cross, Chevenard.[30]

Since cobalt has a larger *d* shell than has nickel, one would expect that the substitution of some cobalt for nickel in the Fe-Ni alloys would result in a larger β_{Mag} and hence in a smaller net thermal expansion coefficient. This effect of cobalt was first observed by Brace and led to the development of super-Invar by Scott.[29]

We now pass from the nickel, cobalt, iron triad in the first transition row to manganese. Whereas in nickel the *d* shells are so small as to give a negligible interaction, as we pass to close-packed γ iron, the *d* shells are sufficiently large to prevent a ferromagnetic alignment. As we continue to manganese, the overlap between *d* shells has further increased. The effect of this increased overlap may be best seen in the γ phase of manganese, a phase which may be retained upon quenching if small additions of copper are made. This phase is face-centered-cubic at high temperatures. Now in a close-packed structure, nearest neighbor atoms cannot have their spins antiparallel to one another, since nearest neighbors of a specific atom are nearest neighbors to one another. In a face-centered-cubic structure it is possible, however, to have an ordered arrangement of spins in which each atom has more nearest neighbors with spins antiparallel than parallel to its own spin. Such an arrangement is given if alternate 100 planes have alternate spin directions.* The four nearest neighbors in the same 100 planes then have parallel spins, whereas the eight nearest neighbors in adjacent 100 planes have antiparallel spins. Having parallel spins, the nearest neighbors in the same 100 plane will have an exchange repulsion, a repulsion which will not be present between nearest neighbors in adjacent 100 planes. The ordered spin arrangement therefore would be tetragonal, the *c/a* ratio being less than unity. Such a face-centered-tetragonal structure with *c/a* less than unity was, in fact, found in quenched Mn-Cu alloys some 25 years ago by Persson and Ohman.[31]

* Sidhu has kindly informed the author of a report by Meneghetti and Sidhu, *Physical Review* (1954) 96, p. 666, which confirms by neutron diffraction the antiferromagnetic spin structure of Mn-Cu alloys.

Such an ordered arrangement of spins has, of course, a lower entropy than has a random arrangement and hence is expected to take place only at lower temperatures. From the heavily twinned structure of these alloys first noted by Worrell,[32] the writer[33] predicted that these alloys were face-centered-cubic at high temperatures, becoming tetragonal during quenching. This prediction has been verified by Zwicker[34] who found that this transition from face-centered-cubic to face-centered-tetragonal occurred at about 250°C for nearly pure manganese and at gradually decreasing temperatures as nickel was added.

As one passes from the face-centered-tetragonal to the face-centered-cubic structure in Mn-Cu alloys with a rise in temperature, one passes from a spin arrangement in which the spins of nearest neighbors are dominantly antiparallel to one in which they are randomly oriented. The face-centered-tetragonal → face-centered-cubic transition is associated therefore with an increase in the number of nearest neighbors with repulsive exchange interactions. This transition therefore must be associated with an anomalously high thermal expansion. That this is indeed the case is demonstrated in Fig. 13, taken from the data of Basinski and Christian.[35]

We are now in a position to specify the materials for an ideal bimetallic strip. For the metal with a small expansion coefficient, we must choose one which is ferromagnetic, the Curie temperature being at the upper limit of the operating range and the *d* shells being as large as is consistent with the presence of ferromagnetism. For the metal with a large expansion coefficient, we must choose one which is antiferromagnetic, the Curie temperature being at the upper limit of the operating range. For such a bimetal, a rise in temperature through the operating range is associated in one-half of the bimetal with a decrease in the number of nearest neighbors with repulsive exchange interactions, in the other half of the bimetal with an increase in the number of nearest neighbors with repulsive exchange interactions.

As we now continue to the left along the first transition row through manganese to chromium and vanadium, the *d* shell continues to expand. Whereas in manganese the resonance interaction between the *d* shells was not sufficiently great to modify the structure from face-centered-cubic until the temperature was lowered to 250°C, in chromium the increased interaction modifies the face-centered-cubic structure only 100° or so below the melting temperature.[36] The lower temperature phase is body-centered-cubic, a structure which is even more effec-

tive than the face-centered-tetragonal structure in reducing the number of nearest neighbors with parallel spins, i.e., with a repulsive exchange interaction. In a body-centered-cubic structure, all nearest neighbors may have antiparallel spins. Finally in vanadium where the *d* shells are still larger than in chromium, the metal crystallizes directly into the body-centered-cubic phase.

Relation between Magnetism and Mechanical Properties

The three preceding applications of magnetism to metallurgy have required some insight into the detailed magnetic structure of the first row transition metals. In contrast, our final application of magnetism to metallurgy requires only a familiarity with macroscopic concepts.

It has long been known that magnetostriction furnishes a coupling between magnetism and mechanical properties of ferromagnetic materials. A common measure of the strength of this coupling is the magnetostriction constant λ. This constant is defined as follows: Suppose we start with a specimen in which the elementary domains are magnetized at random along the various directions of easy magnetization. When we now apply a magnetic field of sufficient strength to magnetize the specimen to saturation, the accompanying tensile strain along a line parallel to the magnetic field is given by λ.

Becker and Kornetzki[48, 49] demonstrated that magnetostriction may have a profound effect upon the damping capacity of a ferromagnetic material. Their argument may best be understood by considering a ferromagnetic material with an ideal *B-H* curve of the type shown in Fig. 14A. The stress-strain curve of such a material will then be of the form shown in Fig. 14B. Now the pressure exerted upon a 90° domain wall by a magnetic field H is essentially JH, by a stress σ is essentially $\lambda\sigma$. Hence the relation between the critical H and the critical σ for domain wall movement is

$$\sigma_c \cong J H_c/\lambda$$

where J is the saturation intensity of magnetization. The area of the mechanical hysteresis loop is given by

$$\triangle E = 2\lambda \sigma_c \cong 2 J H_c$$

and hence is approximately one-half the area of the magnetic hysteresis loop. The variation with stress of the damping capacity ($\triangle E/E$) associated with this magnetoelastic coupling is shown in Fig. 14C.

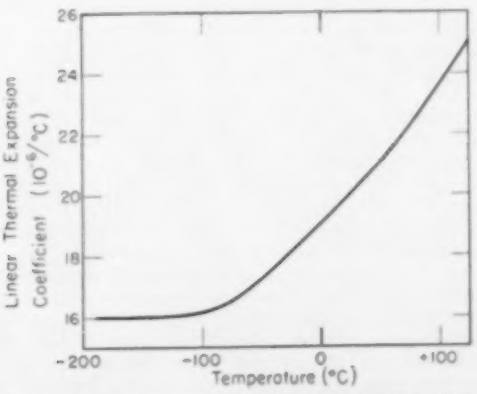

Fig. 13—Thermal expansion coefficient of CuMn alloy, after Houk from data of Basinski and Christian,[45] is shown.

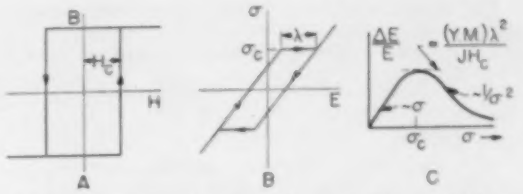

Fig. 14—Magnetoelastic coupling is illustrated. H_c is coercive force; λ, magnetostriction constant; (Y.M.), Young's modulus; and J, saturation intensity of magnetization. Drawing *A* is a representation of ferromagnetic material with an ideal *B-H* curve. *B* is the stress-strain curve of such material. *C* shows the variation with stress of the damping capacity ($\Delta E/E$) associated with magnetic coupling.

Cochardt has recognized that the magnetoelastic damping illustrated in Fig. 14 is the principal source of damping in the common turbine-blading high chrome steel. Following this recognition, he has made a thorough and brilliant study of magnetoelastic damping and its practical applications.[46, 47] Because of this work, metallurgists are now able to design the desired damping capacity into their materials through a control of the appropriate magnetic characteristics.

Conclusion

From the preceding discussion, it is apparent that our insight into magnetism has already had a profound influence upon our understanding of many aspects of metallurgy. As this insight becomes deeper and becomes more widespread among metallurgists, it is to be expected that magnetism will have an ever-widening influence upon metallurgy.

References

[1] J. C. Slater: *Review of Modern Physics* (1953) **25**, p. 199.

[2] W. J. Carr: *Physical Review* (1953) **72**, p. 28.

[3] F. Bader: *Ztsch. für Naturforschung* (1953) **8a**, p. 498.

[4] A readable account of atomic shells is given by A. H. Cottrell: *Theoretical Structural Metallurgy*. (1948) chap. 1. London. Edward Arnold & Co.

[5] Atomic Energy Levels. *Circular No. 467* National Bureau of Standards (1949).

[6] D. R. Hartree and W. Hartree: *Proceedings* Royal Soc. (1936) **157**, p. 490. References to all calculations by the Hartree method are given in Landolt-Bornstein: *6 Auflage I* **1**, pp. 276-283.

[7] The chemical bond is described fully by L. Pauling: *Nature of the Chemical Bond*. (1940) Ithaca. Cornell University Press.

[8] C. Zener: *Physical Review* (1951) **81**, p. 440; (1951) **82**, p. 403; (1951) **83**, p. 299; (1952) **85**, p. 324.

[9] R. R. Heikes: *Physical Review* (1951) **84**, p. 376.

[10] W. J. Carr: *Physical Review* (1952) **85**, p. 590; (1953) **92**, p. 28.

[11] C. Zener and R. R. Heikes: *Review of Modern Physics* (1953) **25**, p. 191.

[12] C. Zener: *Acta Crystallographica* (1950) **3**, p. 346.

[13] H. B. Huntington: *Physical Review* (1952) **91**, p. 1092.

[14] G. J. Dienes: *Physical Review* (1952) **86**, p. 228.

[15] A. E. H. Love: *Mathematical Theory of Elasticity*. (1906) 2nd Ed., p. 535. Cambridge. Cambridge University Press.

[16] C. Zener: *Physical Review* (1947) **71**, p. 323.

[17] C. Zener: *Trans.* AIME (1946) **167**, p. 513; METALS TECHNOLOGY (January 1946).

[18] W. West: *Trans.* AIME (1946) **167**, p. 535; METALS TECHNOLOGY (January 1946).

[19] J. C. Fisher: *Trans.* AIME (1949) **185**, p. 688; JOURNAL OF METALS (April 1949).

[20] F. W. Jones and W. I. Pumphrey: *Journal* Iron and Steel Inst. (1949) **163**, p. 121.

[40] W. Rostoker: *Trans.* AIME (1951) **191**, p. 1203; JOURNAL OF METALS (December 1951).
[41] H. Johansson: *Archiv für Eisenhuttenwesen* (1937) **11**, p. 241.
[42] R. Smoluchowski and J. S. Koehler: *Ann. Review of Physical Chemistry* (1941) **2**, p. 187.
[43] P. Oberhoffer and H. Esser: *Stahl und Eisen* (1927) **47**, p. 255.
[44] J. H. Hollomon and L. D. Jaffe: *Ferrous Metallurgical Design* (1947) p. 47. New York. John Wiley and Sons Inc.
[45] E. P. Klier and A. R. Troiano: *Trans.* ASM (1944) **32**, p. 516.
[46] V. Zyuzin, V. Sadovski, and S. Baranchuk: *Metallurg* (1939) **14**, p. 75.
[47] E. Wigner and F. Seitz: *Physical Review* (1933) **43**, p. 804. Reviewed in F. Seitz: *Modern Theory of Metals.* (1940) chap. X. New York. McGraw-Hill Book Co. Inc.
[48] L. Pauling: *Physical Review* (1938) **54**, p. 899.
[49] Selected Values of Chemical Thermodynamic Properties. *Circular No. 500* National Bureau of Standards (1952).
[50] H. L. Johnston and A. L. Marshall: *Journal* Amer. Chemical Soc. (1940) **62**, p. 1382.
[51] J. W. Edwards, H. L. Johnston, and W. E. Ditmore: *Journal* Amer. Chemical Soc. (1953) **75**, p. 2467.
[52] E. C. Stover: *Acta Metallurgica* (1954) **2**, p. 265.
[53] P. Chevenard: *Comptes Rendus* (1920) **170**, p. 1499.
[54] L. Patrick: *Physical Review* (1954) **93**, p. 384.
[55] H. Scott: *Trans.* Amer. Soc. for Steel Treating (1928) **13**, p. 829.
[56] E. Persson and E. Ohman: *Nature* (1929) **124**, p. 333.
[57] F. Worrell: *Journal of Applied Physics* (1948) **19**, p. 929.
[58] C. Zener: *Elasticity and Anelasticity of Metals.* (1948) p. 162. Chicago. The University of Chicago Press.
[59] U. Zwicker: *Ztsch. für Metallkunde* (1951) **42**, p. 246.
[60] Z. S. Basinski and J. W. Christian: *Journal* Inst. of Metals (1952) **19**, p. 659.
[61] D. S. Bloom and N. J. Grant: *Trans.* AIME (1951) **191**, p. 1009; JOURNAL OF METALS (November 1951).
[62] R. Becker and M. Kornetski: *Ztsch. für Physik* (1934) **88**, p. 634.
[63] R. Bozorth: *Ferromagnetism.* (1951) p. 707. New York. D. Van Nostrand Co. Inc.
[64] A. W. Cochardt: *Trans.* ASME (1953) **75**, p. A-196; (1954) **76**, p. A-256.
[65] A. W. Cochardt: *Journal of Applied Physics* (1954) **25**, p. 91.
[66] A. W. Cochardt: To be published. *Trans.* ASM (1955) **47**.
[67] J. W. Edwards, H. L. Johnston, and P. E. Blackburn: *Journal* Amer. Chemical Soc. (1951) **73**, p. 4727.
[68] J. W. Edwards, H. L. Johnston, and W. E. Ditmore: *Journal* Amer. Chemical Soc. (1951) **73**, p. 4729.

Experimental Production of Al-Si Alloys In A Three-Phase Furnace

by Lloyd H. Banning and William F. Hergert

Experimental production of Al-Si alloys, containing from 33 to 55 pct Al, by direct reduction of aluminum silicates in a three-phase arc furnace is described. Advantages of a smelting technique utilizing hogged wood waste as part of the reductant and for temperature control are discussed.

WORK on the problem of producing aluminum by smelting has been in progress since the middle of the eighteenth century. Early work met with little success and in 1782 Lavoisier, an eminent French chemist, expressed the belief that alumina could not be reduced by carbon. It was almost a century later when the Cowles brothers developed a process for the production of aluminum alloys by reducing alumina coincident with the reduction of other metal oxides. In practice, the other metal oxide was usually copper. In 1907 it was first shown that alumina alone could be reduced by carbon at a temperature of 2200°C. The metal produced was volatilized and lost or recombined with the oxides of carbon formed in the reaction.[1]

For a number of years after the Cowles brothers abandoned production of Cu-Al alloys because their product was not commercially competitive with the aluminum produced by the Hall process, there was little interest in thermal reduction processes. After World War I interest in such processes was renewed and a number of patents were issued on processes for the production of Al-Si alloys.[2, 3] The function of the silicon in these processes was the same as the function of the copper in the Cowles brothers process, namely, to prevent the reduced aluminum from recombining with the oxides of carbon and to promote absorption of the aluminum vapors set free at the high temperature required for the reduction reaction. The advantage of using silicon in place of copper for this function is that silicon has a higher boiling point (2600°C) than copper (2310°C) and its oxides, combined with aluminum oxides, occur in nature in almost unlimited quantities.

No Al-Si alloys have been produced commercially in the United States, as far as is known. However, considerable experimental smelting of aluminum silicate materials has been done by the TVA at Wilson Dam, Ala.[4] The most extensive development and commercialization of the electrothermal production of Al-Si alloys took place in Germany before and during World War II.[5] The furnaces used in the

German smelting process were of the single-phase open-top pit type. The usual voltage was about 55 and amperage about 20,000 when amorphous carbon electrodes 26.5 in. diam were used. Apparently no commercial quantity of Al-Si alloys was produced in three-phase furnaces at that time in Germany although such furnaces were operated on an experimental basis.[6]

Alumina is not necessary as a raw material for the production of Al-Si alloys, and depletion of high grade bauxite deposits on the North American continent has fostered interest in thermal reduction processes for the production of these alloys from nonbauxitic raw materials. Almost every report on future North American resources of aluminum emphasizes the necessity for developing methods for utilizing low grade aluminum-containing raw materials, such as clay, shale, and even high iron laterites. Electric furnace smelting of aluminum silicate materials to produce a crude Al-Si alloy is the first step on one method of obtaining supplementary aluminum from the nonbauxitic materials. A number of potential large volume uses for this crude Al-Si alloy are: 1—supplying silicon for and supplementing primary aluminum or scrap aluminum in the manufacture of silicon-containing aluminum alloys;

2—in the production of aluminum by processes, such as one patented by Dr. Hirsch Loevenstein, involving extraction of the aluminum by a solvent metal followed by vacuum distillation of the solvent metal;[7, 8]

3—in the production of usable Al-Si alloys, such as silumin, an alloy containing 12.8 to 13.2 pct Si,[9, 10] or further *modified silumin* produced by fluxing silumin with a mixture of sodium chloride and sodium fluoride, as patented by Dr. Aladar Pacz;

4—as a reductant in the production of magnesium by the Pidgeon process; and

5—as a reductant and a deoxidizing agent in the steel and ferroalloy industries.

Description of Smelting Process

The smelting tests on the production of Al-Si alloys were carried out in two electric furnaces which had been installed for experimental production of ferroalloys. Both furnaces are three-phase, with automatic electrode regulation; they are of the cylindrical open-top pit type. The large furnace uses 8 in. graphite electrodes and has a shell 96 in. diam and 78 in. high. The small furnace uses either 3 or 4 in. graphite electrodes and has interchangeable shells of different sizes. Carbon linings are used in both furnaces. A complete description of the smelting equipment and facilities used at the Albany Station of the Bureau of Mines is contained in a previous paper.[11]

In the smelting operation, aluminum silicates are mixed with reductant and shoveled into the furnace. The reductant may be coke, charcoal, sawdust, hogged fuel, or mixtures of these materials. When the furnace is operating normally, the charge is kept at a uniform depth. The electrodes extend through the charge, and the useful heat for conducting the reduction reaction is provided by arcing on the molten bath. The charge feeds continually into this smelting zone, and alloy is tapped from the furnace at regular intervals.

When the charge between the electrodes becomes conducting, part or all of the current flows through the charge, and little or no heat is developed at the electrode tips by arcing. Under these conditions little smelting occurs because electric arc temperatures are needed to reduce aluminum silicates.

Table I. Carbon and Energy Requirements for Reducing Charge Constituents

	Al	Si	Ti	Fe
Lb carbon per lb	0.668	0.856	0.501	0.215
Kw-hr per lb	3.03	2.80	1.702	0.355

Under ideal smelting conditions, there is just enough carbon in the charge to reduce all of the oxides to metal, and no slag is formed in the furnace. When there is a deficiency of carbon in the charge, a high melting point slag is produced which is difficult to tap; with an excess of carbon in the charge, infusible silicon carbide forms and collects on the bottom of the furnace, and the charge between the electrodes becomes conducting. The type of reductant, as well as the amount of reductant, also affects the conductivity of the hot charge. Hogged fuel—a mixture of wood chips, splinters, and sawdust—has been found to be the most effective type of reductant for minimizing charge conductivity. Other advantages of using hogged fuel as a major portion of the reductant in the furnace charge are: 1—The charge is porous, and gases formed by the reduction reaction in the smelting zone can escape readily. 2—The charge serves as an insulating blanket over the smelting zone and this permits less radiation and makes for more comfortable operating conditions. 3—The temperature of the smelting zone may be controlled by the adjustment of the proportion of hogged fuel to coke in the charge. 4—There is much less bridging and crusting in the furnace. 5—Vaporization and dust losses are minimized.

Assuming that the carbon in the charge reacts with the Al_2O_3, SiO_2, TiO_2, and FeO to form carbon monoxide and metal, the theoretical carbon and energy requirements can be calculated. The carbon requirements are calculated from the equations for the reactions; the energy requirements are calculated from the heats of formation.[12] Carbon and energy requirements for reducing the charge constituents are shown in Table I.

The actual carbon requirement is not always the same as the theoretical requirement but may be increased by oxidation and by formation of carbides and decreased by the formation and volatilization of silicon monoxide and possibly by the volatilization of some lower oxides of aluminum. The optimum carbon requirements can be determined only by operation.

Description of Smelting Tests

The purpose of the Bureau's electrothermal smelting research has been to determine the chemical composition range of Al-Si alloys that it is practical to produce, to make studies on the use of hogged fuel in the furnace charge, and to determine optimum furnace operating conditions. To date, six continuous-type smelting tests have been made in a small furnace and two in a large furnace. These tests

L. H. BANNING, Member AIME, and W. F. HERGERT are Chief, Pyrometallurgical Branch, and Head, Light Metals Section, Pyrometallurgical Branch, respectively, Northwest Electrodevelopment Laboratory, U. S. Bureau of Mines, Region II, Albany, Ore.

Discussion of this paper, TP 3924D, may be sent, 2 copies, to AIME by July 1, 1955. Manuscript, Apr. 23, 1954. New York Meeting, February 1954.

Papers by authors on the Bureau of Mines Staff are not subject to copyright.

have been aimed at producing Al-Si alloys containing approximately 35, 45, and 55 pct Al.

The analyses of clays used in smelting tests are shown in Table II. Eastern clay was used in three tests. Alumina was used in one large-scale test to increase the Al_2O_3 content of the charge. The Columbia clay used was a standard-brand high duty fireclay mined near Renton, Wash. The raw Cowlitz clay, from an extensive deposit near Castle Rock, Wash., was calcined in the Bureau's rotary kiln. Various types of hogged wood waste, wood chips, and coke were used for reductants.

Five exploratory tests were conducted in the small furnace, all aimed at establishing and maintaining operable smelting conditions for fireclays containing approximately 45 pct alumina. In the first two tests, calcined eastern clay was used. Western Columbia calcined clay was used in the third, fourth, and fifth tests.

Table II. Analysis, Pct, of Raw Materials Used in Smelting Tests

Material	Al_2O_3	SiO_2	Fe_2O_3	TiO_2	Loss on Ignition	CaO	NaO	Fixed Carbon
Eastern raw clay	37.8	43.5	1.08	0.07	15.4	0.29	—	—
Eastern calcine clay	42.7	46.9	1.14	0.03	6.18	—	—	—
Columbia calcine clay	43.1	48.2	4.50	2.50	0.3	0.9	0.8	—
Cowlitz calcine clay	46.1	43.2	5.00	2.82	0.15	1.1	0.9	—
Silica rock	—	99.2	—	—	—	—	—	—
Petroleum coke								96.3
Hogged fuel, average								13.0
Wood chips, average								12.0

The major change in the operation of the furnace from one test to the next was the use of a progressively higher power input per pound of clay. This was achieved by using a higher proportion of hogged fuel to coke in the furnace charge. All of these tests were terminated when a gradual accumulation of material effectively blocked the tap hole and made tapping of the alloy virtually impossible. The fifth test was conducted primarily to determine whether the exclusive use of hogged fuel would result in a high enough smelting temperature to make tapping of the alloy less difficult. The charge proportions consisted of 100 lb clay and 280 lb hogged fuel. This lasted 60 hr. A gradual buildup of a mass of silicon carbide on the furnace hearth resulted in a blocking of the tapholes. Apparently, the use of hogged fuel only as reductant resulted in too slow a feed rate into the smelting zone and in high electrode consumption. Extremely high temperatures were developed as evidenced by tapping temperatures of 1950°C. However, this extreme temperature did not aid materially in tapping silicon carbide from the furnace with the alloy.

The carbon content of the changes in this series of tests was varied over a considerable range; however, the optimum range proved to be between 95 and 102 pct of the stoichiometric requirements. Electrical conditions were varied slightly; but no appreciable effect was evident, other than that, when a higher amperage was used to improve smelting conditions, the 3 in. electrodes become incandescent owing to their inadequate current carrying capacity.

After evaluating the results of this series of five tests, a sixth test was made in the small furnace. Four major changes were made in the operating conditions for this test based on the experience gained from previous tests: 1—Silica rock was added to the charge mixture to simulate a 35 pct alumina clay. 2—Electrodes, 4 in. diam, were substituted for the 3 in. ones used previously. 3—A lower voltage and higher amperage at approximately the same power input were used. 4—A uniformly sized wood chip product, free of sawdust and bark, was substituted for the run-of-the-mill hogged fuel previously used.

The average charge proportions were 74 lb Cowlitz calcined clay, 26 lb silica rock, 232 lb wood chips, and 9 lb coke. The operating voltage was 38 v, phase-to-phase, at a power input of about 140 kw. After 102 hr of operation under ideal and uniform operating conditions, the furnace was shut down as scheduled with every indication that this test could have been continued indefinitely.

The pertinent data for the series of five tests on calcined 45 pct alumina clay and the sixth test on the simulated 35 pct alumina clay are summarized in Table III.

The first test in the large furnace was an attempt to smelt a simulated 55 pct alumina raw material. After 113 hr of operation the test was terminated as unsuccessful, owing to an accumulation of material that would not tap from the furnace. This result was similar to that experienced in many of the tests in the small furnace.

The charge relations used in a second test in the large furnace were 100 lb calcined Cowlitz clay, 216 lb wood chips, and 11 lb coke. The carbon content of the charge averaged about 102 pct of the stoichiometric requirement. The electrical conditions were the same as for the previous test in this furnace. The operating technique used was based on the experience gained from previous tests. After 209 hr of continuous operation, the furnace was in operable condition. Alloy production had been maintained at a normal rate for most of this period. Opening the tap hole was the most troublesome feature of this test and often required the use of an oxygen lance.

For comparison, the pertinent data on two tests in the large furnace are summarized in Table IV.

Discussion of Test Results and Conclusions

The use of hogged fuel or wood chips as part of the reductant is believed to be the most important single factor responsible for the successful smelting of alumina silicates in a three-phase electric arc furnace. The smelting temperature and the tapping temperature were controlled by varying the proportion of hogged fuel to coke. These temperatures must be kept high to operate successfully. However, when only hogged fuel was used for the reductant, as in the fifth test, the temperature was so high that carbon was robbed from the electrodes and a large quantity of silicon carbide formed on the furnace hearth. When too little hogged fuel was used, tapping temperatures dropped, resulting in excessive crusting and furnace blowing. When the correct proportion of hogged fuel was used, the feed rate of the ore into the smelting zone could be correlated easily with the power input, and a definite ratio of kw-hr per pound of aluminum silicates charged could be maintained without having open arc conditions or an excessively deep dry top.

Specific electrical conditions must be maintained to insure a continuing smelting operation. These electrical conditions have been expressed by the formula $R = E/I \sqrt{D}$.[10] Experience has shown that the R factor should be maintained between 0.12 and 0.15 in both the small and large furnace when using

Table III. Summary Data on a Series of Small-Scale Tests

	Test Number					
	1	2	3	4	5	6
Operating Conditions						
Length of smelting test, hr	22	34	48	72	60	102
Charge proportions, lb						
Clay, calcined, eastern	100	100	—	—	—	—
Clay, calcined, Columbia	—	—	100	100	100	—
Clay, calcined, Cowlitz	—	—	—	—	—	74
Silica rock	—	—	—	—	—	26
Coke, 96 pct fixed carbon	20	12	6	9	none	9
Hogged fuel, 13 pct fixed carbon	150	200	220	224	280	—
Wood chips, 12 pct fixed carbon	—	—	—	—	—	232
Carbon, pct stoichiometric	106	98	92	102	97	98
Electrode diameter, in.	3	3	3	3	3	4
Electrode voltage, phase-to-phase	52	45	45	52	45	58
Current, amp, average	1400	1700	1800	1600	1700	2100
Power input, kw, average	130	140	145	135	140	140
Electrode current density, amp per sq in.	197	238	254	212	238	170
R, ohm, in.	0.20	0.18	0.14	0.19	0.15	0.13
Operating Results						
Consumption of ore, lb per hr	77	68	60	53	38	50
Alloy production rate, lb per hr	10	13	15.5	19	12.5	21
Power consumption, kw-hr per lb of ore	1.7	2.1	2.4	2.54	3.7	2.78
Power consumption, kw-hr per lb of alloy	14.0	10.7	9.4	7.1	11.2	6.7
Electrode consumption, graphite, lb per ton of alloy	—	560	475	322	530	358
Composition (typical) of alloy, pct						
Aluminum	65*	54*	47	46	58*	33
Silicon	25	42	46	43	37	59
Iron	3.4	3.5	4.8	5.8	2.2	5.0
Titanium	1.6	1.6	1.5	2.2	1.1	3.0
Alloy recovery, pct	50	66	78	94	72	103†

* High aluminum content due to formation of silicon carbide which resulted in tapping only an aluminum-rich fraction.
† Due to slag inclusions.

graphite electrodes. Under these conditions from 6.2 to 7.2 kw-hr are required per pound of alloy produced. The actual electrical energy requirements compared to the theoretical requirements indicate smelting efficiencies of between 39 and 46 pct.

The difficulty of smelting aluminum silicates increases as the alumina content of the charge increases. Little difficulty was experienced in one of the more recent tests when an Al-Si alloy analyzing 33 pct Al was produced from a charge of clay and quartz. A continuing operation was maintained when producing an Al-Si alloy, analyzing 49 pct Al, from clay. With more experience, it may be possible to continuously produce alloys containing higher percentages of aluminum.

Acknowledgments

This paper is a report of one of the investigations carried out by the Bureau of Mines, Region II, Albany, Ore., under the general supervision of S. M. Shelton, Regional Director. Credit is due to H. W. St. Clair, former Chief of the Light Metals Branch of the Bureau of Mines for suggesting the project titled "Production of Aluminum-Silicon Alloy."

Discussion of this paper, if any, will appear in JOURNAL OF METALS, November 1955, and in AIME Metals Branch *Transactions*, Vol. **203**, 1955.

References

[1] *Encyclopaedia Britannica*. vol. 1, p. 713.

[2] Societé D Ugine: *The Manufacture of Aluminum-Silicon Alloys*. British Patent 302,692 (Dec. 20, 1927).

[3] C. von Girsewald: *Process for Production of Aluminum-Silicon Alloys Free From Carbide*. U.S. Patent 1,747,197.

[4] M. M. Striplin, Jr. and W. M. Kelly: Aluminum-Silicon Alloys by Electrothermal Reduction of Clay with Coke. *Chemical Engineering Process* (1947) **43**, No. 10, pp. 569-578.

[5] F. C. Frary and A. J. Rice: Electrothermal Production of Aluminum-Silicon Alloy. *FIAT Final Report No. 992* (Nov. 12, 1946).

[6] A. Cunningham: Technology of Aluminum and Aluminum Alloy Production in Germany Including Early Fabrication and Recoveries from Scrap. *FIAT Final Report No. 731* (Feb. 8, 1946).

Table IV. Summary Data on Tests in the Large Smelting Furnace

	Inoperable	Operable
Operating Data		
Length of period, hr	113	209
Charge proportions, lb		
Clay, calcined, Cowlitz	—	100
Clay, raw, eastern	100	—
Alumina	15	—
Coke, 96 pct fixed carbon	16	11
Hogged fuel, 13 pct fixed carbon	200	—
Wood chips, 12 pct fixed carbon	—	216
Carbon in charge, pct stoichiometric	106	102
Electrode voltage, phase-to-phase	48	45
Current, amp, average	5500	5500
Electrode current density, amp per sq in.	109	109
Average power input, kw	410	410
Electrode diameter, in.	8	8
R, ohm, in.	0.12	0.12
Operating Results		
Consumption of ore, lb per hr	190	162
Alloy production rate, lb per hr	20	60
Power consumption, kw-hr per lb of ore	2.1	2.5
Power consumption, kw-hr per lb of alloy	15.2	6.8
Graphite electrode consumption, lb per ton of alloy	475	360
Composition (typical) of alloy, pct		
Aluminum	77*	49
Silicon	22	38
Iron	2.5	9.6
Titanium	0.4	2.4
Alloy recovery, pct	80	196†

* High aluminum content due to formation of silicon carbide, which resulted in tapping only an aluminum-rich fraction.
† High alloy recovery figure attributed to slag inclusions in alloy tapped.

[7] H. Loevenstein: *Process for the Manufacture of Aluminum*. U.S. Patent 2,198,673 (Apr. 30, 1940).

[8] H. W. St. Clair and D. D. Blue: Recovery of Aluminum from Crude Aluminum-Silicon Alloy by Extraction with Molten Zinc. *Report of Investigation 4535* U.S. Dept. of Interior, Bureau of Mines (1949).

[9] E. Mathiey, R. Perrin, A. Gereffe, and S. Cavalier: *Process of Manufacture of Aluminum-Silicon Alloys*. U.S. Patent 1,831,023 (Nov. 10, 1931).

[10] C. von Girsewald and O. Schober: *Production of Pure Aluminum-Silicon Alloys*. U.S. Patent 1,972,432 (Sept. 4, 1934).

[11] R. T. C. Rasmussen: Electric Smelting at Bureau of Mines Seeks Utilization of Northwest Ores. JOURNAL OF METALS (1952) **4**, No. 12, pp. 1273-1279.

[12] F. H. Getman and F. Daniels: *Outlines of Physical Chemistry*. 7th Ed., pp. 115-116. New York. John Wiley & Sons.

[13] M. M. Striplin, Jr. and W. M. Kelly: U.S. Patent 2,448,568 (Nov. 22, 1949).

Kosaka Smelter, The Dowa Mining Co., Japan

Hydrometallurgy of Copper-Zinc Concentrates

by Hidesaburo Kurushima and Suketoshi Tsunoda

An investigation of the hydrometallurgy of Cu-Zn concentrates by The Dowa Mining Co. of Japan is described and a detailed flowsheet of the Kosaka hydrometallurgical plant is given. Sufficient operating experience has shown that the Dorrco FluoSolids system has proven successful for recovery of both zinc and copper by roasting in a fluidized bed. At present, 2400 metric tons of concentrates per month are being treated and recoveries of 93 pct Cu and 65 pct Zn are being effected.

A SURVEY of the Japanese chemical industry in 1949 revealed, among other things, that sulphur-bearing blast furnace gas from the Kosaka smelter of The Dowa Mining Co. Ltd., Kosaka, Japan, was being exhausted to the atmosphere as waste. In addition, it was costing that company an average of ten million yen ($28,000) annually for damages to the surrounding property caused by the sulphur dioxide in the gas. It was recommended by this survey that the gas be utilized for the production of sulphuric acid by the contact process.

Mr. Kurushima visited the United States in May 1950 to investigate the engineering, construction, and operation of a contact acid plant. Any acid produced at Kosaka would necessarily have to be 98 pct H_2SO_4 to prevent corrosion in railroad tank cars transporting it to the point of use. However, the production of 98 pct acid requires constant volume and SO_2 content of the gas. As the converter gas at Kosaka fluctuates in both volume and quality, it was decided to evaluate the smelting process with relation to other methods of recovery.

This evaluation revealed a relatively new type of roaster, the Dorrco FluoSolids reactor, which was reported to be capable of roasting the copper sulphide concentrate in an excess of air with the production of an SO_2 gas strong enough for acid production and a water-soluble copper sulphate calcine. The copper sulphate then could be leached from the roasted ore and electrolytic copper recovered from the leach solution in much the same manner as practiced by the Chile Exploration Co. for treating naturally occuring copper sulphate ores. Use of a reactor of this type would eliminate the need for a blast furnace and converter and, in addition, would effect savings in labor and fuel.

The Kosaka ore is a microscopically fine mixture of copper, zinc, and lead sulphides. The lead and a small amount of the barite present can be separated by flotation, but any separation of copper and zinc proved extremely difficult. In blast furnace operation at Kosaka, zinc had been slagged off until a stockpile of about 12,000,000 tons containing 5 pct Zn had been accumulated. Mr. Kurushima felt that if any of the zinc in the concentrate was sulphatized and leached with the copper, it also could be recovered electrolytically.

The Dorr Co., sponsors of fluidization technique in the metallurgical field, suggested that sulphate roasting be tested out on a laboratory scale and that, if successful, a commercial Dorrco FluoSolids system be constructed. They indicated that the results from such laboratory tests could be transposed to a commercial scale without pilot planting the roasting operation. It was therefore decided to send samples of flotation concentrate to the Westport Mill, laboratories of The Dorr Co., for testing.

Table I. Calcine Solubilities

	Acid Soluble, Pct	Water Soluble, Pct
Cu	98.4	96.3
Zn	95.0	94.6
Fe	4.2	2.7

Table II. Condition of Electrolyte, Copper Section

	Initial State of Bath, G per L	Change, G per L
Copper	60	15 to 17
H_2SO_4	Nil	60
Zinc	100	100
Current (dc) density at cathode		13.1 to 14 amp per sq ft
Consumption of electricity		3600 kw-hr per metric ton of cathode copper
Quality of cathode copper		99.97 pct Co 0.0019 pct Fe 0.0042 pct Zn

The objective of Mr. Kurushima's visit to the United States thus had changed from investigation of sulphuric acid plants to a fundamental examination of the hydrometallurgy of copper and zinc.

Testing Program

In February 1951, Mr. Tsunoda went to the United States to witness the application of the FluoSolids system to sulphate roasting at The Dorr

H. KURUSHIMA and S. TSUNODA, Members AIME, are President and Chief Metallurgist, respectively, The Dowa Mining Co. Ltd., Kosaka, Japan.

Discussion of this paper, TP 3994D, may be sent, 2 copies, to AIME by July 1, 1955. Manuscript, Sept. 21, 1953. New York Meeting, February 1954.

Co.'s laboratory. The flotation concentrates tested analyzed 8.7 pct Cu, 15.4 pct Zn, 21.6 pct Fe, 2.93 pct Pb, 32.7 pct S, and 11.3 pct insoluble. These concentrates were 80.3 pct −200 mesh.

Laboratory tests indicated that copper and zinc of high solubility were present in the calcines produced in the FluoSolids reactor for subsequent leaching. Roasting at 700°C with 50 pct excess air produced calcines which, when leached with 5 pct sulphuric acid and water, yielded the solubilities given in Table I.

Table III. Condition of Solution, Sponge Copper Section

	Initial State of Bath, G per L	Change, G per L
Copper	15 to 17	1.1
H_2SO_4	65	90
Zinc	100	100
Current (dc) density at cathode	15.8 to 18.6 amp per sq ft	
Consumption of electricity	4500 to 5000 kw-hr per metric ton of sponge copper	

The conclusions drawn from these tests were: 1—95 pct of the copper is converted to copper sulphate, 2—90 pct of the zinc is converted to zinc sulphate, 3—5 pct of the iron is converted to ferrous and ferric sulphate, and 4—a suitable roasting temperature is 700°C.

Greatly encouraged by the results of the roasting tests, a further study was undertaken to devise methods for the recovery of the copper and the zinc from the solutions by electrolysis and to secure the data needed for the design of a commercial plant. To secure this information, a 300:1 scale pilot plant was constructed at Kosaka. Tests were made there to secure data on the electrolyses of the copper and zinc, on the purification of the liquor for the elimination of iron, cobalt, nickel, etc., and on the neutralization of the solution.

Table IV. Condition of Electrolyte, Zinc Section

	Initial State of Bath, G per L	Change, G per L
Zinc	100	25 to 30
H_2SO_4	Nil	110
Current density at cathode		37 amp per sq ft
Tank voltage		3.5 v
Ampere efficiency		about 80 pct
Quality of cathode zinc		99.95 pct

Since no published data could be found on the electrolytic recovery of copper and zinc from the mixed solution, it was fortunate that the authors had the guidance of Dr. S. Tokunaga, Director of Mitsui Mining Co., who had operated a plant for the electrolytic recovery of these metals from scrap brass anodes. This part of the process as developed consists, in outline, of 1—the electrolysis of the leach solution of mixed sulphates to obtain sound cathode copper, 2—electrolytic stripping of the solution to remove the final copper as sponge, and 3—purification and electrolysis of the solution to obtain electrolytic zinc.

As a result of the pilot plant tests, the optimum conditions, outlined subsequently, were established as being suitable for the operation of the commercial plant.

Optimum Conditions for Commercial Operation

Copper Electrolysis Section: It was established that the electrolysis of the copper should be carried out under the conditions given in Table II.

Sponge Copper Section: At this point the solution is so depleted in the copper ion that most of the remainder must be removed as sponge copper. Conditions in the sponge section should be as given in Table III.

Zinc Electrolysis Section: After neutralization and purification of the solution, the low acid, low current density method for the recovery of the zinc was used. The optimum conditions for the zinc electrolysis plant were established, see Table IV.

Anticipated Operating Conditions for Commercial-Scale Plant

Upon the completion of successful pilot plant tests, a commercial-scale plant was designed to treat 2400 tons per month of flotation concentrates with an expected average analysis as given in Table V.

From this concentrate, recovery of the products of purities and amounts given in Table VI was anticipated.

The plant was expected to effect yields of 92 pct of the copper and 75 pct of the zinc.

Plant Flowsheet

A detailed flowsheet of the Kosaka hydrometallurgical plant is given in Fig. 1.

Table V. Anticipated Average Analysis of Concentrates

Element	Pct
Copper	10.6
Zinc	16.7
Lead	2.4
Sulphur	39.0
Iron	26.0

Concentrates Handling: The flotation concentrates are produced at the Hanaoka mine, which is situated about 24 miles south of Kosaka. The mill and smelter are connected by a railroad having two different track gages. Flotation concentrates are placed in steel boxes of two-ton capacity and loaded onto standard gage flat cars at the mill. These boxes are transferred to flat cars of the narrow gage railroad at the junction point of the two systems by a crane. On reaching the smelter, the concentrate is dumped into the storage bin.

The concentrates are discharged from the storage bin onto a belt conveyor that leads to a repulper tank where spent zinc electrolyte is added to make up a slurry of about 75 pct solids. This slurry is charged into the FluoSolids reactor by a Moyno pump.

Table VI. Anticipated Recoveries

Electrolytic copper (99.98 pct Cu)	237 metric tons per month
Electrolytic zinc (99.98 pct Zn)	303 metric tons per month
Metallic cadmium	1500 kg per month (under construction)
Chemically precipitated gypsum, as a byproduct	1700 tons per month

Roasting: The Dorrco FluoSolids reactor, 20 ft ID by 16 ft high, roasts the concentrates at 700°C, and an automatic control holds this temperature within ±5°C. Roaster gas, containing fine dust, passes to a waste heat boiler for heat recovery and then to a two-stage cyclone and Venturi scrubber system for recovery of the fine dust. Calcine product weight distribution is as follows: reactor over flow, 48 pct; waste heat boiler, 19 pct; cyclones, 28 pct; Venturi scrubber, 4.75 pct; and stack loss, 0.25 pct.

The reactor overflow, waste heat boiler, and cy-

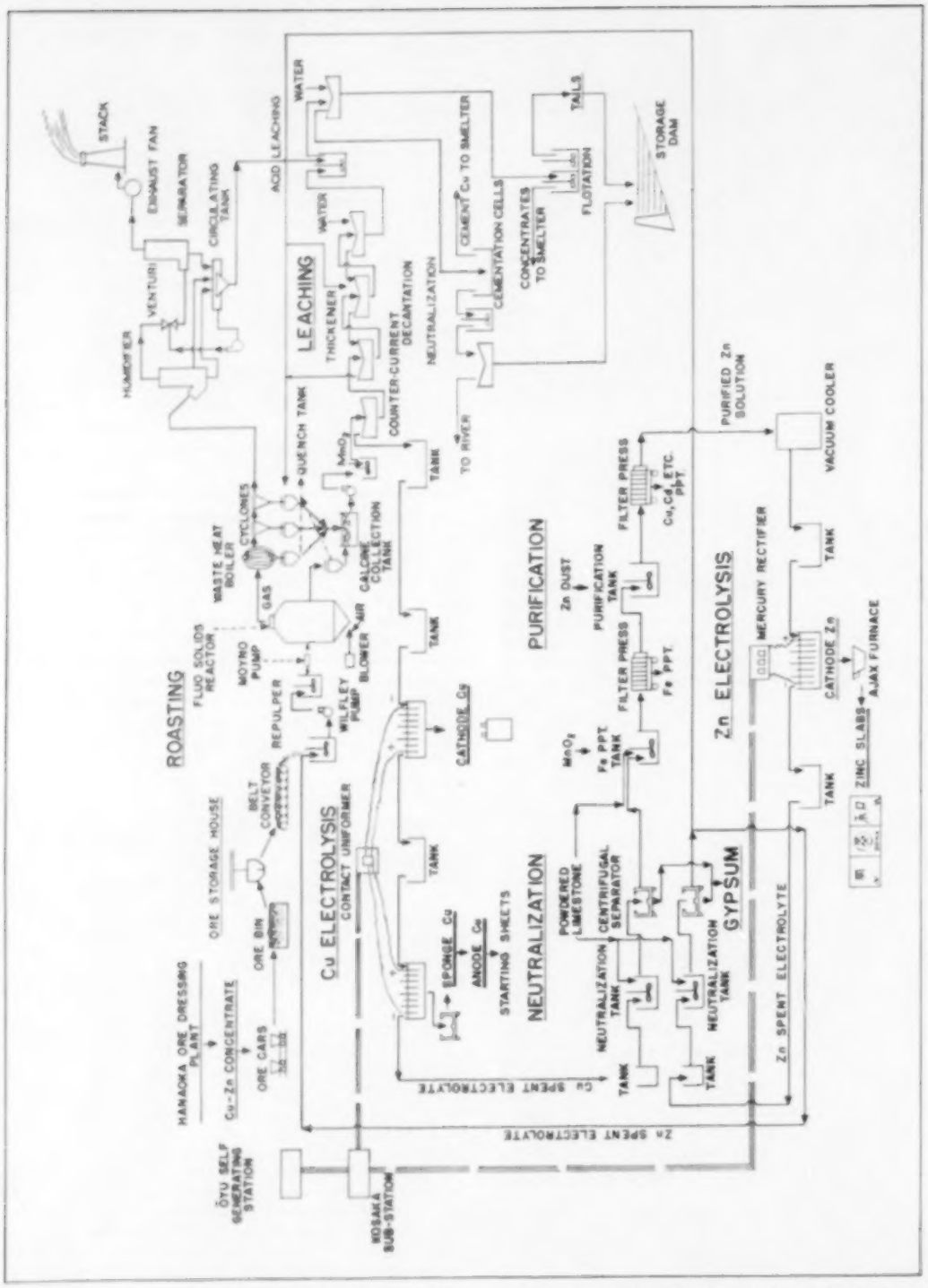

Fig. 1—Flowsheet of the Kosaka Hydrometallurgical Plant, The Dowa Mining Co.

clone products are caught in quench tanks and flow by gravity to a collection tank from which they are pumped to the leaching circuit. The solution added to the quench tanks is taken from the overflow of the secondary thickener in the residue washing circuit. The scrubber product is treated separately.

The waste heat boiler, with a capacity of 6600 lb steam per hr, supplies all of the heat required for leaching, zinc purification, etc.

Leaching: Two separate leach circuits are used. In the primary circuit, solids collected from the reactor overflow, waste heat boiler hoppers, and the cyclones, amounting to 95 pct of the total solids, are given a 5 hr leach at 70°C in a series of three

Table VII. Copper Tank House Data

	1st Stage*	2nd Stage	3rd Stage (Sponge Copper)
Current density, amp per sq ft	10.9	8.5	24.5
Cell voltage, v	2.5	2.2	3.7
Electrolyte flow, gal per min	4.25	2.64	1
Copper in feed solution, g per l	54	25	12
Copper in spent solution, g per l	25	12	1
Temperature of electrolyte, °C	50	43	60
Number of cells	40	50	40
Cell size, ft	10.6x2.8x3.4	6.0x4.0x3.9	10.6x2.8x3.4
Anode size, in.	25.6x30.3x0.3	18.1x28.0x0.3	25.6x30.3x0.2
Cathode size, in.	28.4x31.4	20.5x29.5	25.6x27.6
Number of anodes per cell	24	22*	14
Number of cathodes per cell	23	20*	13
Anode spacing, in.	4.7	3.1	6.0
Kw-hr per metric ton Cu, ac	2600	2300	3100
Current efficiency, pct	82	80	80
Electrical system	Walker	Thophan	Walker
Holding time, days	7	14	5
Weight of cathode, lb	72	38	—
Percentage of total copper	54.7	24.5	20.8
	Copper Analysis		
Cu, pct	99.97	99.97	70 to 80
Pb, pct	Trace	Trace	—
Zn, pct	Trace	Trace	4
Fe, pct	0.0030	0.0030	0.4
S, pct	0.0050	0.0045	—
Bi, pct	Trace	Trace	—
Au, g per ton	0.05	0.05	0.2
Ag, g per ton	4	4	22
Sb, pct	0.0005	0.0005	0.34
Ni, pct	Trace	Trace	—
As, pct	Trace	Trace	2.37

* Two sets of cathodes and anodes per cell.

wooden agitators equipped with acid-proof mechanisms. Pulverized manganese ore, 60 pct MnO_2, is added to the primary agitator at the rate of 200 lb per hr for precipitation of iron. Acid strength at the start of leaching is 5 to 7 g per l and decreases to 2 g per l in the final agitator.

Solids collected in the Venturi scrubber plus residue from the primary circuit are leached together in the secondary circuit where they are given a 4 hr leach at 70°C with 50 g per l sulphuric acid solution which is collected in the Venturi scrubber.

Overall leach solubility is 94 pct Cu and 88 pct Zn.

Solution and Residue Treatment: Solution and residue in the main circuit are separated in a four-stage Dorr countercurrent decantation system. As an aid to washing, some of the neutralized solution from the zinc tank house, containing 27 g per l Zn, is added to the second-stage thickener and fresh water is added to the fourth stage. The solution from the primary thickener is sent to the copper tank house after clarification at the following analysis: 54 g per l Cu, 100 g per l Zn, and 2 g per l Fe.

Residue from the final thickener of the countercurrent decantation circuit is pumped to the secondary leaching tank where it joins the pulp from the scrubber. The solution from the single-stage washing thickener used in this circuit is sent to iron cementation cells for recovery of the copper. The solution from the cementation cells is then neutralized and discharged into the river. The cement copper recovered in this circuit is refined in the smelter. The residue from the single-stage washing thickener passes through a conditioner and 12 flotation cells where a scavenger concentrate is made. In the flotation step, 20 pct of the gold, 60 pct of the silver, 30 pct of the copper, and 60 pct of the zinc values of the residues are skimmed off and sent to the blast furnace for recovery of the precious metals and the copper. The flotation tailings are pumped to a storage dam where they are being held for future utilization, a problem now being investigated. The washed residue contains 1.0 pct Cu, 2.0 pct Zn, and 40 to 45 pct Fe. Washing efficiency is 98 pct for the copper and 95 pct for the zinc. The pregnant solution is clarified before going to copper electrolysis.

Electrolysis of Copper: Copper electrolysis is carried out in three stages with insoluble hard lead anodes containing 5 pct Sb. Cathode copper is produced in the first two stages and sponge copper is produced in the third stage. The sponge copper is sent to the pyrometallurgical section where it is smelted and cast into anodes.

Starting sheets are made from soluble anodes. The copper starting sheet blanks, 2 mm thick, are coated with oil and soap solution. After 20 hr of plating, the starting sheets are stripped from the blanks, cut to size, and the hangers are then attached. For copper tank house data, see Table VII.

Cathodes in the sponge copper section are made of lead plate. Equal weights of gum arabic and thio-urea are added to the first and second sections as follows: No. 1 section, 60 g per metric ton of cathode, and No. 2 section, 12 g per metric ton of cathode. In addition to the foregoing reagents, a nonsoluble higher alcohol is added to the cells to control acid mist. The five rows of cells in the secondary copper circuit are arranged in a parallel wiring or Thophan system. Dc power at 250 v, 6000 amp is supplied by a 1500 kw contact converter manufactured by Fuji Denki Co.

Spent Solution Neutralization and Precipitation of Values: Solution leaving the copper tank house contains 1 g per l Cu, 100 g per l Zn, and 90 g per l H_2SO_4. Solution neutralization and iron precipitation by adding pulverized limestone is carried out in tanks. The precipitated gypsum thus produced is separated from the solution by centrifuging. The copper, cadmium, nickel, cobalt, etc., are removed by the addition of zinc dust and β-naphthol. The purified solution, before going to zinc electrolysis, is cooled to 20°C by means of a vacuum cooler.

Electrolysis of Zinc: Zinc electrolysis is carried out at 36° to 38°C with insoluble lead anodes containing 1 pct Ag. Solution enters the zinc tank

house at 100 to 110 g per l Zn at 20°C. The fresh solution is run into a circulation tank and mixed with cell solution to give the necessary acid strength. Electrolysis starts at about 50 g per l Zn and 70 g per l H_2SO_4. The cells are flat setting rather than a cascade arrangement. This solution is circulated at 3.25 gal per min until electrolysis is finished at 27 g per l Zn and 110 g per l H_2SO_4.

Table VIII. Zinc Tank House Data

Current density, amp per sq ft	37.5
Cell voltage, v	3.4 to 3.7
Electrolyte flow, gal per min per cell	3.25
Zinc in feed solution, g per l	100 to 110
Zinc in spent solution, g per l	23 to 27
Temperature of electrolyte, °C	36 to 38
Number of cells	130
Cell size, ft	2.3x6.2x1.9
Anode size, in.	20.4x30x0.2
Cathode size, in.	22.0x29.5x0.12
Number of anodes per cell	14*
Number of cathodes per cell	12*
Anode spacing, in.	4.7
Kw-hr per metric ton zinc, ac	4700
Current efficiency, pct	77
Electrical system	Walker
Holding time, hr	24
Weight of cathode, lb	13 to 18
Slab Zinc Analysis†	
Zinc, pct	99.98
Lead, pct	0.005 to 0.01
Iron, pct	0.0007 to 0.0011
Cadmium, pct	Trace to 0.001

* Two sets of cathodes and anodes per cell.
† The cathode zinc is melted in an Ajax Wyatt electric furnace and cast into slabs for the market.

Power to the zinc section is supplied by single pole mercury rectifiers. No smoothing reagents are used in the zinc tank house but soy bean cake is added to the cells at the rate of 270 g per metric ton of cathode for control of acid mist. Zinc tank house data may be found in Table VIII.

Initial Operating Problems and their Solution

Plant erection was started in April 1952 and completed in November of the same year. During the following months of operation, difficulties were encountered that occurred despite the time and effort expended on pilot plant testing in order to hold these troubles to a minimum. At times these troubles curtailed production and at other times it has been necessary to shut down to make corrections. Despite these difficulties, it is felt that sufficient experience has been gained so that the new process may be called a success.

Tank Leakage: The first trouble encountered was tank leakage. Many of the solution tanks and the thickeners were made of asphalt-lined concrete. Very shortly after the start of operations, leakage of solution from some of these tanks was detected. This leakage was highly troublesome, not only because of the loss of values but also because the acid could cause serious corrosion of concrete and reinforcing steel. The asphalt lining was applied to the tanks at the beginning of winter at Kosaka and the sudden cooling of the melted asphalt caused cracks that were difficult to locate. The leaky tanks could not be relined until warm weather set in and this caused some delay. This problem has now been corrected.

Precipitation of Gypsum in Pipe Lines: The second problem was caused by the precipitation of gypsum. In the process, the gypsum-saturated spent electrolyte is circulated and, on cooling, deposited solid gypsum in the pipe between the leaching section and the copper tank house and also in the vertical pump in the solution sump. This problem was overcome by replacing the pipe lines with open launders that could be inspected easily and any deposit found promptly scraped off. In places where it was not possible to install open launders, double pipe has been laid with one pipe held as a spare. The deposition of gypsum had been anticipated but the rapidity, quantity, and location of this scale was far beyond expectations.

Corrosion of Stack Interior: The third problem is associated with the exit gas from roasting. If an acid plant had been installed, this difficulty would never have been encountered. An acid plant was not installed originally because of the large investment needed, the uncertainty as to the quantity and quality of the gas, and the problem of the transportation of the sulphuric acid. The most important reason was difficulty of a financial nature, since many members of the staff, even including the metallurgical experts, had expressed a great deal of anxiety about this new process. As it was expected that this gas would be used after a few years, a temporary stack, 200 ft high, 4 ft diam at the top, and built of reinforced concrete, was installed. The lower 73 ft of the stack was lined with acid-proof brick. The exhaust gas from roasting contains 5.5 pct SO_2, and in full operation the volume is 154 cfs.

Six months after the start of operations the bottom of the stack was found to be nearly closed from corroded concrete fragments that had fallen from the top of the stack. Inspection of the stack revealed that corrosion was so bad at the top that some of the reinforcing bars were exposed. This corrosion was caused by the presence of SO_3 and water vapor in the gas.

To correct this problem, it was decided to erect a new stack, lined with acid-proof porcelain brick, and to install one of the Chemical Construction Co.'s Venturi scrubbers which removes most of the SO_3 and dust. Also, to eliminate the smoke damage problem, a fan capable of introducing 35,000 cfm air into the stack was installed. By air dilution, the stack now delivers 1 pct SO_2 gas at 50 fps and smoke damage should no longer be troublesome.

Conclusions

Certain operating difficulties have been encountered which at times have made it necessary to shut down or reduce capacity while corrections are being made. Nevertheless, sufficient experience has been obtained to justify the statement that the Dorr FluoSolids system has been a success at the Kosaka plant of The Dowa Mining Co.

Formerly, effective roasting of mixed Cu-Zn-Fe sulphides to produce highly soluble copper and zinc was considered to be extremely difficult because of the difference between the formation or decomposition temperatures of copper and zinc sulphates. This operation has proved that it is possible to recover both the copper and zinc by roasting in a fluidized bed. It is the authors' opinion that the closely controlled atmosphere and temperature within the reactor, that are not obtainable in other types of roasters, are responsible for the ability to secure a strong SO_2 gas for acid manufacture and a highly water soluble calcine of copper and zinc sulphate for treatment in the electrolytic sections.

At the present time, The Dowa Mining Co. is treating 2400 metric tons of concentrates per month and obtaining 93 pct Cu and 65 pct Zn recoveries.

Discussion of this paper, if any, will appear in JOURNAL OF METALS, November 1955, and in AIME Metals Branch *Transactions*, Vol. **203**, 1955.

Topochemical Aspects of Iron Ore Reduction

by Gust Bitsianes and T. L. Joseph

The gaseous reduction of dense iron ore is a topochemical process in which reduction takes place at distinct interfaces between solid phases or layers. Under normal conditions, these interfaces remain parallel to the exterior surface of the ore body as they move inward. Certain conditions, such as cracking, high porosity, impurities, entrapped residual oxides, may cause departures from normal topochemical behavior.

THE gaseous reduction of dense iron ore proceeds at interfaces between several solid phases or layers.[1,2] Under normal conditions, these interfaces progress inward and remain parallel to the exterior surface of the ore body. This topochemical behavior is clearly illustrated in Fig. 1 which shows partially reduced specimens of natural and synthetic hematite.

Using a coordinated sequence of macro, micro, and X-ray examinations, the authors[3-6] found that the number of interfaces and participating phases was in agreement with the Fe-O system. Above 570°C, reduction of the ore involved a maximum of three common boundaries between four solid phases: iron, wüstite (Fe_xO), magnetite (Fe_3O_4), and hematite (Fe_2O_3). Below 570°C, reduction proceeded through two interfaces between three phases: iron, magnetite (Fe_3O_4), and hematite (Fe_2O_3). The decrease in the number of phases below 570°C was due to the instability of wüstite below this temperature.

The sequence of phases was also consistent with the equilibrium requirements. For example, the layers of iron oxides that were formed in topochemical fashion were always orientated in the order of increasing oxygen content. Thus, in Fig. 1 an outer layer of metallic iron is followed in turn by a thick intermediate band of black wüstite, by a thin layer of light magnetite, and finally by a relatively large core of hematite. This arrangement of the oxide layers was due to restrictions in reducing conditions which were imposed by the physical structure of the solid. The highly reducing gas on the outside of the particle gradually lost its reducing power as it penetrated into the specimen.

On a macro scale, the layers of the various oxides appeared to be sharply defined and uniform in composition. Microexamination of the sections, however, revealed that the interfaces did possess measurable *widths* which varied with the porosity and chemical activity of the oxide phase undergoing reduction. For example, Fig. 2 shows three interfaces in a dense hematitic ore which was partially reduced at 850°C. At the iron-wüstite interface where the greatest porosity developed, the reaction proceeded over a zone 25 to 30 microns in width. Toward the interior, the interfaces became progressively narrower until at the magnetite-hematite boundary the reaction zone was about 1 micron wide. In this region the structure was exceedingly dense; the hematite possessing a porosity on the order of 3 pct.

G. BITSIANES and T. L. JOSEPH, Members AIME, are Assistant Professor and Professor of Metallurgy, respectively, School of Mines and Metallurgy, University of Minnesota, Minneapolis.

Discussion of this paper, TP 3934C, may be sent, 2 copies, to AIME by July 1, 1955. Manuscript, June 30, 1954. Blast Furnace, Coke Oven, and Raw Materials Conference, Chicago, April 1954.

A careful micro study across polished layers of the various oxides revealed generally homogenous and single-phase structures. As reported in a previous paper,[7] the wüstite layer was characterized by an increase in oxygen content with depth of penetration.

The topochemical behavior of reduction was studied in six types of ore of different origin, composition, and physical structure. In most cases, reduction proceeded at the boundaries of well defined layers or phases, and this behavior may be regarded as normal for most dense fine grained ores.

Deviations from Ideal Topochemical Behavior

A number of deviations from the normal topochemical behavior were noted. In these cases, the continuity of the reduction interfaces was disrupted in one of four ways:

1—*Cracking* of the specimen interrupted the geometric configuration, and the interfacial advance was no longer parallel to the exterior surface.

2—As a result of *high porosity*, the interfaces were spread over an appreciable distance and all but obliterated.

3—*Impurities* in the ore promoted a variety of deviations, including cracking.

4—A *residual oxide phase* was entrapped in the reaction product and left behind the advancing macro interface.

Results from Cracking: A crack leading into the interior of an ore specimen presents a path of least resistance for the counter-flow of reducing gases and gaseous reduction products. Higher reducing conditions can be maintained along such cracks and reduction accordingly will propagate well ahead of the normally advancing reduction interfaces.

Cracking was caused by a number of factors, one of which was the thermal spalling of impurities in the massive form. A more general type of cracking was due to reduction and was found in all dense varieties of natural and synthetic hematite, particularly in the temperature range of 500° to 700°C. The effect is shown clearly in Fig. 3. In this case, a dense sphere of pure hematite was partially reduced at 650°C for 100 min. The macrosection shows that one large reduction crack had penetrated the specimen and disrupted the normal topochemical advance of the interfaces. The outer layer of iron was only slightly affected but the thin dark layer of wüstite, adjacent to the ferrite, had widened perceptibly as it progressed along the crack. Farther inward, the magnetite layer was greatly disrupted and had penetrated irregularly to form islands of unaltered white hematite. A great deal of internal cracking is evident in the magnetite phase.

From a practical point of view, the cracking of dense ores in the blast furnace could lead to desirable as well as undesirable effects. The general result

would be a decrease in particle size and a more complete reduction in the upper reaches of the furnace. Excessive cracking, however, could increase the amount of fines and the rate of dust production.

Effect of Porosity: The effects of porosity on the topochemistry of reduction are similar to those of cracking. In the extreme case of an infinite amount of cracking, each iron oxide grain is separated from its neighbor and the reduction system is actually the same as one of high porosity. The reducing gas can diffuse around the individual oxide grains and create a reducing atmosphere over a finite depth of penetration. Under these conditions, well defined and continuous macro interfaces will not form and the actual interface will be spread over an appreciable distance. Within this reaction zone, each individual grain may act as a minute topochemical system. The macrostructure of such a system is shown in Fig. 4. This porous hematite was partially reduced in hydrogen and the resulting structure shows a wide deviation from an ideal topochemical state. At the magnification of 4.5 diameters, a peripheral band of iron is apparent, but its boundary with the interior oxide material is not sharply defined. Fig. 5 shows the interior of the specimen near its geometric center at high magnification. Evidently several waves of reduction had swept through the specimen and reduced the interior to a lacelike network of wüstite grains. Conditions in some areas of the interior had favored the selective reduction of certain wüstite grains to metallic iron.

Two reasons may be advanced for such a selective type of reduction: 1—Because of uneveness in the porosity of the specimen, hydrogen could have built up to a higher reducing potential near certain crystalline aggregates. 2—From the viewpoint of chemical kinetics, certain of the wüstite grains could have been more reactive than others.

Porosity effects in the reduction of iron ores have been studied by Joseph[3] who found a distinct correlation between increased porosity and increased reducibility. With dense ores, the internal reduction reactions are restricted to narrow interfaces with a relatively small amount of surface available to the gaseous reducing agent. The porous ore, however, allows the reactions to proceed over zones of considerable depth and thus over a proportionately larger surface. This increased reaction surface in the interior of porous ores is a big factor in increasing their overall reducibility.

Effect of Impurities: Impurities may play a role in the topochemism of reduction but their effect is quite varied. Quartz, for instance, behaves as an inert impurity and will produce some physical disturbances such as cracking, but only if it is present in the massive form. During normal reduction, neither the temperature nor the time is sufficient for the silica to react with any of the iron oxides. The microexamination of ore 8B in Fig. 2 shows many interlocked silica inclusions but none of these had reacted with any of the oxide phases or had any other substantial effect on the progress of reduction. Another clear-cut case of inert impurity behavior is shown in Fig. 6 which depicts the magnetite-hematite interface in partially reduced dense India ore. The silica inclusions here are of a dendritic nature

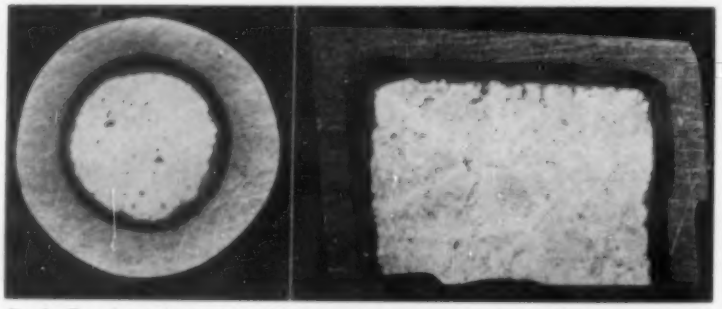

a—Sample of synthetic ore sphere 7, partially reduced in hydrogen at 750°C for 40 min and etched. X4.5. Area reduced approximately 35 pct for reproduction.

b—Specimen of natural dense ore 8A. Half section of rectangular prism, partially reduced at 850°C for 35 min and etched. X4.5. Area reduced approximately 35 pct for reproduction.

Fig. 1—Topochemical aspects of dense ore reduction are illustrated by the two examples of partially reduced specimens of natural and synthetic hematite.

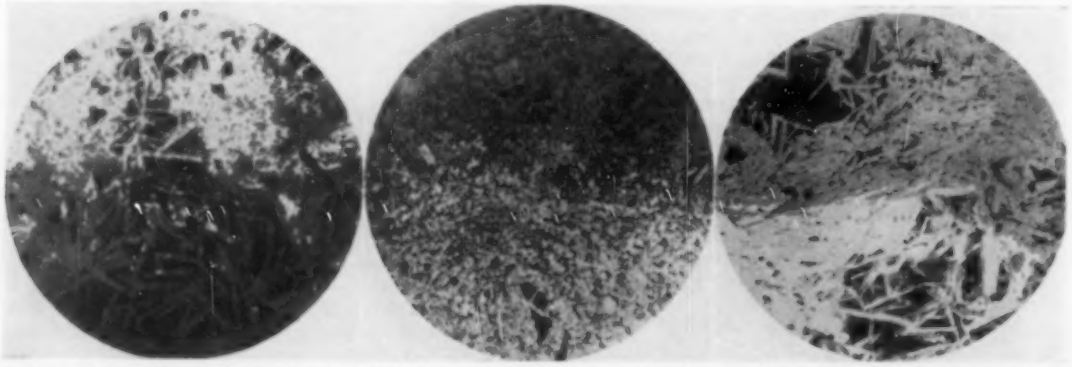

a—Iron-wüstite interface. White phase is iron; dark-gray phase, wüstite; and black inclusions, silica.

b—Wüstite-magnetite interface. Dark-gray phase is wüstite and light-gray phase, magnetite.

c—Magnetite-hematite interface. Light-gray phase is magnetite; light phase, hematite; and black inclusions, silica.

Fig. 2—Three reduction interfaces of natural ore 8B are shown. The specimens were reduced in hydrogen at 850°C for 35 min and etched. X500. Area reduced approximately 35 pct for reproduction.

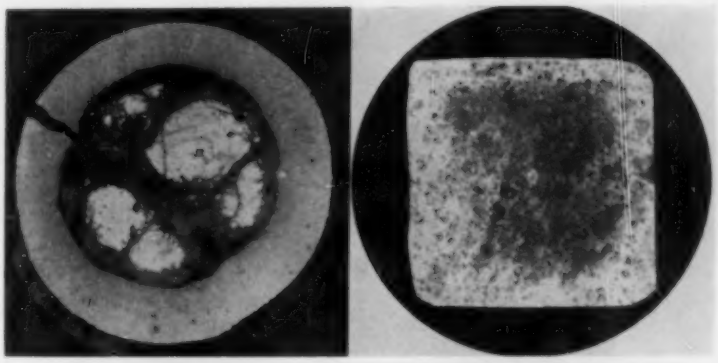

Fig. 3—Effect of cracking is clearly shown in this macrostructure of synthetic ore sphere 15. Specimen was reduced in hydrogen at 650°C for 100 min and etched. X4.5. Area reduced approximately 25 pct for reproduction.

Fig. 4—Macrostructure of porous hematite ore is shown. Specimen was reduced in hydrogen at 850°C for 10 min and etched. X4.5. Area reduced approximately 25 pct for reproduction.

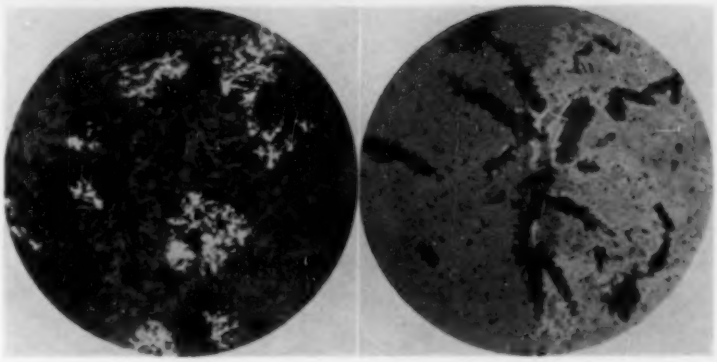

Fig. 5—Micrograph, taken near cube center, shows interior of specimen of partially reduced porous ore. Sample etched. White phase is iron; gray phase, wüstite; and black area, plastic filling representing pores. X500. Area reduced approximately 25 pct for reproduction.

Fig. 6—Magnetite-hematite interface of dense India iron ore is depicted. Specimen reduced in hydrogen at 850°C for 40 min and etched. Gray phase is magnetite; white phase, hematite; and black inclusions, silica. X500. Area reduced approximately 25 pct for reproduction.

and do not appear to have had any direct influence on the progress of reduction.

Impurities may also exist in iron oxide material in the combined form or as an integral part of the oxide lattice. Magnetite, in particular, possessing a spinel type of structure may contain foreign atoms as substitutes in the ferrous and ferric ion positions of its lattice. The effect of such impurities on the progress of reduction is not well known. From an equilibrium point of view, Schenck, Franz, and Willeke[4] have shown that foreign oxides such as MgO, MnO, CaO, ZnO, Al_2O_3, etc., can combine with the iron oxides under certain conditions and that these combinations drastically upset the conventional equilibrium conditions and the reducibility of the products formed. However, little information is available concerning the effects of such impurities on the kinetics of reduction.

Some partially reduced Arkansas lodestone is shown in Fig. 7 and illustrates the effect of combined impurities on reduction. The polished section of this species of magnetite revealed a uniform phase structure with not more than 2 to 3 pct of foreign matter as distinct and separate minerals. Its chemical analysis, however, indicated 20 pct of impurities, most of which must have been present as an integral part of the magnetite lattice. On being reduced, the specimen formed an irregular layer of white iron at its periphery. Reduction also occurred along cracks and fissures of the ore as shown by the gray wüstite and white iron phases within the basic magnetite structure. An X-ray examination of zones *A*, *B*, *C*, and *D* of the specimen clearly established these phase relationships.

Microexamination of the specimen gave the results shown in Fig. 8. A portion of the iron layer has an unusual appearance in that the ferrite is agglomerated into masses of small and distinct spheroids, Fig. 8a. These spheroids were probably kept from intergrowing by the precipitation of oxide impurities from the spinel type of lattice during reduction. In a section located at one of the interior cracks of the specimen, iron, wüstite, and magnetite are seen to be oriented in the proper topochemical order with respect to the crack, Fig. 8b. Even with the porous type of iron layer that had formed and with the effects of cracks and fissures as shown, this lodestone reduced very slowly. This resistance to reduction could be attributed to some effect of the impurities in the magnetite lattice.

Effect of Residual Oxide: The final deviation noted was that of incomplete reduction at the iron-wüstite interface. Certain of the larger and more inert wüstite grains reduced slowly, so that the sponge iron that formed around them had time to undergo a definite sintering action. The sintering action encased these grains of wüstite with ferrite, retarded their reduction at the moving iron-wüstite interface, and permitted their retention well out into the iron layer. At the same time a large amount of

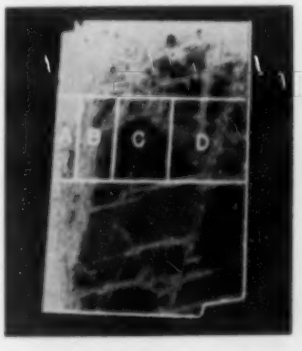

Fig. 7—Macrostructure of partially reduced Arkansas lodestone is shown. Sample was reduced in hydrogen at 850°C for 120 min and etched. *A*, *B*, *C*, and *D* are zones, examination of which established phase relationships. X6.

a—Microstructure of the outer iron layer. Specimen shows porous iron sponge with dark areas of reduction porosity.

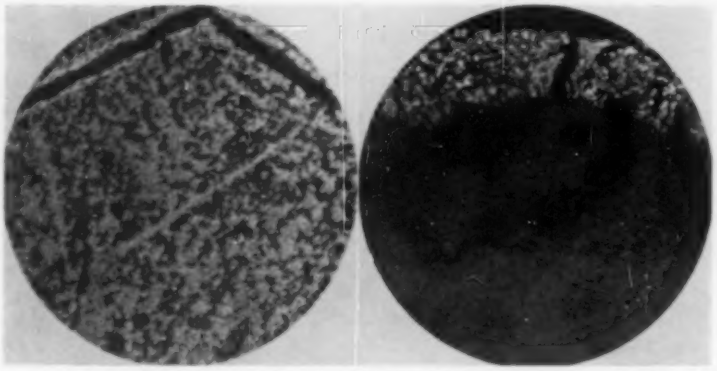

b—Micrograph shows reduction on an interior crack. Porous sponge iron bounds crack surface; dark wüstite follows and is bounded by light-gray magnetite.

Fig. 8—Microexamination of partially reduced Arkansas lodestone gave the results shown in *a* and *b*. Specimen was etched. X500. Area reduced approximately 25 pct for reproduction.

Fig. 9—Iron-wüstite interface of synthetic ore (cylinder No. 9) is depicted. Sample reduced in hydrogen at 850°C for 70 min and etched. White phase is iron; gray phase, wüstite; and black areas, pores. X500. Area reduced approximately 25 pct for reproduction.

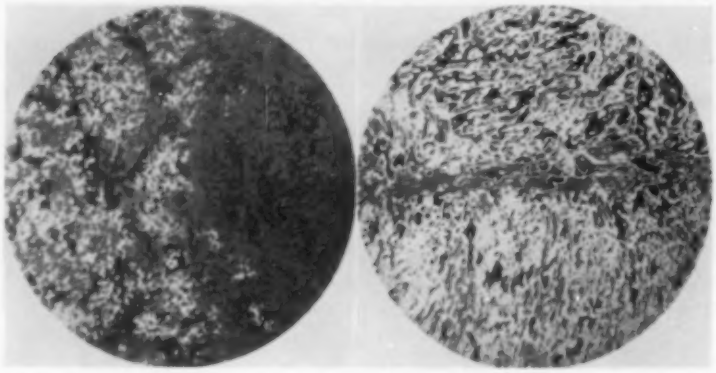

Fig. 10—Micrograph shows structure of sponge iron layer in Elba crystal mass. Specimen reduced in hydrogen at 850°C for 20 min and etched. White phase is iron; gray phase, wüstite; and black areas, pores. X500. Area reduced approximately 25 pct for reproduction.

reduction porosity was formed. A typical case is shown in Fig. 9 which depicts the iron-wüstite boundary condition in a partially reduced cylinder of chemically pure hematite. Another such case is illustrated in Fig. 10 which shows some wüstite retention in the iron layer of a partially reduced mass of single hematite crystals from Elba. Such sintering action and its consequent effects have been observed to be more prevalent in the purer iron layers resulting from the reduction of pure oxide materials.

Wüstite Retention Effect on the Rate of Magnetite Reduction

An exaggerated case of the *wüstite retention* effect was found to occur in a species of New York magnetite. This ore was characterized by a fissured-type structure, and its magnetite fraction was well crystallized and of a relatively pure composition. On being reduced in hydrogen, the ore exhibited a strange anomaly in reduction behavior. The effect is shown in Fig. 11 which summarizes the rate data as obtained for this ore by Wernick and Bitsianes.[3] Rates of reduction are expressed as "the time to reach a definite percentage of reduction." The data for the 40 pct curve show clearly that the reduction rate had followed a normal increase with temperature in the earlier stages of the process. In the later stages of reduction (80 pct data), the rate increased with temperature up to about 600°C and then diminished markedly to an extremely slow rate at about 800°C. Analysis of these data implies that some processes had occurred to create a *rate minimum* condition between 650° and 900°C. This same rate anomaly has been noted by Udy and Lorig[4] in New Jersey magnetite, by Specht and Zapffe[5] in New York magnetite, by Wiberg[6] in Kiruna magnetite, and by Chufarov and Tatievskaya[7] in a species of Russian magnetite. Some reference has been made to the rate effect as a *rate maximum* condition for magnetite at 600°C, but this conclusion was reached without the benefit of rate data above 800°C. There has also been a tendency to associate the anomaly with the behavior of magnetite in general, but certain grades of magnetite such as the Arkansas lodestone and western magnetites do not show a rate minimum.

In the present investigation, a rough block of the New York magnetite was reduced in hydrogen at 850°C for a period of 2 hr. The reducing conditions were chosen to produce a specimen which would be reduced to a point well within the minimum rate field. From the macro result shown in Fig. 12, it is evident that the reduction behavior had been quite

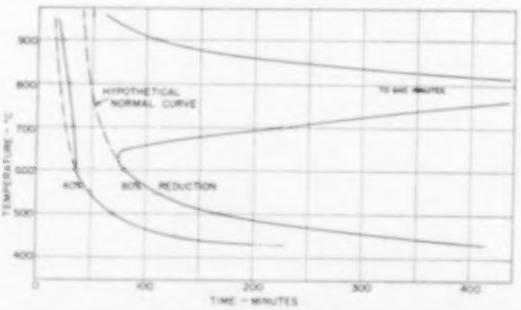

Fig. 11—Curves show the reduction rates of New York magnetite as a function of temperature. −6+8 mesh material was reduced in hydrogen.

different from that encountered previously. A rough topochemical shell of white metallic iron is seen penetrating the specimen at its periphery. Beyond this shell, the reduction had propagated into the interior through countless fissures. The penetration had been surprisingly uniform, so that fine stringers of iron are seen to be evenly distributed throughout the interior of the specimen.

An X-ray examination showed that the outer layer was composed entirely of iron while the interior was a mixture of iron and wüstite. More information was gained from a microexamination. Fig. 13a shows an interior portion of the specimen at X250 and the microstructure is most unusual. Without exception, the large grains of wüstite were coated by thin films of iron 2 to 3 microns in thickness. This coating was apparent along every visible fissure, pore, and hole within the interior of the specimen. At the higher magnifications, the layers of iron appeared to be extremely dense and to have encased the unreduced wüstite grains with a solid ferrite coating, Fig. 13b. Within the iron shells, the wüstite was present as an exceedingly dense phase similar to that of the original magnetite. There is some question as to whether these wüstite grains were in the form of single crystals.

The macro, micro, X-ray, and kinetic studies correlated well in showing that the reduction had started out in a normal fashion but had deviated into an abnormal behavior after about 40 pct of the process had been completed. These two stages will be considered in turn.

Normal Behavior in the Early Stages of the Reduction of Magnetite

In this period, the original magnetite was reduced to wüstite without any adverse kinetic effects. The wüstite at the surface of the specimen also began to reduce and form metallic iron in a normal topochemical fashion. A study of the kinetic data for this specimen reveals that the normal period was completed within the first 30 min of the run and under rate conditions which were 50 pct slower than those found for natural dense hematite ore. On a relative basis, this was not a great difference in rate and could be attributed to the dense and coarse grained structure of the magnetite and resulting wüstite phases.

Abnormal Behavior in the Later Stages of the Reduction of Magnetite

Only the iron and wüstite phases were present during the abnormal period of reduction and the anomaly can be attributed to the following effect on the conversion of wüstite to iron: Near the end of the normal period, the dense wüstite phase was reducing slowly enough so that relatively large amounts of hydrogen could diffuse past the macro interface, through the many fissures, and into the interior of the specimen. A sufficient concentration of hydrogen thus built up in the interior to reduce all the available wüstite surfaces to metallic iron. Further reduction of the dense wüstite grains was so slow that their thin surface layers of pure sponge iron could sinter into relatively impermeable coatings. The outward diffusion of oxide ions or water molecules through such coatings was necessarily a very slow process. As a result, the rate of reduction of the New York magnetite at 800°C was *one-tenth* of the rate at 600°C, see Fig. 11.

The hydrogen reduction anomaly has been shown to be actually an exaggerated case of the wüstite retention effect mentioned previously. In practical application, this retention of wüstite phase could have an important bearing on the manufacture of pure sponge iron products from magnetite ores or concentrates. In carbon monoxide reduction, the effect has not been found to be as serious. Wiberg[9] has studied the relative behavior of hydrogen and carbon monoxide on Kiruna magnetite at 1000°C and has concluded that iron film formation is minimized with the carbon monoxide reductant. His theory is based on the large pressures that can be generated at the iron-wüstite interface due to the equilibrium requirements of the Fe-C-O system. These pressures have been calculated to approach 40 atm at 1000°C and could conceivably rupture any thin films of iron.

Differences in the Rates of Magnetite and Hematite Reduction

Hematite ores generally reduce more rapidly than magnetite ores or sinters. Actually, the hematite phase must pass through the magnetite stage during reduction, and it might be inferred that a hematite ore should reduce more slowly than one composed of magnetite. In considering this question, Bitsianes[10] has concluded that the following physical and chemical factors are important:

1—The grain size of magnetite ore is usually coarser than that of hematite ore. When dense ore bodies are considered, this difference in grain size along with other factors may have a profound effect on the mechanisms and rates of reduction. In coarse grained magnetite, for instance, the reduction reactions are restricted to extremely narrow interfaces with a relatively small amount of internal reduction surface. These ores thus reduce more slowly than fine grained hematitic ores in which reduction porosity causes the interfaces to spread out and create a larger amount of internal reaction surface.

2—The crystallographic orientation of the oxide surface being reduced may have an effect on the reduction mechanisms. Hydrogen molecules would behave differently in bombarding and initiating reactions on a lattice surface of cubic magnetite as compared to that of hexagonal hematite. Moreover, the lattice surface of natural magnetite could react differently than that of artificial magnetite produced by gaseous reduction of hematite at elevated temperatures.

3—Even more important is the matter of crystallographic orientation in the reduction products as they are being formed. In reducing magnetite to iron, Buinov and his coworkers[11] found the orientation relationships to be the same as those found by Mehl and McCandless[12] for the oxidation of iron. These relationships are such that the conversions of magne-

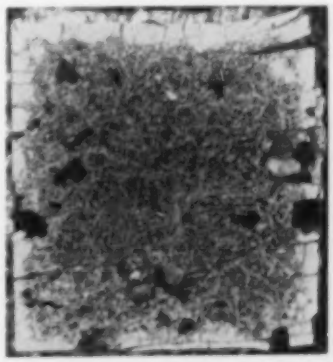

Fig. 12—Macrostructure of New York magnetite is shown. Specimen was reduced in hydrogen at 850°C for 120 min and etched. X4.5.

a—Unreduced core is shown. White phase is iron; gray phase, wüstite; and black areas, fissures. X250. Area reduced approximately 25 pct for reproduction.

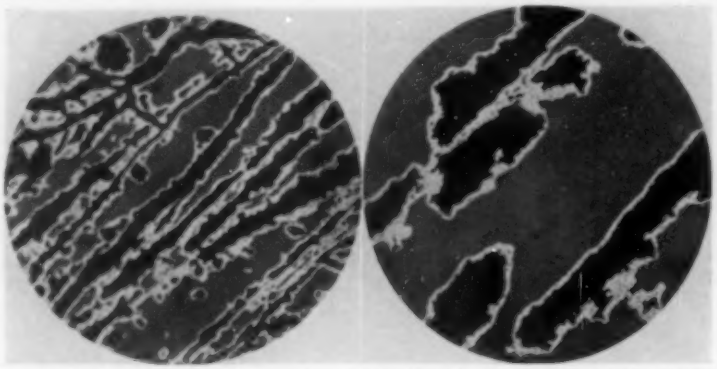

b—Micrograph of unreduced core was taken at a higher magnification. White phase is iron; gray phase is wüstite; and black areas, fissures. X500. Area reduced approximately 25 pct for reproduction.

Fig. 13—Micrographs show structures of partially reduced New York magnetite. Specimens were lightly etched.

tite to wüstite to iron are carried out so that the crystallographic axes of the three cubic systems remain mainly parallel to one another. The three lattices are of such dimension and orientation[10] that the transformations are accomplished along the simplest crystallographic path, and this generally involves the element of parallelism.

Crystalline transformations of one phase into another along parallel directions should be accomplished with the least disruption of the structure as a whole. The preservation and growth of large single crystalline products should be promoted by these circumstances. Such a case was illustrated in the reduction of the New York magnetite with its exaggerated wüstite retention effect.

No direct information is available in the literature as to the effect of crystallographic orientation on the reduction of hematite to magnetite. The closest approach is in the work of Gruner[14] who studied oxidation at the surface of magnetite crystals. Gruner found that hematite developed at the magnetite surface in such a way that its basal (00.1) plane lay parallel to the octahedral (111) plane of the magnetite. If this condition were also true in the reduction process, there would be a drastic shift in the position of the main crystallographic axis when hematite is converted to magnetite. The magnetite would grow as crystallites on the hematite surface and considerable grain refinement could occur. In a rigid system, the change in crystallographic orientation could also lead to physical discontinuities and volume expansion as found by Anderson[15] in the early stages of reduction. The reducibility of small and discrete crystals of magnetite could easily be higher than that of coarse grained magnetite in natural ores.

Edström[16] has shown recently that wüstite formed on reducing single crystals of hematite is usually more porous than the wüstite obtained from reducing single crystals of magnetite. The higher reducibility of hematite is explained on this basis. Crystal orientation effects may well control the porosity resulting from reduction.

4—The influence of impurities in the spinel structure of magnetite has already been discussed. The Arkansas lodestone is one such example and its reducibility was affected in an adverse way by its impurity content.

Conclusions

Iron ore is normally reduced in a topochemical manner. By this mechanism, reduction takes place at solid phase interfaces which remain parallel to the exterior surface as they progress into the piece of ore. Such topochemical behavior was observed in six types of ore of different origin, composition, and physical structure and may be regarded as normal for hard dense ores that do not crack excessively during reduction.

Departures from the normal topochemical behavior were noted. In these cases, the layered structure and the continuity of reduction interfaces were disrupted in one of four ways:

1—Cracking of the specimen interrupted the advance of continuous interfaces between well defined layers.

2—The interface was spread over an appreciable width due to high porosity.

3—Impurities promoted structural irregularities, including cracking.

4—A residual oxide phase was entrapped in the reaction product and left behind the reacting interface. Wüstite thus could be encased in a relatively impervious layer of iron which had been consolidated by sintering. This condition was largely responsible for a minimum rate of reduction of certain magnetite ores at 800°C.

Most of these deviations were caused by conditions which allowed a relatively high concentration of hydrogen to be maintained beyond the advancing interface.

Crystal size and crystal orientation before and during reduction are important factors which make hematite more reducible than magnetite.

Discussion of this paper, if any, will appear in JOURNAL OF METALS, November 1955, and in AIME Metals Branch *Transactions*, Vol. **203**, 1955.

References

[1] G. Bitsianes and T. L. Joseph: Solid Phase Identification in Partially Reduced Iron Ore. *Trans.* AIME (1953) **197**, pp. 1641-1647; JOURNAL OF METALS (December 1953).

[2] G. Bitsianes and T. L. Joseph: The Wüstite Phase in Partially Reduced Hematite. *Trans.* AIME (1954) **300**, pp. 150-153; JOURNAL OF METALS (February 1954).

[3] T. L. Joseph: Porosity, Reducibility, and Size Preparation of Iron Ores. *Trans.* AIME (1936) **120**, pp. 72-90; METALS TECHNOLOGY (February 1936).

[4] R. Schenck, H. Franz, and H. Willeke: Equilibrium Relations in the Reduction, Oxidation, and Carburization Processes of Iron. IX. 10. The Influence of Foreign Oxides upon the Equilibria. *Ztsch. anorg. allgem. Chemie* (1929) **184**, pp. 1-38.

[5] J. Wernick and G. Bitsianes: Unpublished work.

The Effect of Temperature on the Hydrogen Reduction Rates of Eleven Iron Ores. (1948) Dept. of Metallurgy, University of Minnesota, Minneapolis.

[6] M. C. Udy and C. H. Lorig: The Low-temperature Gaseous Reduction of a Magnetite. *Trans.* AIME (1943) **154**, pp. 162-181; METALS TECHNOLOGY (October 1942).

[7] O. G. Specht and C. A. Zapffe: The Low-temperature Gaseous Reduction of Magnetite Ore to Sponge Iron. *Trans.* AIME (1946) **167**, pp. 237-280; METALS TECHNOLOGY (June 1946).

[8] M. Wiberg: The Reduction of Iron Ores with Carbon Monoxide, Hydrogen, and Methane. *Jernkontorets Ann.* (1940) **124**, pp. 179-212.

[9] G. I. Chufarov and E. Tatievskaya: The Reaction Zones in the Reduction of Magnetite and Hematite with Hydrogen. *Acta. Physicochim.* URSS (1935) **3**, pp. 957-974.

[10] G. Bitsianes: *The Mechanisms Involved in the Hydrogen Reduction of Iron Ores.* (1951) Ph.D. Thesis, Dept. of Metallurgy, University of Minnesota, Minneapolis.

[11] N. Buinov, A. Komar, M. Zhuravleva, and G. Chufarov: Orientation of the Phases Formed during the Reduction of Magnetite by Hydrogen. *Acta Physicochim.* URSS (1939) **11**, pp. 571-584.

[12] R. F. Mehl and E. L. McCandless: Oxide Films on Iron. *Trans.* AIME (1937) **125**, pp. 531-559; METALS TECHNOLOGY (February 1937).

[13] H. J. Goldschmidt: The Crystal Structures of Fe, FeO, and Fe_3O_4 and their Interrelations. *Journal* Iron and Steel Inst. (1942) **146**, pp. 157-174.

[14] J. W. Gruner: Magnetite-Martite-Hematite. *Economic Geology* (1926) **21**, pp. 375-393.

[15] L. B. Anderson: Master's Thesis, Dept. of Metallurgy, University of Minnesota, Minneapolis (1951).

[16] J. O. Edström: The Mechanism of Reduction of Iron Oxides. *Journal* Iron and Steel Inst. (1953) **175**, pp. 289-304.

Technical Note

Oxidation of Oxygen-Saturated Titanium

by M. Simnad, Aija Spilners, and O. Katz

THE oxidation of titanium has been studied in recent years by a number of investigators.[1-5] One of the most important aspects of the reaction of titanium with oxygen, which has been observed by several of the investigators, is the extremely high solubility of oxygen in the metal. A detailed study of the Ti-O system[6] has shown that the solubility limit of oxygen in α-titanium is approximately 14.5 wt pct O from 800° to 1700°C. The unusual oxidation behavior of titanium may be ascribed to this phenomenon, since part of the oxygen uptake enters into solid solution in the metal and only a part is available for scale formation. A more complete study of the kinetics of oxidation of titanium would require information on the influence of oxygen in solution in the metal upon the oxidation rate. Such information would also be of interest in regard to the theory of oxidation of metals.

The authors have measured the oxidation rates of oxygen-saturated and oxygen-free titanium between 800° and 1200°C and have found appreciable differences in their rates of oxygen uptake and in the activation energies.

The experimental set-up was similar to that described in a previous paper.[11] The course of oxidadation was followed continously by attaching the specimen to a sensitive spring balance and observing the extension of the spring with time of oxidation. High purity electrolytic oxygen was used and precautions were taken to purify the gases employed. The specimens were prepared from iodide titanium and were ground on metallographic polishing papers to a fineness of 4/0. The furnace was first evacuated and filled with argon; the specimen was lowered into the furnace, which was then evacuated and filled with oxygen, after the specimen had reached the oxidation temperature in argon.

The samples were presaturated with oxygen by means of the following procedure: Each specimen was first heated in oxygen at 1200°C until its increase in weight indicated 13.8 pct by weight uptake of oxygen. The furnace was then immediately evacuated and filled with purified argon five times. The specimen was heated in the argon atmosphere for a period of 72 hr at 1200°C in order to saturate the metal with oxygen by complete absorption of the scale. The temperature was lowered to the oxidation temperature, the furnace was evacuated and filled with oxygen, and the oxidation rate was followed by noting the extension of the spring balance. No oxide film was visible on these specimens at the start of the oxidation experiments.

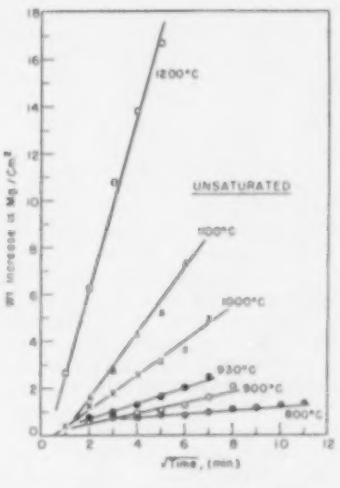

Fig. 1 — Oxidation of oxygen-free titanium.

Titanium samples in the oxygen-free as-received condition were also oxidized and their oxidation rates measured.

The results are shown in Figs. 1, 2, and 3, which indicate that the initial rates of uptake of oxygen by both the oxygen-saturated and oxygen-free specimens are parabolic at these temperatures. The rate of uptake of oxygen is, however, appreciably lower

M. SIMNAD, Associate Member AIME, A. SPILNERS, and O. KATZ are associated with Metals Research Laboratory, Carnegie Institute of Technology, Pittsburgh.

TN 269E. Manuscript, Aug. 2, 1954.

for the oxygen-saturated titanium than for the oxygen-free titanium at temperatures above 950°C.

The results may be explained as follows: The total oxygen uptake of an oxygen-free specimen is equal to the sum of the amounts of oxygen diffusing into the metal and that present in the oxide formed on the surface; whereas in the oxygen-saturated specimens, the total oxygen uptake is equivalent to that required to form the oxide. In the former, the rate of thickening of the oxide is governed by the oxygen concentration gradient in the metal; part of the oxide formed will always be absorbed into the metal. The oxidation rate is governed by the rate of diffusion of oxygen through the scale, which in turn is controlled by the thickness of the oxide present. At a given temperature, the rate of growth of oxide will be lower on the oxygen-free specimen (since it dissolves part of the oxide formed). The diffusion rate of oxygen through this oxide will, however, be greater than in the relatively thicker oxide layer formed in the same period on the oxygen-free specimen. The rate of total oxygen uptake is greater in the oxygen-free titanium, since the amount of oxygen diffusing into it exceeds the quantity of oxygen present in the extra thickness of the oxide formed on the oxygen-saturated specimens.

Fig. 4 shows plots of the logarithms of the rate constants vs the reciprocals of the absolute temperatures for both the oxygen-free and oxygen-saturated specimens. The activation energies calculated from the straight lines obtained give values of 25,000 cal per mol for the oxygen-saturated titanium, and 32,000 cal per mol for the oxygen-free specimens. These values compare with the previously reported values of 26,000 cal per mol by Gulbransen and Andrew[7] for the low temperature oxidation of titanium, and between 40,000 and 47,000 cal per mol reported by Davies and Birchenall,[8] 47,000 cal per mol by Grant and Richardson,[12] and 30,500 cal per mol by Jenkins.[9]

The agreement of the authors' value for oxygen-saturated specimens with the value found by Gulbransen and Andrew is probably due to the fact that at the low temperatures studied by them the diffusion of oxygen into the metal may be negligible, so that their results are comparable with those obtained by the authors with oxygen-saturated specimens at high temperatures.

The disagreement with the reported values for the oxygen-free specimens at high temperatures may be due to the fact that the authors report the results of initial rates of oxidation rather than the rates based on the long times studied by the other investigators. The agreement with the value reported by Jenkins is satisfactory.

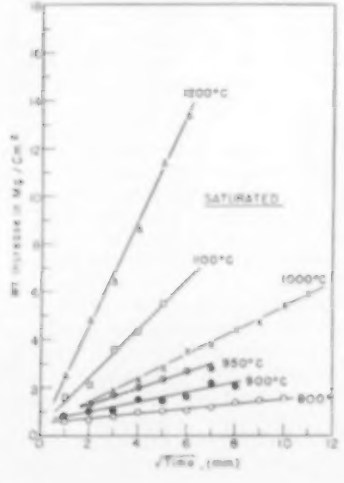

Fig. 2 — Oxidation of oxygen-saturated titanium.

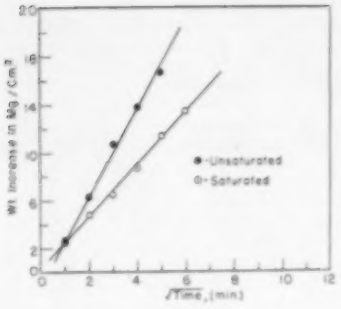

Fig. 3 — Oxidation rates of titanium at 1200°C.

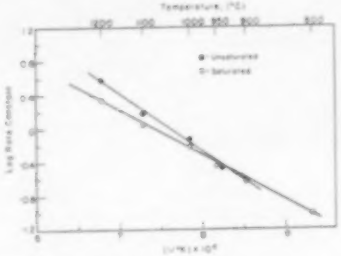

Fig. 4 — Plots of logarithms of rate constants vs reciprocals of absolute temperatures for oxygen-free and oxygen-saturated specimens.

These studies are being continued with other metals having high oxygen solubilities in order to elucidate the influence of oxygen in solution upon the mechanism of oxidation of metals. The result of this work corroborates the theory put forward by Jenkins[9] that oxygen diffusion within the core is an accelerating factor in the oxidation of titanium. The rate of oxide formation will be governed by the existing oxygen gradient in the core.

Acknowledgments

The authors acknowledge the support of the Office of Naval Research in this work, and express their appreciation of advice from Robert F. Mehl and C. E. Birchenall.

References

[1] E. A. Gulbransen and K. F. Andrew: *Trans.* Electrochemical Soc. (1946) **96**, p. 364.
[2] E. A. Gulbransen and K. F. Andrew: *Trans.* AIME (1949) **185**, p. 741; JOURNAL OF METALS (October 1949).
[3] J. W. Hickman and E. A. Gulbransen: *Analytical Chemistry* (1948) **20**, p. 158.
[4] D. J. McPherson and M. G. Fontana: *Trans.* ASM (1951) **43**, p. 1098.
[5] M. H. Davies and C. E. Birchenall: *Trans.* AIME (1951) **191**, p. 877; JOURNAL OF METALS (October 1951).
[6] P. H. Morton and W. M. Baldwin, Jr.: *Trans.* ASM (1952) **44**, p. 1004.
[7] L. G. Carpenter and F. R. Reavell: *Metallurgia* (1948) **39**, p. 63.
[8] W. A. Alexander and L. M. Pigeon: *Canadian Journal of Research* (1950) **B-28**, p. 60.
[9] A. E. Jenkins: *Journal* Inst. of Metals (1954) **82**, p. 213.
[10] E. S. Bumps, H. D. Kessler, and M. Hansen: *Trans.* ASM (1953) **54**, p. 1008.
[11] M. H. Davies, M. Simnad, and C. E. Birchenall: *Trans.* AIME (1951) **191**, p. 889; JOURNAL OF METALS (October 1951).
[12] L. S. Richardson and N. J. Grant: *Trans.* AIME (1954) **200**, p. 69; JOURNAL OF METALS (January 1954).

Integration of Metallurgical Engineering Education

by R. Schuhmann, Jr.

As a response to rapidly growing specialization in various branches of metallurgy, it is proposed that undergraduate education in metallurgical engineering should be built up around four principal scientific themes: 1—thermodynamics, 2—structure, 3—mechanics, and 4—rate processes.

THE following quotation from a recent article by von Bertalanffy[1] describes very well the situation which today challenges curriculum designers in all branches of science and engineering:

"Modern scientific education is presented with a well known dilemma. The amount of facts in modern science, and in any of its smallest branches, is enormous. Life in general, and the academic curriculum in particular, is short. The abundance of factual data, as well as the intricacy of modern scientific techniques, experimental and theoretical, necessitates utmost specialization. This specialization, unavoidable though it is, involves serious danger for both the education of the scientist and the social function of science.

"In so far as the advancement of science is concerned, history shows that interconnection of different fields and problems is a most important basis of progress. Many of the paramount achievements of science arose on borderlines, and from the synthesis of formerly separate fields . . ."

Specialization in subfields of metallurgy has become a serious educational problem only in about the last decade. The growth in specialization, almost as a necessity, has paralleled the rapid growth in metallurgical knowledge during this period. Moreover, in planning future educational policies, the educator must be concerned not only with the rate of increase in metallurgical knowledge and with the concomitant rate of increase in specialization, but also with the second derivatives, that is, with the rates of increase of the rates of increase. These second derivatives are positive and large; the growths being dealt with are self-catalyzing, or like a chain reaction.

As a measure of specialization, the length of the list of different kinds of metallurgies can be considered, the kinds of metallurgy which represent one person's particular interests and those of other practicing metallurgists. To start with, there are physical metallurgy, process metallurgy, and mineral dressing, then mechanical metallurgy, metal processing, foundry metallurgy, corrosion, solid state physics, high temperature metallurgy, welding, powder metallurgy, nuclear metallurgy, etc. Each of these fields is growing so rapidly that any one metallurgist can hope at best to keep up to date in only one or two.

What is the impact of all these "metallurgies" on metallurgical education and metallurgical curricula? In answering this question, it can be said, first, that educators have resisted fairly well the temptations to split up metallurgy, with different curricula, different options, degrees with different labels, and the like—degrees are still given in plain *Metallurgy* and *Metallurgical Engineering*. In other ways, though, the pressures of specialization have had noticeable effects. There is a tendency to think of these "metallurgies" as the important subdivisions of Metallurgical Engineering and to work up

R. SCHUHMANN, JR., Member AIME, is Professor of Metallurgical Engineering, Purdue University, Lafayette, Ind.

Discussion of this paper, TP 3998D, may be sent, 2 copies, to AIME by July 1, 1955. Manuscript, Aug. 13, 1954. New York Meeting, February 1954.

special courses in each one; there is a feeling of some sort of obligation to teach these subjects because these represent the kinds of things graduates will be doing. Perhaps the most serious demarcation is that between physical metallurgy and extractive metallurgy. The dichotomy between physical metallurgy and extractive or process metallurgy has been handled differently in different institutions. One philosophy is that the two fields are so different they represent substantially different professions—this point of view leads to a curriculum treating one field thoroughly and the other in orientative or survey fashion. Undergraduate curricula of this kind enable the specialist teacher to do a more thorough and satisfying job, but the result is a narrower view of the profession, or in the end perhaps two professions instead of one. On the other hand, when the tendency to specialize in one or the other branches is resisted and the curriculum is designed to cover both in a balanced fashion, neither the physical metallurgist nor the process metallurgist may be satisfied with the compromise. Another alternative is a five-year undergraduate program, but this will not be a practical solution unless it is adopted for all engineering education.

The response of metallurgical education to the present challenge of rapid growth in knowledge and increasing specialization is important to the future of the profession. A strong and lasting metallurgy profession must be built on a broad firm base, not on the shifting sands of currently prominent specialized activities. The profession must have some essential unity of knowledge and purpose, which clearly distinguishes its members from other engineers and which defines a field of activity where its members are uniquely qualified above all other scientists and engineers. It is not clear that the present approaches to metallurgical education meet these tests of breadth and unity. Programs emphasizing one branch of metallurgy achieve unity, but at the expense of breadth. Programs designed to cover metallurgy more broadly seem in some respects to have compromised rather than integrated the various fields of metallurgy.

The purpose of this paper is to present a possible basis for integration of metallurgical engineering education in such a way as to promote both breadth and unity in the metallurgical profession.

Approaching a New Curriculum

As a first step, it is necessary to forget temporarily all the traditional arrangements of subject matter as represented by present metallurgy courses. No substantial improvement in metallurgical engineering curricula will be achieved merely by juggling presently available courses, readjusting time distribution between these courses, changing sequence, and other tricks of the curricular trade. Likewise, major improvement through the invention and development of one or two new courses cannot be counted upon, since such development will have to be limited in scope to avoid cutting across all the established courses that are retained.

The fact that the curriculum is to provide the opportunity for a good general education and is to fulfill other important requirements common to all engineering education is implicit here.

As the basis for building a new curriculum, it is necessary first to delineate the few general areas of basic science, beyond elementary mathematics, physics, and chemistry, which are important to *all* metallurgists in common—these will be the areas of scientific knowledge which characterize the metallurgist and the metallurgical engineer. If these fields of knowledge are made the foundations of the curriculum, certain of them will require separate basic courses designed specifically to develop the body of principles and the point of view of each field. Even these courses should utilize illustrative metallurgical applications and should be developed with the objective of getting the student to learn, or start to learn, how to apply basic principles to real engineering situations. Subsequent courses should bring out interrelations between the different fields and should develop the student's ability to bring all points of view to bear on more complex metallurgical situations and realistic metallurgical problems.

A curriculum built up in this way from the basic sciences probably will cover metallurgical technology and metallurgical practices rather poorly. Some processes, some alloys, and some arts which are of considerable industrial importance and which have been habitually included hitherto in metallurgy courses will be left out. A few tears may have to be shed over some of the deliberate omissions, but consolation is to be found in the fact that coverage of important metallurgical practices is already impossible and with another ten years' growth will be ridiculous even to consider.

Fields of Metallurgical Science

Beyond elementary mathematics, physics, and chemistry, the field of metallurgy may be characterized by four principal scientific themes: 1—thermodynamics, 2—structure of matter, 3—engineering mechanics and mechanical behavior of materials, and 4—rate processes. In this list, order is not significant and further caution must be exercised because the labels selected for these four fields may mean different things to different people. Undoubtedly, additions will have to be made to the foregoing list to prepare men for certain specialized metallurgical activities. Some may need nuclear science beyond that given in undergraduate physics; others may need advanced mathematics, inorganic chemistry, advanced electricity and magnetism, etc. Such additions as these, justifiable though they may seem in special cases, do not come in the category of being essential for all metallurgists. On the other hand, it is difficult to conceive of a man calling himself a metallurgist who cannot call on all four of the approaches listed previously. In fact, most metallurgists reading this paper will find it easy to think of problems in which all four of these points of view have contributed simultaneously to the overall solutions.

Thermodynamics: Courses in metallurgical thermodynamics are required in many present metallurgy curricula. Originally introduced as a basis for process metallurgy, this science now is generally recognized as a powerful tool in all branches of metallurgy. An excellent summary of the relationship between thermodynamics and metallurgy was given recently by Austin[1] as part of an ASM symposium on *Thermodynamics in Physical Metallurgy*. Still other recent and convincing evidence of the major role of thermodynamics in all branches of metallurgy is to be found in such books as Wagner's *Thermodynamics of Alloys* and Darken and Gurry's *Physical Chemistry of Metals*.

In most schools it is likely that the responsibility for teaching metallurgical thermodynamics will fall ultimately in the metallurgy or metallurgical engineering department. The undergraduate will fall far short of mastering the whole philosophy of thermodynamics, so it is well that his attention be directed at an early stage toward applications of thermodynamics to metallurgical systems. If he acquires some familiarity with the First and Second Laws, a little skill in applying these laws to processes in metallurgical systems, and a deeply rooted appreciation of the power of the thermodynamic method of tackling metallurgical problems, the course should be considered successful.

The traditional three-year sequence of freshman chemistry, analytical chemistry, and physical chemistry which is now usually considered prerequisite to thermodynamics represents a serious and perhaps unnecessary delay to the introduction of thermodynamics. As far as this author is concerned, the traditional chemistry sequence has outlived its usefulness, and it is time the chemists and the metallurgists together worked out a new arrangement. One sequence which seems worthy of careful consideration is freshman chemistry, physical chemistry in the sophomore year, and a full year of metallurgical thermodynamics in the junior year. However, it is doubtful that this arrangement will work out well if obtained merely by moving present junior courses in physical chemistry back one year, or by putting metallurgy sophomores into physical chemistry with juniors from chemistry and chemical engineering.

Structure of Matter: A good case can be made for the thesis that the distinguishing mark of a metallurgist is his understanding of structure and his ability to interpret all manner of problems in terms of structure. Crystallography, metallography, and X-ray metallography have long been cornerstones of metallurgy curricula. Far-reaching developments have occurred in recent years and continue to occur, which demonstrate that the metallurgist must delve deeper and deeper into structure at all levels. Moreover, it has become clear that these studies should not be confined to the metallic state or even to the solid state. Liquid metals, slags, mattes, fused salts, glasses, minerals, and other classes of matter also have structures of interest to the metallurgist. In view of the extensive growth which has occurred in this field in large measure by accretion onto existing courses and curricula, the time may be ripe for reorganization to obtain a more logical approach and perhaps also to introduce some new material.

Structural concepts should form a continuous thread throughout the curriculum, so that the student is led automatically into examining new situations in terms of structure. Moreover, a substantial start can be made early in the curriculum, since these concepts do not require advanced mathematical or physico-chemical treatment. The fact that the development of the present knowledge of atomic structure, chemical bonds, crystal structure, and other structural concepts has involved difficult and complex researches and a series of brilliant scientific discoveries should not mislead educators into thinking that the resulting structural theories themselves are too difficult for the undergraduate. On the contrary, structure is a natural place to start the untrained mind because it can be seen, drawn on paper, and modeled, and does not require initially, at least, the abstract thinking of calculus or of thermodynamics, for example. Accordingly, it seems entirely logical to give in the sophomore year a substantial one-year course covering atomic structure, the periodic table, chemical bonds, crystal structure (ionic crystals, silicates, and minerals as well as metals), crystal imperfections, structure of liquids and glasses, elementary theory of the metallic state, etc. Insofar as practicable, the emphasis should be placed on understanding what the structure is and on its use to account for material properties rather than on historical development or on experimental and theoretical proofs. Thus, the course might well be developed in the metallurgy department, as *Elementary Structural Metallurgy*, and might serve as the principal or only metallurgy subject in the sophomore year.

In the last two years of the metallurgical engineering curriculum, the structure theme inevitably will develop further in the student's mind as he undertakes the studies of metallography, constitution of alloy systems, mechanical behavior of metals, X-ray metallurgy, etc. because this theme already dominates these topics regardless of how they are arranged in separate courses.

Mechanics and Mechanical Behavior of Materials: The necessity of training metallurgical engineers in the field of engineering mechanics needs no great amplification here. Perhaps it is sufficient to note only that a metallurgical engineer must understand quantitatively the mechanical behavior of metals in machines and structures because the most important criteria of metal and alloy worth are mechanical properties under various conditions of use.

Before World War II, the required service courses in applied mechanics and strength of materials were not always regarded highly by metallurgy students. However, during and since the war, a number of important developments have occurred in the field of mechanics of materials, most conspicuously in the portions of the field which are important to metallurgists. As a result, it may be time for metallurgical engineers to look for more advanced service courses which go into mechanics of materials more deeply than the courses taken by other engineers.

Rate Processes: Diffusion, nucleation, crystal growth, solidification, precipitation, oxidation and scaling, martensitic reactions, carburizing, nitriding, galvanizing, desulphurization of liquid iron, gas evolution from liquid and solid metals—here is just a partial listing of metallurgical processes which attest the importance of a unified and generalized treatment of rates and mechanisms of metallurgical reactions. The indication is clear that the metallurgist of the future will have many new opportunities to apply rate-process thinking to the solution of engineering problems. Accordingly, consideration should now be given to the development of a basic course in this field, general enough to serve all branches of metallurgy.

Fields of Metallurgical Engineering

Undergraduate training in metallurgy and metallurgical engineering, even though based on a curriculum with a high content of basic science, must produce, in the final analysis, men who are engineers first and scientists second. The minority of metallurgy students who eventually are to become metallurgical scientists in research laboratories and colleges will benefit from exposure to the engineering point of view as undergraduates in any event.

In a broad sense, the various courses discussed in

Table I. Illustrative Metallurgical Engineering Curriculum

Year	Subject, Fall	Subject, Spring
First	Mathematics Physics Chemistry Humanities	Mathematics Physics Chemistry Humanities
Second	Mathematics Physics Elementary Physical Chemistry Structural Metallurgy I Humanities	Mathematics Physics Elementary Physical Chemistry Structural Metallurgy II Humanities
Third	Metallurgical Thermodynamics I Metallurgical Engineering I (stoichiometry, heat balance, fluid flow, heat flow, etc.) Structural Metallurgy III (metallography, constitution, phase diagrams, etc.) Engineering Mechanics I Humanities	Metallurgical Thermodynamics II Metallurgical Engineering II (unit processes) Rates of Metallurgical Processes Engineering Mechanics II Humanities
Fourth	Metal Processing I Mechanical Behavior of Metals X-Ray Metallography Humanities Elective	Metal Processing II Extractive Metallurgy Humanities Thesis, special problems, and/or electives

the previous section of this paper, "Fields of Metallurgical Science," should be considered as applied science or engineering courses. Applications to real metallurgical systems will be stressed through illustrative examples, and the primary purpose is to bring the student to use scientific principles in solving engineering problems, not to educate him as a scientist. For this reason, many of these courses dealing with thermodynamics, crystal structure, reaction rates, and other scientific topics probably will be taught by metallurgists rather than by chemists or physicists.

Recognizing the fact that metallurgical engineering is much more than applied science and the fact that engineering activities involve a balance of applied science, empiricism, economics, and judgment, the courses in the curriculum which emphasize the engineering approach now need to be considered.

A few years ago the author described a sequence of three courses designed to cover the engineering of process metallurgy.[2] In several years' experience with this sequence at Massachusetts Institute of Technology, many changes were made in arrangement of material within the courses and in time allotted to various topics, but the overall plan is thought to be sound. The three courses cover the following material: 1—stoichiometry, heat balance, fuels and combustion, fluid flow, heat flow, and refractories; 2—unit processes of extracting metals: reduction of metal oxides, refining of liquid metals, gas-solid reactions, and smelting; and 3—integrated processes and flowsheets: ferrous metallurgy and extractive metallurgy of selected nonferrous metals.

Metal Processing: The manner in which the field of metal processing is handled in the undergraduate course of study is perhaps more critical than has been generally realized. When the label *metal processing* is taken literally, it covers a major part of the actual engineering activities of metallurgical engineering graduates. Thus, much of the justification for a substantial program in metallurgical sciences, such as that discussed previously, will have to be found ultimately in the impact of these sciences on metal processing. There has been a tendency to handle metal processing as a *shop* course, stressing the art, and to place the course early in the curriculum before the student has acquired an appreciable background in metallurgy science. This point of view perhaps has some advantages in as far as student motivation is concerned, but seems questionable as a basis for advancing metallurgical engineering.

Another matter to be considered in curriculum planning is that in the past much of the meat of metal processing has been given in other metallurgy courses, especially traditional courses in physical metallurgy. The handling of heat treatment illustrates this point. Heat treatment is a complex art which draws on scientific principles relating to structure, equilibria, mechanics, rate processes, etc., but in addition, leans heavily on engineering tests and on intelligent engineering use of empirical data and empirical or semi-empirical correlations.

Accordingly, a good case can be made for giving metal processing a larger and more vital role in the metallurgical engineering curriculum. Such a shift would require raising the level of instruction, a new balance between science and art, incorporation of material previously considered as part of physical metallurgy courses, and an increased time allotment. A two-semester course of this kind in metal processing, placed in the fourth year, would afford an excellent opportunity for integrating scientific principles and engineering practices at the time when such integration is most important: just before the student enters engineering practice.

Curriculum

An illustrative four-year curriculum embodying the ideas discussed previously is shown in Table I. No attempt is made to show the detail of time allotments, laboratory time, credits, etc., since these matters depend very much on local conditions.

It should be emphasized again that the curriculum arrangement shown is not contemplated as a rearrangement of already existing courses of the same names. Rather, the final arrangement is associated with the substantial redistribution of the subject matter of metallurgy around four main themes of metallurgical science and, in the last two years, a series of terminal and integrative engineering courses.

Conclusion

Curricular discussions are never concluded, so perhaps it is appropriate to end this paper by quoting a brief statement attributed to Dr. Raymond Kirk, Dean of the Graduate School, Polytechnic Institute of Brooklyn: "Both the teacher and the taught must continually reorganize their knowledge and continually rephrase their own generalizations."

Discussion of this paper, if any, will appear in JOURNAL OF METALS, November 1955, and in AIME Metals Branch *Transactions*, Vol. **203**, 1955.

References

[1] L. von Bertalanffy: Philosophy of Science in Scientific Education. *Scientific Monthly* (1953) **77**, No. 11, pp. 233-239.

[2] J. B. Austin: Contribution of Thermodynamics to Metallurgical Research and Operations. ASM *Seminar on Thermodynamics in Physical Metallurgy* (1950).

[3] R. Schuhmann, Jr.: The Unit Processes of Chemical Metallurgy. *Trans.* AIME (1949) **185**, pp. 321-326; JOURNAL OF METALS (May 1949).

AIME OFFICERS:
President—H. DeWitt Smith
Vice-Presidents—T. B. Counselman, W. A. Dean, Harold Decker, L. E. Elkins, A. B. Kinzel, W. W. Mein, Jr.
President-Elect—C. E. Reistle, Jr.
Treasurer—G. F. Moulton
AIME STAFF:
Secretary—Ernest Kirkendall
Secretary Emeritus—E. H. Robie
Ass't. Secretaries—J. B. Alford, H. N. Appleton, E. J. Kennedy, Jr.
Field Secretary & Ass't. Secy—R. E. O'Brien
Ass't. Treasurer—P. J. Apol

aime NEWS

AIME Bessemer Steel Committee Meets in Hamilton, Ontario, Canada

AN outstanding meeting in all respects was the general opinion of members attending the AIME Bessemer Steel Committee meeting April 4 to 5 in Hamilton, Ont., Canada. The meeting held at the Royal Connaught Hotel was attended by 52 members and was highlighted by a plant trip through the oxygen steel shop of Dofasco (Dominion Foundries & Steel Ltd.).

The plant trip took place Monday, April 4, and members studied the oxygen steelmaking process first hand with the wholehearted cooperation of Dofasco's expert staff. At the luncheon, F. J. McMulkin gave a resume of the process and discussed the questions put to him by members. Afer lunch the group returned to the plant and observed the oxygen steel being rolled. (For a description of the plant and the steel produced see *Oxygen Steel Produced at Dofasco Can Compete with Open Hearth*, by F. J. McMulkin, JOURNAL OF METALS, April 1955, p. 530).

Monday evening Dofasco was host to the members of the committee at cocktails and dinner. Tuesday the roundtable off-the-record technical discussions were held. After the meeting adjourned, members were invited to visit the plant of the Steel Co. of Canada.

A. B. Wilder, Chairman of the Bessemer Steel Committee, was in charge of the arrangements of the meeting. He was assisted by Art Thornton, Chairman of the Iron and Steel Committee, and F. J. McMulkin who was Dofasco's representative to the group.

A. B. Wilder, U. S. Steel Corp. and Chairman of the AIME Bessemer Steel Committee, is shown with J. R. Atkinson, F. J. McMulkin, and D. M. McFarlane all of Dofasco's oxygen steelmaking plant.

Art Thornton, Chairman of the Iron and Steel Div. AIME, talks with H. W. Graham, Walther Mathesius, and G. M. McMorran who are among the first organizers of the AIME Bessemer Steel Committee.

Progress Report of AIME Advisory Committee to Bureau of Standards

The AIME Advisory Committee to the metallurgy div. of the National Bureau of Standards is one of 12 similarly constituted committees established to provide a direct connection between the National Bureau of Standards and the organized science and technology of the U. S.

These committees were set up in 1954 on the recommendation of another committee appointed earlier by Secretary of Commerce Sinclair Weeks to study the activities of the Bureau of Standards. The members of these advisory committees represent their technical society which has appointed them and interprets its point of view with respect to the Bureau's program. In addition, these committees are of assistance to their respective divisions in formulating programs and discussing problems.

The AIME Advisory Committee has met twice with Bureau personnel at Washington and again during the past Annual Meeting at Chicago. At the earlier sessions the committee became acquainted with the division personnel, its projects and problems. At the present time the committee is giving consideration to the program and the objectives toward which the division might work.

Members of the Advisory Committee to the metallurgy div., National Bureau of Standards attended the meeting held in Chicago during the AIME Annual Meeting. Left to right, C. E. Sims, E. C. Smith, E. Schumacher, C. S. Smith, and W. A. Dean.

The committee has enjoyed the fullest of cooperation from A. V. Astin, director of the Bureau, J. G. Thompson, chief of the metallurgy div., and all other Bureau personnel with whom it has come in contact.

Spokane Section Hears Talk on Uranium

Paul Franklin, Jr., of Merrill, Lynch, Pierce, Fenner & Beane outlined the growth of the uranium industry to the Spokane Subsection at a recent meeting. Facing an audience of 150, Mr. Franklin outlined the financial methods involved in uranium development.

He advised those who want to offer shares to the public to find a small broker of good reputation. One avenue of finance described by Mr. Franklin was recourse to Government loans. Defense Minerals Exploration Administration will provide a large share of the cost if the showing is of sufficient promise.

Philadelphia Section Holds Dinner Meeting

The Mining and Metals Branches of the AIME Philadelphia Section met jointly for cocktails and dinner. Subsequently, each group adjourned for its own lecture.

The mining group heard a talk on *The Flotation of Fluorspar at Wilmington, Del.*, by Edward S. Frohling, flotation engineer, St. Lawrence Fluorspar Corp.

F. D. Rosi of the RCA Laboratories, Princeton, N. J., spoke on *Stress-Strain Characteristics and Slip Band Formation on Metal Crystals.* He correlated the effects of the various slip systems with the stress-strain curves for very pure, single crystals of copper, silver, and aluminum. The effects of small amounts of impurities were also discussed.

Excellent illustrative material consisting of diagrams and photomicrographs was used to clearly show the mechanism of the slip systems.

A highly informative discussion period followed the talk.

Magnetism Conference To Be Held in June

The AIME, American Physical Society, and Carnegie Institute of Technology will participate in a symposium to be held by the magnetics subcommittee of the Basic Science Committee of AIEE. The conference will be held June 14 to 16 at the William Penn Hotel, Pittsburgh. Presentation of original and review papers will be held on two or more days and organized trips to companies and institutions in the Pittsburgh area also are planned. Companies will be encouraged to have exhibits of apparatus of interest to those in attendance. Time will be reserved for informal discussion.

Programs containing abstracts of the talks will be distributed before the meeting. Abstracts of 200 to 500 words are to be sent to R. M. Bozorth, Bell Telephone Laboratories, Murray Hill, N. J. The meeting is open to all interested and publication of the complete proceedings is planned.

The program committee consists of: J. E. Goldman, J. F. Libsch, W. H. Meiklejohn, J. A. Osborn, C. Zener, and R. M. Bozorth. Local arrangements are in charge of A. C. Beiler.

DIRECTORY

A new all-Institute directory was announced in the March issue. Members may obtain a copy of the directory without cost by sending in the coupon which appeared on p. 492, March 1955, JOURNAL OF METALS. Please use the coupon because it will serve as a label for mailing.

EUROPEAN MEETING—ISD MAY DINNER

There are still several places available for conferees to the Joint Metallurgical Societies Meeting to be held in Europe this June. See p. 491, March 1955, JOURNAL OF METALS. If interested, write Ernest Kirkendall, Secretary, AIME, immediately. Because of this meeting, the May dinner of the Iron and Steel Div., normally held in New York during the AISI annual meeting has been cancelled.

Sept. 15, 1955 is the deadline for the Institute of Metals Div. papers for the 1956 New York Annual Meeting and the deadline for all Iron & Steel Div., and Extractive Metallurgy Div. papers to be preprinted. Papers received by this deadline but requiring revision may not be processed in time to permit scheduling for this meeting.

William R. Bond is vice president, operations, Woodward Iron Co., Woodward, Ala. Mr. Bond had been associated with the Lone Star Steel Co., Lone Star, Texas.

Henry Epstein has joined the research dept., Bethlehem Steel Co., Bethlehem, Pa.

Adolph E. Palty formerly of the chemical engineering dept., New York University, New York, has joined the SAE dept., General Electric Co., West Lynn, Mass.

Carl J. Forkum has been transferred to the Columbia Geneva steel div., U. S. Steel Corp., Provo, Utah, as assistant to the division superintendent, open hearth and foundry. Mr. Forkum had been assistant division superintendent, steel works, for the American Steel & Wire div., Worcester, Mass.

Eric Kula is associated with the Watertown Arsenal Laboratory, Watertown, Mass.

Delwin D. Blue has been appointed chief of the bureau of mines electrometallurgical branch at Boulder City, Nev. He succeeds **Frank S. Wartman** who is entering into private industry. Mr. Blue has had 13 years of experience with the bureau in light metals research. He will direct experimental work on metals as titanium and manganese.

Roger M. Ferryman, formerly associated with Horizons, Inc., Cleveland, has been named production manager of the Metalphoto Corp., Cleveland.

Walter J. Barrett has been announced as president of the United Engineering Trustees, Inc. Mr. Barrett is electrical coordination engineer, N. J. Bell Telephone Co., Newark, N. J. He has been a member of the Board of Trustees of UET for four years, serving as vice president and on various committees. Mr. Barrett represents the AIEE on the board and is treasurer and a director of AIEE. He is also a director of the Engineers Joint Council.

William P. Saunders, formerly research and development engineer, Dow Chemical Co., Midland, Mich., is now laboratory division leader at the Madison, Ill. plant of the company.

A. Eugene Schubert has been named manager, engineering, General Electric Co., chemical materials dept., Pittsfield, Mass.

A. Craig Hood and **George E. Clauser** have joined the technical div., Superior Tube Co., Norristown, Pa.

Hamnett P. Munger has been named a technical advisor at Battelle Memorial Institute. He has been on the staff at Battelle since 1948.

P. T. STROUP

Philip T. Stroup and **Ernest C. Hartmann** have been appointed assistant directors of research by the Aluminum Co. of America at the research laboratories, New Kensington, Pa. **Harry N. Hill** succeeds Mr. Hartmann as chief of the engineering design div. **Allen S. Russell** replaces Dr. Stroup as chief of the process metallurgy div. **Luther M. Foster** has been named chief of the physical chemistry div. Dr. Stroup is a member of the AIME Metals Branch Council.

Hugh C. Land will succeed **William P. Drake** as head of the industrial chemicals div., Pennsylvania Salt Mfg. Co. Mr. Drake was named executive vice president.

John F. Tyrrell was appointed senior associate editor *Metals Progress*. For the past four years Mr. Tyrrell has been an advertising representative.

Robert A. Willey has been named assistant technical and research director for the Steel Founders' Society of America, Cleveland. Mr. Willey had been chief metallurgist for the Commercial Steel Casting Co., Marion, Ohio.

R. A. WILLEY

Kenneth A. DeLonge has been placed in charge of the iron and nonferrous castings section, development and research div., International Nickel Co., Inc.

Charles B. Tillson, Jr., has been appointed general superintendent of the Crucible Co. of America mine at Crucible, Pa. Mr. Tillson was mine superintendent since 1953. **A. V. Faull** was named mine superintendent, **U. P. Rembold** was appointed superintendent, coal preparation, and **Earl N. Burnham** was named general foreman, coal preparation.

Howard M. Dess joined the staff of Electro Metallurgical Co., metals research laboratories as senior research assistant in the engineering research group.

O. A. Pfaff, president and general manager of the American Wheelabrator & Equipment Corp., Mishawaka, Ind., was elected to the board of directors of the Bell Aircraft Corp., Buffalo, N. Y.

Anton deSales Brasunas, associate professor of metallurgical engineering, University of Tennessee, has been appointed to the newly created post of director of educational activities for ASM.

E. Paul Lange, assistant secretary of Engineers Joint Council, has become secretary. He succeeds **Brig. Gen. S. E. Reimel,** USA (Ret.). Prior to joining EJC, Mr. Lange had been an engineer with C. Tennant Sons & Co., New York.

William L. Walsh has been appointed assistant to the president, Kennecott Copper Corp. His duties will be in the titanium field.

Augustus B. Kinzel, director of research for the Union Carbide & Carbon Corp., received the International Acetylene Assn. Morehead Award. Dr. Kinzel was cited for his contributions to the use of acetylene. Dr. Kinzel is a Vice President of AIME.

J. O. Brittain has joined the staff of the dept. of metallurgy, Technological Institute of the Northwestern University, Evanston, Ill. He had been a research associate at the School of Mines, Columbia University, New York.

L. C. Duncan was appointed general manager of American Cyanamid Co.'s Lederle Laboratories div. **V. E. Atkins** was named general manager of the organic chemicals div.

Anson B. Albree has joined Aluminum Foils, Inc., Jackson, Tenn., as sales manager. He had been associated with Rolled Alloys, Inc., Detroit, Mich.

Obituaries

Elmer Judson Tompkins (Member 1946) died during August 1954. He was born at Lake City, Iowa and attended Iowa State and the University of Illinois. In 1916 he was associated with the Illinois Steel Co., Gary Works. From 1924 to 1929 he was associated with the LaSalle Steel Co. at Hammond, Ind. He then joined the Central Steel & Wire Co., Chicago. At the time of his death, Mr. Tompkins was residing at Skokie, Ill.

Ray G. Gibson (Member 1945) died on Oct. 16, 1954. Mr. Gibson had been associated with the Michigan Smelting & Refining Co., Detroit, for the greater part of his career. For one year he was an analytical chemist for the Dodge Bros. While at Michigan Smelting, Mr. Gibson held the positions of analytical-chemist, chief chemist, chief metallurgist, and technical superintendent.

Crosby F. Baker (Member 1921), former chairman of the dept. of chemistry, Tufts College, Medford, Mass., died on Dec. 9, 1954. Professor Baker was born at Hampden, Maine and attended Tufts College. He was an instructor in chemistry at the college from 1911 to 1918. He was appointed an assistant professor of chemistry in 1918. From 1917 to 1921 he did consulting work in metallurgy and chemistry for the Eastern Metal & Refining Co.

Robert L. Hardy (Member 1952) died on Dec. 29, 1954. Mr. Hardy was born in Newton, Mass., and received a B.S. in general engineering from Massachusetts Institute of Technology.

Necrology

Date Elected	Name	Date of Death
1917	D. W. Butner	Feb. 10, 1955
1941	Thomas C. Cheasley	Mar. 17, 1955
1912	Hugh M. Crankshaw	Mar. 25, 1955
1925	Francis H. Crockard	Mar. 3, 1955
1912	J. W. H. Hamilton	Jan. 11, 1955
1928	Elton Hoyt, II	Mar. 16, 1955
1928	Franklin Leonard	Mar. 13, 1955
1947	Leslie A. Rainier	Dec. 3, 1954
1920	John Roger	Mar. 7, 1955
1932	I. J. Simcox	Feb. 13, 1955
1897	Alpheus F. Williams	Unknown

Proposed for Membership

— Metals Branch AIME —

Total AIME membership on Feb. 28, 1955 was 22,402; in addition 1383 Student Associates were enrolled.

ADMISSIONS COMMITTEE

P. D. Wilson, Chairman; F. A. Ayer, Vice-Chairman; A. C. Brinker, R. H. Dickson, T. D. Jones, F. T. Hunsan, Sidney Rolle, O. B. J. Fraser, F. T. Sisco, Frank T. Weems, R. L. Ziegfeld, R. B. Caples, F. W. McQuiston, Jr., A. R. Lytle, H. R. Wheeler, L. P. Warriner, J. H. Scuff.

The Institute desires to extend its privileges to every person to whom it can be of service, but does not desire as members persons who are unqualified. Institute members are urged to review this list as soon as possible and immediately to inform the Secretary's office if names of people are found who are known to be unqualified for AIME membership.

In the following list C/S means change of status; R, reinstatement; M, Member; J, Junior Member; A, Associate Member; S, Student Associate.

Arizona
Superior—Ellis, Loren E. (M)
Superior—Mahoney, Bartholomew F. (M)
Colorado
Leadville—De Santis, Peter A. (A) (R. C/S—S-A)
Connecticut
Watertown—Lynch, John P., Jr. (M)
Delaware
Wilmington—Trombly, Arthur J. (M)
District of Columbia
Washington—Epremian, Edward (M) (C/S—A-M)
Florida
Vero Beach—Houlehan, Thomas J. (M) (R. C/S—S-M)
Illinois
Chicago—Jackson, David A. (A)
Chicago—Rausch, John J. (J)
Chicago—Treat, Charles N. (M)
Elmhurst—Young, Henry A. (M)
Hinsdale—Graham, John D. (M)
Homewood—Pierce, David W. (M)
Park Forest—Taussig, Charles A. (A)
Western Springs—Meissner, Robert C. (A)
Wheaton—Shaner, Herbert V. (M)
Winnetka—Bayless, Robert N. (A)
Indiana
Hobart—Frame, Charles P. (M) (C/S—A-M)
Kokomo—Miller, Arthur L. (M)
Munster—Bellows, Edmund R. (M)
Kansas
Overland Park—Patterson, Edward P. (M) (C/S—A-M)
Kentucky
Louisville—Hadley, Robert L. (A) (R. C/S—S-A)
Louisiana
Shreveport—Grady, Dan J. (M) (R. C/S—J-M)
Maryland
Baltimore—Schaufus, Henry S. (M) (R.)
Massachusetts
Springfield—Silver, Gordon H. (M)
West Medford—Reed, Norman L. (A) (R. C/S—J-A)
Michigan
Detroit—Roberts, Sidney G. (M) (C/S—A-M)
Montana
Great Falls—Stephens, Tracy V. (M)
Nevada
Carson City—Guild, Clark J. (A)
Castleton Pioche—Frailey, William M. (M)
McGill—Kinneberg, David A. (J)
New Jersey
East Paterson—Zysk, Edward D. (M) (C/S—A-M)
New York
Newtonville—Dyrkacz, Wasil W. (M)
Niagara Falls—Geary, Arthur L. (M)
Niagara Falls—Stern, Milton (J)
Port Washington—Rubenstein, Lester S. (J)
Schenectady—Satz, Leo H. (M) (C/S—A-M)
Star Lake, St. Lawrence County—EshBack, Alton R. (A)
Ohio
Alliance—Ganslein, Earl W. (A)
Cambridge—Johnson, Gordon W. (M)
Cincinnati—Stroppel, Gail L. (A)
Cleveland—Forsmark, Stig O. (A)
Parma—Weber, Edward P. (M)
Shaker Heights—Petersen, Robert P. (M)
Willoughby—Strong, Douglas H. (J)
Pennsylvania
Bethlehem—Gee, Kenneth H. (M)
Bridgeville—Robertshaw, Thomas L. (J)
New Castle—McFeaters, Harry L. (M)
New Kensington—Judge, William Q. (J)
Pittsburgh—Bach, Joseph H. (M) (C/S—A-M)
Pittsburgh—Donaldson, Vernon V. (A)
Pittsburgh—Dulis, Edward J. (M) (R. C/S—M)
Pittsburgh—McClintock, Alma S. (A)
Pittsburgh—Welch, Charles G. (M)
Pittsburgh—Wolf, John S. (A)
St. Marys—Butler, Edward W. (M)
Tennessee
Oak Ridge—Fretague, William J. (M) (C/S—A-M)
Texas
Pasadena—Guidi, Arthur F. (A)
Washington
Tacoma—Henderson, James M. (C/S—A-M)
Canada
Ontario—Cavanagh, Patrick E. (M) (R. C/S—M)
Ontario, Toronto—Jowsey, Robey J. (A)
Saskatchewan, Eldorado—Mancantelli, Robert W. (M)
England
London—Evans, Gerald J. (J)
Fiji Islands
Vatukoulo—Koruh, Danilo (J)
France
Paris—Dupont, Max (M)
Mexico
Monterrey—Mijares, Carlos J. (M)
Monterrey—Morris, Stanford R. (M)

Advertisers' Index

Air Reduction Co., Inc. *G. M. Basford*	*
Ajax Electrothermic Corp. *The Harry P. Bridge Co.*	*
Ajax Engineering Corp. *Eldridge, Inc.*	*
American Bridge Div., U. S. Steel Corp. *Batten, Barton, Durstine & Osborn, Inc.*	583
American Machine & Metals Inc. *The L. W. Ramsey Adv. Agency*	589
Bailey Co., Wm. M. *Walker & Downing*	*
Basic Refractories Inc. *The Griswold-Eshleman Co.*	*
Bell Telephone Labs. *N. W. Ayer & Son, Inc.*	*
Braun & Co., C. F. *The McCarty Co.*	585
Buehler Ltd. *Kreicker & Meloan, Inc.*	586
Consolidated Vacuum Corp. *Charles L. Rumrill & Co., Inc.*	*
Dow Chemical Co. *MacManus, John & Adams, Inc.*	597
Electro Met. Div., Union Carbide & Carbon Corp. *J. M. Mathes, Inc.*	587
Ferro Engineering Co. *C. A. Reece Ind. Publicity*	*
General Electric Co., X-Ray Dept. *Klau, Van Pietersom-Dunlap Assoc.*	600
Great Lakes Carbon Corp. *Davis, Parsons & Strohmeier, Inc.*	593
Harbison-Walker Refractories Co. *Walker & Downing*	*
Hevi Duty Electric Co. *Camm, Costigan, Inc.*	581
International Nickel Co. *Marschalk & Pratt*	598
McKee & Co., Arthur G. *Meermans, Inc.*	*
Molybdenum Corp. of America *Smith, Taylor & Jenkins, Inc.*	592
Morgan Construction Co. *Davis Press, Inc., The*	*
National Carbon Div., Union Carbide & Carbon Corp. *William Esty Co., Inc.*	*
North American Philips Co. *Associated Art Service*	582
Pittsburgh Lectromelt Furnace Corp. *Fuller & Smith & Ross Inc.*	Second Cover
Ramtite Co., The *Marsteller, Rickard, Gebhardt and Reed Inc.*	*
Smooth-Harwood Co. *Allbright Associates Adv.*	*
Smidth & Co., F. L. *The Stuart Co.*	*
Stokes Machine Co., F. J. *John Mather Lupton Co., Inc.*	578, 579
Swindell-Dressler Corp. *Walker & Downing*	*
Taylor Sons Co., The Chas. *The Keelor & Stites Co.*	*
United States Graphite Co., The *Price, Tanner & Willox, Inc.*	Fourth Cover
U. S. Steel Corp. **Columbia-Geneva Steel Div.** **Tennessee Coal & Iron Div.** **U. S. Steel Supply Div.** **U. S. Steel Export Co.** *Batten, Barton, Durstine & Osborn, Inc.*	590, 591
Valley Mould & Iron Corp.	*
Walsh Refractories Corp. *Ralph Smith Adv.*	*
Wyman-Gordon Co. *John W. Odlin Co., Inc.*	Third Cover

* Previous issue.

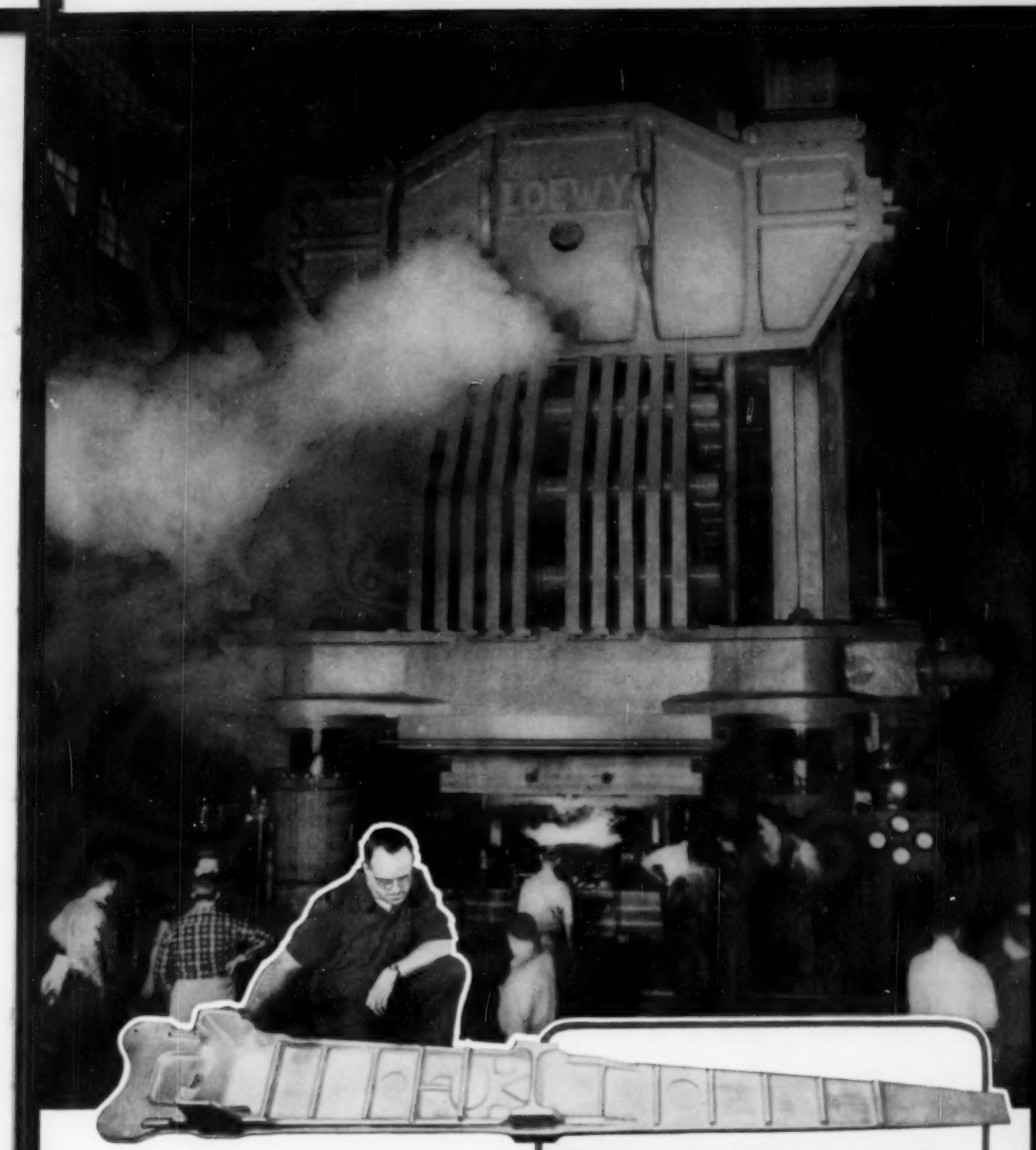

FIRST die forging press in the Air Force Heavy Press Program — 35,000-ton capacity. Now in operation and capable of producing forgings larger than heretofore attempted. Again, as from the beginning of the aviation age, Wyman-Gordon pioneers in scientific advance.

WYMAN-GORDON CO.

Established 1883

FORGINGS OF ALUMINUM • MAGNESIUM
STEEL • TITANIUM

WORCESTER 1, MASSACHUSETTS
HARVEY, ILL. • DETROIT, MICH.

USG® PRODUCTS IMPROVE STEEL MAKING FROM CHARGE TO FINISHED INGOT

The United States Graphite Company has served the steel industry for a half century with products to improve steel making from the furnace to the finished ingot. Our engineering service and laboratories are constantly working on new products to solve your steel production problems. The products listed here are a few of the most popular and widely used — why not investigate them — they can cut your costs.

RECARB-X®

(engineering bulletin #11)

insures carbon specifications

RECARB-X is ideal for off-carbon heats. A fifty pound bag per 100-tons of steel will raise carbon two points when added to the ladle. RECARB-X dissolves quietly, gives uniform, dependable carbon recovery at all carbon levels. There are grades of RECARB-X for the furnace charge.

MEXICAN® MOLD WASHES

(engineering bulletin #15)

for better ingot surfaces

For as little as ¾c per ingot ton, you can insure quicker, easier mold stripping with MEXICAN Ingot Mold Washes. MEX and 90-B can be applied at any temperature and are easy to prepare and use. Where a high volatile "gas kick" is needed, VOLMEX or XF-81 will supply the answer. For an inert, non-carbonaceous mineral coating, XF-88 will do the job.

MEXATOP®

(engineering bulletin #5)

gives sounder ingots

MEXATOP is a powder compound which spreads easily over molten ingot heads and casting risers. A ⅛" layer over the molten surface works effectively to prevent cavitation and insure sounder castings.

Write for Engineering Bulletins describing these products.

196

THE UNITED STATES GRAPHITE COMPANY

DIVISION OF THE WICKES CORPORATION • SAGINAW, MICHIGAN

Journal of METALS

MAY 1955

TRANSACTIONS SECTION

VOL. 7, NO. 5, IN TWO SECTIONS—SECTION TWO

High Temperature Properties of Iron-Rich Fe-Mo Alloys
S. F. Kiefer, W. R. Hibbard, Jr. 655

Viscous Flow of Copper at High Temperatures
A. L. Pranatis, G. M. Pound 664

Curie Temperatures of Binary and Ternary Sigma Phases
M. V. Nevitt, P. A. Beck 669

Effect of the Structure of Dislocation Boundaries on Yield Strength
J. Washburn 675

Creep Deformation of Magnesium at Elevated Temperatures by Nonbasal Slip
A. K. Chaudhuri, H. C. Chang, N. J. Grant 682

Discussion—Institute of Metals Div. 689

Copyrighted by American Institute of Mining and Metallurgical Engineers, Inc., 1955
Printed in U.S.A.

High Temperature Properties of Iron-Rich Fe-Mo Alloys

by S. F. Reiter and W. R. Hibbard, Jr.

A survey of the effect of heat treatment on the room temperature hardness of Fe-Mo alloys has been made. Constant strain rate tensile tests were performed between room temperature and 1800°F. These data were analyzed to determine the effect of temperature and composition on the strain hardening coefficient and strain rate sensitivity. Constant load creep-rupture tests were made on these alloys and the results related to composition and structure. A relation between the high temperature strength of the precipitation hardened alloys and the volume of precipitate has been observed.

IN view of the extensive use of ferritic materials at elevated temperatures, it is surprising to note the limited amount of information relating the variables of plastic deformation, i.e., composition, structure, temperature, stress, strain, and strain rate. Hollomon and Lubahn[1] showed how the several variables of plastic flow might be treated analytically. No data were available on carbon-free iron and its alloys in a form suitable for this analysis. Several German investigations[2-4] constitute most of the experimental work relating high temperature properties to the constitution of these types of materials.

In order to obtain new data, the iron-rich alloys of the Fe-Mo system were selected for detailed investigation for the following reasons: 1—Some of the important effects of molybdenum on the mechanical properties of iron have already been studied.[5, 6, 7, 8] 2—By suitable heat treatment of selected alloys, it is possible to study strengthening effects of four types: A—γ-α transformation, B—substitutional, C—precipitation, and D—dispersion of hard intermetallic compound.

Materials and Treatment

Four-pound ingots were vacuum cast, employing the same melting schedule previously used.[7] The raw materials were electrolytic iron and lamp-grade molybdenum. The ingots were forged to ½ in. sq. rod and one portion swaged to 0.350 in. diam rod for the production of 1 15/16 in. long button-head specimens. The button-head specimen blanks were solution treated for 16 hr at 2100°F in hydrogen of −70°C dewpoint and then water quenched. They were subsequently plunge ground to the standard 0.160 in. diam test bar.[7] Micrographs of the solution treated alloys are given in Figs. 1a through 1d. The higher molybdenum alloys contained large equiaxed ferrite crystals similar to those in Fig. 1d.

Table I. Chemical Composition of the Fe-Mo Binary Alloys

Mo	C	Si	Mn	S	P
0	0.001	<0.01	0.001	0.002	†
1.09	0.003	0.02	*	0.003	†
2.05	0.006	0.02	*	0.006	†
4.32	0.004	0.02	*	0.001	†
5.74	0.004	0.02	*	0.004	†
8.75	0.004	0.02	*	0.002	†
10.69	0.004	0.01	*	0.003	†
15.70	0.004	0.02	*	0.003	†
15.90	0.002	<0.01	0.002	0.002	0.004

* A slight trace of manganese was detected spectrographically.
† The phosphorous contents were in the range from 0.002 to 0.003 pct.

A portion of the ½ in. rod was hot rolled to 0.100 in., sandblasted, and cold rolled to 0.020 in. Strip tensile specimens having a 0.020x0.200 in. cross-section and a 2.25 in. gage length were machined from the sheet. The alloys containing molybdenum were subsequently annealed 1 hr at 1560°F. The iron strip was annealed 4 hr at 1300°F in wet hydrogen. The resultant structures are shown in Fig. 2a through h. The ASTM grain sizes were 1 to 3 as solution heat treated or 3 to 4 as annealed.

The chemical analyses of the alloys are given in Table I. Carbon contents were obtained after the heat treatments in hydrogen. Alloy 15.9 pct Mo was tested as a cast alloy.[7]

S. F. REITER, Junior Member AIME, formerly associated with Research Laboratory, General Electric Co., is Technical Manager, Rome Fastener Corp., New Haven, Conn., and W. R. HIBBARD, JR., Member AIME, is associated with Metallurgy Research Dept., Research Laboratory, General Electric Co., Schenectady.

Discussion of this paper, TP 3987E, may be sent, 2 copies, to AIME by July 1, 1955. Manuscript, Aug. 2, 1954. Chicago Meeting, February 1955.

The Transactions papers appearing in the Journal of Metals during 1955 will subsequently appear in AIME Transactions Volume 203, and may be permanently referenced to that volume.

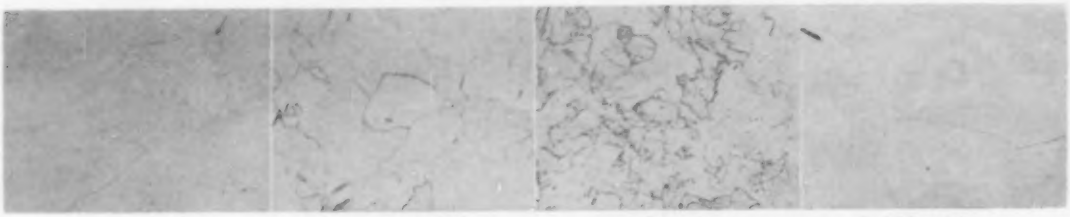

a—Iron. b—1.09 pct Mo. c—2.06 pct Mo. d—4.32 pct Mo.

Fig. 1—Fe-Mo alloys in the solution heat-treated condition. Heat treated at 2100°F for 16 hr, water quenched. Etched with nital. X100. Area reduced approximately 50 pct for reproduction.

The electrolytic iron melt will be designated "iron," and the binary alloys will be referred to by their molybdenum contents.

Equipment

Constant load creep-rupture tests were run in an argon atmosphere at 1200°F. Strain was read from a dial gage linked to the shoulders of the specimens. The specimen was exposed to the bare heating element in the furnace. The temperature was measured and controlled by three Pt—Pt-Rh thermocouples positioned along the specimen during the test. The maximum temperature difference at 1200°F along the 1⅛ in. gage length was 2°F, approximating the accuracy of the three thermocouples. The short-time cycling of the furnace was ±0.2°F, while the long-time overnight cycling of the furnace was ±1.0°F.

Tensile tests were carried out in air using the Instron testing machine previously described.[8]

Hardness Survey

Samples were heated to 2100°F in hydrogen, held 16 hr at temperature, and quenched in water. Individual specimens were aged 2 hr at various temperatures in hydrogen and water quenched to room temperature. Fig. 3 summarizes the results of the study, giving the average hardness value obtained from five impressions.

Three types of curves are shown in Fig. 3. The first is shown by the dashed curves of iron, 1.09, and 2.06 pct Mo. These compositions transform from γ iron when water quenched, producing an irregular martensitic-type structure. When heated above 1000°F, the alloys soften rapidly. At 1800°F, iron 1.09, and 2.06 pct Mo have the γ structure, so that quenching from this temperature and from 2000°F increases the hardness as a result of martensitic-type transformation.

The second characteristic hardness temperature curve is that of 4.32 pct Mo. This alloy undergoes no phase change between room temperature and its melting point and no significant change in room temperature hardness occurs as a result of heating to 2000°F. 5.74 pct Mo has essentially the same hardness temperature behavior. However, at 1200°F, 5.74 pct Mo precipitates a very small amount of ϵ phase. The amount of precipitation is not large enough to produce appreciable hardening.

The third type of curve is displayed by 8.75, 10.69, and 15.70 pct Mo. At 1200°F, measurable precipitation hardening occurs. The hardening effect is greater the larger the molybdenum content.

Fig. 4 relates the maximum and minimum hardness values to the Fe-Mo constitution diagram. Both transformation and precipitation reactions are shown to be very effective hardeners.

Tensile Data

True Stress-True Strain Plots: The true stress-true strain plots were determined for all the Fe-Mo

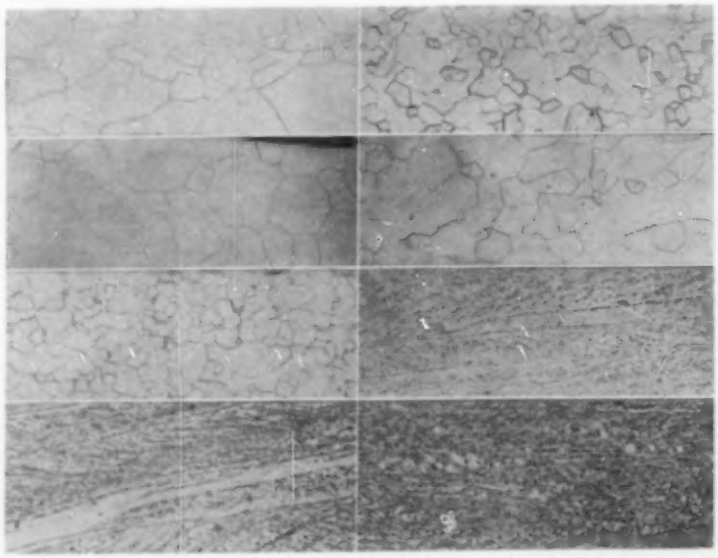

a—Iron, annealed 1 hr at 1300°F. b—1.09 pct Mo annealed 1 hr at 1560°F. c—2.06 pct Mo annealed 1 hr at 1560°F. d—4.32 pct Mo annealed 1 hr at 1560°F. e—5.74 pct Mo annealed 1 hr at 1560°F. f—8.75 pct Mo annealed 1 hr at 1560°F. g—10.69 pct Mo annealed 1 hr at 1560°F. h—15.70 pct Mo annealed 1 hr at 1560°F.

Fig. 2—Fe-Mo alloys in the annealed condition after 80 pct cold work. Etched with nital. X100. Area reduced approximately 50 pct for reproduction.

1955 will subsequently appear in AIME Transactions Volume 203, and may be permanently referenced to that volume.

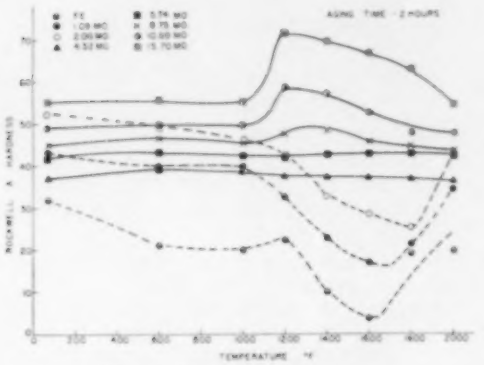

Fig. 3—Aging studies of Fe-Mo alloys.

alloys. They were tested after a water quench from 2100°F and at a strain rate of 0.09 min^{-1}. The samples were 0.160 in. diam rods, except for 15.70 pct Mo, which was tested as 0.020x0.200 in. strip. This alloy cracked during swaging so that no bar stock was available.

In Fig. 5, the ultimate tensile strengths at the several testing temperatures are shown as a function of composition for the solution treated alloys. Data for stress at constant strain values as a function of composition resulted in plots essentially similar to those in Fig. 5.

The interesting feature of Fig. 5 is a maximum in strength which is apparent at about 2 pct Mo for the alloys tested at room temperature and 1000°F. This peak is associated with the transformation hardening reaction. At higher testing temperatures, transformation hardening is not effective. The iron and 1.09 pct Mo alloys are stronger in the face-centered-cubic structure at 1800°F than they are at 1600°F in the body-centered-cubic form. Another interesting feature of Fig. 5 is the increase in tensile strength at 1400° and 1600°F in alloys that precipitate a significant amount of ϵ phase during the tensile test.

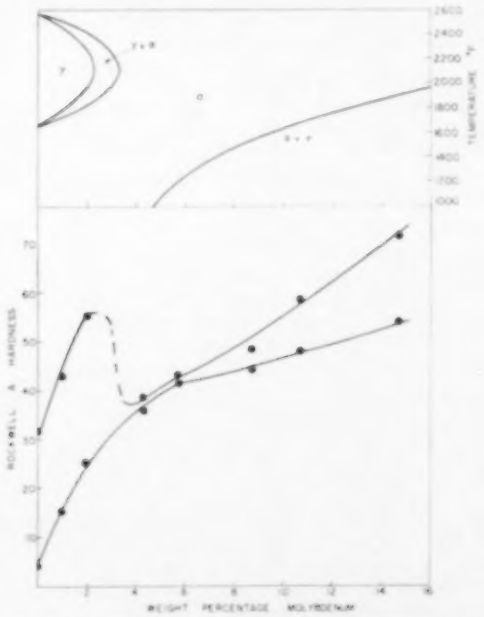

Fig. 4—A portion of the Fe-Mo constitution diagram and the maximum and minimum hardness data.

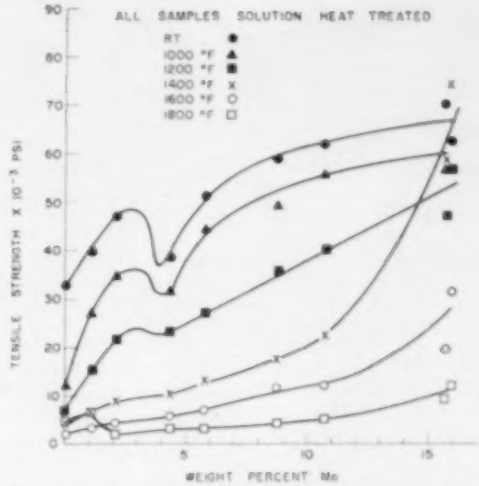

Fig. 5—The effect of temperature on the tensile strength of Fe-Mo alloys tested in the solution heat-treated condition.

True stress-true plastic strain plots were also determined for the Fe-Mo alloys tested in the annealed condition at a strain rate of 0.09 min^{-1}. In all cases, the test samples are 0.020x0.200 in. strip. Fig. 6 gives the tensile strengths of these alloys in the annealed condition as a function of composition. Data for stress at constant amounts of plastic strain produced similar plots. Alloys with more than 5.74 pct Mo contain some ϵ, and a significant increase in their strength results from the dispersed phase. The curves are shown dotted connecting 10.69 and 15.70 pct Mo because the condition or dispersion of the second phase is not constant for these materials.

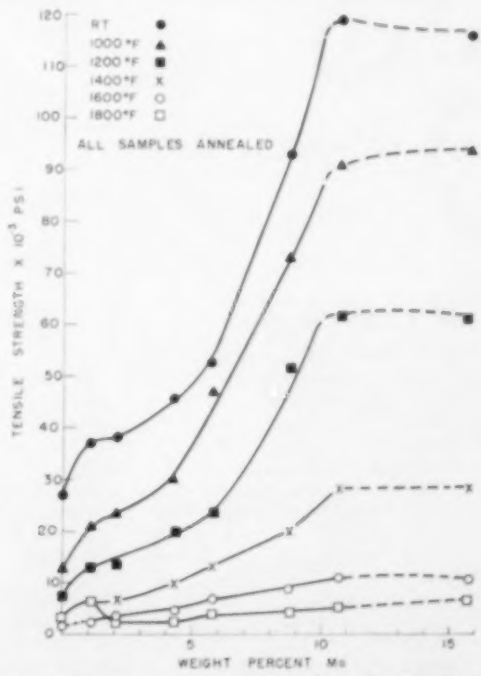

Fig. 6—The effect of temperature on the tensile strength of Fe-Mo alloys tested in the annealed condition.

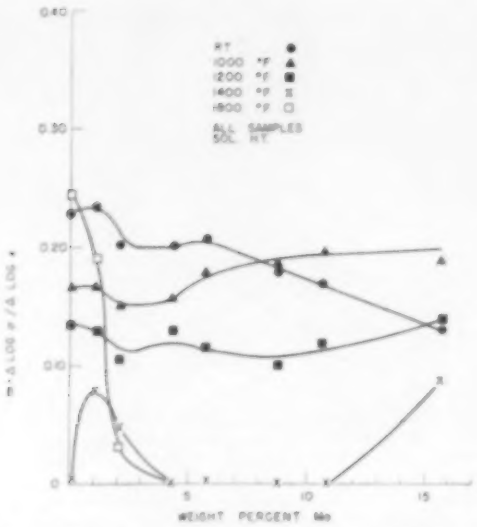

Fig. 7—The effect of temperature on the strain hardening exponent of Fe-Mo alloys tested in the solution heat-treated condition.

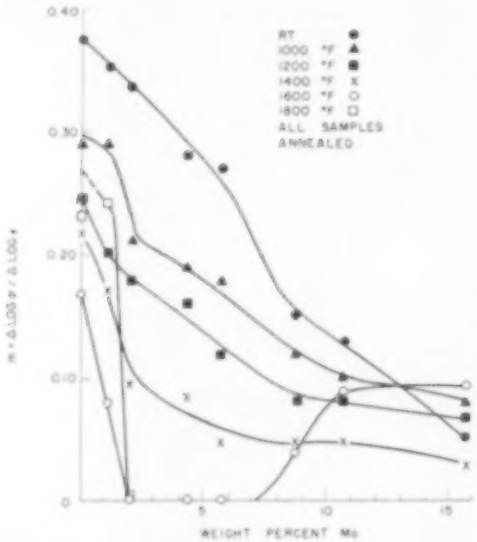

Fig. 8—The effect of temperature on the strain hardening exponent of Fe-Mo alloys tested in the annealed condition.

Yield Points: Yield points were not found in the stress-strain curves for specimens of any of the alloys tested at room temperature after solution heat treating at 2100°F in dry hydrogen and water quenching. These specimens were plunge ground after heat treatment and tested days after heat treatment. It is suggested that the absence of the yield point is the result of either quenching or of the removal of carbon during the 16 hr 2100°F treatment in dry hydrogen[20] and is not related to the presence of molybdenum.[20]

Specimens cold rolled and annealed at 1560°F were found to have small yield points at room temperature when the alloy content was less than 8.75 pct Mo, i.e., single-phase alloys at the annealing temperature (see Fig. 4). The prominence of these yield points was related to the carbon content in

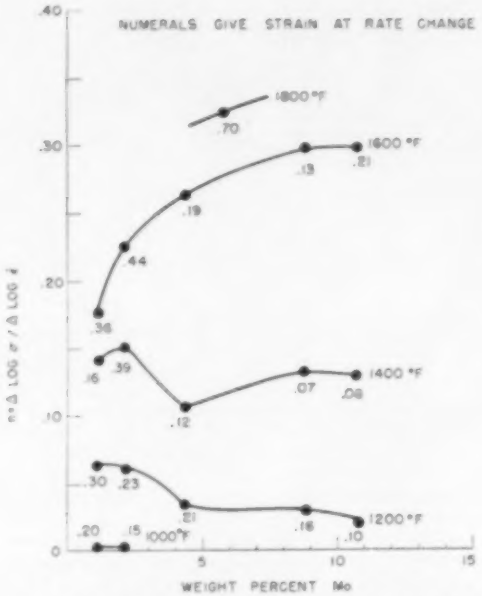

Fig. 9—Effect of temperature on the strain rate sensitivity, *n*, of Fe-Mo alloys. The values given with the data points are the true plastic strain, *ε*, at the rate change.

Table I, not to the molybdenum content. (For example, the 2.06 pct Mo alloy containing 0.006 pct C had the most prominent yield point.) The alloys containing 8.76 and 10.69 pct Mo were annealed at a temperature where Fe_2Mo_2 was precipitated. These alloys had no yield points at room temperature, probably because the carbon was partitioned from the solid solution and dissolved in the intermetallic compound. These results are also consistent with the results of Edwards, Phillips, and Jones,[20] who found that the presence of molybdenum in solid solution does not counteract the effects of carbon in causing yield points in iron.

Strain Hardening: The true stress-true plastic strain data for the alloys in the solution heat treated and annealed conditions were plotted on logarithmic coordinates. These plots result in straight lines for the majority of the alloys tested and can be interpreted in terms of the expression given by Hollomon and Lubahn[1]

$$\sigma = K_1 \epsilon^m |_{\dot{\epsilon},T} \qquad [1]$$

where σ and ϵ are the true stress and true plastic strain, respectively, K_1 is a constant, and m is the strain hardening exponent. The strain rate, $\dot{\epsilon}$, and temperature, T, were constant for these tests.

Fig. 7 shows the effect of temperature on the strain hardening exponent for alloys in the solution heat treated condition. At room temperature, m decreases with increasing alloy content. However, at 1000° and 1200°F, age hardening alloys are associated with essentially constant strain hardening exponents. The pure iron sample tested at 1400°F had a very small m value which may be the result of recovery. Tensile tests performed on the alloy series at 1600°F yielded m values close to zero and are not plotted. At 1800°F, the large values of m for the iron and 1.09 pct Mo alloys are believed to be the result of the face-centered-cubic structure.

In Fig. 8, m values are shown for the alloys tested in the annealed condition. At room temperature up

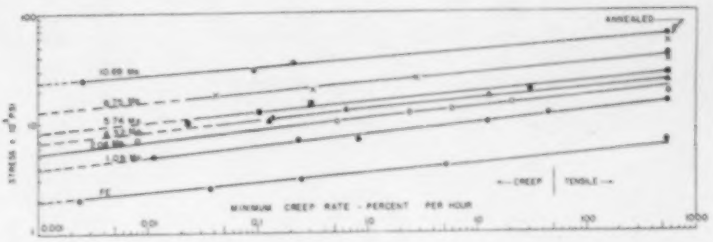

Fig. 11—Stress vs minimum creep rate of Fe-Mo alloys quenched from 2100°F.

to 1400°F, there is a decrease in the strain hardening exponent value with increasing molybdenum content similar to that observed by French and Hibbard in copper alloys.[7] At 1600°F, the m value falls off to zero at 2 pct Mo but rises again in alloys containing more than 8 pct Mo. This rise is believed to be related to the contribution of dispersion hardening. At 1800°F, only the two face-centered-cubic materials displayed significantly large strain hardening exponents.

Effect of Strain Rate: During many of the tensile tests previously described, the strain rate was decreased by a factor of ten after the maximum load had been reached. The strain rate sensitivity given as the exponent in Eq. 2 was calculated, and the results are shown in Fig. 9.

$$\sigma = K_2 \dot{\epsilon}^m|_{\epsilon,T} \qquad [2]$$

K_2 is a material constant and the strain, ϵ, and temperature, T, are also invariant. Also shown in Fig. 9 are the values of strain at which the rate was changed. There is significant increase in the rate sensitivity with increasing temperature above 1000°F. At this time, the shape of the curves cannot be rationalized possibly because of the experimental variation in strain, ϵ.

Tensile Tests in Vacuum

The 1800°F tensile data for pure iron showed irregularities. Tensile tests were run on 0.160 in. diam iron samples in vacuum for purposes of comparison. In Fig. 10, the nominal stress-nominal plastic strain curve for specimens tested in air (curve *a*) may be compared with the test run in vacuum under similar strain rate conditions (curve *b*) and at slower strain rates (curves *c* and *d*). The maxima appeared at essentially the same strain values and therefore are believed to be a manifestation of a strain-dependent softening reaction at this temperature. The tests at lower strain rates (shown by curves *c* and *d*) exhibit smaller load values, indicating a relatively large strain rate sensitivity at this temperature. Localized necking had started in several locations in each of these specimens. The final grain size in the necked areas was essentially similar to that in the rest of the gage length.

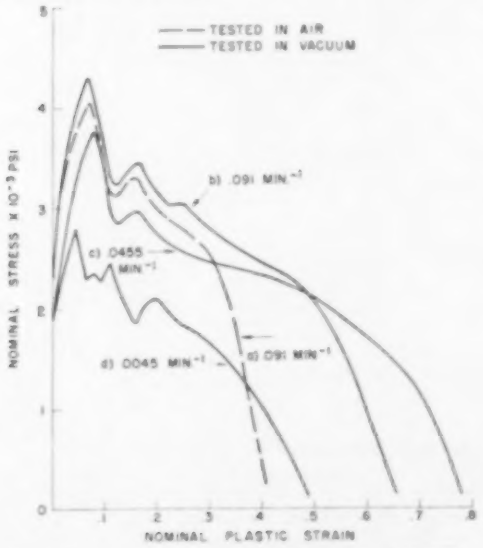

Fig. 10—Comparison of tensile tests of pure iron at 1800°F in air and in vacuum.

Creep and Rupture Data

All of the creep-rupture tests were performed at 1200°F. Since all of the creep tests were taken to rupture, an inversion point with respect to creep rate was observed. This minimum creep rate is shown plotted in Fig. 11 as a function of initial stress. The maximum load in a tensile test is shown plotted against the strain rate for the tests in air at 1200°F. The maximum load stress was selected because it is considered to be analogous to the conditions reflecting minimum creep rate in a creep test. The straight line connecting the creep data intersects the tensile data in this plot for the alloys that do not exhibit particularly strong aging re-

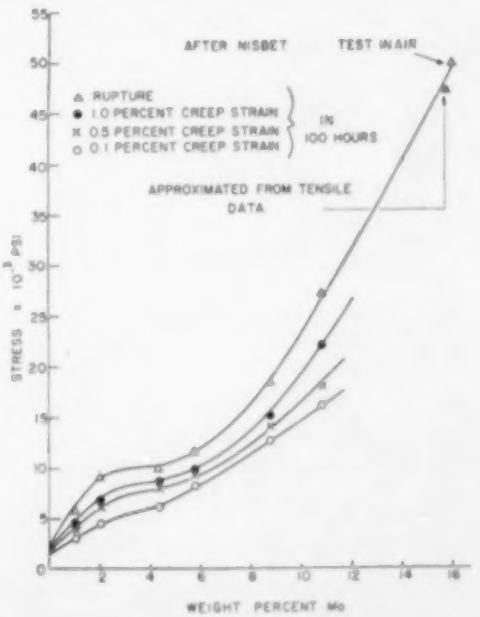

Fig. 12—Effect of composition on the stress to produce 0.1, 0.5, and 1.0 pct creep strain and rupture in Fe-Mo alloys at 1200°F. Nisbet data from *ref. 7*.

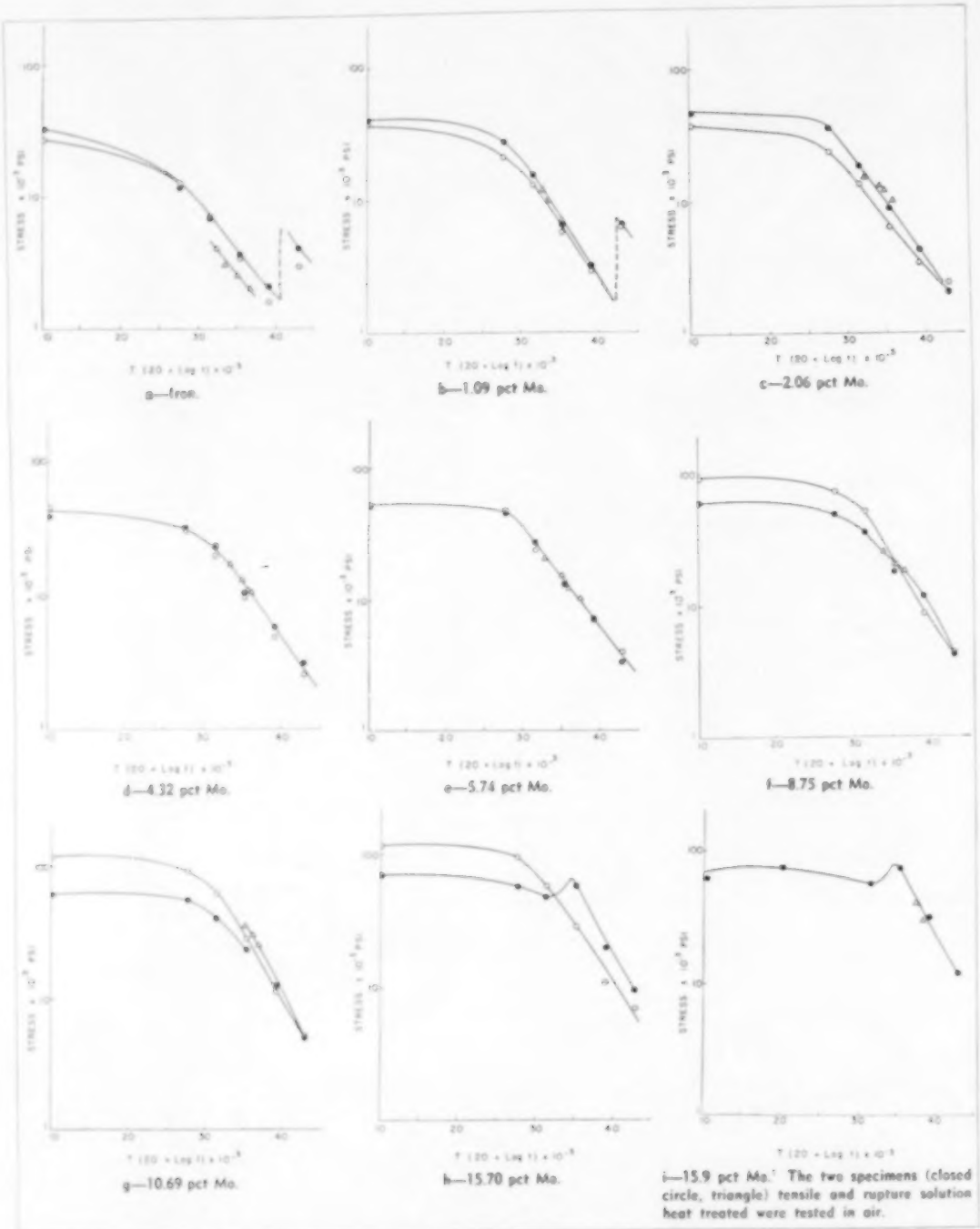
a—free.
b—1.09 pct Mo.
c—2.06 pct Mo.
d—4.32 pct Mo.
e—5.74 pct Mo.
f—8.75 pct Mo.
g—10.69 pct Mo.
h—15.70 pct Mo.
i—15.9 pct Mo. The two specimens (closed circle, triangle) tensile and rupture solution heat treated were tested in air.

Fig. 13—Parametric plots including tensile and rupture data. In each plot, closed circle represents tensile solution heat treatment; open circle, tensile annealed; and triangle, rupture solution heat treatment.

actions. For the two high molybdenum alloys, the line falls between the tensile strengths for the solution heat treated and annealed specimens.

Similar straight-line logarithmic plots were obtained for initial stress plotted against time for rupture, 1.0 pct creep strain, 0.5 pct creep strain, or 0.1 pct creep strain. In Fig. 12, composition is related to the initial stress to cause rupture, 1.0, 0.5, and 0.1 pct creep strain in 100 hr at 1200°F. The knee in the rupture curve at 2 pct Mo is believed to be related to the strengthening effect produced by transformation hardening. This effect is more pronounced with increasing strain. The most significant effects of composition on strength occur in the range of compositions involving precipitation hardening alloys.

Parameter Plots

The rupture and tensile data previously reported

are assembled in a series of plots in Figs. 13a to 13f, wherein temperature and time are combined according to the Larson-Miller[9] parameter expression

$$P_m = T(20 + \log t)10^{-4} \qquad [3]$$

where T is test temperature in degrees Rankine and t the duration of the test in hours. A rather large difference between the rupture and tensile data for iron is shown in Fig. 13a. This difference is believed to be due to precipitation of FeO[8] during the 1200°F creep-rupture tests and the accompanying loss of ductility, which greatly reduced the rupture life. The temperature of the phase change for a tensile test is indicated by a vertical dashed line in this plot and also in Fig. 13b for 1.09 pct Mo. From Fig. 13c, 2.06 pct Mo is strengthened by the martensite transformation more than iron and 1.09 pct Mo alloys. The rupture data fall on the same line as the solution heat treated tensile data. Alloy 4.32 pct Mo (Fig. 13d) undergoes no phase change during heat treatment and there is good agreement between the rupture and tensile data for both heat treatments. The same agreement is found for 5.74 pct Mo, shown in Fig. 13e, since the amount of ϵ precipitated in long-time tests at 1200°F is extremely small. For the higher molybdenum alloys, Fig. 13f illustrates the larger strengthening due to precipitation hardening at higher testing temperatures (solution heat treated) and of dispersion hardening at lower testing temperatures (annealed). The difference is believed to be of degree rather than kind, i.e., the alloy previously solution treated precipitates a very fine dispersion, while the annealed materials have large coarse particles in their structure.

Discussion

The linear logarithmic creep-rupture plots similar to Fig. 11 suggest the following relationship between initial stress, S, and the time, t, for a predetermined amount of creep

$$S = K_s t^{-n'}|_{\epsilon,T} \qquad [4]$$

where the creep strain, ϵ, and the test temperature, T, are constant, and K_s and n' are material constants. Eq. 4 follows from Eq. 2, since at constant stress $\dot{\epsilon}$ is proportional to $1/t$. Eq. 4 can also be written in the form

$$t = K_s S^{-n'}|_{\epsilon,T}. \qquad [5]$$

Values of n' have been determined graphically and the values tabulated in Table II. It is interesting to note that the n' values are consistently larger than the rate sensitivity, n, which was determined from tensile data by the use of Eq. 2. Alloys 1.09, 2.06, and 4.32 pct Mo show a smaller slope ($\Delta n'$ is negative) with increasing amounts of creep, i.e., they are becoming more stress sensitive with increasing amounts of creep. These alloys are tempered or softened in the conventional sense at 1200°F. Alloys 5.74, 8.75, and 10.69 pct Mo, the age hardening alloys, display increasing slopes ($\Delta n'$ is positive) with increasing amounts of creep, i.e., these alloys are becoming less stress sensitive at larger creep strains. Iron, when tested at 1200°F, shows a behavior with regard to $\Delta n'$ similar to that of the age hardening high molybdenum alloys, probably due to a precipitate thought to be FeO[8].

The relative effectiveness of solution and precipitation hardening in Fe-Mo alloys may be estimated from Fig. 12. At 1200°F, the maximum amount of solution strengthening at the solid solubility limit of 5 pct Mo in iron results in a 100 hr rupture strength of 10,500 psi. By the dispersion of a stable intermetallic compound, three to five times the rupture strength of the saturated solution may be obtained.

Table II. Comparison for n' and n for Solution Heat-Treated Fe-Mo Alloys Tested at 1200°F

Wt Pct Mo	n', Negative Slope of Log Stress-Log Time Plot				Rate Sensitivity from Tensile Tests	
	Creep, In. per In.					Strain at Rate Change, In. per In.
	0.001	0.005	0.01	Pct $\Delta n'$	n	
0	0.093	0.093	0.111	19	—	—
1.09	0.103	0.090	0.085	−18	0.062	0.30
2.06	0.101	0.092	0.084	−17	0.078	0.10
4.32	0.082	0.078	0.075	− 9	0.034	0.21
5.74	0.074	0.076	0.083	12	—	—
8.75	0.061	0.065	0.068	38	0.030	0.16
10.69	0.072	0.092	0.095	32	0.02	0.10

The increase in creep and rupture strength due to precipitate hardening is plotted in Fig. 14 as a function of the equilibrium volume fraction of Fe_2Mo_3 calculated from the stoichiometric composition and assumed densities of α and ϵ, 7.9 and 9.0, respectively.[10] A line of slope 1.5 in Fig. 14 is in fair agreement with the rupture data.

On the basis of dislocation theory, Fisher, Hart, and Pry[11] described the increment in tensile flow stress, $\Delta\sigma$, in this way

$$\Delta\sigma = Kf(r)f^{1/2} \qquad [6]$$

where k is a constant, $f(r)$ is a function of the particle radius, and f the volume fraction. The rupture data indicate a correlation between the contribution of hard particles to rupture strength and to increased flow stress in tensile tests. It is assumed that the effective particle radii were sufficiently constant to conform to this relationship. The particles measured at X500 are approximately 0.1 micron in diameter.

In the present study, three of the conditions of

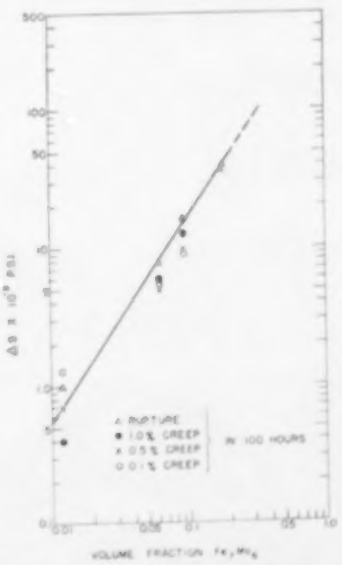

Fig. 14—Increase in rupture and creep strengths over the saturated solid solution plotted against volume fraction Fe_2Mo_3.

the mechanical equation of state given by Hollomon and Lubahn[7] were evaluated, namely, that log σ_o, m, and n should be linear functions of temperature. In Fig. 15, the yield stress at 0.005 strain is plotted against the absolute temperature on semilogarithmic coordinates. The high temperature portion of the curve is linear, but the data do not clearly delineate the effect of composition on the slope. In Fig. 16, the strain hardening exponent is plotted as a function of temperature, and again the high temperature portion may be considered as a family of straight lines. Plotting the strain rate sensitivity, n, against absolute temperature yields another set of straight lines in the high temperature area shown in Fig. 17. In the preceding plots, only the solid solution alloys in the annealed condition were considered. Solid solution alloying may be considered to increase the transition temperature between low and high temperature behavior in the three preceding plots. In Fig. 16 the temperature dependence of the strain hardening exponent appears to increase with increasing alloy content. Similarly, in Fig. 17, the strain rate sensitivity's temperature dependence also increases with molybdenum content.

In Fig. 18, the strain hardening exponent is related to the yield stress at constant temperature values for the solution strengthened alloys in the annealed condition. The slope appears to increase in a regular manner as the testing temperature is increased.

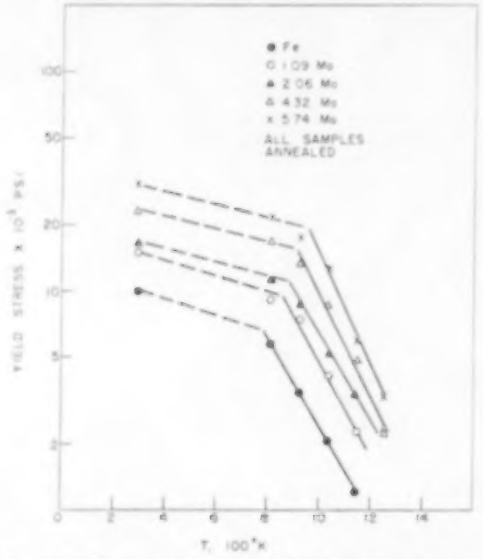

Fig. 15—Yield stress of annealed solid solution alloys vs absolute temperature.

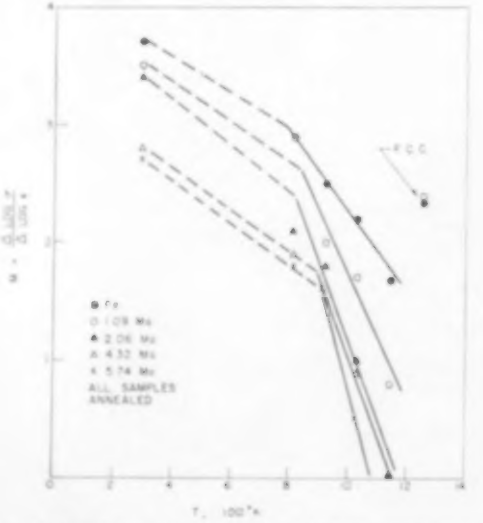

Fig. 16—Strain hardening exponent vs absolute temperature.

Alloying Principles

Previous investigators[4-6] have contended that, in the low alloy area of the phase diagram, maximum high and low temperature strengthening is achieved by quenching from a saturated solution of austenite. This effect is strongly time and temperature dependent. The tensile data (Fig. 5) for quenched alloys show that the relative contribution of transformation hardening decreases from a maximum at room temperature to essentially zero at 1400°F.

The temperature and time dependence of transformation hardening is also illustrated in the parameter plots given in Figs. 13a, b, and c. The strengths of quenched samples approach those of annealed material at parameter values that increase with increasing molybdenum content. This effect may be

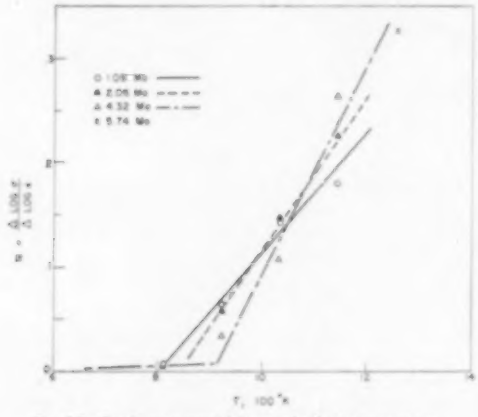

Fig. 17—Strain rate sensitivity vs absolute temperature.

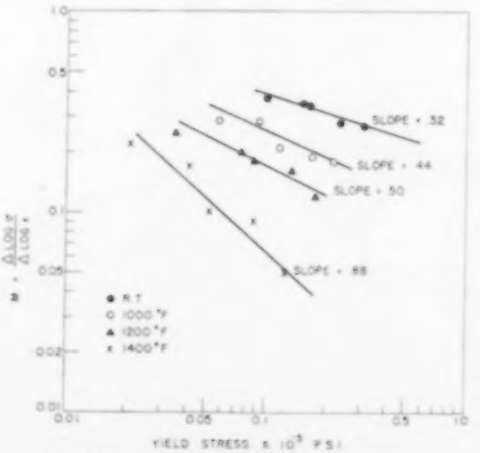

Fig. 18—Strain hardening exponent vs yield stress.

related to 1—the increase in transformation temperature, and 2—increased stability of the ferrite grain boundaries with increasing alloy content.

As shown in Figs. 5, 6, and 12, a fine and relatively stable dispersion is a much more potent strengthening factor at high temperatures than is solution or transformation strengthening. This finding is in accord with the fact that currently available high temperature ferritic alloys contain a fine dispersion of alloy carbides.

In agreement with Nisbet and Hibbard,[7] an allotropy-free material and one of very low precipitation hardening potential give single-line parametric strength curves (Figs. 13d and e), regardless of heat treatment. Alloys that contain a fine dispersion of a precipitate show marked superiority in strength at high temperatures over the annealed or overaged structures (Fig. 13f).

Summary

1—A survey of the effect of heat treatment on the room temperature hardness of Fe-Mo alloys has been made, and the results have been related to the constitution diagram.

2—Constant strain rate tensile tests on polycrystalline electrolytic iron and its alloys with molybdenum have been performed between room temperature and 1800°F. The data were analyzed as true stress-true strain plots and also as plots of tensile strength at several temperatures which may be related to the constitution diagram. The effects of temperature and composition on the strain hardening exponent and strain rate sensitivity were determined.

3—Constant load creep-rupture tests were performed and the results related to composition and structure. A relation between the high temperature strength of the precipitation hardened alloys and the volume of precipitate has been observed.

4—Support for the concept of a mechanical equation of state was obtained. The influence of alloying on some of the parameters of the equation of state has been demonstrated.

Acknowledgments

The authors are indebted to J. D. Nisbet for valued suggestions and guidance during the progress of this study. The creep-rupture tests were performed by W. E. Rollins and R. F. Berning. Mrs. J. Paquette made the large number of calculations connected with this report. The authors also wish to thank the many members of the Alloy Studies Section of the Research Laboratory, General Electric Co., who presented stimulating discussion.

Discussion of this paper, if any, will appear in JOURNAL OF METALS, November 1955, and in AIME Metals Branch *Transactions*, Vol. **203**, 1955.

References

[1] J. H. Hollomon and J. D. Lubahn: The Flow of Metals at Elevated Temperatures. *General Electric Review* (February, April 1947).

[2] P. Grün: Creep of Steel as a Function of Alloy Content and Heat Treatment. *Archiv für Eisenhüttenwesen* (1934) **8**, p. 205.

[3] W. Holtmann: Influence of Alloy on Tensile Strength and Creep Limit of Heat-Treated Steels. *Mitteilungen Kohle und Eisenforschung* (1941) **3**, p. 1.

[4] F. Wever and W. Peter: Precipitation Hardening and the Creep Limit of Fe-Cb Alloys and Cb-Alloyed Steels. *Archiv für Eisenhüttenwesen* (1941-1942) **15**, p. 357.

[5] P. Bordenheuer and W. A. Fischer: Influence of Titanium on the Creep Limit of Steel. *Archiv für Eisenhüttenwesen* (1942-1943) **16**, p. 31.

[6] W. Peter and W. A. Fischer: Relationship Between the Phase Diagram and Mechanical Properties, Particularly the Creep Behavior, of Fe-Cb and Fe-Ti Alloys. *Archiv für Eisenhüttenwesen* (1949) **19**, p. 161.

[7] J. D. Nisbet and W. R. Hibbard, Jr.: A Rationalization of Measured High-Temperature Properties of Fe-Cr-Co-Ni Alloys. *Trans.* AIME (1953) **197**, p. 1149; JOURNAL OF METALS (September 1953).

[8] E. R. Parker: The Development of Alloys for Use at Temperatures Above 1000°F. *Trans.* ASM (1940) **28**, p. 797.

[9] C. R. Austin, C. R. St. John, and R. W. Lindsay: Creep Properties of Some Binary Solid Solutions of Ferrite. *Trans.* AIME (1945) **162**, p. 84; METALS TECHNOLOGY (August 1945).

[10] W. P. Sykes: The Iron-Molybdenum System. *Trans.* Amer. Soc. for Steel Treating (1926) **10**, p. 839.

[11] D. T. Seljesater and B. A. Rogers: Magnetic and Mechanical Hardness of Dispersion-Hardened Iron Alloys. *Trans.* Amer. Soc. for Steel Treating (1932) **19**, p. 553.

[12] W. P. Sykes: Precipitation-Hardening in the Heavy Alloys. *ASM Symposium on Age-Hardening of Metals* (1939) p. 82.

[13] W. P. Sykes: Further Notes on Precipitation Hardening in the Heavy Alloys. *Trans.* ASM (1940) **28**, p. 892.

[14] C. E. Lacy and M. Gensamer: The Tensile Properties of Alloyed Ferrites. *Trans.* ASM (1944) **32**, p. 88.

[15] C. R. Austin: Effect of Elements in Solid Solution on Hardness and Response to Heat Treatment of Iron Binary Alloys. *Trans.* ASM (1943) **31**, p. 321.

[16] C. R. Austin, L. A. Luini, and R. W. Lindsay: Annealing Studies on Cold-Rolled Iron and Iron Binary Alloys. *Trans.* ASM (1945) **35**, p. 446.

[17] D. Harker and M. J. Murphy: A Study of Age-Hardening Using the Electron Microscope and Formvar Replicas. *Trans.* AIME (1945) **161**, p. 75; METALS TECHNOLOGY (June 1945).

[18] H. Arnfelt: On the Constitution of the Fe-W and the Fe-Mo Alloys. *Carnegie Scholarship Memoirs* Iron and Steel Inst. (1928) **17**, p. 1.

[19] T. Takei and T. Murakami: *Trans.* Amer. Soc. for Steel Testing (1929) **16**, p. 339.

[20] H. Arnfelt and A. Westgren: The Crystal Structure and the Composition of the Intermediate Phases Present in Fe-W and Fe-Mo Alloys. *Jernkontorets Annaler* (1935) **119**, p. 185.

[21] *Metals Handbook*. (1948) Cleveland. ASM.

[22] J. R. Low, Jr. and M. Gensamer: Aging and the Yield Point in Steel. *Trans.* AIME (1944) **158**, p. 218; METALS TECHNOLOGY (December 1943).

[23] F. R. Larson and J. Miller: A Time-Temperature Relationship for Rupture and Creep Stresses. *Trans.* ASME (1952) **74**, p. 765.

[24] R. P. Carreker and W. R. Hibbard, Jr.: Tensile Deformation of High-Purity Copper as a Function of Temperature, Strain Rate, and Grain Size. *Acta Metallurgica* (1953) **1**, p. 654.

[25] A. U. Seybolt: Private communication.

[26] J. C. Fisher, E. W. Hart, and R. H. Pry: The Hardening of Metal Crystals by Precipitate Particles. *Acta Metallurgica* (1953) **1**, p. 336.

[27] R. S. French and W. R. Hibbard, Jr.: Effect of Solute Elements on the Tensile Deformation of Copper. *Trans.* AIME (1950) **188**, p. 53; JOURNAL OF METALS (January 1950).

[28] O. D. Sherby, R. L. Orr, and J. E. Dorn: Creep Correlations of Metals at Elevated Temperatures. *Trans.* AIME (1954) **200**, p. 71; JOURNAL OF METALS (January 1954).

[29] C. Zener and J. H. Hollomon: Plastic Flow and Rupture of Metals. *Trans.* ASM (1944) **33**, p. 163.

[30] C. A. Edwards, D. L. Phillips, and H. N. Jones: The Influence of Some Special Elements Upon the Strain-Aging and Yield-Point Characteristics of Low-Carbon Steels. *Journal* Iron and Steel Inst. (1940) **142**, p. 199.

Viscous Flow of Copper at High Temperatures

by A. L. Pranatis and G. M. Pound

Changes in length of copper foils of varying thickness and grain size were measured under such conditions of low stress and high temperature that it is believed that creep was predominately the result of interboundary diffusion of the type recently discussed by Conyers Herring. The surface tension of copper was calculated and results confirmed previous work within the limits of experimental error. Under the assumption of viscous flow, viscosities were calculated as a function of temperature and grain size. Predictions of the Nabarro-Herring theory of surface grain boundary flow were borne out fully and the Herring theory of diffusional viscosity is strongly supported.

ONLY a relatively few techniques for obtaining the surface tension of solids are presently available. Of these, the simplest and most straight forward is the direct measurement of surface tension by the application of a balancing counterforce. Thin wires or foils are lightly loaded and strain rates (either positive due to the downward force of the applied load or negative if the contracting tendency of surface tension is sufficiently greater than the applied stress) are observed. By plotting strain rates against stress, the load which exactly balances the upward pull is found and a simple calculation yields a value for the surface tension.

The technique is of comparative antiquity, and solid surface tension values were reported by Chapman and Porter,[1] Schottky,[2] and Berggren[3] in the early part of the century. Later, the filament technique became fairly well established as a method for determining the surface tension of viscous liquids, and Tammann and coworkers,[4, 5] Sawai and coworkers,[6-8] and Mack[9] showed good agreement between the values of surface tension for glasses and tars obtained by the filament technique and by more conventional methods.

With the increased confidence in the technique gained in these experiments, the method was applied to solid metals and the first reliable values of surface tension of solid metals were reported by Sawai and coworkers[10, 11] and by Tammann and Boehme.[12] More recently, Udin and coworkers[13-15] have reported the results of experiments with gold, silver, and copper wires. Similar experiments with gold wires were carried out by Alexander, Dawson, and Kling.[16]

The excellent review articles of Fisher and Dunn[17] and of Udin[18] should be referred to for detailed criticism of the foregoing work and for discussion of underlying theory.

In all the foregoing calculations, it is assumed implicitly that the material contracts or extends uniformly along the length of the specimen and also that it flows in a viscous fashion, i.e., that strain rates are proportional to stress. For an amorphous material, such as glass, tar, or pitch, the assumptions are quite valid and good agreement is obtained with values of surface tension measured by other techniques. The values reported for metals, however, are occasionally regarded with misgiving, since it can be argued that, because of their crystalline nature, true solids can not deform in a viscous fashion. If this is true, then the results reported for solid metals over a long period of years are of only doubtful value.

Thus it is clearly necessary that a mechanism be established that would explain both the viscous flow and the uniform deformation that has been assumed. Such a mechanism has been proposed by Herring.[19] Briefly, he suggests that, under the conditions of the experiment, deformation takes place by means of a flow of vacancies between grain boundaries and surfaces. This is a direct but independent extension of the theory proposed by Nabarro[20] in an attempt to explain the microcreep observed by Chalmers.[21]

In a condensed form the Herring viscosity equation is

$$\eta \sim \frac{TRL}{D}$$

where η is the viscosity, T the absolute temperature, R and L grain dimensions, and D the self-diffusion coefficient. In its complete form, all constants are calculable and it includes such factors as grain shape, specimen shape, and degree of grain boundary flow. When applied to existing data, good agreement was obtained between predicted and observed flow rates.

The theory received provisional confirmation from the work of Buttner, Funk, and Udin[22] who observed viscosities in 5 mil Au wire much higher than those in the 1 mil wire used by Alexander, Dawson, and Kling.[16] More significant were the completely negligible strain rates found by Greenough[23] in silver single crystals. Opposed to these observations were those of Udin, Shaler, and Wulff[24] who found indications of viscosity decreasing as grain size increased.

Thus, complete confirmation of the theory was lacking in that the data to which it could be applied contained only a limited number of grain sizes. Hence, it was proposed that a series of experiments be carried out with thin foils of varying grain size up to and including single crystals, where, according to the Herring theory, deformation would occur only at almost infinitely slow rates.

A. L. PRANATIS, formerly Graduate Student, Dept. of Metallurgical Engineering, Carnegie Institute of Technology, is Research Engineer, Atomic Energy Div., Sylvania Electric Products Inc., Bayside, N. Y., and G. M. POUND, Member AIME, is Assistant Professor, Dept. of Metallurgical Engineering, Carnegie Institute of Technology, Pittsburgh.

Discussion of this paper, TP 3946E, may be sent, 2 copies, to AIME by July 1, 1955. Manuscript, Sept. 15, 1954. Chicago Meeting, February 1955.

This paper is based on a thesis by A. L. Pranatis submitted, in partial fulfillment of the requirements for the degree of Doctor of Philosophy in Metallurgical Engineering, to the Graduate Faculty, Carnegie Institute of Technology.

Experimental Procedure

Three grades of copper were used to prepare the specimens: electrolytic foil of 4 nines purity, extra-pure OFHC copper of at least 5 nines purity, and ordinary OFHC of 4 nines purity. No difference in creep behavior for the different grades of copper could be detected and no effort has been made to separate the effect of starting material in the presentation of the data.

After rolling the copper down to size, specimens about ⅝ in. wide and about 5 in. long were cut from the sheet. Triangular gage marks then were cut through the specimens and copper suspension hooks attached to the folded ends. It is believed that the gage marks were far enough from the ends of the specimens so that end effects could be ignored.

The hard-rolled specimens were washed in a degreasing solution and then dipped in a ½ pct H_2SO_4 solution and chemically polished in a solution of 8 g $K_2Cr_2O_7$, 10 cc saturated NaCl solution, 30 cc H_2SO_4, and 40 g CrO_3 in 8000 cc H_2O. They then were returned to the H_2SO_4 solution and finally washed in distilled water and then in alcohol. After this treatment, the specimens showed the typical salmon-pink color of clean unoxidized copper. It cannot be pretended that the chemical polishing resulted in perfectly plane surfaces, but it was necessary to resort to chemical polishing, since no satisfactory electropolishing technique could be developed. After the final cleaning, the specimens were suspended in the furnace chamber, to be described later, each with a 4 g weight attached.

The specimens were then held at 1060°C for 8 hr for annealing and straightening. It was found that this treatment resulted in a reproducible grain diameter R for all specimen thicknesses. Inasmuch as each grain extended completely through the foil, the grain thickness is the same as the foil thickness L. This preliminary anneal at 1060°C was at a higher temperature than that of any of the creep tests in order to prevent secondary recrystallization during the runs. Another factor preventing grain growth was thermal etching of the grain boundaries which tended to inhibit boundary movement. In those few cases that grain growth occurred (usually caused by damage to the specimens during measurement), the "ghosts" of the former grain boundaries were quite apparent in the recrystallized grains and these specimens were then discarded.

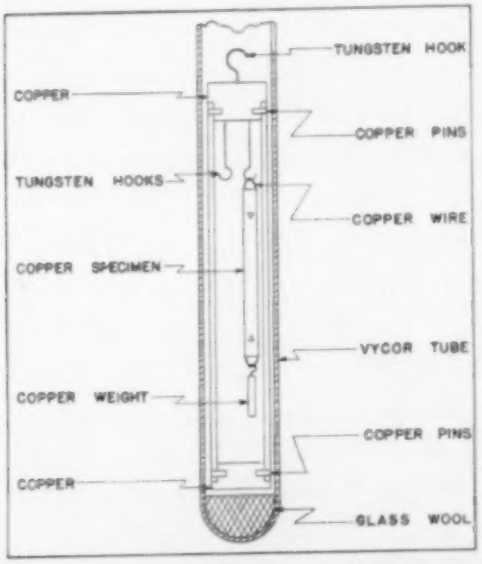

Fig. 1—Arrangement of specimens in copper furnace chamber.

After annealing, gage lengths were measured at room temperature and a preliminary grain size count was made. For purposes of grain size measurement, the grains were considered as circular and the number of grain boundaries intercepted by the cross-hairs, as the cathetometer moved between the gage marks, was counted. This gave an average chord of the circular grains which was converted to average grain diameter by the formula

$$\text{Average Diameter} = \left(\frac{\pi}{2}\right) (\text{average chord}).$$

Table I shows the average grain diameter for each of the specimen thicknesses.

Table I. Grain Size for Various Foil Thickness

L, Foil Thickness, In.	Average Chord, In.	R, Average Grain Diameter, In.	R/L	$R \times L$ (10^{-4}) Sq In.
0.0015	0.004	0.0063	4.2	9.45
0.002	0.0061	0.008	4	16
0.003	0.00525	0.00825	2.75	24.8
0.004	0.00445	0.007	1.75	28
0.005	0.0051	0.008	1.6	40

As far as could be determined from the evidence of slip lines in deliberately strained crystals, all specimens had the standard texture with (001) planes in the surface and the 100 direction parallel to the length of the specimen.

Single crystal foils were used in a number of preliminary creep tests. These were prepared by secondary recrystallization in a horizontal moving furnace. As discussed later, no length changes could be detected in the single crystals and only a limited number of these specimens were prepared.

Furnace and Specimen Chamber: Three double-wound Kanthal furnaces were used for the creep tests. One winding was adjusted by resistances so that line voltage held it about 50° to 75°C below the desired temperature. The second winding was controlled to hold the test temperature. Over short periods of time, temperatures were held to within ½ °C and it is believed that variations of temperature over long periods of time were less than 3°.

The specimens were suspended in a copper chamber (illustrated in Fig. 1) from tungsten hooks attached to the cover block which then was pinned to the chamber wall. The whole chamber was then lowered into a 3 ft Vycor tube sealed at the bottom. The Vycor tube was then connected to the gas purification train by means of ground-glass joints.

Atmospheres: All runs were made in either purified hydrogen or helium. The hydrogen was purified in the following train: 1—deoxo tube; 2—indicating alumina; 3—copper gauze, 550°C; 4—indicating alumina; 5—platinized asbestos, 550°C; 6—indicating alumina and ascarite; 7—cold trap, dry ice and acetone; and 8—10 liter storage flasks.

The following train was used to purify the helium: 1—mixed alumina and ascarite; 2—copper oxide, 550°C; 3—indicating alumina; 4—copper gauze, 550°C; 5—indicating alumina; 6—cold trap, dry ice and acetone; and 7—10 liter storage flasks.

Experimental Procedure: After cleaning and annealing, the initial gage lengths of the specimens

Table II. Surface Tension of Copper Foils

L, specimen thickness, in.	0.0015	0.002	0.003	0.004	0.005
R, average grain diameter, in.	0.0063	0.008	0.00833	0.007	0.008
L/R	1/4.2	1/4	1/2.75	1/1.75	1/1.6
Equation	$P = 0.96\gamma W$	$P = 0.958\gamma W$	$P = 0.94\gamma W$	$P = 0.905\gamma W$	$P = 0.896\gamma W$
		Surface Tension, Dynes per Cm			
Temperature, °C					
1051	1780	1690	1760	1680 (assumed)	1680 (assumed)
1024	1660	1740	1690	—	—
1002	1680	1720	1800	—	—
975	1680	—	—	—	—
900	1680	—	—	—	—

were measured while still suspended from the chamber cover and then the specimen assembly was replaced in the furnace chamber. The chamber then was carefully lowered into the Vycor furnace tube which was sealed to the gas train. The Vycor tube was then alternately evacuated and flushed with hydrogen at room temperature and then carefully lowered into the vertical furnace. Another series of alternate evacuations and flushings at temperature with the desired atmosphere then followed and the tube was then sealed off from the gas train so that the specimens remained in a static atmosphere during the run.

After a desired period of time, usually 4, 8, or 12 hr, the Vycor tubes were removed from the furnace and allowed to cool to room temperature. This usually took about 10 min, but the time at which diffusion was appreciable was probably no more than 2 or 3 min. The specimen chamber was then removed from the Vycor tube and the cover plate was unpinned and removed. Gage lengths were then measured with the specimens still suspended from the cover plate. A Gaertner cathetometer with a specially adapted draw tube to give magnifications of X75 and a claimed accuracy of 0.0002 in. was used to measure length changes in the specimens. In practice, accuracy was somewhat less than this, but it was found that results were reproducible within 0.0003 in.

On completion of the runs, which usually lasted 5 to 10 days, another grain size count was made and the specimens cut in two for weighing.

A number of unweighted single crystal specimens of 0.0015 in. thickness were used in a preliminary test, but no shrinkage could be detected even when the specimens were lying flat on carbon blocks with only friction between the specimen and block opposing the surface stress. It was concluded therefore that deformation of the viscous type did not occur at a detectable rate in single crystals.

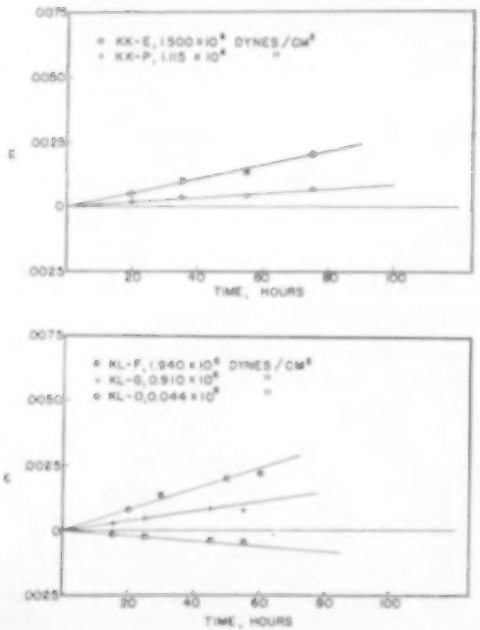

Fig. 2—Results of typical creep test. Data are plotted as $(l - l_o)/l_o$ vs time. 0.002 in. specimens, 1002°C.

Results

Results of a typical creep test are shown in Fig. 2. The data are plotted as $(l - l_o)/l_o$ (where l_o is the original gage length) vs time. The slopes of these curves are shown plotted against the corresponding stresses in Fig. 3. From these strain rate vs stress curves, surface tension is calculated from the equation

$$P = W\gamma\left[1 - \frac{L}{6R}\right]$$

where L/R is the ratio of specimen thickness to grain diameter, W the specimen width, γ the surface tension, and P the intercept on the stress axis corresponding to zero creep rate. It is assumed that the grain boundary energy is 1/3 that of the surface and that the grain boundaries form a hexagonal network.[11] Table II shows a summary of the surface tension calculations. The values for the thinner specimens are believed to be the more reliable and,

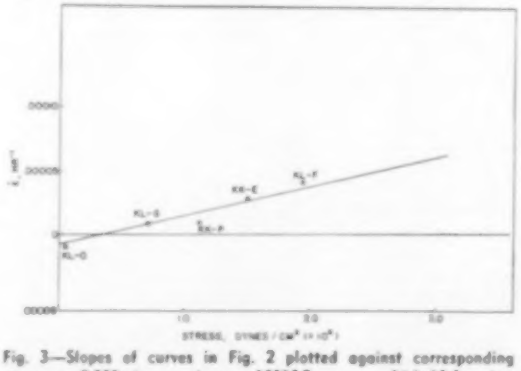

Fig. 3—Slopes of curves in Fig. 2 plotted against corresponding stresses. 0.002 in. specimens, 1002°C. $\eta = 16.1 \times 10^{-4}$ poise; $\gamma = 1720$ dynes per cm.

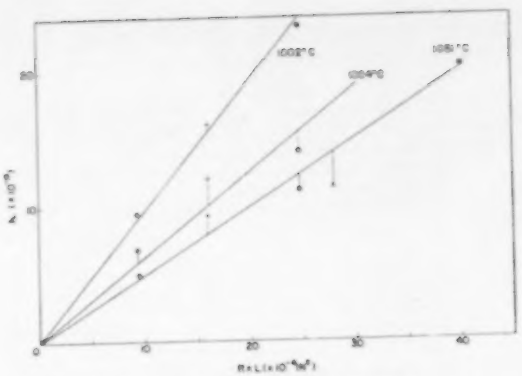

Fig. 4—Viscosity as a function of grain size.

in fact, the average calculated from the 0.0015 in. data is interpolated in some of the data for the thicker specimens in order to establish the slope of the strain rate vs stress curves.

By definition, the reciprocals of the slopes of the strain rate vs stress curves are the viscosities, that is

$$\sigma = \eta \dot{\epsilon}.$$

Since one of the purposes of this work has been to establish the validity of the Herring viscous flow mechanism, which defines viscosity

$$\eta \sim \frac{T R L}{D}$$

where T is the absolute temperature, R and L grain size parameters, and D the self-diffusion coefficient, the viscosity has been plotted as a function of these parameters in Figs. 4, 5, and 6. In Fig. 4, viscosity is plotted against the product of the grain dimensions. In Fig. 5, the natural logarithm of the viscosity is plotted as a function of the inverse temperature for each of the three smallest grain sizes. Strictly, of course, the data should be plotted as ln η/T vs $1/T$ but failure to do this in Fig. 5 introduces an error of less than 1 pct in the slopes. And finally in Fig. 6, where ln η/TRL is plotted against $1/T$, all the viscosity data is combined to yield one straight line with a slope corresponding to an activation energy of 56,800 cal per mol. Values of the coefficient of volume self-diffusion have been variously reported from 39,000 to 61,400 cal per mol, the higher values being the more reliable. In Table III, the observed values for the coefficients of viscosity are

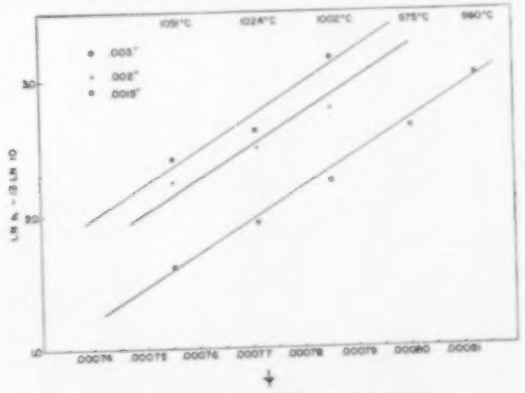

Fig. 5—Viscosity as a function of temperature.

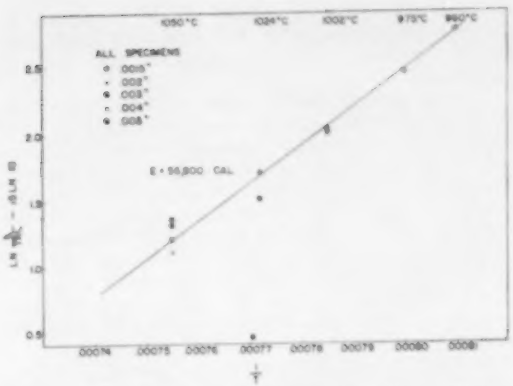

Fig. 6—Viscosity as a function of grain size and temperature.

compared with those predicted by the equation

$$\eta = \frac{1}{10}\left(\frac{3}{4}\right)^{\frac{2}{3}}\left(\frac{k\,T}{D\,\Omega}\right)V_s^{\frac{2}{3}}$$

where k is the Boltzman constant, T the absolute temperature, D the self-diffusion coefficient, Ω the atomic volume, and V_s the average grain volume.

Table III. Comparison of Observed and Predicted Values of the Viscosity Coefficients of Copper

Specimen Thickness, In.		Viscosity, Poise (10^{12})				
		1051°C	1024°C	1002°C	975°C	950°C
0.0015	Observed, He	6.58	7.04	9.5	—	—
	Observed, H_2	5.00	6.93	9.35	11.1	18.6
	Predicted	1.64	2.56	4.00	6.3	9.7
0.002	Observed	9.35	13.1	16.1	—	—
	Predicted	4.1	6.33	7.93	—	—
0.003	Observed	11.16	13.9	23.4	—	—
	Predicted	8.8	9.24	11.55	—	—
0.004	Observed	11.15	—	—	—	—
	Predicted	11.1	—	—	—	—
0.005	Observed	20.4	—	—	—	—
	Predicted	15.4	—	—	—	—

The self-diffusion coefficient was calculated from the relationship $D = 47 \exp.\ (61{,}400/kT)$, which is the equation given by Rollin.[22] The foregoing equation for viscosity has been developed by Herring[20] for the case of flow in a mass of equal quasi-spherical grains with tangential stresses relaxed at the boundaries and is not strictly applicable to the present geometry. However, it has been pointed out by Herring[20] that, for those cases where the grain diameter is not much greater than the specimen thickness, the use of the foregoing equation for foils will not introduce too great an error. In view of the errors inherent in the experiment and in the approximations necessary in the derivation of the equation, the unexpectedly good agreement in the absolute values is possibly no more than fortuitous. It is felt, however, that the variation of the observed viscosity with grain size and temperature is significant and powerful evidence in favor of the Herring mechanism of viscous flow.

Conclusions

In spite of the approximations used in the development of the Herring theory of diffusional viscosity and the unavoidable experimental error, agreement between calculated and observed values of the coefficient of viscosity is good, differing only by an almost constant factor of 2. It is believed, however, that in assessing the validity of the Her-

ring theory, greater weight should be given to comparison of observed behavior with that predicted by the individual terms of the Herring equation.

The activation energy obtained from the slope of the plots of ln η vs $1/T$ compares favorably with that of the more reliable values for the self-diffusion coefficient of copper, as is predicted by the Herring theory. It is not, however, incompatible with that for other modes of deformation, such as slip or diffusion between mosaic boundaries. The activation energies to be expected for kinking and offsetting cannot be predicted at present due to inadequate understanding of the mechanisms of these processes. However, Rhines[27] has found that the activation energy for grain boundary slip in aluminum bicrystals, a process closely related to offsetting, is only 11,000 cal per mol, indicating no relationship to a self-diffusion process.

Greatest significance is attached to the linear relationship between viscosity and grain size shown in Figs. 4 and 6. This, together with the zero creep rate observed for single crystals and the observed temperature dependence, constitutes behavior that seems to be completely explicable only by the Herring theory of diffusional viscosity.

The additional evidence in favor of the Herring theory of viscous flow permits the values of surface tension obtained by the wire and foil-pulling techniques to be regarded with increased confidence. This corroboration of the basic assumption of the technique is believed to be of greater importance than the mere confirmation of the values of surface tension of copper obtained by earlier investigators.

Summary

Rates of contraction and extension of thin copper foils were measured as a function of stress, temperature, and grain size. Foil thickness varied from 0.0015 to 0.005 in., with grain diameters ranging from 4.2 times the foil thickness in the 0.0015 in. specimens to 1.6 times the thickness in the 0.005 in. ones; tests were carried out in the temperature range 960° to 1050°C; stresses varied from $0.01 \cdot 10^7$ dynes per sq cm to about $2.5 \cdot 10^7$ dynes per sq cm resulting in strain rates ranging from about $1 \cdot 10^{-3}$ hr^{-1} to about $4 \cdot 10^{-2}$ hr^{-1}.

From these data, the following results were obtained: 1—an average value of surface tension for solid copper, in reasonable agreement with values previously reported; 2—viscosity values ranging from $3 \cdot 10^{12}$ to $20 \cdot 10^{12}$ poises, depending on temperature and grain size; 3—an infinite viscosity for single crystals, i.e., no detectable creep; 4—linear relationships between viscosity and the square of the grain size and between the log of the viscosity and the inverse temperature; and 5—good agreement between observed viscosity values and those predicted by the Herring theory of diffusional viscosity.

The observed relationships between viscosity and grain size and viscosity and temperature, as well as the absolute magnitudes of observed viscosities, strongly support the conclusion that deformation under the conditions of the experiment takes place almost entirely by means of vacancy diffusion. It is believed that slip, kinking, offsetting, and grain boundary sliding made only a limited contribution to deformation.

Acknowledgment

The research described in this paper was sponsored by the U. S. Office of Naval Research.

Discussion of this paper, if any, will appear in JOURNAL OF METALS, November 1955, and in AIME Metals Branch *Transactions*, Vol. **203**, 1955.

References

[1] J. C. Chapman and H. L. Porter: On the Physical Properties of Gold Leaf at High Temperatures. *Proceedings* Royal Society (1909) **A183**, p. 65.

[2] H. Schottky: Gesell. Wiss. Göttingen. *Nachr. Math.-Phys. Klasse* (1912) **4**, p. 480.

[3] B. Berggren: Methoden zur Bestimmung der Oberflächenspannung, usw. *Annalen der Physik* (1914) **44**, p. 61.

[4] G. Tammann and R. Tomke: Über die Skinnfähigkeit, Oberflächenspannung und die Wärme von Glasen. *Ztsch. Anorg. Allgem. Chemie* (1927) **162**, p. 1.

[5] G. Tammann and H. Rabe: Die Abhängigkeit der Oberflächenspannung hochviscoser Flussigkeiten von der Temperatur. *Ztsch. Anorg. Allgem. Chemie* (1927) **162**, p. 17.

[6] I. Sawai and Y. Ueda: Über die Schrumpfung des Glasfaden beim Erhitzen. *Ztsch. Anorg. Allgem. Chemie* (1929) **180**, p. 287.

[7] I. Sawai and M. Nishida: Über die Langenänderung von Glasfaden bei hoher Temperatur. *Ztsch. Anorg. Allgem. Chemie* (1930) **193**, p. 133.

[8] I. Sawai and M. Nishida: Über die Temperaturabhängigkeit der Oberflächenspannung des Glases. *Ztsch. Anorg. Allgem. Chemie* (1932) **204**, p. 60.

[9] C. Mack: Physico-Chemical Aspects of Asphalt Pavements. *Industrial Engineering Chemistry* (1935) **27**, p. 1500.

[10] I. Sawai and M. Nishida: Über die Schrumpfungskraft der Blattmetall bei hoher Temperatur. *Ztsch. Anorg. Allgem. Chemie* (1930) **190**, p. 375.

[11] I. Sawai and M. Nishida: Über die Schrumpfung der Blattmetall beim Erhitzen. *Ztsch. Anorg. Allgem. Chemie* (1930) **193**, p. 119.

[12] G. Tammann and W. Boehme: Die Oberflächenspannung von Gold Lamellen. *Annalen der Physik* (1932) **12**, p. 820.

[13] H. Udin, A. G. Shaler, and J. Wulff: The Surface Tension of Solid Copper. *Trans.* AIME (1949) **185**, p. 186; JOURNAL OF METALS (February 1949).

[14] E. R. Funk, H. Udin, and J. Wulff: Surface Tension of Solid Silver. *Trans.* AIME (1951) **191**, p. 1206; JOURNAL OF METALS (December 1951).

[15] F. H. Buttner, H. Udin, and J. Wulff: Surface Tension of Solid Gold. *Trans.* AIME (1951) **191**, p. 1209; JOURNAL OF METALS (December 1951).

[16] B. H. Alexander, M. H. Dawson, and H. P. Kling: Deformation of Gold Wire at High Temperature. *Journal of Applied Physics* (1951) **22**, p. 439.

[17] J. C. Fisher and C. G. Dunn: Imperfections in Nearly Perfect Crystals. *Surface and Interfacial Tensions of Single Phase Solids.* (1952) Ch. 12. New York. John Wiley and Sons Inc.

[18] H. Udin: Measurement of Solid Gas and Solid Liquid Interfacial Energies. *Metal Interfaces.* ASM (1952).

[19] C. Herring: Diffusional Viscosity of a Polycrystalline Solid. *Journal of Applied Physics* (1950) **21**, p. 437.

[20] F. R. N. Nabarro: *Report of a Conference on the Strength of Solids.* Physical Society, London (1948) p. 75.

[21] B. Chalmers: Micro plasticity in Crystals of Tin. *Proceedings* Royal Society, London (1936) **A156**, p. 427.

[22] B. V. Rollin: *Physical Review* (1939) **55**, p. 231.

[23] C. Herring: Private communication.

[24] F. N. Rhines, W. E. Bond, and M. A. Kissel: Grain Boundary Behavior in the Creep of Aluminum Bicrystals. *Report to the NACA* (April 1954) Carnegie Institute of Technology.

[25] F. H. Buttner, E. R. Funk, and H. Udin: Viscous Creep of Gold Wires Near the Melting Point. *Trans.* AIME (1952) **194**, p. 401; JOURNAL OF METALS (April 1952).

[26] A. P. Greenough: The Deformation of Silver at High Temperatures. *Philosophical Magazine* (1952) **43**, p. 1015.

Curie Temperatures of Binary and Ternary Sigma Phases

by M. V. Nevitt and P. A. Beck

All binary and a number of ternary σ alloys formed by first long period transition elements were examined and found to be ferromagnetic at low temperatures. The Curie temperatures for these alloys were measured. It was found that the correlation of the Curie temperature with composition may be described qualitatively in terms of the contributions of the various component atomic moments to the saturation moment of the alloy. Ternary Fe-Cr-Mo σ phase alloys were also found to be ferromagnetic, with a Curie temperature dependent on the iron content and largely independent of the unit cell dimensions. Similar relations were found for the Co-Fe-Cr and the Co-Cr-Mo σ alloys, where the Co + Fe content appears to determine the Curie temperature.

RECENTLY, it has become increasingly evident that the σ phase is some kind of an "electron compound." Several papers[1-3] discussed the empirical correlation between the composition of the various σ phases in alloys of the transition elements and the distribution of electrons in the partially filled d-levels of the component atoms. However, a picture of the latter can be formed only in a more or less intuitive manner, as in the Pauling theory,[4] and the rigorous treatment of these problems is at present prevented by lack of adequate knowledge of the electronic structure of the transition elements in the metallic state.

It appeared reasonable to expect that investigation of the magnetic properties, which are related to d-shell electrons, may help in clarifying the physical nature of the foregoing empirical correlation. Qualitative tests of samples of various compositions have shown that certain σ alloys become ferromagnetic at liquid nitrogen temperature.[5] The present investigation was undertaken to determine whether or not low temperature ferromagnetism is characteristic of a large variety of σ alloys and to establish how the Curie temperatures of ferromagnetic σ alloys are influenced by changes in composition and in lattice parameter. In the first portion of the investigation, Curie temperatures were measured for a series of σ alloys containing either vanadium or chromium with one or two of the elements manganese, iron, cobalt, or nickel. In the second phase of the work, data were obtained on the Curie temperature of ternary (Fe, Co, Cr)σ, (Fe, Cr, Mo)σ, and (Co, Cr, Mo)σ alloys, as a function of composition and of interatomic spacing.

M. V. NEVITT, Junior Member AIME, formerly Graduate Student, University of Illinois, is Head, Dept. of Metallurgical Engineering, Virginia Polytechnic Institute, Blacksburg, Va., and P. A. BECK, Member AIME, is Research Professor of Physical Metallurgy, University of Illinois, Urbana, Ill.

Discussion of this paper, TP 3960E, may be sent, 2 copies, to AIME by July 1, 1955. Manuscript, Aug. 12, 1954. Chicago Meeting, February 1955.

This paper is based on a thesis by M. V. Nevitt submitted, in partial fulfillment of the requirements for the degree of Doctor of Philosophy, to the Graduate College of Engineering, University of Illinois.

Experimental Procedures

High frequency vacuum melting in high purity recrystallized alumina crucibles was employed in the preparation of the σ alloys, using metals whose lot analyses are given in Table I. Approximately two-thirds of the alloys were analyzed chemically, the analytical results being in acceptable agreement with the intended compositions, as seen in Tables II and III. The specimens were annealed for homogenization in an atmosphere of purified 92 pct He and 8 pct H_2 mixture or in evacuated and sealed Vycor tubes at temperatures from 780° to 1300°C, depending on the temperature range of the σ phase field for the particular composition. The annealing temperature and time for each alloy are given in Tables II and III.

Curie points were determined by an induction method; the change with temperature of mutual inductance between two coils was observed when the σ specimen was inserted into the flux path between the coils. The transformer consisted of three coils each containing 1200 turns of 0.0050 in. diam enameled copper wire. The center coil, P in Fig. 1, served as the primary coil, and was linked magnetically with each of the two secondary coils, S_1 and S_2, which were connected in series opposition. The primary coil, P, was energized by an audio-oscillator, set at a frequency of 500 cycles per sec, while the signal from the transformer secondary circuit,

Table I. Lot Analyses of Metals Used in Making σ Alloys, Wt Pct

Element or Compound	Vanadium	Electrolytic Cr	Electrolytic Mn	Electrolytic Fe	Electrolytic Co	Electrolytic Ni	Mo
Al	—	—	—	—	0.008	—	—
C	0.08	0.01	0.005 max	0.010	0.028	—	0.003 max
Co	—	—	—	—	Balance	0.6 to 0.8	—
Cr	—	Balance	—	0.015	—	—	—
Cu	—	Trace	—	0.03	0.004	0.01	—
Fe	—	0.05	0.001 max	Balance	0.14	0.01	0.005 max
H_2	0.01	0.045	0.015 max	0.01	Nil	—	—
Mn	—	—	Balance	0.015	—	—	Balance
Mo	—	—	—	—	—	—	—
N_2	0.077	0.10	—	—	—	—	—
Ni	—	—	—	0.03	Trace	Balance	—
O_2	0.062	0.51	—	—	—	—	0.003
P	—	—	—	0.003	—	—	—
Pb	—	0.001	—	—	—	—	—
S	—	0.012	0.024 max	0.002	0.004	0.001	—
Si	—	—	Trace	—	0.002	—	—
SiO_2	—	—	—	0.03	—	—	—
V	Balance	—	—	—	—	—	—

S_1 and S_2, was fed to a variable gain amplifier and the output from the amplifier was read with an ac voltmeter. When a sample of sigma linked the primary, P, with one of the secondaries, S_2, the extent to which the electrical balance of the transformer was disturbed depended on the magnetic state of the sample. When the σ sample was ferromagnetic, the difference in mutual inductance between P and S_1 and P and S_2 was large so that the opposing voltages of the two secondary windings were of greatly different magnitude and a correspondingly large voltage difference was indicated by the voltmeter. As the temperature of the sample was changed between values above and below the Curie temperature, a sharp change in the output voltage was observed at the Curie temperature. The σ samples used in the transformer consisted of cast and annealed material, ground to approximately −60 mesh and packed tightly into a gelatin capsule. The sample and the coils were heated by means of a heater coil of nichrome wire which jacketed the transformer, as shown in Fig. 1. The assembly was housed in a vacuum container which could be exhausted to a pressure of less than 1 micron Hg, and the vacuum container was immersed in a low temperature reservoir which was contained in a suitable cryostat. Either liquid nitrogen or liquid helium was used as the coolant, depending upon the range of temperatures over which the measurements were made. The temperature was measured in °K with a previously calibrated copper vs gold plus 2.1 atomic pct Co thermocouple which was embedded in the σ sample. By adjusting the dc current to the heater coil, the temperature of the σ sample could be maintained at any point at or above the temperature of the coolant. The heater current was kept constant at each temperature of measurement long enough to assure constant temperature in the sample. When the induced secondary voltage was measured over a range of temperatures, the Curie point could be determined by noting the temperatures at which a sharp change in voltage occurred. In this manner, Curie points were determined for 58 σ alloys in 16 different binary and ternary systems.

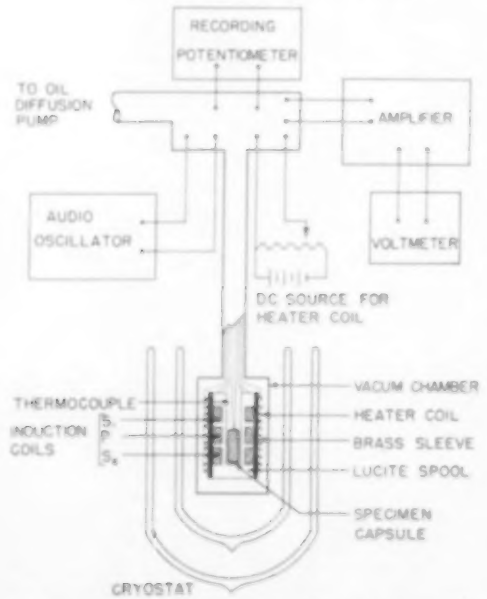

Fig. 1—Apparatus used to determine Curie temperatures by induction method. P is the primary coil and S_1 and S_2 are the secondary coils.

Results of Investigation

The alloys in Table II are listed by system, together with their compositions in atomic percent and their Curie temperatures. The binary σ alloys were chosen, as closely as possible at the time, near the center of the σ composition range in each alloy system. The σ boundaries in most of the ternary systems concerned have not been reported previously, but they were determined in a concurrent investigation.[6] In each case, a continuous field of ternary σ solid solutions connects the two binary σ phases. The composition of the ternary alloys used for the Curie point determinations was selected so that the corresponding points in the triangular composition coordinate system lay approximately on the straight line connecting the two binary σ compositions. Accordingly, it should be noted that, in cases like that of the V-Mn-Fe system, where the two binary σ phases have different composition, the corresponding curves in Figs. 2, 3, and 4 represent alloys in which the amount of the component not indicated on the abscissa (vanadium or chromium) also varies. It is seen that the Curie temperatures are low for all the compositions studied, and this observation is in accord with the work of previous investigators, as reported by Bozorth,[7] where the σ phase was consistently observed to be "nonmagnetic" at room temperature.

For purposes of interpretation, it was necessary to establish some basis for comparison of all the data. Consideration of the data for the binary alloys suggested that at least a rough correlation could be made between the Curie temperature and the saturation magnetization of certain of the component elements of the alloys. The nature of this correlation is shown in Fig. 2, where the Curie temperature of the three binary alloys containing chromium and the Curie temperatures of the four binary alloys containing vanadium are plotted against the atomic number of the other component element in each alloy, namely, manganese, iron, cobalt, or nickel. The general shape of these curves resembles the dashed curve which expresses the variation of saturation magnetic moment with the average atomic number for the ferromagnetic elements of the first transition period and their alloys. The similarity of these curves implies that the variation in Curie temperature for the σ phase may reflect a corresponding variation in its magnetic moment, and this hypothesis is in general accord with the relationship that obtains between Curie temperature and saturation moment for ferromagnetic substances[4]

$$k\theta/Z = \beta N I_s/Z$$

where θ is the Curie temperature; Z is the number of nearest neighbors; β is the Bohr magneton; N is the Weiss molecular field constant; and I_s is the saturation magnetic moment. Thus, an increase in the saturation moment of σ would be expected to produce an increase in the Curie temperature, if other factors did not intervene.

However, Figs. 3 and 4 show that the ternary alloy data do not conform to this simple correlation. In Fig. 3, the Curie points of the ternary σ alloys containing vanadium are plotted against the weighted average atomic number of the other two alloy components. In Fig. 4, the Curie points of ternary chromium σ alloys are plotted in a similar manner. In both of these figures the data for the binary alloys are the same as those in Fig. 2. It may be noted that there is a general depressing effect on the Curie temperature when a third element is added to any one of the binary σ alloys.

One interpretation of this behavior can be made in terms of the effect of 3d-shell diameter in allowing the occurrence of a positive exchange force between the 3d-shell electrons of neighboring atoms. A relationship due to Bethe[5] predicts that the alignment of magnetic moments of neighboring atoms is parallel or antiparallel, depending on the extent of the overlap of the charge distributions of the partially filled d-shells of the transition metals concerned. The lattice dimensions of the σ phase remain relatively constant in binary and ternary systems of the first transition period elements, but the component elements have considerably different 3d-shell diameters. Thus, the overlap of the adjacent 3d-shells is changed when one transition element atom is substituted for another on a particular lattice site, depending on the relative diameters of the 3d-shells of the atoms concerned. The possibilities for ferromagnetic coupling in a given σ lattice can be analyzed qualitatively, when the interatomic spacings are known, by using Néel's[10] values for the 3d-shell diameters of the elements and his criterion for positive exchange coupling: $d - 2r \geq 1.05$Å, where d is

Table II. Curie Temperatures of Binary and Ternary σ Alloys

Intended Composition, Atomic Pct	Chemical Analysis, Atomic Pct	Annealing Temperature, °C	Annealing Time, Hr	Curie Temperature, °K
80 Mn, 20 Cr	80.1 Mn, 19.9 Cr	1000	120	91
60 Mn, 11 Fe, 29 Cr	—	810	264	90
36 Mn, 25 Fe, 39 Cr	—	810	264	85
37 Fe, 16 Mn, 47 Cr	37.7 Fe, 15.3 Mn, 47.0 Cr	810	264	106
53 Fe, 47 Cr	53.6 Fe, 46.4 Cr	780	336	163
46 Fe, 7 Co, 47 Cr	46.5 Fe, 7.5 Co, 46 Cr	820	336	163
40 Fe, 14 Co, 46 Cr	—	820	336	162
40 Fe, 10.5 Co, 49.5 Cr	38.9 Fe, 11.9 Co, 49.2 Cr	820	120	128
30 Fe, 18.5 Co, 51.5 Cr	—	820	120	116
27 Co, 16 Fe, 57 Cr	26.8 Co, 16.1 Fe, 55.1 Cr	1000	120	91
42.1 Co, 57.9 Cr	41.3 Co, 58.7 Cr	1000	120	73
60 Mn, 10 Co, 30 Cr	—	1000	144	76
39 Mn, 20 Co, 41 Cr	38.9 Mn, 20.8 Co, 40.3 Cr	1000	144	71
29 Co, 20 Mn, 51 Cr	29.8 Co, 19.3 Mn, 50.9 Cr	1000	144	73
83.5 Mn, 16.5 V	83.4 Mn, 16.6 V	1000	120	106
16 Fe, 37 Mn, 27 V	16.1 Fe, 37.4 Mn, 26.5 V	1000	120	99
42.3 Fe, 15.6 Mn, 42 V	43 Fe, 16.3 Mn, 40.7 V	1000	120	106
52.7 Fe, 47.3 V	52.4 Fe, 47.6 V	1000	120	205
41 Fe, 12 Co, 47 V	42.8 Fe, 11.6 Co, 45.6 V	1000	120	149
29.2 Fe, 23.9 Co, 46.9 V	30.7 Fe, 24.4 Co, 44.9 V	1000	120	128
51.3 Co, 48.7 V	50.4 Co, 49.6 V	1000	120	98
37 Co, 10 Ni, 53 V	37.2 Co, 9.5 Ni, 53.3 V	1000	120	62
20.9 Co, 18.6 Ni, 53.5 V	20.8 Co, 18.6 Ni, 55.6 V	1000	120	58
36.3 Ni, 63.7 V	35.8 Ni, 64.2 V	1000	120	82
20.5 Co, 47.5 Mn, 32 V	—	1000	120	95
36 Co, 17 Mn, 47 V	36.1 Co, 17.0 Mn, 46.3 V	1000	120	90

Table III. Curie Temperatures of (Fe, Cr, Mo) σ and (Co, Cr, Mo) σ Alloys

Intended Composition, Atomic Pct	Chemical Analysis, Atomic Pct	Annealing Temperature, °C	Annealing Time, Hr	Curie Temperature, °K
48.1 Fe, 29.7 Cr, 22.2 Mo	55.1 Fe, 25.6 Cr, 19.3 Mo	1200	72	191
55.5 Fe, 28.5 Cr, 16.0 Mo	56.7 Fe, 26.9 Cr, 16.4 Mo	1200	72	191
54 Fe, 34 Cr, 23 Mo	54.5 Fe, 24.6 Cr, 20.9 Mo	1200	72	181
54.5 Fe, 28.0 Cr, 17.5 Mo	—	1200	72	177
51 Fe, 29 Cr, 20 Mo	52.4 Fe, 27.4 Cr, 20.2 Mo	1200	72	156
51.6 Fe, 28.0 Cr, 20.4 Mo	—	1200	72	150
52 Fe, 26 Cr, 22 Mo	51.9 Fe, 25.7 Cr, 23.4 Mo	1200	72	145
51 Fe, 29.5 Cr, 19.5 Mo	—	1200	72	134
50 Fe, 28 Cr, 22 Mo	51.0 Fe, 27.2 Cr, 21.8 Mo	1200	72	136
49.5 Fe, 31.5 Cr, 19.0 Mo	—	1200	72	130
51 Fe, 26 Cr, 23 Mo	51.5 Fe, 25.2 Cr, 23.2 Mo	1200	72	125
49 Fe, 26.0 Cr, 25.0 Mo	—	1200	72	117
48.5 Fe, 29.3 Cr, 22.2 Mo	49 Fe, 28.9 Cr, 22.3 Mo	1200	72	112
47 Fe, 32.5 Cr, 19.5 Mo	47.5 Fe, 33.3 Cr, 19.2 Mo	1200	72	109
47 Fe, 26 Cr, 27 Mo	47.3 Fe, 25.3 Cr, 27.4 Mo	1200	72	109
53 Fe, 47 Cr	53.6 Fe, 46.4 Cr	780	336	163
51.5 Fe, 46.0 Cr, 2.5 Mo	—	780	336	142
49 Fe, 44.5 Cr, 6.5 Mo	—	780	336	120
47 Fe, 43 Cr, 10.0 Mo	48 Fe, 41.9 Cr, 10.1 Mo	780	240	109
45 Fe, 42 Cr, 13.0 Mo	—	1000	120	90
42 Fe, 42 Cr, 16 Mo	42.1 Fe, 41.7 Cr, 16.2 Mo	1200	72	91
41 Fe, 41 Cr, 18 Mo	41.2 Fe, 40.1 Cr, 18.7 Mo	1160	120	81
38.5 Fe, 38.5 Cr, 23 Mo	38.8 Fe, 38.5 Cr, 22.7 Mo	1200	72	74
43.1 Co, 57.9 Cr	41.3 Co, 58.7 Cr	1300	72	73
38 Co, 55 Cr, 9 Mo	—	1300	48	66
38 Co, 48 Cr, 14 Mo	—	1300	72	69
41 Co, 50 Cr, 9 Mo	—	1300	72	77
43.5 Co, 41 Cr, 15.5 Mo	—	1300	72	68
49.5 Co, 41 Cr, 9.5 Mo	—	1300	72	105
47 Co, 50.5 Cr, 2.5 Mo	46 Co, 51.6 Cr, 2.4 Mo	1300	72	108

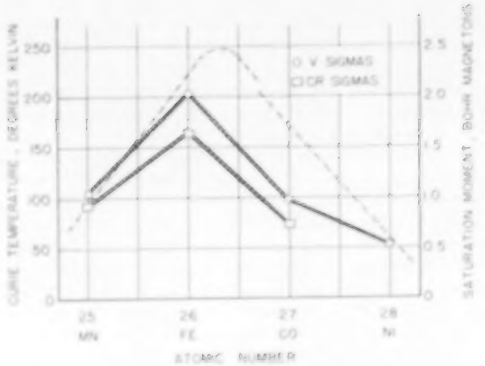

Fig. 2—Curie temperatures of binary alloys containing chromium and vanadium are plotted against the atomic number of the other component element in each alloy.

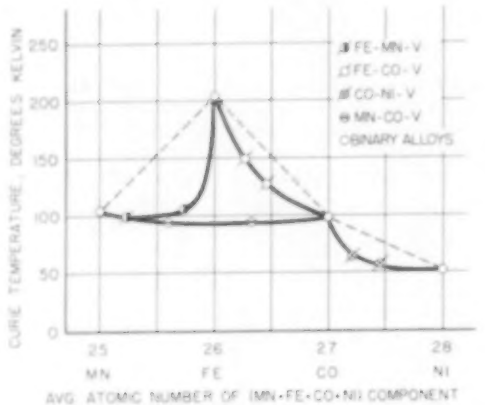

Fig. 3—Curie points of ternary σ alloys containing vanadium are plotted against the weighted average atomic number of the other two alloy components.

the distance between atom centers and $2r$ is the average diameter of the 3*d*-shell. The interatomic distances in various binary σ alloys can be approximated by converting the spacings given by Bergman and Shoemaker[14] for (Fe,Cr)σ by means of the multiplying factors of Carlisle, Christian, and Hume-Rothery.[15] When the structure of (Fe,V)σ is analyzed in this way, it is found that the substitution of manganese atoms for iron atoms on certain of the lattice sites results in a decrease in the number of positive exchange couplings in the lattice because positive Fe-Fe interactions are replaced by antiferromagnetic Fe-Mn, Mn-Mn, or Mn-V interactions. The same result occurs when manganese atoms are substituted in the (Fe,Cr)σ lattice. The fact that the Curie temperatures of (Fe,V)σ and (Fe,Cr)σ are markedly lowered by the addition of manganese may be explained satisfactorily on this basis. However, the foregoing interpretation is not adequate to explain the depression of the Curie temperature caused by the addition of atoms with 3*d*-shells smaller than those of the original atoms. Figs. 3 and 4 show dips in the Curie temperature curves when cobalt is added to (Fe,V)σ and to (Fe,Cr)σ, when nickel is added to (Co,V)σ and, to a lesser extent, when cobalt is added to (Mn,V)σ and to (Mn,Cr)σ. In most of these cases, the analysis in terms of the

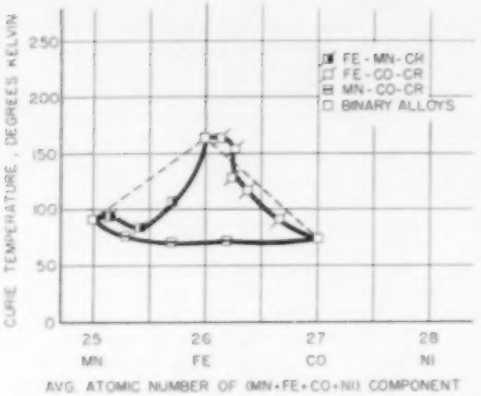

Fig. 4—Curie points of ternary chromium σ alloys are plotted against the weighted average atomic number of the other two alloy components.

Néel criterion shows that there should be an increase rather than a decrease in the number of possible positive 3*d*-shell exchange interactions.

An alternative explanation that may be valid even in the instances just described is based on the assumption that a transfer of electrons among certain atoms takes place in σ alloys and that the resultant decrease in the magnetic moment of the structure is reflected in a decrease in the Curie temperature. Although there is as yet no experimental verification of such electron transfer in the σ phase, it has been shown by Shull[16] that the unusually large decreases in the magnetic moment and in the Curie temperature, for instance, in cobalt-base hexagonal Co-Cr solid solutions are due to electron transfer of this type.

In an effort to clarify the effects of magnetic moment and overlap of unfilled *d*-shells on the Curie temperature of σ alloys, additional Curie temperature data were obtained for (Fe,Cr,Mo)σ and (Co,Cr,Mo)σ alloys as a function of composition. In the isolated atom, molybdenum has five 4*d* electrons corresponding to chromium's five 3*d* electrons, so that these two elements might be expected to make equal contributions to the magnetic moment of the structure. However, molybdenum has a very much larger atomic diameter and *d*-shell diameter than chromium.

In Table III, the compositions and Curie temperatures of 30 (Fe,Cr,Mo)σ and (Co,Cr,Mo)σ alloys are shown. In Fig. 5, the (Fe,Cr,Mo)σ data are plotted on a portion of the ternary diagram. The 1100° and 650°C σ phase boundaries are due, respectively, to Putnam, Potter, and Grant[14] and to Duwez and Baen.[13] The *a* dimension of the tetragonal cell, also plotted, was obtained by converting the value of Bergman and Shoemaker[14] for (Fe,Cr)σ by means of a factor expressing the lattice expansion in (Fe,Cr,-Mo) σ observed by Duwez and Baen.[13]

As seen in Table III and Fig. 5, the Curie temperature falls as molybdenum is added to (Fe,Cr)σ. However, contours of constant Curie temperature follow lines of constant iron content and they are not influenced by the change in lattice dimension. Fig. 6 shows the compositions and Curie temperatures of 7 (Co,Cr,Mo)σ alloys. The 1300°C phase boundary was determined by Darby and Beck.[9] In this system, the *a* dimension of the unit cell was determined by converting the value for (Co,Cr)σ of

Dickens, Douglas, and Taylor[28] by means of the lattice expansion in (Co,Cr,Mo)σ observed by X-ray measurements. Fig. 6 shows that the Curie temperature is apparently insensitive to the expansion of the lattice that molybdenum produces. In Fig. 7 the Curie temperatures of (Fe,Cr,Mo)σ, (Co,Fe,Cr)σ, and (Co,Cr,Mo) σ alloys are plotted as a function of the Co + Fe content, regardless of the variations of the Mo/Cr ratio or the Co/Fe ratio. It may be seen that in a first approximation the iron and cobalt content determine the Curie temperature in these alloys.

The dependence of Curie temperature upon the concentration of iron or cobalt again suggests that the number of ferromagnetic atoms in the structure is of decisive influence. The fact that the Curie temperature is not affected by the lattice stretching due to the addition of molybdenum is rather remarkable. When the Néel criterion is used, as described previously, to analyze the possibilities for ferromagnetic exchange between adjacent atoms in the binary (Fe,Cr)σ lattice, it is found that many adjacent lattice sites are properly spaced for positive Fe-Fe and Fe-Cr coupling, while for others the interatomic distances are too short. When molybdenum is added, new Fe-Fe and Fe-Cr positive exchanges are created because molybdenum increases the interatomic distances. On the other hand, the 4d-shell radius of molybdenum is too large to permit any positive exchanges with either iron or chromium, so that the replacement by molybdenum atoms of either iron or chromium atoms must result in a decrease in the number of positive exchange couplings. If the magnitudes of these two effects were the same, the Curie temperature of σ would be indifferent to molybdenum additions, as observed experimentally. The compensation of these two counteracting effects is apparently fortuitous, there being no evident theoretical reason for expecting it.

The widespread occurrence of ferromagnetism among the various σ phases confirms the view expressed earlier[2] that the electronic structure of σ proposed by Sully[1] is not likely to be correct. In terms of the Pauling theory, the present results are consistent with the picture that for each atom the bonding subband is filled up with electrons and that the atomic subband, which is responsible for ferromagnetism, is only partially filled.

In Fig. 8 all of the Curie point data of this investigation are plotted as a function of a quantity which may be called the *hypothetical saturation moment* of the σ alloys. The hypothetical moment for each alloy is taken as the sum of the products of atom fraction of each component times the atomic moment value for that element. The experimentally determined saturation moments for the elements iron, cobalt, and nickel are, respectively, 2.218,[27] 1.715,[28] and 0.604[29] Bohr magneton. As derived from Pauling's[29] postulated distribution of hybridized 3d and 4s electrons for elements of the first transition period, moment values of 0, 0.22, and 1.22 Bohr magnetons per atom were used for the elements vanadium, chromium, and manganese. A value of 0.22 Bohr magnetons per atom was also used for molybdenum. These hypothetical moment values are based on the greatly oversimplified picture of additivity of all atomic moments, so that they should not be considered as even crude approximations of the true saturation moments of the alloys. Nevertheless, in the absence of actual measured values for the saturation moments, they may be conveniently used in presenting certain features of the data for a wide variety of σ compositions. The extensive scatter in Fig. 8 clearly shows that the measured Curie tem-

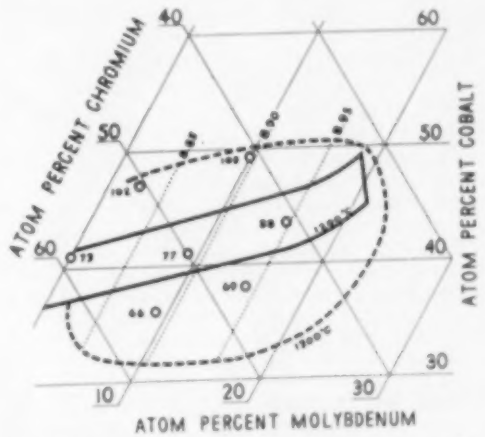

Fig. 6—Compositions and Curie temperatures of seven (Co, Cr, Mo)σ alloys.

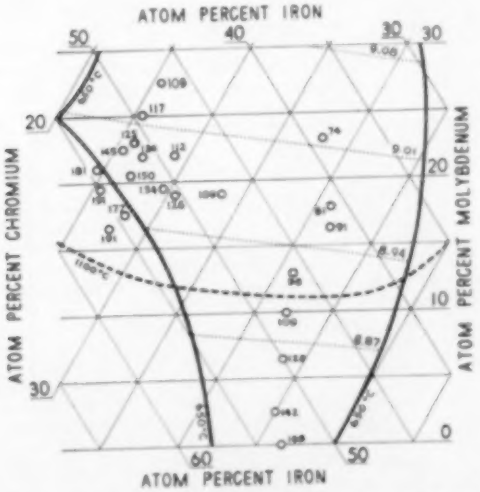

Fig. 5—Curie temperatures for (Fe, Cr, Mo)σ alloys are plotted on a portion of the ternary diagram.

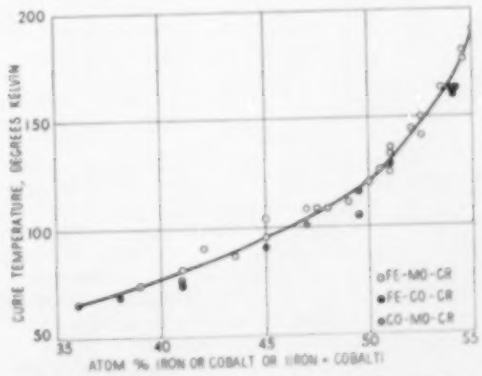

Fig. 7—Curie temperatures of σ alloys are plotted as a function of the Co + Fe content.

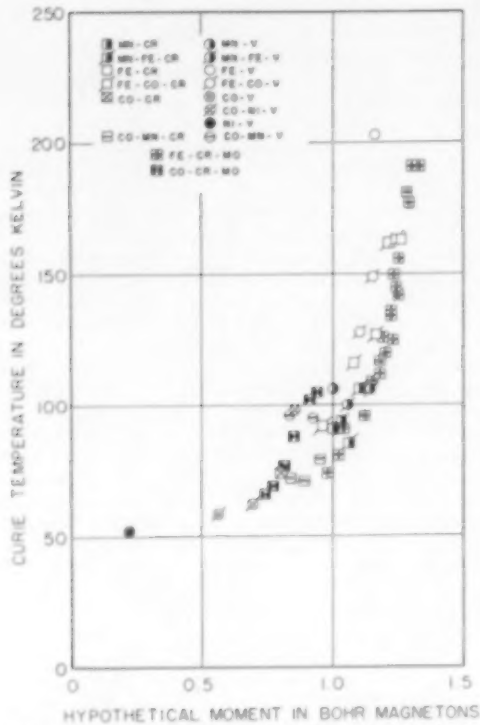

Fig. 8—Curie point data plotted as a function of the hypothetical saturation moment of the σ alloys.

peratures and the hypothetical saturation moments are not uniquely related, but it seems likely that the steady rise in Curie temperature that accompanies the transition from the nickel σ phase through manganese and cobalt to the iron-containing σ alloys in effect reflects a steadily rising saturation moment for these alloys. If this view is accepted, the results suggest strongly that the σ phase may not be ascribed a unique or characteristic value of the saturation moment, and that, therefore, the empirical correlation between the composition and the number of atomic subband electron vacancies[1, 6, 7] should not be given the interpretation that the σ structure as such has a Pauling atomic subband of its own with a characteristic number of electrons independent of composition.

Conclusions

1—Ferromagnetism is a characteristic low temperature property in a wide variety of σ alloys.

2—The correlation of the Curie temperature of the σ phase with composition may be reasonably well described qualitatively in terms of the contributions of the various component atoms to the saturation moment of the alloy.

3—The insensitivity of the Curie temperature to an increase in the interatomic distances in the (Fe,Cr)σ phase when molybdenum is added suggests that molybdenum additions produce two mutually compensating effects: an increase in the number of positive exchange interactions in the structure due to the stretching of interatomic distances, and a decrease in the number of positive interactions due to the substitution of strongly negative Fe-Mo, Cr-Mo, and Mo-Mo interactions for some of the positive Fe-Fe, Fe-Cr, and Cr-Cr 3d-shell exchange couplings.

4—It is unlikely that the σ structure can be ascribed a Pauling atomic subband of its own with a characteristic number of electrons independent of the composition. The present investigation did not lead to a rational interpretation of the empirical correlation between σ boundary compositions and electron vacancies in the atomic 3d-subbands of the component elements.

Acknowledgments

The authors wish to acknowledge gratefully the Research Fellowship of the Union Carbide and Carbon Research Laboratories Inc., established at the University of Illinois through the courtesy of Dr. A. B. Kinzel, granted one of them. The investigation was supported by the Office of Ordnance Research, Contract No. DA-11-022-ORD-1175.

Discussion of this paper, if any, will appear in JOURNAL OF METALS, November 1955, and in AIME Metals Branch *Transactions*, Vol. **203**, 1955.

References

[1] A. H. Sully: The Sigma Phase in Binary Alloys of the Transition Elements. *Journal* Institute of Metals (1951) **80**, p. 173.

[2] S. Rideout, W. D. Manly, E. L. Kamen, B. S. Lement, and P. A. Beck: Intermediate Phases in Ternary Alloy Systems of Transition Elements. *Trans.* AIME (1951) **191**, p. 872; JOURNAL OF METALS (October 1951).

[3] D. S. Bloom and N. J. Grant: Regarding Sigma Phase Formation. *Trans.* AIME (1953) **197**, p. 88; JOURNAL OF METALS (January 1953).

[4] P. Greenfield and P. A. Beck: The Sigma Phase in Binary Alloys. *Trans.* AIME (1954) **200**, p. 253; JOURNAL OF METALS (February 1954).

[5] P. A. Beck: Magnetic Behavior of Intermediate Phases in Alloys of Transition Elements. *Trans.* AIME (1952) **194**, p. 420; JOURNAL OF METALS (April 1952).

[6] J. Darby and P. A. Beck: Research in Progress, University of Illinois.

[7] R. M. Bozorth: *Ferromagnetism.* (1951) New York. D. Van Nostrand.

[8] R. M. Bozorth: The Physical Basis of Ferromagnetism. *Bell System Technical Journal* (1940) **19**, p. 26.

[9] H. Bethe: *Handbuch der Physik* (1933) **24**, Part 2, p. 595.

[10] L. Néel: *Annales de Physique* (1937) **8**, No. 11, p. 237.

[11] B. G. Bergman and D. P. Shoemaker: Space Group of the Sigma-FeCr Crystal Structure. *Journal of Chemical Physics* (1951) **19**, p. 515; *Journal* American Chemical Society (1950) **72**, p. 5793.

[12] S. J. Carlisle, J. W. Christian, and W. Hume-Rothery: The Equilibrium Diagram of the System Chromium-Manganese. *Journal* Institute of Metals (1950) **76**, p. 169.

[13] C. C. Shull: Private communication to P. A. Beck.

[14] J. W. Putman, R. D. Potter, and N. J. Grant: The Ternary System Chromium-Molybdenum-Iron. *Trans.* ASM (1951) **43**, p. 824.

[15] S. R. Baen and P. Duwez: Constitution of Iron-Chromium-Molybdenum Alloys at 1200°F. *Trans.* AIME (1951) **191**, p. 331; JOURNAL OF METALS (April 1951).

[16] G. S. Dickens, A. M. B. Douglas, and W. H. Taylor: Sigma-Phase in the Co-Cr and Fe-Cr Systems. *Journal* Iron and Steel Institute (1951) **167**, p. 27.

[17] P. Weiss and R. Forrer: *Annales de Physique* (1929) **12**, p. 279. (As reported by R. M. Bozorth: *Ferromagnetism.* (1951) New York. D. Van Nostrand.)

[18] P. Weiss, R. Forrer, and F. Birch: *Comptes Rendus* (1929) **189**, p. 189. (As reported by R. M. Bozorth: *Ferromagnetism.* (1951) New York. D. Van Nostrand.)

[19] P. Weiss: *Actes VII Cong. Inst. Froid* (1937) **1**, p. 508. (As reported by R. M. Bozorth: *Ferromagnetism.* (1951) New York. D. Van Nostrand.)

[20] L. Pauling: The Nature of the Interatomic Forces in Metals. *Physical Review* (1938) **54**, p. 899.

Effect of the Structure of Dislocation Boundaries On Yield Strength

by Jack Washburn

Two simple types of dislocation distribution were introduced into zinc crystal specimens and the effect of each on the stress-strain curve was investigated. Quantitative results were obtained for simple edge dislocation arrays and for an array of screw dislocations lying in the slip plane.

ACCORDING to present knowledge, the dislocations present in large annealed metal crystals can be divided into two somewhat arbitrary groups: 1—single dislocation lines distributed more or less at random or forming elements of a three-dimensional network in which the distance between adjacent dislocations is of the order of 10^{-5} to 10^{-4} cm and 2—widely separated planar arrays of edge dislocations forming dislocation walls or small angle boundaries within which adjacent dislocation lines are spaced at much smaller distances (10^{-7} to 10^{-6} cm). The former can be considered as a dislocation interpretation of the *mosaic crystal* proposed by Darwin and Ewald[1, 2] 40 years ago to account for anomalously high integrated intensities of X-ray diffraction maxima. Small angle boundaries, although now known to be present in most single crystals used for mechanical testing, were not generally recognized by the early workers. This was partly due to the fact that only recently have improved X-ray and metallographic techniques been available for checking the macroscopic perfection of crystals.[3-5]

It has long been known that changes in growth conditions and in annealing procedure, which might logically be expected to cause variations in the structural details of both the dislocation network and of dislocation boundaries, produce marked variations in some mechanical properties such as yield strength.[6] However, no quantitative experimental correlations between changes in dislocation distribution and changes in mechanical properties have yet been made. Such a correlation has been difficult to obtain because, even when great care is exercised to keep the histories of a number of single crystal specimens identical, it usually has not been possible to avoid considerable variation in macroscopic perfection.[7] The number and orientation of dislocation boundaries vary from specimen to specimen. This has probably been an important contributing factor to the large scatter in the results of most mechanical measurements on pure single crystals.

Some recent experiments[8, 9] with single crystals of zinc have shown that the presence of dislocation boundaries in a specimen can increase its resistance to deformation by slip. With polycrystalline aluminum and nickel, there is also evidence that dislocation boundaries within the individual grains of the aggregate can increase the resistance of the material to plastic deformation, either as measured by tension tests at room temperature or by creep tests at higher temperatures.[10, 11]

Although the foregoing observations seem to have established the fact that substructure can have a strengthening effect, the test conditions were too complex to give much information concerning the mechanism. In the foregoing cases, a network of intersecting boundaries having various orientations and boundary angles were present. Before their apparent strengthening effect can be understood, it will be necessary to isolate and study separately the effect of a number of variables: 1—boundary angle, 2—boundary orientation with respect to the active slip direction, 3—number of boundaries, 4—intersections of boundaries, 5—detailed structure of the boundaries, and 6—interaction of impurity atoms with dislocations in boundaries.

The object of the present work was to study the effect of dislocation boundaries on flow stress under the following simple experimental conditions: 1—substantially pure shear deformation and 2—boundaries of controlled angle, orientation, and number. In this way, it might be possible to distinguish the important variables from the relatively unimportant ones.

Experimental Procedure

Stress-strain curves of hexagonal metals are generally nearly linear even out to very large strains.[6]

J. WASHBURN, Member AIME, is Assistant Professor of Metallurgy, University of California, Berkeley, Calif.

Discussion of this paper, TP 3980E, may be sent, 2 copies, to AIME by July 1, 1955. Manuscript, Oct. 21, 1954. Pacific Northwest Metals and Minerals Conference, April 1954.

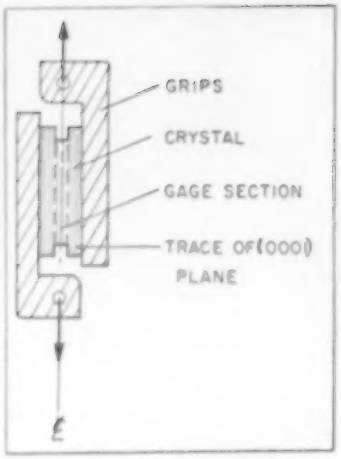

Fig. 1—Normal method of loading in shear. Stress is applied in the slip plane along a slip direction.

The magnitude of the minimum strain at which linearity begins depends upon the uniformity of applied stress and upon the structural perfection of the crystal in the gage section. In a tension test the shape of the initial portion of the stress-strain curve is extremely sensitive to the straightness of the specimen and to the axiality of loading. See, for example, the curves obtained by Jillsen.[3] Other objections to the tensile testing of soft single crystals arise from the rotations accompanying extension.[4] Some of these difficulties can be avoided by testing of single crystals in shear. Previous work[4] has shown that a particularly uniform distribution of slip throughout the gage section of a specimen can be obtained by this type of loading. A section through a shear specimen showing the normal method of application of the load is shown in Fig. 1.

Fig. 2 shows another type of shear specimen which was used for some of the tests. The shearing load is applied at 90° to both the slip plane and active slip direction rather than parallel to the slip plane and direction. The orientation of crystal axes and the estimated elastic shear-stress distribution on the slip plane in the slip direction are shown. When a shearing load is applied to such a specimen, the crystal deforms by slip on the (0001) planes. The active gage section is indicated in Fig. 2 by the shading. The boundary of the slipped volume, instead of being a free surface on four sides as in the usual type of shear specimen, consists of a small angle tilt boundary at the two extremeties. Figs. 3 and 4 are photographs of a specimen of this type before and after a 25 pct shear strain. The tilt boundaries at the end of the gage section are visible on the side surfaces because of the change in intensity of reflected light (due to the relative rotation of the etch pit faces across the boundary). Fig. 5 shows a specimen which had been cleaved through the center after a 1 pct strain. The small angle boundary is visible on both the cleavage surface and the side surface of the specimen. To distinguish it from the normal type of shear specimen, this new specimen hereafter will be referred to as a *kink specimen*.

The grip and roller extensometer assembly used with kink specimens is shown in Fig. 6. Strain in the specimen was determined by measuring the relative displacement of the two opposite halves of the grip. The extensometer was capable of an accuracy of ±0.000025 in. and could be operated by a force of less than 0.004 lb.

The load applied to the specimen was measured to an accuracy of ±0.01 lb by means of a load measuring beam, the curvature of which was indicated by S-R-4 strain gages. The maximum strain rate employed in the tests was 0.01 pct per min.

The crystals were grown from Horse Head Special zinc which had a nominal purity of 99.99 pct. Long rectangular crystals, from which the desired specimens were cut by acid sawing, were grown. The orientation of crystollographic axes in the large crystals was controlled by a seed crystal having the desired orientation relative to specimen directions.

As mentioned previously, a kink specimen was characterized by the formation during testing of a pair of pure edge dislocation boundaries at the extremeties of the gage section. The angle of the boundaries was directly related to the relative displacement of the two grips. This specimen geometry was used because it provided a means for introducing simple edge dislocation boundaries of controlled angle across the gage section of a specimen. Fig. 7 shows the type of specimen used for this purpose. At any stage during a series of tests, the specimen could be gripped at the inner set of notches and a pair of boundaries of known angle could be introduced by shearing the specimen a measured amount. The accuracy within which the boundary angle could be controlled was ±0.01°.

A second type of distortion, which it was thought might be involved in complex substructures, was a

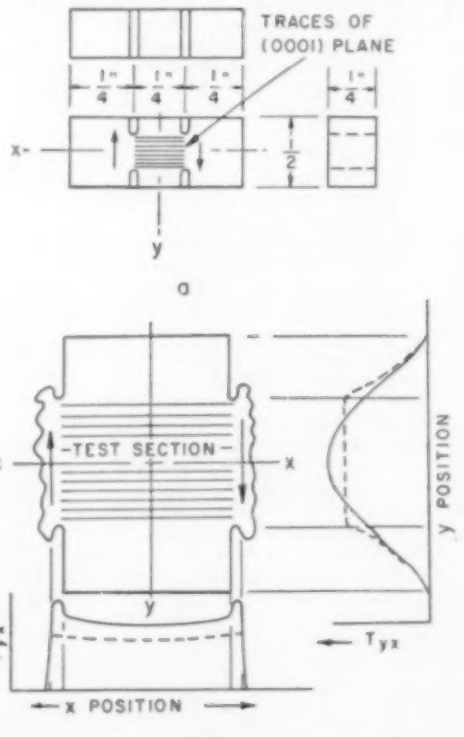

Fig. 2—Alternate type of shear specimen. a—Specimen dimensions are shown. The test section is shaded. Slip planes of the crystal are the Y = constant planes of the sketch. b—Enlarged view of the test section shows estimated elastic shear-stress distributions in the slip planes along X and Y axes. Solid lines are before start of plastic deformation and dashed lines, after start of plastic deformation.

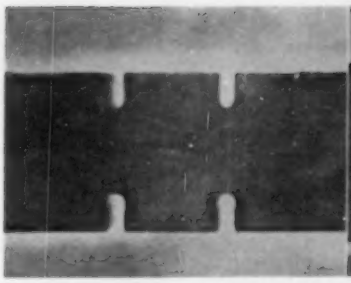

Fig. 3—Photograph shows an undeformed kink specimen.

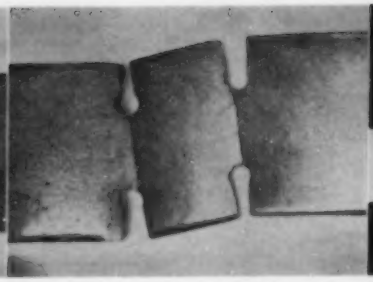

Fig. 4—Kink specimen is shown after a shear strain of 25 pct.

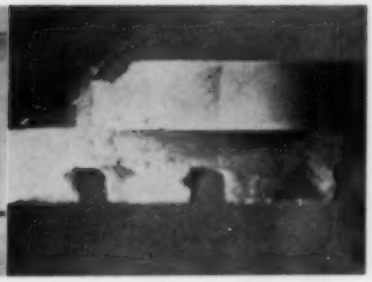

Fig. 5—Photograph of a kink specimen cleaved through the center after a 1 pct strain shows the small angle boundary on both cleavage and side surfaces.

twist about an axis normal to the slip plane. In order to study the effect of such a twist, shear specimens of the normal type were used in which there was initially no observable substructure. The cylindrical gage section was ideally suited for the introduction of a pure twist deformation. A twist about the [0001] axis should result in a network of screw dislocations lying in the (0001) planes. After a small measured twist, the specimen could be tested in the usual manner by loading in shear along the median $[2\bar{1}\bar{1}0]$ direction. The largest twist employed was such that the greatest deviation of the $[2\bar{1}\bar{1}0]$ direction of the applied shear stress was 0.6° which caused a negligible variation in resolved shear stress.

Cottrell states[11] that, "Soft single crystals are not the easiest materials to consider from the theoretical point of view because the process of making them involves the deliberate removal, as far as is possible, of all known sources of hardening and thereby makes the cause of their residual hardness uncertain." Introducing known arrays of dislocations and observing the changes in plastic properties caused thereby may eventually lead to a more detailed model of the annealed state of a crystal.

Previous experience with the mechanical testing of single crystals indicates that, even when great care is exercised to keep the history of a number of specimens identical, an appreciable scatter in yield strength from crystal to crystal can be expected. The only way of avoiding this difficulty was to measure the yield stress of each specimen initially and select those with lowest yield strength, assuming them to be the most perfect. All comparisons were then made on the basis of results from a single specimen. In order to measure the initial yield stress, however, it was necessary to deform the crystal plastically. Therefore, when a series of tests was to be made, it was essential that any strain hardening introduced by the measurement could be removed completely by a recovery treatment. It had already been demonstrated [8, 10] that with shear specimens it was possible to reproduce the stress-strain curve over and over again if the crystal was heated to 400°C after each test. The scatter in yield stress observed in a series of tests on a single specimen was usually less than half as much as would be obtained from the same number of carefully selected separate specimens.

It was necessary to determine whether similar reproducibility also could be obtained with kink specimens. In this kind of specimen, the gage section was terminated by a pair of edge dislocation boundaries which continuously increased in angular magnitude throughout a series of tests and might therefore exert an influence on the shape of the stress-strain curve. The shaded areas of Figs. 8, 9, and 11 show the scatter observed for several tests on three different crystals. No regular change in successive stress-strain curves was observed. The magnitude of the yield stress (as computed from the minimum cross-section between the bottoms of the notches) and the rate of strain hardening in kink specimens were found to be comparable with the same quantities obtained from tests on conventional shear specimens.

From the previous work[8] it was suspected that the strengthening effect of dislocation boundaries might be greatly influenced by the annealing procedure employed. Since it was desired to determine the change in yield strength of crystals containing boundaries as a function of annealing temperature,

Fig. 6—The loading and strain-measuring assembly employed for testing of kink specimens.

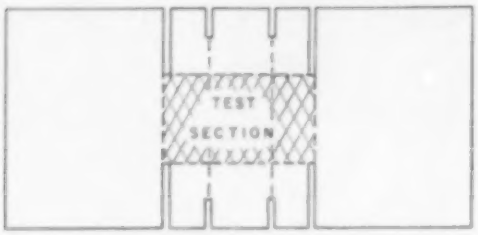

Fig. 7—This type of specimen was used for introduction of a pair of simple tilt boundaries of controlled angle through the test section.

it was necessary to know whether the base yield stress was affected by changes of annealing temperature. It was found that for a good crystal (one having a yield of about 30 psi) a change in annealing temperature from 300° to 400°C resulted in a negligible shift in the level of the stress-strain curve. It was therefore possible to determine the base yield stress employing a 400°C annealing temperature and be reasonably certain that nearly the same value would have been obtained if a 300°C anneal had been used instead. All annealing was carried out in a helium atmosphere. Two standard cycles were used: 1 hr at 400°C or 2 hr at 300°C. Cooling to room temperature was accomplished by turning off the power to the furnace, which resulted in a maximum cooling rate of 10°C per min. All tests were conducted at a temperature of 78°K.

Experimental Results

Results for Simple Edge Dislocation Boundaries: A pair of pure edge dislocation boundaries lying at right angles to the active slip direction was the first type of substructure to be studied. In this case the dislocations forming the boundary array all had the same Burgers vector as the dislocations contributing to the strain. Fig. 8 shows the effect of introducing a pair of such boundaries on the stress-strain curve of a kink specimen. The base curve, as represented by the shaded area, was obtained before the boundaries were introduced; the crystal was annealed at 400°C between tests. The boundaries were then formed by gripping the specimen at the inner set of notches and shearing the crystal a predetermined amount at liquid nitrogen temperature; the specimen was then annealed at 300°C. The stress-strain curve fell exactly in the center of the shaded area enclosing the initial stress-strain curves. There was no apparent strengthening effect produced by the boundaries.* The same specimen was then annealed at 400°C and a second stress-strain curve was obtained. A 22 pct increase in yield stress was then observed. The experiment showed that a pair of edge dislocation boundaries had an almost negligible strengthening effect unless the crystal containing the boundaries had been heated to a temperature close to the melting point prior to testing. Another interesting feature of these curves was the constant value of the strain hardening coefficient; the presence of substructure affected only the yield stress and, in some cases, the sharpness of the yield.

* However, the base yield stress for this crystal was a litt'e higher than that obtained for the most perfect specimens tested. It is likely that a 300°C anneal before introduction of the boundaries would have resulted in a slightly lower set of base curves. Therefore, it is probable that the pair of 1° boundaries annealed at 300°C did have a small strengthening effect.

The relationship between boundary angle and strengthening effect was investigated with the same type of kink specimen. Fig. 9 shows the results ob-

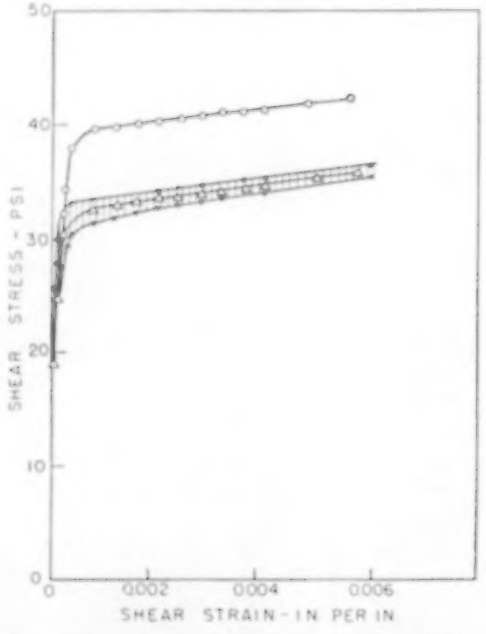

Fig. 8—Effect of annealing temperature on the strengthening due to a pair of 1° edge dislocation boundaries. Shaded area shows the limits of scatter for four tests on the specimen before introduction of boundaries. Annealing temperature was 400°C. Triangles: after introduction of a pair of 1° boundaries and an anneal at 300°C. Circles: same pair of boundaries after an anneal at 400°C.

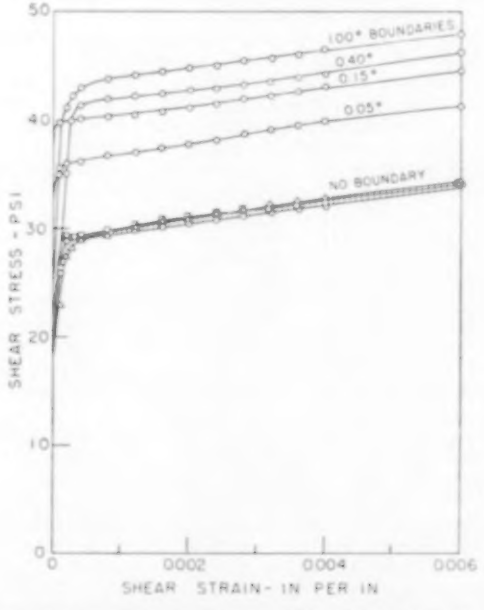

Fig. 9—Stress-strain curves from a single specimen show the effect of introducing a pair of pure tilt boundaries of controlled angle. The crystal was annealed at 400°C before each test and the temperature of testing was —196°C. The shaded area shows band of scatter for three tests on the specimen before introduction of boundaries.

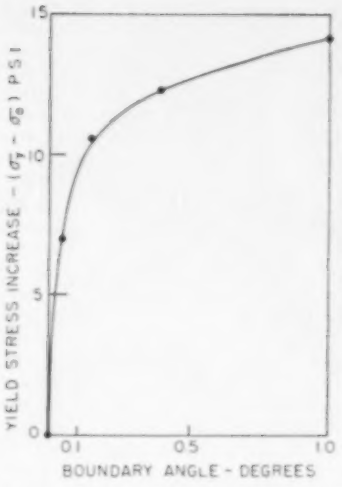

Fig. 10—Curve indicates increase in yield stress as a function of boundary angle for a pair of simple edge dislocation boundaries annealed at 400°C.

tained with boundaries of various angles. All of the tests were preceded by an anneal at 400°C. The crystal used for this series of tests was initially quite perfect, as evidenced by the relatively low base yield stress and the small amount of scatter for the first three tests. Yield-stress increase as a function of boundary angle is plotted in Fig. 10. The yield stress rose rapidly at very small boundary angles but appeared to saturate by the time an angle of 1° had been reached.

Results for an Array of Screw Dislocations: The effect of twisting about an axis normal to the slip plane thus introducing screw dislocations into the (0001) planes is shown by Fig. 11. The numbers opposite the curves indicate the sequence of the tests. 300°C annealing was used for the base curves and for the first two curves after twisting 0.11° per mm. Unlike the edge dislocation arrays, the screw array had a significant strengthening effect even after 300°C annealing. After twisting, the yield was poorly defined with the linear part of the curve only being reached after a strain of 0.006. Again, as in the case of edge arrays, no change in the slope of the linear part of the curve was observed. 400°C annealing produced an additional increment of strengthening as shown by the third curve for the 0.11° twist. The increase in yield stress as a function of twist angle is plotted in Fig. 12. The relation is analogous to that obtained for edge boundaries. A sharp rise for small angles of twist was followed by decreasing increments in strengthening effect for additional increments of twist.

Discussion

Prior to each of the tests, the crystals were in the annealed condition in the sense that they had been heated to a temperature close to the melting point. The annealing treatments were sufficient to accomplish complete recovery in a homogeneously deformed specimen.[6, 10] Therefore, although parts of the specimen underwent plastic deformation during the introduction of the simple substructures, it can be assumed that all of the attendant work hardening was removed by the heat treatment. The only remaining differences were those in the arrays of like dislocations which made up the substructures.

By measurement of boundary angle in the case of pure tilt boundaries, it is possible from geometrical considerations alone to calculate the spacing be-

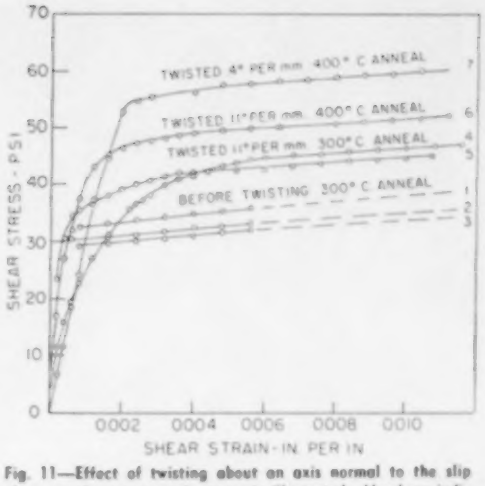

Fig. 11—Effect of twisting about an axis normal to the slip plane on the stress-strain curve is illustrated. Numbers indicate sequence of tests.

tween the excess dislocations of the same sign which make up the boundary. Similarly, in the case of a twisted crystal if the twist angle per unit length along the twist axis is known, the density of excess screw dislocations of the same sense is fixed by geometry. However, the precise distribution of these dislocations among the possible parallel slip planes cannot be determined by any available means. Since climb of edge dislocations becomes possible at high temperatures, it is reasonable to assume that changes in vertical distribution occur during annealing. However, in view of the importance of annealing temperature in determining the strengthening effect of a given substructure, it seemed desirable to obtain some experimental evidence that changes in boundary structure actually occurred at the annealing temperature employed.

The following experiment shows clearly that vertical redistribution of dislocations in a tilt boundary does occur when a zinc crystal is heated to 400°C. Fig. 13 describes the experimental conditions. A bend plane was formed at right angles to $[2\bar{1}\bar{1}0]$ by local slip having a slip vector $[2\bar{1}10]$. The intersection of the bend plane with the (0001) surface is readily observable.[9] The position of the bend plane intersection with the $(11\bar{2}0)$ surface coincided with the ends of the slip markings which were visible in the plastically deformed part of the crystal.

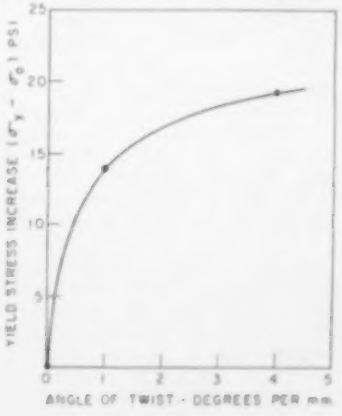

Fig. 12—Curve shows increase in yield stress as a function of twist angle.

Fig. 13 — Diagram shows formation of a small angle boundary by localized shear strain. Intersection of boundary with (1210) surface as seen on cleavage face coincides with ends of slip markings as seen on (1210) surface.

Directly after formation, the boundary was diffuse. Rather than being a sharp bend, it was a narrow zone of curvature. The distribution of slip as shown by the slip markings on the (1120) surface required that the boundary had a structure like that pictured in Fig. 14a. Most of the dislocations must have been clustered in groups at the termination of visible bands of slip. If such a boundary were to move in the direction of the slip vector of its component dislocations, all of the dislocations remaining in their original slip planes, then the slip markings as seen on the (1120) surface would either extend or contract depending on the direction of the motion of the boundary. If, on the other hand, the dislocations were allowed to redistribute themselves vertically by climb into a uniformly spaced array such as Fig. 14b prior to motion of the boundary, then the slip markings which terminated at the original position of the boundary should remain unchanged by the motion. Motion of the regularly spaced array would cause such small closely spaced steps on the surface as to be unresolvable by the microscope. Fig. 15 shows that this was the case when a boundary was caused to move at a temperature of 400°C. The original slip markings remained unchanged as the position of the boundary changed.

These results mean that after annealing at 400°C the boundaries which were present did have a structure which approached a regular array. However, there are still unknown details of the distribution which may be extremely important. For example, if it were possible to follow one of the dislocation lines in the boundary, it is probable that every so often there would be jogs where the line stepped from one close-packed plane of atoms to the next parallel one. The number of these jogs per unit length of dislocation line is probably an important factor in determining the properties of a boundary.

The qualitative result that unannealed boundaries or those which had only been annealed at low temperatures showed little or no strengthening effect is reasonable on the basis of the simple dislocation model of boundary structure presented in Fig. 14a. Many of the boundary dislocations would be attracted only weakly, if at all, to the region of curvature. Such a boundary might be expected to act as a source of dislocations rather than as a barrier to slip.

The quantitative results, however, are difficult to explain on the basis of the ideal boundary structure and present theories of slip. For example, if the strengthening effect is assumed to be related to the local stress necessary to separate two edge dislocations spaced at the same vertical distance as those in the boundary, then the strengthening effect should increase linearly with boundary angle as long as the angle is less than a few degrees.[8] The results showed a marked deviation from linearity at boundary angles which were only a fraction of a degree. Furthermore, if the boundary is considered as a local barrier against which a number of dislocations must pile up on each active slip plane before a slip avalanche can break through, then the same simplified model referred to previously gives 20 to 200 dislocations, depending on boundary angle, as the maximum number of piled-up dislocations. Consideration of the details of the growth of visible slip bands suggests that sufficient stress concentration to penetrate the boundary should always be present at the tip of an advancing band of slip. On the basis of a barrier model of the strengthening effect, it is also difficult to understand why the yield was sometimes observed to be just as sharply defined when boundaries were present as it was before any had been introduced, Fig. 9. The two curves were sometimes parallel beyond a strain of 0.0001 although the yield stress differed by 25 pct. It would be more reasonable to expect yielding to occur at approximately the same stress and to be followed by rapid strain hardening when a boundary was present until stress concentrations could build up at the barrier. This type of behavior was observed, for example, in the twisted crystals, Fig. 11.

Summary and Conclusions

Two simple types of dislocation distribution were introduced into zinc crystal specimens and the effect of each on the stress-strain curve was investigated. For simple edge dislocation boundaries lying at right angles to the active slip direction, a quantitative study of yield stress as a function of boundary angle was made. The presence of a pair of 0.05° simple edge dislocation boundaries across the gage section of a specimen caused a 25 pct increase in the yield stress. Further increases in boundary angle were accompanied by smaller increments in strengthening effect. A saturation value of about 50 pct increase in yield stress appeared to be approached for boundary angles above 1°.

For a given boundary angle, the strengthening effect was determined by the temperature at which the specimen containing a boundary had been annealed. A pair of 1° boundaries introduced by plastic bending at liquid nitrogen temperature produced no strengthening at all if the crystal had been heated only to room temperature, very little strengthening if heated to 300°C, but a large increase in yield stress if heated to 400°C.

An array of screw dislocations was introduced into the (0001) planes by twisting about the c-axis.

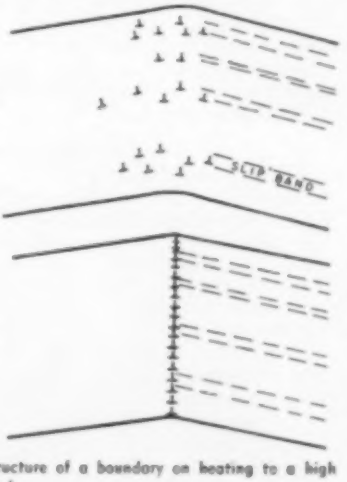

a—Immediately after formation by localized shear strain at low temperature.

b—Change in structure of boundary after heating to 400°C.

Fig. 14—Change in structure of a boundary on heating to a high temperature is illustrated.

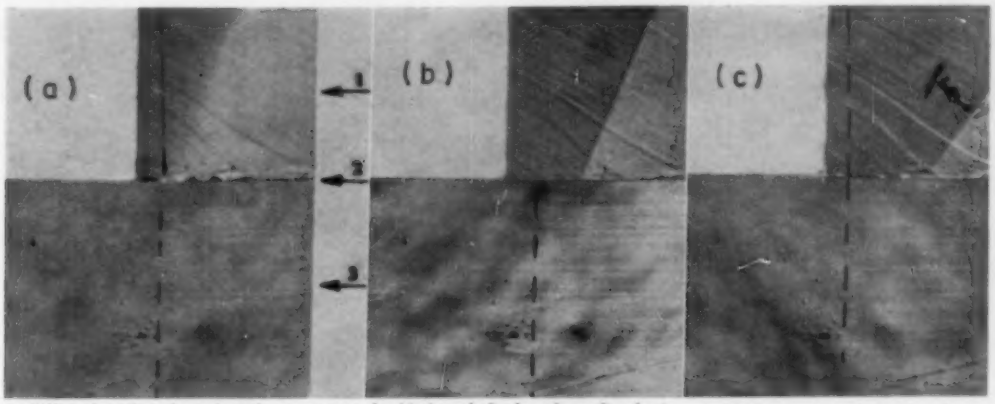

a—Diffuse boundary formed at low temperature as indicated in Fig. 13. Arrow 1 points to (0001) surface, arrow 2 to common edge, and arrow 3 to (1$\bar{2}$10) surface.

b—Motion of the boundary after heating to 400°C. Since visible slip markings on (1$\bar{2}$10) surface are unchanged, dislocations must have rearranged themselves vertically by climb as indicated in Fig. 14 before the boundary started to move.

c—Further motion of the boundary.

Fig. 15—Three parts of the figure show experimental evidence for dislocation climb in zinc. X100.

Quantitative measurements of strengthening effect as a function of angle of twist gave results similar to those for simple edge dislocation boundaries; the first small increment of twist angle produced the largest increment in yield stress. A somewhat smaller dependence on annealing temperature was observed for this type of array.

Two further qualitative observations were common to most of the tests: 1—No change in the slope of the linear part of the stress-strain curve was observed. 2—The yield was usually not as sharp as in macroscopically perfect crystals; appreciable plastic strain accompanied by rapid strain hardening occurred before the *linear* part of the curve began. This was not always true for the case of pure edge dislocation boundaries.

The following conclusions can be drawn from the results:

1—The yield strength of a metal crystal is determined not only by the submicroscopic or microscopic distribution of dislocations throughout the crystal but also by concentrations of dislocations on a macroscopic scale forming isolated small angle boundaries.

2—Rate of strain hardening at larger strains is not affected by edge dislocation boundaries or by an array of screw dislocations in the slip planes. Therefore it seems probable that the small linear rate of hardening of hexagonal crystals is due to a process occurring on a submicroscopic scale.

3—The *detailed structure* of a small angle boundary, as determined by prior strain and thermal history, determines its effectiveness as a barrier to slip.

4—Boundary intersections do not appear to be a necessary condition for the strengthening effect of a substructure, since a pair of pure tilt boundaries was just as effective in producing a strengthening effect as the complex array studied earlier.

5—Climb of dislocations does occur in zinc crystals when heated to a temperature of 400°C.

Acknowledgments

The author is grateful for the support of the Office of Naval Research, which made it possible to undertake this investigation, and to the General Electric Co. at whose laboratories some of the experimental work was completed during a period of summer employment.

Discussion of this paper, if any, will appear in JOURNAL OF METALS, November 1955, and in AIME Metals Branch *Transactions*, Vol. **203**, 1955.

References

[1] C. G. Darwin: The Theory of X-Ray Reflexion, I and II. *Philosophical Magazine* (1914) **27**, pp. 315, 675.

[2] P. P. Ewald: Zur Begrundung der Kristalloptik. *Annalen der Physik* (1917) **54**, p. 519.

[3] P. Lacombe and L. Beajard: The Application of Etch-Figures on Pure Aluminum (99.99%) to the Study of Some Micrographic Problems. *Journal* Inst. of Metals (1947) **74**, p. 1.

[4] A. Guinier and J. Tennevin: Discussion of a paper by P. Lacombe and A. Berghazan. *Physica* (1949) **15**, p. 167.

[5] A. Guinier: Substructures in Crystals. *Imperfections in Nearly Perfect Crystals.* (1952) New York. John Wiley and Sons, Inc.

[6] E. Schmid and W. Boas: *Kristallplastizitat.* (1935) Berlin. J. Springer.

[7] A. N. Holden: Preparation of Metal Single Crystals. *Trans.* ASM (1950) **42**, p. 319.

[8] C. H. Li, J. Washburn, and E. R. Parker: Variation in Plastic Properties with Annealing Procedure in Zinc Single Crystals. *Trans.* AIME (1953) **197**, p. 322; JOURNAL OF METALS (February 1953).

[9] D. W. Bainbridge, C. H. Li, and E. H. Edwards: Recent Observations on the Motion of Small Angle Dislocation Boundaries. *Acta Metallurgica* (1954) **2**, No. 2, p. 322.

[10] D. McLean and A. E. L. Tate: Influence de la Polygonisation sur certaines propriétés de l'aluminum. *Revue de Métallurgie* (1951) **48**, p. 765.

[11] E. R. Parker and T. Hazlett: Principles of Solution Hardening. *Relation of Properties to Microstructure.* (1954) Cleveland. ASM.

[12] D. C. Jillson: An Experimental Survey of Deformation and Annealing Process in Zinc. *Trans.* AIME (1950) **188**, p. 1009; JOURNAL OF METALS (September (1950).

[13] E. R. Parker and J. Washburn: Deformation of Single Crystals. *Modern Research Techniques in Physical Metallurgy.* (1953) Cleveland. ASM.

[14] A. H. Cottrell: Bristol Conference on the Strength of Solids. (1948). *Dislocations and Plastic Flow in Crystals.* (1953) Oxford. Oxford University Press.

[15] T. A. Read: *Dislocations in Crystals.* (1953) New York. McGraw-Hill Book Co. Inc.

Creep Deformation of Magnesium at Elevated Temperatures by Nonbasal Slip

by A. R. Chaudhuri, H. C. Chang, and N. J. Grant

During the creep of coarse-grained polycrystalline magnesium at elevated temperatures, a nonbasal type of slip was found to play an important role in the deformation processes. The nonbasal slip traces were examined metallographically in eight specimens (13 grains) and the observed glide plane located stereographically for each grain. The tests were run at 500° and 700°F at stresses of 148 to 786 psi. Based on these measurements and theoretical calculations, the crystallographic elements for nonbasal slip were determined.

WHEN a metal deforms by slip, the conventional appearance of the slip bands on the surface of a specimen is that of straight lines. Such is the behavior of the face-centered-cubic metals, as for example, aluminum. The particular slip system on which slip occurs in these metals is governed by the criterion of resolved shear stress.

Work on the body-centered-cubic metals α-iron,[1, 2] molybdenum,[3] and columbium[4] has shown that the process of slip is somewhat more complicated than the simple gliding of one close-packed plane of atoms over another in a close-packed direction and that it results in the formation of wavy and irregular slip traces on the surface. The recent reviews and experiments of Vogel and Brick[5] and Chen and Maddin[6] show that, for the body-centered-cubic metals, the resolved shear stresses along the planes and the degree of close-packing do not necessarily determine the slip system. Theirs and other investigations indicate that a complete understanding of the slip process in the body-centered-cubic metals is not yet possible. However, one behavior displayed by all these metals is that the slip direction is invariably one of the close-packed directions <111>. The wavy nature of the slip-band traces has been explained on the basis of cooperative slip by planes sharing this same slip direction.[1,5,6]

It is generally acknowledged that, when the hexagonal-close-packed metal magnesium (axial ratio $c/a = 1.624$) deforms by slip at room temperature, it does so by basal slip in the close-packed direction $<11\bar{2}0>$. This type of slip has the conventional appearance of straight lines and is governed by the critical shear-stress law. Schmid and coworkers[7] showed that basal slip was operative in the temperature range of −185° to 300°C (−300° to 572°F).

Work by Servi, Norton, and Grant[8] has shown that, during the creep of coarse-grained aluminum at high temperatures, new slip systems come into operation. The existence of a new high temperature slip system at temperatures greater than 225°C (437°F) for magnesium was suggested also by Schmid.[9] This was later indicated by Bakarian and Mathewson[7] to be slip along the pyramidal planes $\{10\bar{1}1\}$ in the close-packed direction $<11\bar{2}0>$.* They observed that this kind of slip resulted in irregular markings on the specimen surface. According to them, a possible cause for the appearance of the markings was due to "limited accessory slip on the pyramidal $\{10\bar{1}2\}$ planes." Burke and Hibbard,[9] on deforming a single crystal of magnesium at room temperature, found evidence of slip on a pyramidal plane $\{10\bar{1}1\}$. They explained it as being due to the effect of grip restraints.

It is pertinent to note at this point that, although basal slip has received a fair amount of attention, only two specimens have been investigated, that of Bakarian and Mathewson and of Burke and Hibbard, to establish the elements of nonbasal slip in magnesium.

During the study of the deformation mechanisms

* Mention will be made in the text of pyramidal planes and prismatic planes. The pyramidal planes referred to are the type I, order 1 of the form $\{10\bar{1}1\}$; and the prismatic planes of the type I of the form $\{10\bar{1}0\}$. For the sake of brevity, they are termed in the text as pyramidal $\{10\bar{1}1\}$ and prismatic $\{10\bar{1}0\}$ planes, respectively. Where reference is made to the pyramidal plane type 1, order 2 of the form $\{10\bar{1}2\}$, they are referred to as the pyramidal planes of the type $\{10\bar{1}2\}$.

A. R. CHAUDHURI, H. C. CHANG, Associate Member AIME, and N. J. GRANT, Member AIME, are Research Associate, Staff Member, Div. of Industrial Cooperation, and Associate Professor, respectively, Dept. of Metallurgy, Massachusetts Institute of Technology, Cambridge, Mass.

Discussion of this paper, TP 3926E, may be sent, 2 copies, to AIME by July 1, 1955. Manuscript, Aug. 6, 1954. Chicago Meeting, February 1955.

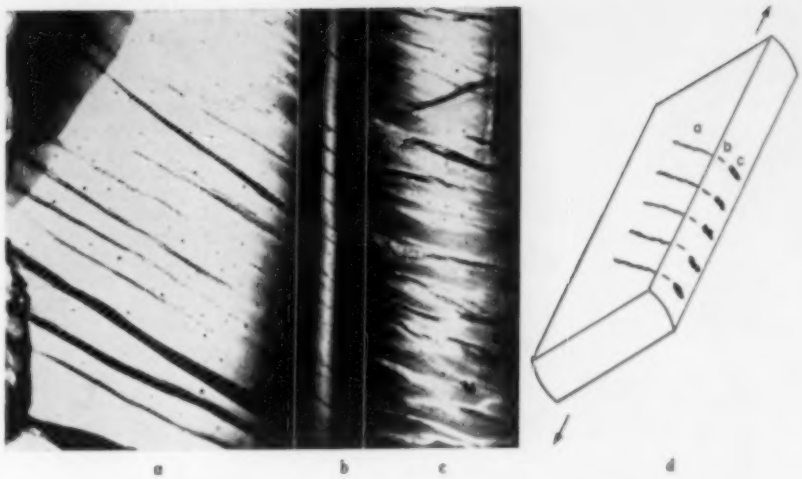

Fig. 1—Examples of nonbasal slip traces, grain 32-1. Inclination of observation plane to plane containing both the slip direction and the axis of tension. Axis of tension is vertical. *a*, flat reference surface, 22°; *b*, 6°; *c*, —57°; and *d*, schematic drawing showing the traces on these three surfaces. X50.

of magnesium in creep at high temperatures, Chaudhuri, Grant, and Norton[5] observed that one of these mechanisms was by nonbasal slip. The nomenclature of pyramidal slip was given to these markings on the basis of the similarity they bore in appearance to those observed by Bakarian and Mathewson. Roberts[6] also has observed this nonbasal type of slip. The extreme irregularity of these bands seemed to suggest that it was unlikely that slip occurring on a single plane of atoms could result in traces of this type. It was felt that their appearance could be more successfully rationalized by using arguments similar to those that have been used to explain the nature of the markings in the body-centered-cubic metals.

Because this type of nonbasal slip plays an important role in the creep of coarse-grained polycrystalline magnesium at high temperatures, it was decided to study it in greater detail.

Experimental Procedure

The magnesium studied in this work was supplied by the Dow Chemical Co. and was of 99.972 pct purity. The originally round specimens had parallel flats milled on opposite sides for the purpose of metallographic examination. The test bar ends were threaded to fit the specimen holders. The test zone had the dimensions of 1x3/16x7/64 in. The average diameter of the grains examined was about 2 to 3 mm and was attained by annealing at 1100°F for about 15 hr. The specimens were polished electrolytically in a solution of orthophosphoric acid and ethyl alcohol prior to deformation. Direct loading of the specimens was used. The details of the preparation and testing of the specimens have been reported previously.[5] The specimens were deformed in air, but the resulting oxidation was only slight. This lead to the formation of small oxidation pits distributed both randomly on the surface and also preferentially along zones of deformation.

Polycrystalline specimens were used in this work but only those grains which occupied nearly the whole of the cross-section were selected for analysis. Micrographs at X50 were taken at several azimuthal positions around the specimen axis. The angles made by the slip traces to the axis of tension were measured from these micrographs. The amount of rotation was measured with respect to one of the flat surfaces of the specimens and was determined by means of a protractor attached to the specimen holder and axially aligned with it. Since the specimens were not round in their cross-sections, the entire circumference of the specimens could not be examined. The orientations of the grains were determined from Laue back-reflection X-ray pictures which were taken on the deformed specimens. In most cases the breaking up of the Laue spots into streaks was small (2°) and they did in no case exceed 5°. In plotting the zones, the hyperbolae passing through the centers of the streaks were used. Consequently, the true orientations could be of the order of $\pm 2\frac{1}{2}$° from the measured ones. The angles made by the slip traces were transferred to the stereographic projections.

A glance at the micrographs (Fig. 1) will show at once that the slip-band traces are very irregular in appearance. Although the bands are wavy, they are, in general, more or less parallel in any one grain. Grains in which too much branching and forking of

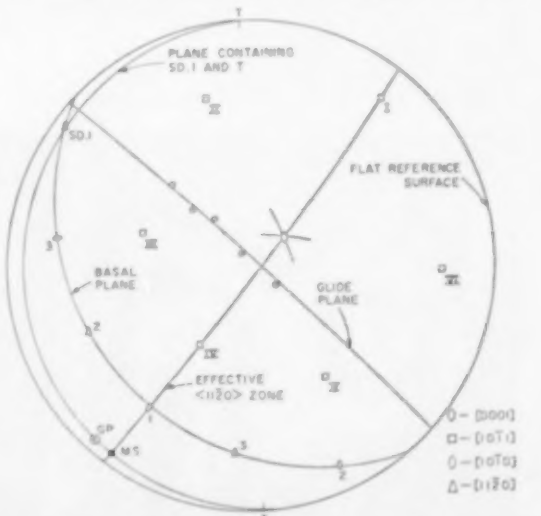

Fig. 2—Projection of grain 48-3, showing location of observed glide plane. *GP* stands for pole of glide plane; *SD. 1*, <11$\bar{2}$0> slip direction in glide plane; *MS*, pole of maximum resolved shear-stress plane on effective <11$\bar{2}$0> zone; and *T*, tension axis.

Fig. 3—Orientations of grains studied.

the slip bands were exhibited were not used in this analysis. At each position of observation, an average was taken of the angles made by several traces; and traces showing too marked a departure from the general direction were not included among those measured. One difficulty encountered in this work was due to the formation of volatilization pits on the specimen surfaces during the annealing to produce the coarse grain size needed. It was attempted to electropolish to a depth below these pits. In most cases, the polished surfaces were free of these imperfections; however, in a few other instances the pits were too deep to be completely removed. Naturally, slip bands on passing through them appeared curved. Such traces were not measured.

The accuracy of the location of a glide plane obtained from such irregular bands might well be questioned and it is best discussed by means of an example. The basic circle in Fig. 2 represents one of the flat surfaces of grain 48-3.* The axis of tension is indicated as *T*. The encircled dots are the directions (with respect to the axis of tension) of the traces on surfaces, which are inclined by known amounts to the flat surface represented by the basic circle. The great circle passing through these dots is the observed glide plane, and its pole is shown as *GP*. For this grain, it will be seen from Fig. 2 that the scatter of the trace directions about the observed glide plane was not at all large. In most other cases, the scatter was such that the angular distance between the pole of the glide plane and each of the trace directions was within 90±7°. A possible reason for the comparatively large amount of scatter in the latter measurements is given subsequently, and it will be shown that it is not so much a question of error as it is of something latent in the nature of this mode of deformation. This reason also will explain the wavy appearance of the bands.

* The first two-digit number indicates the specimen, while the third digit indicates the particular grain in that specimen.

Table I shows the test conditions for the specimens. All the specimens except specimens 31 and 32 were deformed at 700°F. These two were deformed at 507° and 470°F, respectively. Specimens 31 and 33 were deformed to fracture. The grains selected from these specimens for examination were, however, quite far from the fracture zone, and a metallographic study of these grains indicated that the severity of the deformation in the fracture zones did not spread to the grains 31-1, 33-2, and 33-4. In specimen 54 the whole gage section was practically occupied by one grain.

The orientations of the crystals used are shown in Fig. 3. The concentration of the orientations to one small region will be noted at once. This resulted because the coarse grains, grown from the smaller ones in the extruded rods, retained orientations not far removed from the original preferred orientation, namely, one in which the basal planes are nearly parallel to the axis of extrusion. As will be shown later, this particular orientation effect was not only beneficial, but also very necessary for this investigation.

Experimental Results and Discussion

In determining the glide plane, it usually suffices to measure the angles made by the slip traces with respect to a particular direction on two surfaces at a known angle to each other, the particular direction being common to both surfaces. In view of the fact that the slip bands studied in this work were wavy, measurement of the angles made by the traces on more than two surfaces was performed, since this resulted in greater accuracy.

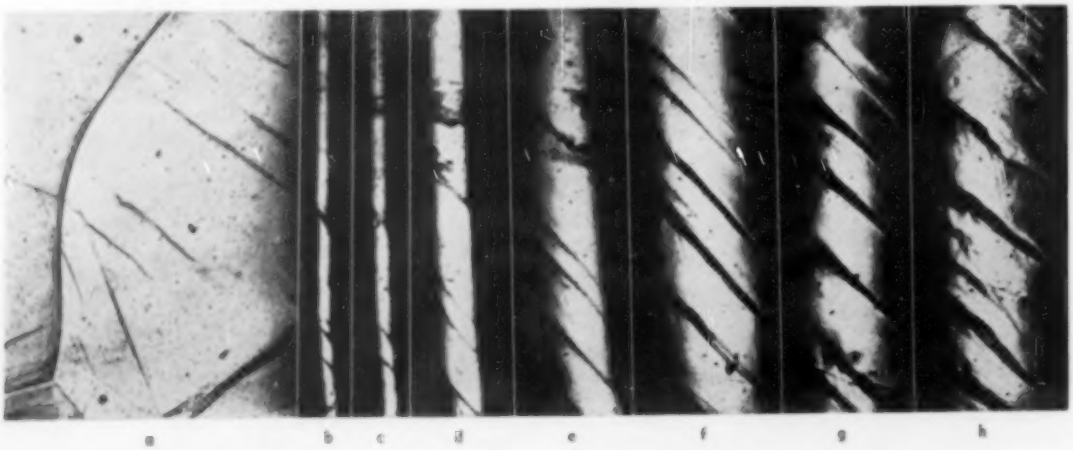

Fig. 4—Nonbasal slip traces in grain 33-4. Inclination of observation plane to plane containing both the slip direction and the axis of tension. Axis of tension is vertical. *a* is flat reference surface, 54°; *b*, 23°; *c*, 12°; *d*, 2°; *e*, —5°; *f*, —15°; *g*, —25°; and *h*, —36°. X50.

Table I. Test Conditions

Specimen No.	Number of Grains Studied	Stress, Psi	Elongation, Pct	Duration, Hr
31	1	670	To fracture	About 330
32	1	788	2.7	717
33	2	426	To fracture	About 9
39	1	302	13	17
48	3	140	4.6	66
51	3	179	5.7	161
52	1	187	2.9	29
54	1	173	4.9	27

Metallographic Observations: Fig. 4a to h shows the traces of the slip bands on the surfaces of grain 33-4. Fig. 5 is a stereographic projection of this grain. Each encircled dot represents the average of the experimentally determined angles between the tension axis *T* and the slip traces on a surface of observation. The inclination of the observation surface was measured with respect to a reference surface (one of the flat surfaces of the specimens) and each surface of observation also was parallel to the tension axis. The best great circle passing through these points is therefore the observed glide plane, and its pole is shown as *GP*. The slip direction of the type $<11\bar{2}0>$ situated closest to the glide plane is shown as *SD*. This typical example shows that the pole of the observed glide plane lies very close (1°) to a $<11\bar{2}0>$ zone and is situated between the poles of a $\{10\bar{1}0\}$ prismatic plane, 1, and a $\{10\bar{1}1\}$ pyramidal plane, I. This pole also lies close (1°) to the pole of the maximum resolved shear-stress plane on this particular zone. The latter pole is indicated as *MS* in Fig. 5 and is located at the intersection of this zone and the plane containing both the axis of tension and the slip direction. Also evident is the fact that the glide plane pole does not coincide with the pole of any low index, and therefore densely packed, plane. Fig. 6 shows the location of the glide plane in the single crystal 54-1. It will be seen that the relationships of the pole of the glide plane to the various other poles are, in general, the same as those of the pole of the glide plane in grain 33-4. It is found again in this grain that the observed glide plane pole lies very close to the maximum resolved shear-stress plane pole, *MS*. Table II shows, for all the grains examined, the locations of the poles of the glide planes with respect to the $<11\bar{2}0>$ zones closest to which they are situated and, also, to the poles of the pyramidal $\{10\bar{1}1\}$ and prismatic $\{10\bar{1}0\}$ planes between which they lie. The following observations can be made from this table of results:

1—The observed glide plane pole does not coincide with the pole of any low index plane.

2—The observed glide plane pole is close to a $<11\bar{2}0>$ zone. The maximum distance was 4°.

3—The observed glide plane lies between a prismatic plane $\{10\bar{1}0\}$ and a pyramidal plane $\{10\bar{1}1\}$ though closer to the former.

4—The angular distance between the glide plane pole and the $\{10\bar{1}0\}$ and $\{10\bar{1}1\}$ poles is not constant, indicating that no unique glide plane can be assigned to this type of nonbasal slip.

No attempts were made in this work to determine the slip direction by determining the rotation of the specimen axis after deformation. Others[4, 5] have found that the slip direction is invariably of the close-packed-type $<11\bar{2}0>$. The fact that there was only one such slip direction situated very close to the glide plane left no ambiguity in the choice of slip direction.

It was found that the appearance of the slip traces was not a constant feature on every surface of observation on a specimen but was, in fact, dependent on the angle made by the surface of observation to the slip direction. A series of traces shown in Figs. 4a through 4h obtained from grain 33-4 illustrates this point very clearly.

Table II. Location of Pole of Observed Glide Plane

Grain	Distance of Pole of Observed Glide Plane From: Closest Slip Direction	$(10\bar{1}1)$	$(10\bar{1}0)$	Maximum Resolved Shear Plane
31-1	87°	27°	3°	4°
32-1	87°	24°	5°	3°
33-2	88½°	25°	4°	6°
33-4	89°	10½°	10½°	1°
39-1	87°	27°	3½°	7°
48-1	86°	19°	10°	8°
48-2	86°	27°	4°	6½°
48-3	85°	12°	18°	5°
51-1	87°	29°	3°	5½°
51-2	87°	25½°	4½°	7½°
51-3	86°	23°	8½°	6¼°
52-1	87°	24½°	6°	4°
54-1	86°	22°	8°	4°

Fig. 4d shows that when the surface of observation was almost parallel to the slip direction, not only were the traces the sharpest of the series, but also there was only one set of parallel traces. This fact is important in that it indicates that only one slip direction, one of the close-packed $<11\bar{2}0>$ directions, is involved in the formation of these bands. Hence, it is reasonable to suppose that the glide process is due to the cooperation between planes sharing this same slip direction and that planes having other slip directions do not take part in this process, at least not to any significant extent. In other words, the planes taking part necessarily belong to the same zone. Since all the planes of a $<11\bar{2}0>$ zone intersect along a line, which is the slip direction, all the planes (of the zone) would each make the same trace on a surface parallel to this

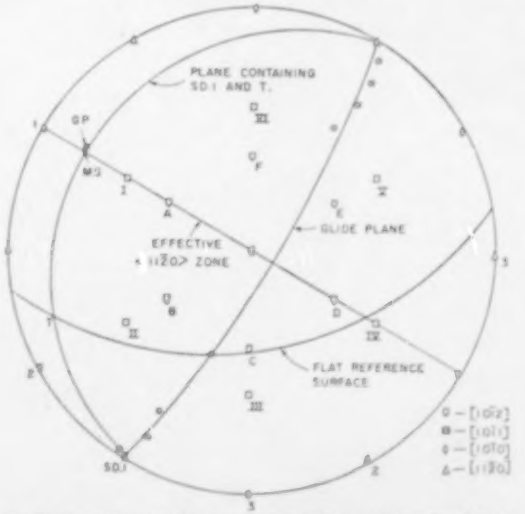

Fig. 5—Location of glide plane in grain 33-4. *GP* is pole of glide plane; *SD. 1*, $<11\bar{2}0>$ slip direction in glide plane; *MS*, pole of maximum resolved shear-stress plane on effective $<11\bar{2}0>$ zone; and *T*, tension axis.

line; and the direction of the trace would be the same as the slip direction. The sharpness of the traces on a surface parallel to the slip direction is then understandable.

As the surface of observation becomes increasingly inclined to the slip direction, Figs. 4c, 4b, and 4a and 4e to 4h show that observed slip traces become progressively wider and coarser. This is to be expected on the basis of the foregoing argument since, as the surface of observation becomes increasingly inclined to the slip direction, the traces of the planes (of the zone) make increasingly larger angles with each other on the plane of observation. Consequently, the observed slip bands would tend to become progressively coarser. In the ideal case, that is, one in which every direction of rotation is available, a plane of observation almost parallel to one of the planes in the effective zone would be the surface on which the coarsest possible traces would be seen.

The tension axis was the axis of rotation used to obtain the different observation surfaces. Hence, the coarsest traces were observed on a surface 90° removed from that on which the sharpest were seen. Due to the specimen shape and the size of the grains, the whole circumference of the specimens could not be examined. As a result it was not possible in every case to view surfaces which would show each of these types (fine or coarse) of traces. However, it was found in all the specimens that the traces became finer as the surface of observation approached a parallel position to the slip direction. Also, they tended to become coarser as the surface of observation approached a surface perpendicular to that parallel to the slip direction. The series of micrographs in Fig. 4 demonstrates these findings.

Surface Atomic Density Factors: It has been demonstrated that the wavy nonbasal slip bands encountered in this work result from cooperative slip between planes belonging to a $<11\bar{2}0>$ zone, and which, therefore, share the same slip direction, a $<11\bar{2}0>$ direction. The fact that the pole of the observed glide plane was, in all cases, located near a $<11\bar{2}0>$ zone and between the poles of a prismatic plane $\{10\bar{1}0\}$ and a pyramidal plane $\{10\bar{1}1\}$, suggests that these may be the two participating planes. One

Fig. 6—Location of glide plane in grain 54-1.

criterion used to determine the ease of slip along a plane is that of the surface atomic density of the plane. An indication of the particular planes of the $<11\bar{2}0>$ zone participating in the slip process is obtained by considering the atomic densities of the more important planes of this zone.

Table III shows these values. It is evident that the atomic density of the basal planes is much higher than those of the other planes. The pyramidal $\{10\bar{1}1\}$ and the prismatic $\{10\bar{1}0\}$ planes have values which are quite close to each other, while that of the pyramidal plane $\{10\bar{1}2\}$ is much less. The slightly higher atomic density of the prismatic planes suggests that if the criterion of the degree of close packing is the only one to determine the ease of slip, then slip on the prismatic planes should be easier than slip on the pyramidal planes $\{10\bar{1}1\}$, the orientation of the planes being suitable.

Consideration of the interplanar spacings for these planes introduces some uncertainty in this reasoning. Due to the presence of the centered atoms, the hexagonal-close-packed structure may be considered as being composed of two interpenetrating simple hexagonal lattices. Fig. 7 shows a hexagonal lattice viewed in a $<11\bar{2}0>$ direction and illustrates the traces of the basal, the two pyramidal $\{10\bar{1}2\}$ and the $\{10\bar{1}1\}$, and the prismatic planes $\{10\bar{1}0\}$ on a $\{11\bar{2}0\}$ plane. It is apparent that, whereas the basal planes are uniformly spaced at intervals of $c/2$, the other planes are not. The ratios of the nonuniform spacings are 1/3:2/3, 1/6:5/6, and 1/3:2/3 for the planes $\{10\bar{1}2\}$, $\{10\bar{1}1\}$, and $\{10\bar{1}0\}$, respectively. These nonuniform spacings and the spacings that would result if the centered atoms are not considered are also shown in Table III. It is obvious that the centered atoms are essential in any consideration of slip in the hexagonal-close-packed metals; and therefore, the largest interplanar spacing listed for each plane (that value obtained by not considering the centered atoms) does not have any significance. Consequently, in addition to the surface atomic density for a plane, the nonuniform interplanar spacing must also be taken into account as a factor in determining the plane for slip. Chalmers and Martius[11] considering, in effect, these arguments have attempted to rationalize the nonoccurrence of prismatic slip and the occurrence of pyramidal slip in magnesium. On the other hand, Rosi, Dube, and Alexander[12] have suggested that prismatic slip should be possible in magnesium. Thus the preference of the one slip system for the other is still in question.

There is no doubt that slip along the basal planes as the predominant slip system in magnesium is supported from considerations of both the atomic densities and the interplanar spacings. Due to the nonuniform spacing of the planes of the $<11\bar{2}0>$ zone, the choice of the slip system (with a $<11\bar{2}0>$ slip direction), which is next likely to be operative, is not quite as unambiguous. However, when basal slip is not possible, it is reasonable to assume that the systems $\{10\bar{1}1\}$ $<11\bar{2}0>$ and $\{10\bar{1}0\}$ $<11\bar{2}0>$ are the next most favorable systems on which slip is likely to occur.

Resolved Shear-Stress Considerations: The possibility of slip along these planes is enhanced by a consideration of the resolved shear stresses along these planes and the critical resolved shear stress for slip.

Bakarian and Mathewson[7] obtained values of 400 and 65.5 g per sq mm, respectively, as the critical resolved shear stresses for pyramidal $\{10\bar{1}1\}$ and basal slip in magnesium. Their values were obtained for magnesium of a purity similar to that used in the present work and at a temperature of 330°C (626°F). Therefore, for pyramidal slip to occur, the orientation factor ($\cos\theta \cos\lambda$, where θ and λ are, respectively, the angles made by the normal to the plane and the slip direction in the plane to the axis of tension) of the pyramidal plane must be about six times as high as that of the basal plane. The critical resolved shear-stress values for slip along the prismatic $\{10\bar{1}0\}$ and the pyramidal $\{10\bar{1}2\}$ planes are not available, slip not having been observed to take place along these planes. However, since the atomic densities suggest that slip will occur at least as easily along the prismatic planes as along the pyramidal $\{10\bar{1}1\}$ planes, it can be assumed that the critical resolved shear stress for prismatic slip will be about the same as that for pyramidal $\{10\bar{1}1\}$ slip.

Table III. Atomic Densities and Interplanar Spacings in Magnesium (c/a, 1.624)

Plane	Atomic Density	Interplanar Spacing, A
(0001)	$\frac{2}{a^2\sqrt{3}} = 0.114$	$c/2 = 2.605$ $c = 5.21$
$(10\bar{1}2)$	$\frac{1}{a\sqrt{3a^2 + c^2}} = 0.0412$	$\frac{ac\sqrt{3}}{6\sqrt{3a^2 + c^2}} = 0.633$ $\frac{ac\sqrt{3}}{3\sqrt{3a^2 + c^2}} = 1.266$ $\frac{ac\sqrt{3}}{2\sqrt{3a^2 + c^2}} = 1.900$
$(10\bar{1}1)$	$\frac{2}{a\sqrt{3a^2 + 4c^2}} = 0.0528$	$\frac{ac\sqrt{3}}{6\sqrt{3a^2 + 4c^2}} = 0.408$ $\frac{5ac\sqrt{3}}{6\sqrt{3a^2 + 4a^2}} = 2.04$ $\frac{ac\sqrt{3}}{\sqrt{3a^2 + 4c^2}} = 2.45$
$(10\bar{1}0)$	$\frac{1}{ac} = 0.0597$	$\frac{a\sqrt{3}}{6} = 0.928$ $\frac{a\sqrt{3}}{3} = 1.856$ $\frac{a\sqrt{3}}{2} = 2.784$

The orientation factors of the $\{10\bar{1}1\}$ and the $\{10\bar{1}0\}$ planes, which share the active $<11\bar{2}0>$ slip direction and are closest to the operative glide plane, were at least 5 to 6 times as high as that of the basal plane in every specimen. This is approximately the relative value of the orientation factor required for pyramidal slip to occur in preference to basal slip on the basis of the Bakarian-Mathewson values. The values of the atomic densities further suggest that if pyramidal slip can occur then prismatic slip should also occur, either to the exclusion of, or in addition to, pyramidal slip. It should also be noted that the planes sharing the active $<11\bar{2}0>$ slip direction (that which lies closest to the observed glide plane) have higher orientation factors than the other similar planes containing either of the other two available slip directions.

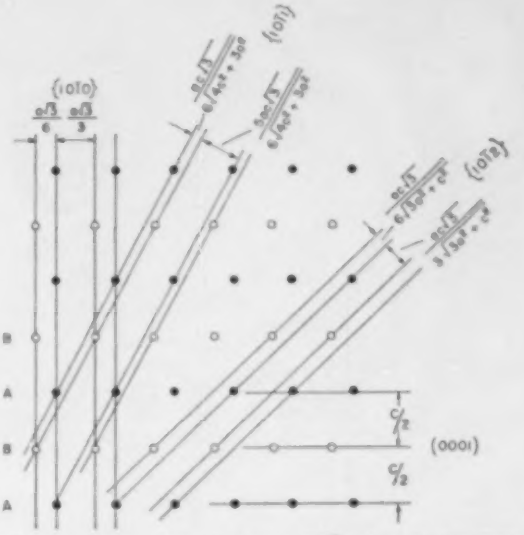

Fig. 7—Projection of atom positions on $\{11\bar{2}0\}$ plane showing traces and interplanar spacings of (0001), $\{10\bar{1}2\}$, $\{10\bar{1}1\}$, and $\{10\bar{1}0\}$ planes. Magnesium $c/a = 1.624$

In the three grains of specimen 51 although the $\{10\bar{1}1\}$ planes, closest to the respective observed glide planes, had slightly lower values of resolved shear stresses than the other $\{10\bar{1}1\}$ plane in each of the effective $<11\bar{2}0>$ zones, the values of these resolved shear stresses still fulfilled the requirement of being at least 5 to 6 times as high as those along the respective basal planes. The position of the observed glide planes could well be due to the fact that the two $\{10\bar{1}1\}$ planes on the effective $<11\bar{2}0>$ zones were nearly equally inclined to the individual axes of tension. It is felt that the behavior exhibited by these three grains does not contradict the mechanism of this type of slip process to be postulated.

Thus when basal slip cannot occur, it is suggested that a nonbasal type of cooperative slip between the $\{10\bar{1}1\}$ and the $\{10\bar{1}0\}$ planes will take place. Of course, this does not exclude the possibility of other planes of the effective $<11\bar{2}0>$ zone from participating, but it is expected that their functions would be relatively small in extent when compared to those of the former two. Slip deformation along the $\{10\bar{1}2\}$ planes is not likely, not only because these planes are less densely packed, but also because the orientations of the crystals studied were such that the $\{10\bar{1}1\}$ and the $\{10\bar{1}0\}$ planes were more suitably oriented.

Nature of the Bands: Table II shows the angular relationships between the glide plane and the maximum resolved shear-stress plane, the prismatic $\{10\bar{1}1\}$, and the pyramidal $\{10\bar{1}1\}$ planes (closest to the operative glide plane) for all the specimens examined. Two facts emerge from this table. First, as has been stated before, the operative glide plane lies between prismatic and pyramidal planes, $\{10\bar{1}0\}$ and $\{10\bar{1}1\}$, respectively, and second, and of greater importance, the observed glide plane invariably lies

close (at most 8°) to the maximum resolved shear-stress plane regardless of its location with respect to the $\{10\bar{1}0\}$ and the $\{10\bar{1}1\}$ planes.

The concept of this cooperative type of slip process then may be formulated as follows: The maximum resolved shear-stress plane determines the operative glide planes. But by itself it cannot be regarded as the actual glide plane because 1—it is not a low index plane and 2—the slip traces do not suggest slip to be taking place on a single plane of atoms.

However, suitable amounts of glide could occur in a consecutive manner mainly along the $\{10\bar{1}0\}$ and the $\{10\bar{1}1\}$ planes and to smaller extents along other planes in the effective zone so as to result in a corrugated slip surface (hence the wavy traces) which would be more or less parallel to the plane of maximum resolved shear stress. This accounts for the closeness of the observed glide plane to the plane of maximum resolved shear stress rather than to either of the two major participating planes.

Examination of the traces in the grains showed that they were only more or less parallel. This fact indicates that the extents of cooperation between the planes is not uniform even in a single grain. Had the extent of cooperation been the same, then quite parallel traces would have been seen. Therefore, in each localized region having the appearance of a slip band, the amount of slip is different and this results in the departure from parallel traces. The micrographs presented show that the width of these slip bands is larger than the conventional ones. In fact, it seems correct to think that the type of nonbasal slip bands described in this paper are more akin to deformation bands than to conventional slip bands.

It is expected that this type of slip must involve very close and frequent cooperation between the participating planes. It is suggested that this process is aided by two factors. First, the lattice geometry of magnesium is such that the two major cooperating planes make an angle of only 28° with each other. Second, the very close values of the atomic densities of these planes suggest that the ease of slip is the same along either of the two planes. It is then possible to understand the nonobservance of conventional cross slip, noted in face-centered-cubic metals, to which this type of nonbasal slip process is really very similar in that the planes cooperating share the same slip direction. Attempts to resolve the slip traces at higher magnifications were not successful. In place of the traces seen at lower magnifications, only shallow channels were visible at higher ones.

Mention must be made of the fact that basal slip was observed in addition to nonbasal slip in these crystals. Small amounts of deformation usually resulted on handling the specimens prior to and during attachment of them in the specimen holders. This resulted in the formation of twins and basal slip bands, but these were usually restricted to the ends of the gage lengths near the grips. It was observed microscopically that basal slip also resulted during creep at elevated temperatures. In some of the grains this was justifiable on the basis of the resolved shear stress of the basal slip system in contrast to that of the pyramidal, $\{10\bar{1}1\}$.

Whereas basal slip was observed frequently to result on the initial loading of the specimens, that is, under conditions involving high strain rates, the nonbasal slip bands developed progressively during creep. Hence, it is possible that strain rate might determine, in part, the type of slip that occurs. It is unlikely that this type of deformation would be exhibited at room temperature, since the higher strain rates can be more easily accommodated by twinning or kinking.

Summary

1—A nonbasal type of slip resulting in the formation of wavy traces, unlike the straight bands of more conventional basal slip, was found to occur fairly extensively during hot creep of magnesium.

2—The appearance of these traces was dependent on the angle between the surface of observation and the plane containing both the axis of tension and the slip direction. When these two surfaces nearly coincided, only one set of straight parallel traces were seen and the traces became coarser as the specimen was rotated away from the latter surface. These facts indicated that only one slip direction was involved in this type of slip process and that more than one plane was taking part in it. These planes would necessarily be planes belonging to the same zone, and they were indicated to be the pyramidal plane of the type $\{10\bar{1}1\}$ and the prismatic plane of the type $\{10\bar{1}0\}$.

3—This cooperative form of slip between at least two planes also follows from considerations of the surface atomic densities and the resolved shear stresses.

4—The observed glide plane did not coincide with any low index plane and was nearly parallel to the plane of maximum resolved shear stress.

5—The fact that more than one slip plane was taking part indicated that the slip plane was, in reality, a corrugated surface formed by suitable amounts of glide occurring in a consecutive manner along the cooperating planes so as to form a corrugated surface which was nearly parallel to the plane of maximum resolved shear stress.

Acknowledgment

The authors wish to thank the Aeronautical Research Laboratory, Wright Field, for sponsorship of this research.

Discussion of this paper, if any, will appear in JOURNAL OF METALS, November 1955, and in AIME Metals Branch *Transactions*, Vol. **203**, 1955.

References

[1] G. I. Taylor and C. F. Elam: *Proceedings* Royal Society, London (1926) **112A**, p. 337.

[2] F. L. Vogel, Jr. and R. M. Brick: *Trans.* AIME (1953) **197**, p. 700; JOURNAL OF METALS (May 1953).

[3] N. K. Chen and R. Maddin: *Trans.* AIME (1951) **191**, p. 937; JOURNAL OF METALS (October 1951).

[4] N. K. Chen and R. Maddin: *Trans.* AIME (1953) **197**, p. 1131; JOURNAL OF METALS (September 1953).

[5] E. Schmid and W. Boas: *Plasticity of Metals Crystals.* (1950) London. F. A. Hughes and Co. Ltd.

[6] I. S. Servi, J. T. Norton, and N. J. Grant: *Trans.* AIME (1952) **194**, p. 965; JOURNAL OF METALS (September 1952).

[7] P. W. Bakarian and C. H. Mathewson: *Trans.* AIME (1943) **152**, p. 226.

[8] E. C. Burke and W. R. Hibbard, Jr.: *Trans.* AIME (1952) **194**, p. 295; JOURNAL OF METALS (March 1952).

[9] A. R. Chaudhuri, N. J. Grant, and J. T. Norton: *Trans.* AIME (1953) **197**, p. 712; JOURNAL OF METALS (May 1953).

[10] C. S. Roberts: *Trans.* AIME (1954) **200**, p. 634; JOURNAL OF METALS (May 1954).

[11] B. Chalmers and U. Martius: *Proceedings* Royal Society, London (1952) **213A**, p. 175.

[12] F. D. Rosi, C. A. Dube, and B. H. Alexander: *Trans.* AIME (1953) **197**, p. 257; JOURNAL OF METALS (February 1952).

Discussion — Institute of Metals Division*

Impact Transition Temperatures of Some Pearlite-Free Mild Steels as Affected by Heat Treatments in the Alpha Range (paper by A. Josefsson. JOURNAL OF METALS, May 1954, p. 652) 689

New York Meeting, February 1954

Investigation of the Heat Treatment of Commercial Titanium-Base Alloys (paper by L. Luini and E. Lee. JOURNAL OF METALS, May 1954, p. 581) 691

475°C (885°C) Embrittlement in Stainless Steels (paper by A. J. Lena and M. F. Hawkes. JOURNAL OF METALS, May 1954, p. 607) 691

Chicago Meeting, November 1954

Strain Hardening of Latent Slip Systems in Zinc Crystals (paper by E. H. Edwards and J. Washburn. JOURNAL OF METALS, November 1954, p. 1239) 692

Effects of Temperature on the Deformation of Beta Brass (paper by C. S. Barrett. JOURNAL OF METALS, September 1954, p. 1003) 693

Quantitative Substructure and Tensile-Property Investigations of Nickel Alloys (paper by B. Ancker and E. R. Parker. JOURNAL OF METALS, October 1954, p. 1155) 694

Stress-Strain Characteristics and Slip-Band Formation in Metal Crystals: Effect of Crystal Orientation (paper by F. D. Rosi. JOURNAL OF METALS, September 1954, p. 1009) 696

Solubility of Oxygen in Alpha Iron (paper by A. U. Seybolt. JOURNAL OF METALS, May 1954, p. 641) 697

Metallographic Study of Equilibrium Relationships in 3S Aluminum Alloy (paper by P. R. Sperry. JOURNAL OF METALS, January 1955, p. 145) 697

Determination of the Self-Diffusion Coefficients of Gold by Autoradiography (paper by H. C. Gatos and A. D. Kurtz. JOURNAL OF METALS, May 1954, p. 616) 698

An Examination of the Decrease of Surface-Activity Method of Measuring Self-Diffusion Coefficients in Wüstite and Cobaltous Oxide (paper by R. E. Carter and F. D. Richardson. JOURNAL OF METALS, November 1954, p. 1244) 700

Electron Optical Study of Oxidation of High Purity Iron at Low Oxygen Pressures (paper by E. A. Gulbransen, W. R. McMillan, and K. F. Andrew. JOURNAL OF METALS, September 1954, p. 1027) 701

Warm Pressing of Beryllium Powder (paper by N. P. Pinto. JOURNAL OF METALS, May 1954, p. 629) 702

Influence of Carbon and Manganese on the Properties of Semikilled Hot Rolled Steel (paper by F. W. Boulger and R. H. Frazier. JOURNAL OF METALS, May 1954, p. 645) 705

Temper Embrittlement of 5140 Steel (paper by S. H. Bush and C. A. Siebert. JOURNAL OF METALS, November 1954, p. 1269) 705

Viscosity and Density of Liquid Lead-Tin and Antimony-Cadmium Alloys (paper by H. J. Fisher and A. Phillips. JOURNAL OF METALS, September 1954, p. 1060) 706

On the Nucleation of Pearlite (paper by M. E. Nicholson. JOURNAL OF METALS, September 1954, p. 1071) 706

Stabilization of the Bainite Reaction (paper by R. F. Hehemann and A. R. Troiano. JOURNAL OF METALS, November 1954, p. 1272) 707

Some Characteristics of the Isothermal Martensitic Transformation (paper by C. H. Shih, B. L. Averbach, and M. Cohen. JOURNAL OF METALS, January 1955, p. 183) 709

Ordering Reaction of the Cu$_3$Pd Alloy (paper by A. H. Geisler and J. B. Newkirk. JOURNAL OF METALS, September 1954, p. 1076) 710

Mechanism for the Origin of Recrystallization Nuclei (paper by J. P. Nielsen. JOURNAL OF METALS, September 1954, p. 1084) 710

Some Observations on Grain Boundary Shearing During Creep (paper by B. Fazan, O. D. Sherby, and J. E. Dorn. JOURNAL OF METALS, August 1954, p. 919) 714

Creep-Rupture Characteristics of Al-Mg Solid-Solution Alloys (paper by A. W. Mullendore and N. J. Grant. JOURNAL OF METALS, September 1954, p. 973) 715

Creep Behavior of Magnesium-Cerium Alloys (paper by C. S. Roberts. JOURNAL OF METALS, May 1954, p. 634) 715

Correlation Between Microstructure and Resistivity of Transforming Ti-Mn Alloys (paper by D. J. DeLazaro and D. W. Levinson. JOURNAL OF METALS, September 1954, p. 1089) 716

Mechanical Properties of Alpha Titanium as Affected by Structure and Composition (paper by R. I. Jaffee, F. C. Holden, and H. R. Ogden. JOURNAL OF METALS, November 1954, p. 1282) 717

Phase Transformations in Titanium-Rich Alloys of Iron and Titanium (paper by D. H. Polonis and J. G. Parr. JOURNAL OF METALS, October 1954, p. 1148) 718

* TP 4001E

Impact Transition Temperatures of Some Pearlite-Free Mild Steels As Affected by Heat Treatments in the Alpha Range

by Åke Josefsson

H. P. Tardif *(Canadian Armament Research and Development Establishment, Quebec)*—Mr. Josefsson is to be congratulated for his study of a most difficult subject and for the theories proposed to explain the results. One point which, however, might not have received proper attention is that of the shape of the stress-strain curve at the yield point of quenched and furnace-cooled specimens and of specimens strain aged

after quenching or furnace cooling. Also, no microscopic observation has been reported comparing the structure of quenched or quench-aged specimens with that of specimens strain aged after quenching or quench aging.

To cover the first point, some results are reported, which were recently obtained on a low carbon rimmed steel of the following analysis: 0.053 pct C, traces of silicon, 0.305 pct Mn, 0.028 pct S, 0.018 pct P, 0.07 pct Ni, 0.1 pct Cu, 0.022 pct Sn, and aluminum nil. Tensile loading experiments were made with a hard machine of the Polanyi type.[14]

Fig. 17 shows the shape of the stress-strain curves for annealed and strain-aged specimens, while Fig. 18 shows curves obtained with specimens quenched from 700°C and then strain aged. The annealed specimens have an upper and a lower yield point and a 3 pct yield-point elongation. The specimens quenched from 700°C only show an inflection in the curve. Mr. Josefsson has observed a yield point and a yield-point elongation in both cases. After straining and aging the annealed specimens, the yield-point elongation is shown to return completely after a certain length of time depending on the activation energy of the process, which has been measured and found to be of the same order as that for the diffusion of carbon and/or nitrogen in iron.[15] In the case of the quenched specimens, strain aging does not produce a yield point even after very long periods of aging. An explanation of this phenomena on the basis of the dislocation theory can be visualized as follows:

After introducing a large number of dislocations by stretching the quenched specimens, the atoms of carbon and nitrogen on aging are prevented from precipitating as large particles and will move to dislocations. This effect has been observed experimentally by Wilson[16] on 0.45 pct C steels quenched, cold worked, and tempered at 200°C for long periods of time. Before this, Andrew and Trent[17] observed that precipitated carbides would return to solution if low carbon steel was deformed after quench aging. If solute atoms in the dislocations are regarded to be in solution, it can be said that the limit of solubility of carbon in iron is increased. If some carbon does precipitate as carbide, it will do so as very fine particles because of the low temperature of aging used in the experiment. In this case, the concentration of carbon in the matrix, in equilibrium with the particles of carbide, is greater than that for normal solubility. This has been discussed by Glasstone[18] and Konebeevski.[19] Because of the foregoing combined effects, it is probable that a dislocation can never free itself completely of an atmosphere because there is too much carbon in solution; and as soon as the atmosphere lags behind the dislocation, new carbon atoms would immediately anchor them.

The fact that, in all tests carried out by the author, the transition temperature was found to be higher in the strain-aged than in the unstrained specimens can be explained on this same basis: the larger number of

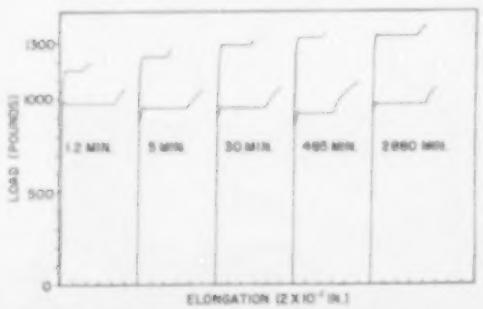

Fig. 17—Stress-strain curves of annealed and strain-aged material, stretched 5 pct after annealing and strain aged at 100°C.

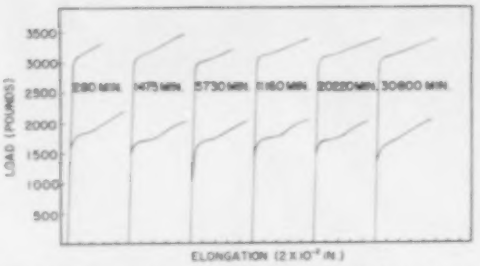

Fig. 18—Stress-strain curves of quenched and strain-aged material, stretched 5 pct after quenching from 720°C and strain aged at 100°C.

carbon atoms in solution will prevent movement of the dislocations and raise the transition temperature.

It would be most interesting to compare the distribution of carbides shown in Figs. 10, 12, and 13 with that observed in the same specimens after strain aging. It is expected that the carbides would break down as carbon and move to the dislocations.

Ake Josefsson *(author's reply)*—The interesting contribution by Mr. Tardif is highly appreciated. According to this author's experiences, the yield point after quenching from 700°C is in some cases conserved, in others eliminated, depending on carbon content, grain size, cooling rate, and aging treatment. In general, the yield-point elongation is eliminated in steels with carbon contents higher than say 0.04 pct, in agreement with the statements of Mr. Tardif. Steel *E*, however, after quenching in oil from 700°C, had a definite, although not very pronounced, yield-point elongation. Another steel with 0.048 pct C and 0.22 pct Mn, showed a clear yield point if tested directly after quenching but a smooth stress-strain curve, appreciably displaced toward higher stress values, if artificially aged at 100°C (3 to 27 days) before testing. The displacement is obviously the consequence of a precipitation hardening due to carbon, but then the disappearance of the yield point must follow a *decrease* in the quantity of carbon in solid solution. The following explanation is suggested: The yield-point phenomenon is assumed to be caused by Frank-Read sources giving off dislocation rings at a lower shear stress (lower yield point) after having themselves been created during the faint "preliminary" deformation when the locking action of interstitial atoms raise the critical shear stress (upper yield point).[20] In order to give a yield point, these secondary dislocation rings must be able to pass over their slip plane without being appreciably hindered by obstacles, otherwise they will be stopped until the shear stress has increased a certain amount over the value that was sufficient to activate the Frank-Read source. In the case mentioned where the yield point had disappeared after aging, finely dispersed carbide precipitates acted as such obstacles. (This dispersion is probably not identical with that which was proposed as a cause for the low transition temperatures.) In other words, the strain hardening due to carbide precipitates (not solute atoms) sets in at an early point and obscures the yield-point elongation.

It is agreed that the quantity of carbide in Figs. 10, 12, and 13 should, in principle, decrease on straining and aging by the mechanism mentioned by Mr. Tardif. However, it has not been possible to verify this microscopically. Actually, the ferrite is probably so supersaturated that it can supply the carbon absorbed by the dislocations without dissolving perceptible quantities from the carbides.

[14] M. Polanyi: *Ztsch. für Physik* (1925) 6, p. 121.
[15] M. P. Tardif: To be published.
[16] D. V. Wilson: *Journal* Iron and Steel Inst. (1954) 176, p. 28.
[17] J. H. Andrew and E. M. Trent: *Journal* Iron and Steel Inst. (1938) 138, p. 241.
[18] S. Glasstone: *Textbook of Physical Chemistry*. (1946) p. 495. New York. D. Van Nostrand Co.
[19] S. T. Konebeevski: *Journal* Inst. of Metals (1943) 69, p. 397.
[20] E. Orowan: Dislocations and Mechanical Properties. *Dislocations in Metals*. (1954) Ed. by M. Cohn, p. 69. New York. AIME.

Investigation of the Heat Treatment of Commercial Titanium-Base Alloys

by L. Luini and E. Lee

DISCUSSION, O. T. Marzke and W. Finlay, Associate Chairmen

D. L. Day and H. D. Kessler *(Titanium Metals Corp. of America, Henderson, Nev.)*—In connection with the authors' discussion of the test results on Ti-150A, the discussers would like to clarify several points involving the physical metallurgy of this alloy. The authors state on p. 583 that "The hardening response of this alloy is apparently due to a martensitic type of transformation of the β phase during rapid cooling." Recent work at several laboratories indicate that the actual quench hardening of this type of alloy is associated with supersaturated β phase which has been masked in the microstructures by the martensitic, but soft, α'. The hardening of the β phase on quenching is due either to a transition product, β' formed during the rejection of α, or to the actual precipitation of α (the latter mechanism being associated with lower quenching rates).

On pp. 586 and 587, the authors discuss a dark etching constituent "observed to precipitate from the acicular transformed β" on aging and refer to Fig. 16 for evidence. They also refer to the work of Phillips and Frey,* who suggested that a dark etching constituent they developed in Ti-150A was related to the eutectoid transformation. It is not clear as to exactly which structures the authors are referring when they discuss the "very fine spheroidal particles" formed at "higher temperatures." Referring to Fig. 16b, there is little question but that the fine spheroidal particles in the transformed β matrix are precipitated α. In the same figure, however, are also dark needlelike structures and these are quite similar to dark etching phase observed by Phillips and Frey. Phase diagram studies have shown that the ternary eutectoid reaction is very sluggish in both high purity and oxygen-contaminated Ti-Fe-Cr alloys,* as the eutectoid could not be identified either metallographically or by X-ray diffraction in samples annealed below the eutectoid for very long times. However, more recent work at the Titanium Metals Corp. of America points to the fact that dark constituents in Ti-150A similar to those observed by the authors is connected with the presence of as little as 0.03 pct H. Whether this constituent is a hydride phase or the ternary or more complex eutectoid which is rejected on short annealing times due to the effect of hydrogen on reaction kinetics has not been determined. The removal of hydrogen by vacuum treatment completely eliminates the possibility of producing this constituent.

Regarding the age hardening response (at temperatures from 500° to 1000°F) of Ti-150A previously quenched at temperatures from 1650° to 1750°F, the authors imply that the precipitation of the dark etching phase may account for the hardening. The discussers would agree if the authors are referring to the fine background phase in Figs. 16b and c which have been identified as α, but would disagree that the hardening is due to the needlelike phase which is associated with hydrogen. There is little question but that the β' reaction or precipitation of α from supersaturated β is also responsible for the hardening curves shown in Fig. 12.

L. Luini and **E. Lee** *(authors' reply)*—The authors welcome the discussion of Messrs. Day and Kessler of the titanium alloy hardening mechanisms and the observed behavior of the Ti-150A alloy. The heat treatment work was based primarily on the controlled decomposition of the β phase through the use of various thermal cycles.

It is likely that quench hardening of the Ti-150A alloy is attributable to a transition product defined as β' or to a low temperature β-transformation product formed from the alloy-lean β solution treated at high temperatures.

The observation that clear etching β phase was associated with quench hardening and the appearance of the martensitic acicular structure coincided approximately with the attainment of maximum quench hardening was noted in the paper, p. 583.

It has been observed in a heat of 7 pct Mn-Ti alloy on which isothermal transformation studies were conducted in addition to continuous cooling studies that water quenching resulted in a structure similar to a hard low temperature isothermal product. It appears that the quenched hardness of these titanium alloys depend partially on the low temperature β transformation products as determined by the alloy concentration.

The discussers appear to miss the statement, illustrated in Fig. 16, that very fine spheroidal particles were described as forming at the lower, not the higher, temperatures. Evidently age hardening is related to the β' reaction but not necessarily attributable to changes in structure visible with the light microscope. It has been observed with a heat of Ti-155AX that aged specimens subjected to different temperatures have similar structures. Furthermore, structures showing very little change on short aging times have similar hardness to those having well defined changes with long aging times.

*R. J. Van Thyne, H. D. Kessler, and M. Hansen: System Titanium-Chromium-Iron. *Trans.* AIME (1953) 197, pp. 1209-1216; JOURNAL OF METALS (September 1953).

475°C (885°F) Embrittlement in Stainless Steels

by A. J. Leno and M. F. Hawkes

DISCUSSION, W. J. Harris, Jr. and L. D. Jaffe, Associate Chairmen

J. F. Brown and **B. J. Connolly** *(Billingham Div., Imperial Chemical Industries Ltd., Billingham, England)*—The authors' postulate of an intermediate body-centered-cubic phase of chromium ferrite in the Fe-Cr alloys is extremely interesting. A similar chromium ferrite has been noted in creep specimens of an 18 pct Mo-10 pct Ti Cr-Ni austenitic steel (analysis is given in Table IV) which were tested under a stress of 18.0 tsi for over 3000 hr. An optical micrograph of the structure of the original fully softened bar from which the creep test pieces were machined is shown in Fig. 16 and shows ferrite grains in an austenite matrix. The structure of the steel after heating for 3340 hr at 500°C under stress is given in Fig. 17 from which it is seen that the ferrite phase has retained its original form but has become blackened completely. Fig. 18 is an electron micrograph showing the fine structure in the ferrite grains which causes the blackening.

The creep specimen was as magnetic as the original bar with about 35 pct ferrite, and X-ray reflection examination showed that both contained ferrite and austenite. The creep specimen was extracted electrolytically in 10 pct HCl and gave a nonmagnetic material

Table IV. Analyses of 18 pct Mo-10 pct Ti Cr-Ni Austenitic Steel

Analyses	N	C	Si	Mn	S	P	Cr	Ni	Mo	Ti	Fe	Residue†
Original steel	n.d.*	0.60	0.56	1.74	0.005	0.021	17.7	9.9	2.84	0.42	n.d.*	—
Extract from original steel	0.35	0.3	n.d.*	n.d.*	n.d.*	n.d.*	20.8	6.0	4.3	2.5	36.9	6.9
Extract from creep specimen, 3340 hr at 500°C	2.0	2.0	n.d.*	n.d.*	n.d.*	n.d.*	32.9	5.9	12.2	5.2	28.2	11.6

* n.d. is not determined.
† Residue includes oxides, silica, etc.

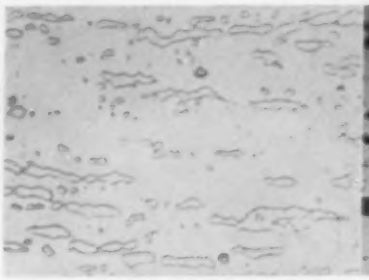

Fig. 16—Structure of original 18 pct Mo-10 pct Ti steel bar. X500. Area reduced approximately 35 pct for reproduction.

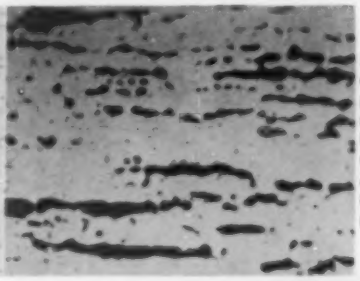

Fig. 17—Structure of creep specimen of 18 pct Mo-10 pct Ti steel tested for 3340 hr at 500°C under stress of 18.0 tsi. X500. Area reduced approximately 35 pct for reproduction.

which X-ray examination showed to be mainly body-centered-cubic phase of cube edge 2.878Å which is identical with that found by Fisher, Dulis, and Carroll[7] in plain high chromium steels. In addition to the body-centered-cubic phases, traces of TiC and TiN but no σ phase were detected. Extracts from the original bar gave a residue which was mainly a body-centered-cubic phase with a cube edge of 2.871Å, but it was strongly magnetic. Complete chemical analyses of the two extracts are given in Table IV. The high chromium content of the creep extracts is in agreement with the high cube edge of the body-centered-cubic phase and its nonmagnetic properties.

The occurrence of this nonmagnetic phase in both this steel and the plain high chromium steels suggests that two forms of ferrite may exist at 500°C. One is the normal magnetic "δ" ferrite which is dissolved preferentially during extraction and the other is the "nonmagnetic" ferrite which is present in a finely divided form, having a high chromium content and in general a composition approximating to σ phase into which it probably transforms.

The formation of σ phase at 500°C was not detected even after 8000 hr heating; but, since Heger[20] has found that the high chromium body-centered-cubic phase transforms to σ after 30,000 hr at 500°C, it is quite possible that the phase in this 18 pct Mo-10 pct Ti Cr-Ni steel also transforms to σ after a very long heat treatment. It was noted, however, that σ phase could be produced in this 18 pct Mo-10 pct Ti steel by heating at 600°C, traces being found in electrolytic extracts after only 300 hr heating, while after 8000 hr all the original ferrite had been transformed to σ.

The authors are to be complimented on a paper which throws considerable light on the reasons for the 475°C embrittlement in the Cr-Fe alloys.

A. J. Lena *(authors' reply)*—The authors would like to thank Messrs. Brown and Connolly for their discussion and consider it a valuable addition to the paper. Their work provides further proof that 475°C embrittlement is caused by the formation of a chromium-rich ferrite and it is interesting to see that this phase also occurs in the ferrite of duplex alloys aged at 500°C. Cina and Lavender[21] earlier had shown by hardness measurements that the ferrite in duplex alloys of the 18 pct Mo-8 pct Ti type is susceptible to 475°C embrittlement and this can now be attributed to the formation of chromium-ferrite.

Fig. 18—Electron micrograph of creep specimen (see Fig. 17). Positive replica, shadowed. X5000.

There can be little doubt that 475°C embrittlement is caused by the formation of chromium-ferrite. However, further work is needed to establish the exact relationship of this phase to the Fe-Cr system. Another point which requires further investigation concerns the mechanism of hardening by the chromium-ferrite. The authors' X-ray work indicates very little lattice straining, which is consistent with the small difference in unit cell size of the two ferrites.

[20] J. J. Heger: Discussion of ref. 26. Trans. AIME (1954) 200, p. 662. Journal of Metals (May 1954).
[21] B. Cina and J. D. Lavender: Journal Iron and Steel Inst. (1953) 174, p. 97.

Strain Hardening of Latent Slip Systems in Zinc Crystals

by E. H. Edwards and Jack Washburn

DISCUSSION, W. A. Backofen and W. M. Baldwin, Chairmen

John J. Gilman *(General Electric Co., Schenectady)*—The authors are to be congratulated for the simple elegance of their experiments. For the first time, they have measured, in a straightforward manner, the effect

of slip on the behavior of latent slip directions in the active slip plane of a crystal. A possible interpretation of the results is offered for their consideration.

The interpretation is based on the original Taylor model of strain hardening. According to this model, one of the causes of strain hardening is the mutual blocking of dislocations that attempt to pass each other on nearby slip planes. This leads to local "Taylor rotations" or "Burger's local curvatures." It was possible to detect these rotations at small strains by means of X-rays and at large strains by microscopic observations of cleavage planes in zinc. At small strains the rotations are partially recoverable at room temperature.

It is believed that the slip planes of a strained zinc crystal are "corrugated" due to the Taylor rotations. The ridges and valleys of the corrugations lie perpendicular to the active slip direction. The corrugations are expected to have no effect on the hardness of a crystal when the slip direction is changed by 180°. As the authors point out, the reduced stress for flow in this case is a result of back stresses. On the other hand, when the slip direction is changed by 60° or 120°, it is expected that slip will be difficult because the "corrugations" cannot move over one another without either being destroyed themselves or tending to destroy the crystal locally. Thus slip in the new direction will be resisted. In other words, the production of "corrugated" slip planes is believed to be inherent in the slip process. When the slip direction is changed, new corrugations tend to be produced which lie perpendicular to the new slip direction. It can be readily imagined that it is easier to produce new corrugations parallel to the old ones (the 180° case), than to produce them at an angle of 60° (the 60° and 120° cases).

Unfortunately, a means for stating this interpretation in an explicit fashion has not been found. However, it has the virtues that it is a natural consequence of the Taylor work-hardening model, and that it can be partially tested. Since the "corrugations" are believed to favor forward or backward motion over sideward motion, there should be a small but measurable strain component in the original slip direction when a crystal is stressed in the 60° or 120° direction.

Effects of Temperature on the Deformation of Beta Brass

by Charles S. Barrett

DISCUSSION, W. A. Backofen and W. M. Baldwin, Chairmen

Eric C. W. Perryman *(Aluminium Laboratories Ltd., Kingston, Ont., Canada; present address, Atomic Energy of Canada Ltd., Chalk River, Ont., Canada)*—The discusser would like to present some results obtained at the British Non-Ferrous Metals Research Assn. (London) which support Professor Barrett's conclusions. For this work an Izod impact machine was adapted so that an elevated temperature tensile test could be performed at a very high rate of straining.

Fig. 7 shows the percentage of elongation as a function of testing temperature for an extruded and annealed binary β brass having a grain diameter of 0.4 mm. It will be seen that the general shape of the curve is the same as that shown in Fig. 6 of Professor Barrett's paper, except that with the impact tensile test the increase in elongation in the temperature range 500° to 600°C is small, whereas with the impact hardness test the hardness appears to be decreasing continuously in this temperature range. Similar results were obtained for a cast β brass having a grain diameter of 3.9 mm, except that in this case no decrease in elongation was observed below room temperature.

Ternary β brasses containing 1 to 4 pct Al were also tested. These gave the same type of curves except that the rapid increase in elongation occurred in the temperature range 500° to 600°C. Fig. 8 shows a typical curve for a cast β brass containing 1 pct Al and having a grain diameter of 0.6 mm. Tests were also done on a β brass containing 0.8 pct Sn annealed at 800°C and quenched in cold water. This material had a grain diameter of 4.9 mm. The results for this brass were the same as those shown in Fig. 7 except that the increase in elongation was continuous in the temperature range 400° to 600°C and furthermore was not as marked as with the binary β brass. With all these different β brasses, the sharp decrease in elongation from

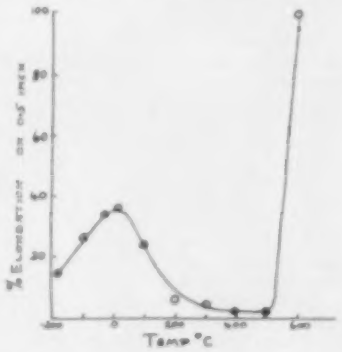

Fig. 8—Cast β brass containing 1 pct Al.

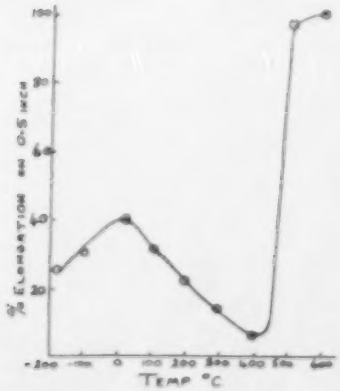

Fig. 7 — Binary β brass extruded and annealed.

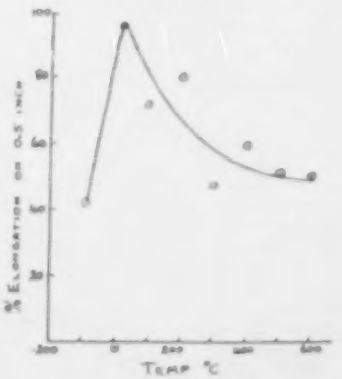

Fig. 9—Cast α brass containing 5 pct Al.

about room temperature to 400°C is in part due to intercrystalline cracking; in fact at 300° to 400°C for the binary and tin-bearing β brass and 300° to 500°C for the aluminum-bearing β brass, the fracture was entirely intercrystalline.

Professor Barrett's suggestion that the rapid increase in ductility is because of the order-disorder transformation is supported by the fact that no such increase in ductility was observed for an α brass containing 5 pct Al, see Fig. 9. In view of the foregoing results on the tin-bearing and aluminum-bearing β brasses, it would be interesting to see if the order-disorder transformation temperature was unaffected by tin and increased by aluminum.

These results confirm Professor Barrett's observations that the ductility of β brasses decreases as the testing temperature is reduced below room temperature. The fact that this decrease is observed both with α and β brasses suggests that this effect is independent of crystal structure.

Quantitative Substructure and Tensile-Property Investigations of Nickel Alloys

by Betsy Ancker and Earl R. Parker

DISCUSSION, W. A. Backofen and W. M. Baldwin, Chairmen

R. W. Guard *(General Electric Co., Schenectady)*—While this paper covers work in a very important field, there are several critical questions which it leaves unanswered. A great number of problems arise in work on substructure because of difficulties in experimental technique. A more detailed account of the method of X-ray microscopy used would have allowed a more critical evaluation of the results. In particular, would the authors care to comment on the following?

1—Was there any difficulty due to overlapping reflections?

2—What is the effect of the fact that all subgrains with large angular differences from the original grain will not give a reflection near the spot corresponding to the original grain?

3—Are Figs. 12b and 12c typical of the X-ray micrographs obtained? If so, don't they tend to emphasize large subgrains to the exclusion of small ones?

4—Since subboundaries having very small angular differences ($<0.10°$) are known to have important effects in zinc, how would the authors' conclusions be affected by the fact that their method will not resolve such differences?

Several alternative propositions may be made to the interpretation of the results. Since the distribution of boundaries is rather heterogeneous, the use of large samples, particularly when such a large number of zero values are obtained, may lead to erroneous results. A reading of zero does not mean zero but means only no boundaries within the limits of the method, which, according to items 2 and 4 given previously, may exclude quite a large number of subgrains. It is also possible that, in the case of such a nonhomogeneous process as deformation of polycrystalline metals, the mean, mode, or median values have little importance and that the properties are governed by the extreme values (high or low) of the distribution.

The application of the Suzuki mechanism to the results seems to be appropriate, but it should be pointed out that Suzuki did not show that high concentrations existed in faulted regions; he simply assumed that such regions did exist and calculated their strengthening effect. Proof of the existence of such concentration differences remains to be shown, and indeed, would be difficult. The postulate of Cottrell atmospheres in Ni-Ti alloys should give a strong temperature dependence to the yield point as compared to the Suzuki atmospheres in Ni-Co alloys. Such data would constitute stronger proof of the postulate than Fig. 13.

The lines in Fig. 13 are drawn to indicate zero flow stress for zero substructure. All of the results are contrary to this, and the figure thus conveys a misrepresentation of the results.

In view of the difficulties attendant in separating effects of subboundaries and the effect of distributed dislocations, it is very desirable to emphasize the tentativeness of conclusions 5 and 6. Proof of these conclusions will require data on a large number of systems taken specifically for that purpose.

Eric C. W. Perryman *(Aluminium Laboratories Ltd., Kingston, Ont., Canada; present address, Atomic Energy of Canada Ltd., Chalk River, Ont., Canada)*—This paper, besides being of theoretical interest, is extremely interesting from the practical point of view. However, the discusser would like to raise a few questions on this paper and then to present some results which in a qualitative way give support to some of the authors' conclusions.

The authors state that their starting material was forged and swaged and then annealed at 1150°C for ½ hr. After this treatment, were the materials fully recrystallized? From Table I it would appear that all the alloys after this initial anneal contained subgrains. Although subgrains have been observed in the center of large grains formed by annealing a lightly strained material, as far as the writer is aware there is no positive evidence for subgrains in heavily worked and recrystallized material. He has tried to find subgrains in fully recrystallized aluminum but have never been successful. If, however, the authors' starting material was in fact in some recovered state, then this makes the interpretation of their results much more difficult. It is well known that during recovery the rate of change of properties of the cold-worked metal is rapid at first and then slows down with increasing annealing time. Recent work[10] has indicated that during this recovery period dislocations are redistributed and the subgrains become more perfect, the maximum in perfection being reached when the hardness or the X-ray half-peak breadth has become constant. Could the authors say on what part of the recovery curve their anneal of 1 hr at 800°C fell?

From the appearance of the X-ray micrographs in Fig. 12, it would appear that the subgrains in Fig. 12b are far from perfect, i.e., not strain free. It is not clear from the paper whether Fig. 12a is from the material before prestrain or whether this subgrain was formed by annealing prestrained material at 1150°C. If it is the latter, then it would seem that these subgrains are more perfect than those formed after annealing at 800°C for 1 hr, and so from the authors' discussion it would be expected that the material annealed at 1150°C would have a higher flow stress than that annealed at 800°C. Did the authors do any measurements after annealing prestrained material at 1150°C? Comparing Fig. 12b with 12c, it would seem that the subgrain size directly after straining was almost the same or slightly larger than that after annealing at 800°C. This is in contradiction to the discusser's results on aluminum[10] and suggests that the annealing treatment of 1 hr at 800°C was not sufficient to produce perfect subgrains. Although no magnification is given for Fig. 12, it would seem that the subgrain size directly after

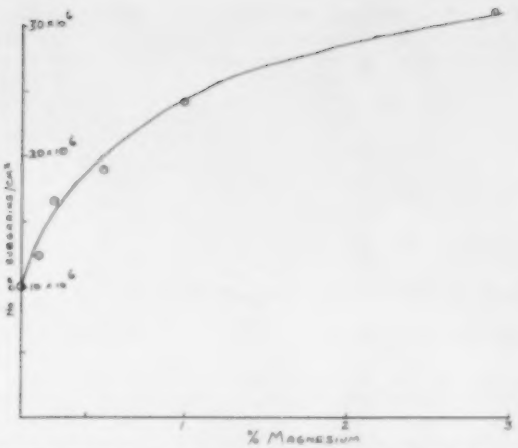

Fig. 19—Effect of magnesium on subgrain size after complete recovery, 20 pct cold work and annealed at 250°C for 1 hr.

straining is considerably larger than that reported by Gay and Kelly.[13] From Table I the subgrain size in nickel strained 2 pct and recovered at 800°C is about 100 microns which is about 20 times larger than that reported by Gay and Kelly.[13] Would the authors comment on this large difference?

During an investigation on the effects of magnesium on the recovery of superpurity aluminum by metallographic examination, the subgrain size has been determined after complete recovery. By this is meant an anneal such that the hardness and X-ray half-peak breadth have fallen to a steady value and recrystallization has not commenced. Fig. 19 shows the number of subgrains per square centimeter as a function of magnesium content. This appears to be very similar to the authors' curve for the Ni-Co alloys. If it is assumed that during recovery dislocations climb out of their slip plane, some become annihilated, and others become blocked at subgrain boundaries, then the hardness of the recovered material minus that of the recrystallized material will represent the residual work hardening. If this is done, it is found that, for a given amount of cold work, the residual work hardening for the different Al-Mg alloys is almost constant. Similarly if the authors' results are taken, it is found that the difference between the flow stress for 1 pct prestrain and the as-annealed value at a given strain is about 2500 psi for all the different materials tested. This strongly suggests that subgrain size alone has no major effect on mechanical properties. In another investigation,[14] it has been found that the recovered hardness value decreases slightly while the subgrain size increases slightly with increasing annealing temperature. This suggests that subgrain size may have a small effect on mechanical properties or that, with increasing annealing temperature, the residual density of lattice defects decreases.

D. McLean and A. E. L. Tate *(National Physical Laboratory, Dept. of Scientific and Industrial Research, Teddington, England)*—The discussers would like to draw attention to some similar work[15] in which the effect of a subcrystal structure on mechanical properties was measured. The metal used in this work was aluminum and the subcrystal structure was produced by hot rolling or by creep. To summarize the relevant results quite briefly, they showed that a subcrystal structure increased the 0.1 pct proof stress very considerably (up to about ten times) but had a much smaller effect on ultimate tensile strength or hardness. This was regarded as understandable, since, although the subboundaries could be expected to have an important effect at the start of plastic deformation, they should cease to be a significant factor after extensive deformation. Miss Ancker and Professor Parker, in their more detailed investigation, also find that a subcrystal structure raises the stress level at the beginning of deformation. They find this in a different pure metal than the discussers used and, in addition, in two alloys. Considering also the theoretical plausibility of the effect, it may be reasonably supposed to be general.

B. Ancker and E. R. Parker *(authors' reply)*—The authors wish to thank Dr. Guard for his detailed analysis of this paper and the questions he has asked regarding the data and its interpretation.

It must first be re-emphasized that the experimental method employed in these investigations is not an absolute one but is relative. The accuracy of the relative data was severely tested and found to be completely satisfactory as described in the text. A detailed description of the X-ray method is found in Barrett as footnoted in the text.[8] Arbitrarily, the following conditions were chosen: focal spot to specimen, 53 cm, specimen to photographic plate, an average of 1 mm. The full focal spot of the X-ray tube, approximately 2 mm, was utilized for convenience.

1—Grains which happened to have overlapping reflections on the photographic plates were disregarded and data were recorded from over 100 grains per specimen whose subgrains could be clearly counted. Since the grains to be observed were arbitrarily chosen in the first place, disregarding overlapping reflections in no way affected the results.

2—In general the reflections from various individual grains were widely separated (on a microscopic scale) from those of other grains (generally only about 20 grains reflected at once) and thus it was easy to detect all the reflections belonging to a certain grain. If there was any doubt, as explained under 1, the data from such grains were not used.

3—Fig. 12c is not typical of the micrographs used in the quantitative investigation, since all the deformed specimens were recovered at 800° or 1150°C as indicated in the text. Figs. 12a and 12b are typical and the subboundaries indicated there can be counted readily.

4—The effect of subboundaries of smaller angles than can be resolved by the method used in this research is the subject of a current investigation on the same materials by Dr. Sigmund Weissmann, Rutgers University. Topology indicates that the various composition polycrystalline aggregates which undergo the same strain develop the same number of dislocations. In the case of the cobalt alloys, these dislocations do not collect readily into boundaries of more than 10′. Thus, as stated in the text, the increase in strength cannot be correlated with the increase of such subboundaries. Results will be published shortly relating density of subboundaries of smaller angle with tensile strength.

The distributions of subboundaries for specimens of identical history were proved by statistical methods to be the same (see "Analysis of the Substructure Data"), i.e., it was proved that various samples (information taken from different photographic plates) from one specimen or from specimens of identical history all came from the same distribution. Therefore, Dr. Guard's objection about the use of large samples of the distributions is invalid. It is true that the distributions are truncated; a zero reading means no subboundaries of 10′ or more, rather than none present. The validity of using the mean, mode, or median as a *comparative* tool is altogether justified, however, since significant differences are observed for specimens of different strain histories. Here again the Wilcoxon test was applied and showed conclusively that specimens of different histories had different distributions. In any case, the properties are not governed by the extreme values of the distribution; rather, properties may be predicted from the mean, mode, or median of the distribution.

The authors certainly agree with Dr. Guard that the data presented in this paper do not constitute proof of the concentration of foreign atoms in faulted regions. No series of experiments on yield strength at the mo-

ment appears feasible as a means of differentiating the effects of Suzuki vs Cottrell atmospheres.

Concerning Fig. 13, whether the lines should be drawn through the zero point or somewhere near it is immaterial. The graph is only meant to emphasize the striking difference between the relationship of substructure density and flow stress for the different alloys. The implications are fully described in the text.

In reply to Dr. Perryman's comments concerning the location of the 800°C temperature on the recovery vs temperature curve, the authors did not make a complete survey over the entire temperature range and consequently cannot answer the question. Since some substructure remained even after the 1150°C treatment, it is evident that the material had not completely recrystallized even at this high temperature.

[16] E. C. W. Perryman: To be published.
[17] P. Gay and A. Kelly: *Acta Crystallographica* (1953) 6, p. 165.
[18] D. McLean and A. E. L. Tate: *Revue de Métallurgie* (1951) 48, No. 10, p. 765.

Stress-Strain Characteristics and Slip-Band Formation in Metal Crystals: Effect of Crystal Orientation

by F. D. Rosi

DISCUSSION, W. A. Backofen and W. M. Baldwin, Chairmen

M. S. Paterson *(Dept. of Geophysics, Australian National University, Canberra, Australia)*—The discusser was particularly interested in Dr. Rosi's paper, having just completed some similar experiments on high purity (99.999 pct) copper when it appeared. It is therefore interesting to compare the results in the light of some differences in the experimental details.

In Fig. 24 are some of the tensile stress-strain curves for copper from Rosi's paper and the discusser's results for copper crystals of similar orientations. Curve 53, the only one that Rosi gives for 99.999 pct Cu, can be compared to curves 69 and 89 for similar orientations. A further comparison can be made between the effect of crystal orientation on the stress-strain curves for Rosi's 99.98 pct Cu (Nos. 41, 37, and 34) and for the discusser's 99.999 pct Cu (Nos. 87, 84, and 69, respectively).

The initial region of low strain hardening, or "easy glide," for orientations near [110] is of much greater extent for Paterson's crystals, in spite of Rosi's conclusion that higher purity crystals show a smaller region of easy glide and the fact that the ends of the crystals were rigidly gripped, thus preventing accommodation of the lattice rotation. However, Paterson's specimens were of 1.5 mm diam, compared to 9.5 mm diam for Rosi's, and it seems likely that the longer region of easy glide in these crystals is related to their smaller diameter. It is also interesting to note that the curve reproduced in Fig. 24 from Lange and Lücke's measurements[20] on high purity aluminum for an orientation near [110] was obtained from a crystal of 1.5 mm diam and shows a very extensive region of easy glide.

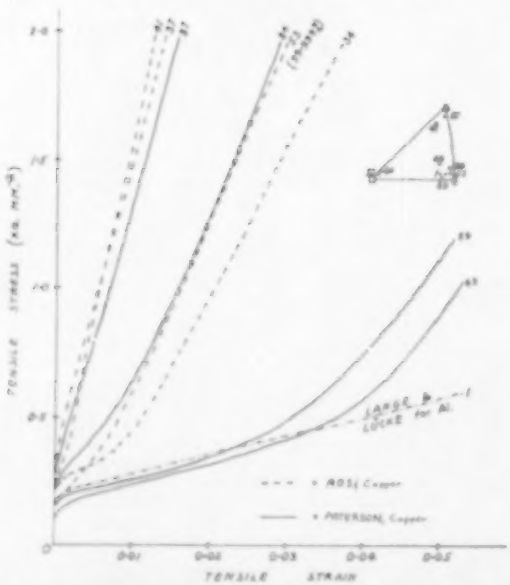

Fig. 24—Comparison of tensile stress-strain curves for copper given by Rosi and results for copper crystals of similar orientations found by Paterson.

The suggestion that a crystal of smaller diameter will show more extensive easy glide favors the idea that in the region of easy glide most dislocations pass out of the crystal and so do not contribute to the hardening,[21] since in a larger crystal there would be a greater chance of a dislocation meeting an obstacle (e.g., a dislocation on another plane) during its passage through the crystal. Further, this effect of diameter would invalidate Rosi's comparison of his results with those of Lange and Lücke and throw doubt on his conclusion that low melting point (or high testing temperature) is favorable to easy glide, a conclusion that is in contradiction to that of Andrade and Henderson.[18]

The discusser's observations of slip markings on the electropolished surfaces of the crystals corresponded in general to Rosi's photographs. However, in contrast to Rosi's conclusion, he found that crystals with orientations far removed from the [100]-[111] line showed the least tendency to clustering of slip lines; the slip in such crystals was very uniform. On the other hand, crystals oriented near [100] or [111] showed very marked clustering of the slip lines, with traces of slip on other planes occurring preferentially between these clusters. Crystals oriented near [110] also showed many kink bands, as Rosi observed, when the ends of the crystals are constrained from rotation.

Further details of these experiments will be published.

F. D. Rosi *(author's reply)*—The size effect, discussed by Dr. Paterson, on the region of low strain hardening is most interesting and not unexpected. In this connection, however, it would be of further interest to know whether there is a size effect on the value of critical resolved shear stress for flow. Assuming other things constant, a larger region of low strain hardening with a greater critical resolved shear stress can be expected.

Another factor in considering a size effect based on a comparison of available data is the method used in producing the single crystals. In the present work, the crystals were produced from the melt, whereas the author presumes that the wire crystals used by Dr. Paterson were produced by the strain-anneal technique. Existing data do suggest that the two techniques could result in significant differences in both the density and distribution of dislocations.

Regarding the reference to the appearance of slip bands, it was brought out in the paper that the effect of crystal orientation on clustering of slip bands was studied only in crystals exhibiting slip on a single primary system (Fig. 19 of the paper). The clustering of slip bands for crystals near <100> or <111> to which Dr. Paterson refers also was observed in the present work (Figs. 16 and 17). It must be remembered, however, that the clustering in these crystals is closely related to the nature of secondary slip-band development.

[9] H. Lange and K. Lücke: Strörungen der Gleitung bei Aluminiumeinkristallen-I. *Ztsch. für Metallkunde* (1953) 44, pp. 183-191.

Solubility of Oxygen in Alpha Iron

by A. U. Seybolt

DISCUSSION, S. C. Carapella, Jr. and B. D. Cullity, Chairmen

N. A. Gokcen *(Michigan College of Mining and Technology, Houghton, Mich.)*—Total oxygen contents reported in this paper do not necessarily represent the dissolved oxygen in α iron for at least two reasons:

1—The oxygen combined with aluminum, calcium, chromium, magnesium, manganese, silicon, titanium, and vanadium would be 0.0055 pct rather than 0.003 pct estimated by the author if it is assumed, as on p. 642, that all of the "oxygen-avid" elements in the iron used are present in half the maximum amount reported in Table I. Since it was shown by Kitchener et al.[1] that manganese at small concentrations is oxidizable, then the choice of preceding elements as "oxygen-avid" is reasonable. Further, the oxides of these elements may dissolve or combine with FeO as indicated qualitatively by Kitchener et al.[2]

2—The surface area to weight ratio is high for the thin strips used in this investigation. Therefore, the surface oxygen content is of the order of 0.003 pct as calculated by using the results of Sloman and Rooney.[17]

A. U. Seybolt *(author's reply)*—The following reply is numbered according to the numbered issues raised by Dr. Gokcen:

1—On checking the arithmetic, it is found that Dr. Gokcen's figure of 0.0055 wt pct O is correct. However, this kind of estimate is not of great value, since the amounts of the impurities present are not known with sufficient precision.

More significantly, the fact that the log solubility—$1/T$ plot is linear within the experimental error of about ± 0.003 wt pct O indicates that there must be a real solubility which is not in error by more than about this amount. Now, if the real solubility were in error by a constant amount of 0.006 pct, as implied by Dr. Gokcen, this amount would have to be added to each experimental point, thus resulting in a nonlinear plot.

In addition, as demonstrated in the paper entitled "Precipitation of Iron Oxide from Alpha Fe-O Solid Solutions,"[18] iron oxide dissolves or precipitates, depending upon heat treatment, according to metallographic evidence.

2—The figure quoted here for the surface oxide (0.003 pct) picked up by pickled iron from air at room temperature agrees well with an estimate by Gulbransen,[19] whose figure was 30Å of iron oxide. This last turns out to be about 0.002 pct O. These estimates fall within the stated uncertainty of the oxygen analysis, ± 0.003 pct.

[17] H. A. Sloman and T. E. Rooney: Journal Iron and Steel Inst. (1943) 148-II, pp. 327p-340p.
[18] A. U. Seybolt: *Trans.* AIME (1954) 200, p. 979; JOURNAL OF METALS (September 1954).
[19] E. A. Gulbransen: Private communication (1954).

Metallographic Study of Equilibrium Relationships in 3S Aluminum Alloy

by Philip R. Sperry

DISCUSSION, S. C. Carapella, Jr. and B. D. Cullity, Chairmen

J. O. Lord *(Ohio State University, Columbus, Ohio)*—The author presents some interesting comments and excellent micrographs of the structural constituents found in the 3S alloy. The interpretation of the structures of the alloys as-cast and cooled at various rates seems quite satisfactory and well in keeping with published phase diagrams.

The reheated structures with eutectic areas depleted in solute material present a controversial problem. This condition well may be likened to eutectoid patterns in low carbon steels and particularly in abnormal steels where carbide particles seem to withdraw from cooperative association with the matrix.

In the case of the 3S alloy, the depletion of the eutectic aluminum undoubtedly takes place on original casting as indicated in Fig. 13. However, is it not possible that this depletion is best explained by the second solid phase in the eutectic acting as nucleating material to prevent supersaturation of the solution in its immediate vicinity? For this to happen, it is only necessary to postulate a moderate rate of diffusion of the solute in the solid solution near its melting temperature.

P. R. Sperry *(author's reply)*—It is satisfying to have acceptance of the concept that the precipitate distribution directly reflects the solute distribution in the cast structure before heating. Some of the statements in the literature imply that certain areas are clear of precipitate because of diffusion during reheating. On the basis of the present evidence this is not so.

Professor Lord's comment on the depletion of the eutectic aluminum suggests that supersaturation occurs in the primary aluminum but not in the eutectic aluminum due to the nucleating effect of the second phase. So far, the evidence does not indicate that supersaturation occurs and certainly not to the extent that is indicated by the precipitate pattern. Admittedly, the evidence is far from conclusive but it can be pointed out that this same type of precipitate pattern can be found in other aluminum alloy systems where the divorced type of eutectic is present but where supersaturation is even less likely to occur.

A better picture of the actual growth mechanism in divorced eutectics is needed, but it appears that the second phase is nucleated and grown at some distance from the dendrite faces on which the eutectic aluminum forms. This, of course, is the reason for the coarse-

ness of these structures as compared with a pure binary eutectic. As the solid phases form, the liquid itself is either enriched further or remains quite rich in alloying elements. This is what the eutectic valley depicts. Therefore, it is difficult to see why there should be less supersaturation in the eutectic aluminum than in the primary, if supersaturation does occur at all.

Determination of the Self-Diffusion Coefficients of Gold by Autoradiography

by Harry C. Gatos and Anthony D. Kurtz

DISCUSSION, J. H. Keeler and R. W. Balluffi, Chairmen

Paul G. Shewmon *(Carnegie Institute of Technology, Pittsburgh)*—The authors have developed a new and potentially very useful technique for the determination of distance-concentration curves in diffusion studies. If this technique is to be developed to its full potential, some correction must be made for radiation which comes from relatively large distances away from the point of observation. In their paper the authors give a correction factor which, in their opinion, corrects for this undesired radiation. The discusser would like to point out what he believes to be errors in the derivation of their correction factor,* and to discuss the effect of this on the applicability of the technique.

* This derivation was not published but was kindly sent to the discusser by the authors.

In their derivation, the authors take the intensity at a point on the sectioned surface, at a distance K from the original interface, to be

$$I = A\int_K^L \exp(-x^2/4Dt)\,\exp\left[-\mu(x-K)\right]dx. \quad [12]$$

In this equation x is the distance from the original interface in the direction of diffusion, L is the range of the β particles, μ is the linear absorption coefficient for the β rays, A is a constant independent of x and K, D is the diffusion coefficient, and t is the time.

Eq. 12 considers radiation coming only from a cylinder directly behind the point P on the surface. Actually, the radiation recorded on the film at the surface point will come from an entire hemisphere of metal whose radius is L and whose center is at p. Not only will the radiation come from this larger volume instead of the cylinder considered in Eq. 12, but the concentration of the radioactive isotope will vary from point to point on any given hemispherical shell due to the concentration gradient in the specimen. One way of setting up this new integral for the intensity is

$$I = 2\pi A\int_0^{\pi/2}\int_K^L \exp\left(-\frac{[r\cos\phi+K]^2}{4Dt}\right) \exp(-\mu r)\,\sin\phi\cos\phi\,d\phi\,dr. \quad [13]$$

The origin is now taken as the cut surface, not the original interface, and ϕ is the polar angle defined so that ϕ is zero in the diffusion direction. $2\pi r^2\sin\phi\,d\phi\,dr$ is the volume element in spherical coordinates, and $\cos\phi/r^2$ is proportional to the fraction of the β particles emanating from the given volume element which hit the element of area taken as the origin.* It is assumed that the base of the hemisphere is parallel to the original interface ($\phi = \pi/2$), not the cut surface. This assumption simplifies the integral considerably and introduces a very small error.

* The discusser would like to thank R. H. Condit for bringing this last term to his attention.

In the authors' work with Eq. 12, they make use of the expansion

$$erf\ (z) = (\sqrt{\pi}/2)\left(1-\frac{\exp(-z)}{z}\right), z>>1 \quad [14]$$

where $erf\ (z) = \int_z^\infty \exp(-z^2)\,dz$.

The correct expansion for large z is*

$$erf\ (z) = \sqrt{\pi}/2 - \frac{\exp(-z^2)}{2z}. \quad [15]$$

The important point is that for large z, $erf\ (z)$ varies not as $\exp(-z)$, but as $\exp(-z^2)$. It is the use of Eq. 14 which makes the authors' correction factor vary as $\exp(-bK)$ instead of $\exp(-bK^2)$.

Finally, the authors take their evaluation of Eq. 12, obtained by using Eq. 14, and use it as an *additive* correction factor to the true solution, i.e., concentration = $A\exp(-K^2/4Dt)$. The reasoning involved in this is not at all clear to the discusser. Actually, Eq. 12 gives this true solution times a *multiplicative* correction factor, provided Eq. 15 is used for the expansion of *erf* (z). This solution of Eq. 12 is

$$I = \frac{a\exp(-K^2/4Dt)}{\dfrac{K}{2\sqrt{Dt}}+\mu\sqrt{Dt}} \quad [16]$$

which is similar to the solution given on p. 669, Eq. 20.

For the case of gold, the correction term used by the authors is negligible. To see if the effect of radiation coming from distant points is actually negligible, Eq. 13 must be evaluated. If the exponential terms in Eq. 13 are grouped together, the equation becomes

$$I = A\exp(-K^2/4Dt)\left[2\pi\int_0^{\pi/2}\int_0^L r^2\exp\left(\frac{-2Kr\cos\phi}{4Dt}-\frac{r^2\cos^2\phi}{4Dt}-\mu r\right)\sin\phi\,d\phi\,dr\right]. \quad [17]$$

The factor in front of the brackets is the variation of concentration with t and K which results from diffusion. The term inside the brackets is a function, hereafter called $F\,(K, Dt, \mu)$, which relates the local concentration to the observed intensity.

The integration over ϕ in F can be avoided by using the definition of an average value. The integrand of F is zero at $\phi = 0$, and it is continuous and monotonic, increasing at all values of ϕ in the range of $0\leq\phi\leq\pi/2$. If $f\,(x)$ is continuous and monotonic, increasing in the range $a\leq x\leq b$, then

$$\overline{f(x)} = \int_a^b \frac{f(x)\,dx}{b-a} = f(h) \quad [18]$$

where h is a unique number, and $a<h<b$. Therefore, there is a unique value of ϕ, hereafter called Φ, which can be substituted in the integrand of F to take the place of the difficult integration over ϕ. A graph of the integrand of F vs ϕ shows that $\Phi = \pi/4$ is a reasonable value to assume. The exact value taken does not change the final result appreciably, since the function F varies slowly with $\cos\phi$ in this range.

To integrate over r, let $y = (r\cos\Phi)/(2\sqrt{Dt}) + U$ where $U = K/2\sqrt{Dt} + \mu\sqrt{Dt}/\cos\Phi$. These substitutions give

$$F = B\exp(U^2)\int_{-U}^{\infty}\exp(-y^2)\,dy. \quad [19]$$

Since the range of the β particles is small compared to the dimensions of the specimen, L can be set equal to infinity. The evaluation of Eq. 19 is then carried out, using Eq. 15 to approximate the expression *erf* (y). (The error introduced in this approximation is 2

pct.) The following is finally obtained

$$F = \frac{C}{U} = \frac{C}{\dfrac{K}{2\sqrt{Dt}} + \dfrac{\mu\sqrt{Dt}}{\cos\Phi}} \qquad [20]$$

where C is a positive constant independent of K.

In order to use this new correction factor, F, in diffusion work, it would be plotted and used to convert the intensities to concentration. In their work the authors, in effect, took the concentration to be proportional to the intensity (since their correction factor was negligible). To check this, Eqs. 20 and 17 are combined to give

$$\left(\frac{\partial(\ln I)}{\partial K^2}\right)_{\mu, Dt} = -\frac{1}{4\,Dt}\left[1 + \left[\frac{\dfrac{\sqrt{Dt}}{K}}{\dfrac{K}{2\sqrt{Dt}} + \dfrac{\mu\sqrt{Dt}}{\cos\Phi}}\right]\right] \cdot \qquad [21]$$

The term in the inner bracket is the contribution of $F\ (\mu, Dt, K)$ to the experimentally determined slope and can be seen to go to zero for sufficiently large μ or K. The application of Eq. 21 to the authors' data using $\mu = 400$ cm^{-1}, $\phi = \pi/4$ or $\pi/3$, and $\sqrt{Dt} = 10^{-4}$ cm or $4.5\text{x}10^{-5}$ cm leads to the following conclusions:

1—The variation of the correction factor with Φ between $\Phi = \pi/4$ and $\Phi = \pi/3$ is only a few percent.

2—The correction factor varies from 15 to 2 pct as K increases from 0.01 to 0.07 cm. If $K \geq 0.03$ cm, the correction to the slope averages out to 3 to 4 pct. This correction makes the D's reported 3 to 4 pct smaller than the true values. However, a correction of 4 pct in the reported values of D is less than the probable error of the work so this change is unimportant.

3—Different values of $\sqrt{Dt}$ were probably used at high and low temperatures. This would not change the correction factor by more than a few percent. Therefore, the fact that the heat of activation ΔH, as determined in this work, is lower than the ΔH of earlier workers could not be explained in this way.

If this technique is used in the future with the more common metals, the range of the β particles will probably be greater, i.e., μ will be smaller. If the reasonable value of $\mu = 100$ cm^{-1} is used in Eq. 21 with $\sqrt{Dt} = 10^{-4}$ cm, the correction to the experimentally measured D ranges from 5 to 50 pct. Therefore, the use of the correction factor described here will be mandatory if accurate data is to be obtained.

J. E. Reynolds *(Battelle Memorial Inst., Columbus, Ohio)*—The authors have drawn some conclusions based on their work with Au^{198} which are not in agreement with observations made by the writer in work with Ni^{63}.

The authors have presented a rigorous treatment (Eq. 3) for correcting the surface intensity for any additional intensity contribution from subsurface radioactive atoms. This treatment utilizes the linear absorption coefficient (μ) for the β rays emitted.

It is established[1, 2] that the average angle of deflection of β particles on traversing thin layers of the absorber varies with the absorber thickness. This fact leads to the conclusion that, for diffusion specimens where the radioactive layer is thin and the thickness of the layer (which also is the absorber) varies, the amount of backscattering and, hence, the adsorption coefficients are also variables. This makes it very difficult to determine reliable absorption coefficients for β particles for diffusion studies.

The authors have stated also that autoradiography under proper conditions provides an accurate and convenient method for determining diffusion coefficients. They further delineate the "proper conditions" based upon their observations with Au^{198} by stating that:

1—The isotope to be used as a trace must emit β rays of sufficiently low energy so that their range is an order of magnitude less than the diffusion distance.

2—The isotope must have a sufficiently long half life so that fairly long diffusion distances may be obtained before its radioactivity is decayed to impractically low levels.

The writer has unsuccessfully attempted to use the autoradiographic method for studying the self-diffusion of nickel in pure nickel using Ni^{63} (half life, 85 years) which emits a β particle of 0.063 mev. This isotope meets the two requirements listed previously (i.e., high absorption of β particles and long half life) but was not amenable to the autoradiographic treatment because the absorption was too great. It is recognized that a higher specific activity of the isotope would counteract high absorption slightly, but it appears from the foregoing that the usefulness of the autoradiographic method, insofar as β emitters are concerned, is limited to isotopes and absorbers with an optimum absorption behavior. On the one hand, high absorption is desirable so that the radiation will be more indicative of the activity of the sectioned face of the specimen, while the other conflicting factor is that the absorptivity must not be so great that registration on a photographic film is prevented.

H. C. Gatos and **A. D. Kurtz** *(authors' reply)*—In determining the self-diffusion coefficients of gold by autoradiography, the correction for radiation originating away from the surface is negligible. The authors agree with Mr. Shewmon, however, that the correction factor which appears under Eq. 3 in the paper should be modified in order to become generally applicable. Following is the derivation of a correction factor which the authors believe meets with the requirements of a general case:

Introducing the parameter shown in Fig. 2 of the paper, y is the distance along original interface, x is the diffusion distance, $x - y \tan\alpha$ is the actual absorption length for β rays and for small α sectioning angles, and I is the intensity of radiation.

$$I(y) = \int_{y\tan\alpha}^{\infty} I(x)\, e^{-\mu(x - y\tan\alpha)}\, dx. \qquad [22]$$

Assuming the Johnson solution of Fick's law

$$I(x) = \frac{I_o}{\sqrt{4\pi Dt}} \exp(-x^2/4Dt \qquad [23]$$

where I_o is constant, the following is obtained

$$\frac{I(y)}{I_o} = \frac{\exp(\mu\, y \tan\alpha)}{\sqrt{4\pi Dt} \displaystyle\int_{y\tan\alpha}^{\infty} \exp(-x^2/4Dt - \mu x)\, dx. \qquad [24]$$

Completing square in the exponent gives

$$\frac{I(y)}{I_o} = \frac{\exp(\mu\, y \tan\alpha + \mu^2 Dt)}{\sqrt{4\pi Dt} \displaystyle\int_{y\tan\alpha}^{\infty} \exp(-x^2/4Dt - \mu x - \mu^2 Dt)\, dx. \qquad [25]$$

Letting $z = \left(\dfrac{x}{\sqrt{4\,Dt}} + \mu\sqrt{Dt}\right)$, $z_o = \left(\dfrac{y\tan\alpha}{\sqrt{4\,Dt}} + \mu\sqrt{Dt}\right)$, and rearranging the limits of integration $\dfrac{I(y)}{I_o} = (\pi)^{1/2} \exp(\mu\, y \tan\alpha + \mu^2 Dt)\left[\int_o^{\infty} \exp(-z^2)\, dz - \int_o^{z_o} \exp(-z^2)\right] dz. \qquad [26]$

By integrating, the following is obtained

$$\frac{I(y)}{I_o} = \frac{\exp(\mu\, y \tan\alpha + \mu^2 Dt)}{2}\,[1 - erf\,(z_o)]\cdot \qquad [27]$$

This expression for $erf\ (z_o)$ may be expanded for large

values of z_o to give

$$\frac{I(y)}{I_o} = \frac{\exp(-y^2 \tan^2 \alpha / 4Dt)}{(4\pi z_o)^{1/2}} \left[1 - \frac{1}{2z_o^2} + \frac{3}{(2z_o^2)^2} + \cdots\right] \quad [28]$$

Neglecting all but first powers of z_o

$$\ln \frac{I(y)}{I_o} = \frac{-(y \tan \alpha)^2}{4Dt} - \frac{1}{2} \ln (4\pi z_o) \quad [29]$$

For values of $\left(\frac{y \tan \alpha}{2\mu Dt}\right)^2 << 1$

$$\ln \frac{I(y)}{I_o} = -\frac{(y \tan \alpha)^2}{4Dt} - \frac{1}{2} \ln\left(1 + \frac{y \tan \alpha}{\mu Dt}\right) + \text{constant} \quad [30]$$

and the slope of a plot of $\ln I(y)/I_o$ vs $(y \tan \alpha)^2$ becomes

$$\text{Slope} = \frac{-1}{4Dt}\left(1 + \frac{2}{\mu y \tan \alpha}\right) \quad [31]$$

The absolute value of the slope is thus larger than $\frac{1}{4}Dt$ and dependent on y, but at sufficiently large values of $(\mu y \tan \alpha)$ the correction becomes negligible and the slope is a constant. By including second-order terms in the expansion, even more rapid convergence is assured.

Regarding Dr. Reynolds' comments, the authors believe that the autoradiographic method, insofar as β emitters are concerned, is not necessarily limited to isotopes and absorbers with an optimum absorption behavior. For a given isotope-absorber system, the optimum autoradiographic conditions are greatly dependent upon the specific activity of the β-ray emitting isotope.

[6] L. Milne-Thomson and L. Comries: *Standard Four-Figure Mathematical Tables*. (1931) p. 211. London, MacMillan. This can also be derived by applying integration by parts to the integral in the expression

$$erf(z) = \sqrt{\pi}/2 - \int_z^\infty (1/x) \exp(-x^2) \times dx.$$

[7] J. A. Crowther and B. F. Schonland: *Proceedings* Royal Soc. A (1922) **100**, p. 526.

[8] S. Glasstone: *Sourcebook on Atomic Energy*. (1950) p. 165. New York, D. Van Nostrand Co. Inc.

An Examination of the Decrease of Surface-Activity Method of Measuring Self-Diffusion Coefficients in Wustite and Cobaltous Oxide

by R. E. Carter and F. D. Richardson

DISCUSSION, J. H. Keeler and R. W. Baluffi, Chairmen

C. Ernest Birchenall *(Princeton University, Princeton, N. J.)*—The authors of this paper are to be warmly commended for several important contributions. It seems to the discusser that this is the first time that a satisfying mechanism has been associated with the concept of surface trapped atoms. There may be another mechanism of trapping for crystals, which conform closely to some fixed composition, by means of which atoms (even atoms of the same kind as one of the elements in the compounds) may be quite insoluble and may exchange too slowly to fulfill the customarily assumed boundary conditions. But the formation of surface crystallites would apply for the larger range of solid materials which are somewhat tolerant of composition variation.

The diffusion coefficients for cobalt in cobaltous oxide and the oxygen pressure dependence should be very useful in investigating the mechanism of cobalt oxidation. The agreement between sectioning and surface-activity methods for diffusion in rough-surfaced cobaltous oxide does indeed cast doubt on the roughness hypothesis which Ruder and Birchenall[9] applied to explain the differences between the cobalt self-diffusion coefficients obtained on electropolished specimens with very smooth surfaces and mechanically polished and etched specimens with rougher surfaces. The former were accepted and reported by these authors and the latter were rejected. Results on welded and sectioned couples to be published soon by H. W. Mead and C. E. Birchenall[10] will show that, in fact, the latter are correct and the former are probably in error due to the surface trapping of the active cobalt. The discusser must second the authors' recommendation for a check by sectioning on all surface-activity measurements.

Naturally it is gratifying to see the results previously obtained on wüstite by Himmel, Mehl, and Birchenall[11] confirmed by these varied procedures. There are references to that earlier work which diverge from the discusser's interpretation of it, and these divergences are stated without explanation. Therefore, I should like to seek the reasons. In Fig. 6 of ref. 11, the diffusion coefficient is plotted at these temperatures as a linear function of the *vacancy concentration*. Although there is some scatter in the data, it is difficult to see why this is now taken as a dependence on the 1.25 power of the vacancy concentration. It is also found that the vacancy concentration at 983°C is proportional to $P_{o_2}^{1/5.5}$ which is rather close to the expected $P_{o_2}^{1/6}$, perhaps closer than would be expected in concentrated solution.

This leads to the Arrhenius-type interpretation placed upon the deviations from ideal behavior in these crystals. Since direct evidence of vacancy-ferric ion groupings with a kinetic identity is lacking in oxides, it seems more useful to favor a Debye-Hückel approach, such as that employed by Wagner and Hammen[12] in their discussion of cuprous oxide. Eq. 8 of the present paper may be rewritten in the form $n_{V''}B_{V''} = n_{e'}B_{e'}$ where the n's are the numbers of iron atoms or vacancies per unit volume and the B's are the mobilities. Using Einstein's relation

$$D^* = B\,kT$$

and taking the values for the composition of wüstite in equilibrium with magnetite (double primes) and the composition of wüstite in equilibrium with iron (single primes), the relation

$$\frac{B_{e'}''}{B_{e'}'} = \frac{n_{V_O}'' D^*_{V_O}'' n_{e'}'}{n_{V_O}' D^*_{V_O}' n_{e'}''}$$

is obtained for a given temperature.

Assuming the relative change in density at high temperature to be about the same as that found at room temperature at 983°C, it is found that

$$\frac{B_{e'}''}{B_{e'}'} = 1.4$$

and at 897°C

$$\frac{B_{e'}''}{B_{e'}'} = 1.3.$$

An increase in mobility (average for all vacancies present regardless of binding) with concentration would seem to be incompatible with the Arrhenius picture. The Debye-Hückel type of approach can recognize the increased electrostatic and elastic repulsions accompanying the increased vacancy concentration. That effects of this type exist is supported by Bertaut's[13] observation that the vacancies in pyrrhotite ("FeS")

can undergo long-range ordering and by Humphrey, King, and Kelley's[20] findings that such interactions are required to explain the thermodynamic measurements on wüstite. The use of dissociation equilibria in this connection recalls the rather monstrous compounds attributed to steelmaking slags until much too recently.

To look at this last point another way, by the time 10 pct or so of the iron lattice sites become vacant with twice as many electron holes in the crystal, it is difficult to imagine any electron holes which are not very close to one or more vacancies. The mobilities of the holes are so much greater than those of the vacancies that the association of any hole with a given vacancy for a time comparable to that for a diffusion jump at these temperatures seems unlikely.

Another way of looking at these data also argues against the association idea. Dr. L. S. Darken has just called the discusser's attention to the fact that, if the more reliable data at the two highest temperatures are extrapolated linearly back to the fictitious stoichiometric composition, the diffusion coefficients go to zero at that point.

R. E. Carter and **F. D. Richardson** *(authors' reply)*—The authors thank Professor Birchenall for his most valuable comments and for pointing out the curious sentence referring to the proportionality found by Himmel, Mehl, and Birchenall[11] between diffusion coefficients and vacancy concentrations in wüstite. This sentence (the second, col. 1, para. 3, p. 1256 of the authors' paper) appears to have arisen from a typing jumble. The facts are, as Fig. 6 of ref. 11 shows, that the proportionality factor which increases with temperature is very small at 800° and substantial at 983°C. Incidentally, the data in Fig. 10 of ref. 11 seems to the authors to lead to a vacancy concentration per atom of oxygen which is proportional to $P_{O_2}^{1/6.7}$ at the higher concentrations and $P_{O_2}^{1/6.9}$ at the lower.

The authors agree with Professor Birchenall that, since direct evidence of vacancy-ferric ion groupings is not available, other ways of looking at the relationships which exist between vacancy concentrations, oxygen pressures, and diffusion rates in nonstoichiometric compounds must be considered. It is believed that he has a strong point regarding relative mobilities of electron holes and vacancies, but the authors would not attach much weight to his final suggestion: like Dr. Darken, the authors had looked to see how the lines in this Fig. 6 extrapolated to zero vacancy concentration, but it is necessary to be rather selective to find the result which Professor Birchenall gives. It is not agreed that consideration of these relationships in terms of association is on a par with the old compound theories for slags. In the oxide case it is known that a lattice built up of ions and cation and electron holes is being dealt with, so the simplest basic units for which there is direct evidence are being started with.

The essential point emerging from this discussion is that at present no adequate theory exists. The most important step now is to measure the relationships which exist between diffusion coefficients, departures from stoichiometry, and oxygen pressures for a *number of oxides over good ranges of temperature and composition*. Only in this way can the kinetic and thermodynamic properties of cation vacancies and electron holes be worked out and the basic data provided for the development of theory. The wrong thing to do is to pile up diffusion data alone or to work on substances for which it is impossible to measure the departures from nonstoichiometry by unequivocal chemical means.

[20] C. Wagner and H. Hammen: *Ztsch. für Physik. Chemie* (1938) **B40**, p. 197.
[21] F. Bertaut: *Acta Crystallographica* (1953) 6, p. 557.
[22] G. L. Humphrey, E. G. King, and K. K. Kelley: *Bulletin 4870* U.S. Bureau of Mines (June 1952).
[23] Mead and C. E. Birchenall: to be published. *Trans.* AIME (1955) 203.

Electron Optical Study of Oxidation of High Purity Iron At Low Oxygen Pressures

by Earl A. Gulbransen, William R. McMillan, and Kenneth F. Andrew

DISCUSSION, A. J. Shaler and W. P. Roe, Chairmen

J. Bardolle and **J. Bénard** *(Faculté des Sciences, Université de Paris, Paris, France)*—The discussers are glad to see that the authors' observations generally agree with the results obtained by them some years ago. Since then, they have improved the precision of their first results by studying the variation of the number of nuclei according to the crystalline orientation of the metal.[14, 15] Moreover, one of the discussers, in collaboration with J. Moreau, recently demonstrated a similar nucleation phenomenon in the oxidation of Ni-Cr alloys.[16] It has now been proven beyond a doubt that the oxidation of a metal may be discontinuous under certain conditions of pressure and temperature.

The discussers would like to call the authors' attention to a few observations on the following points:

1—It seems necessary to point out that the first of the discussers' experiments, to which the authors refer,[8] was carried out not only on Armco iron but also on pure electrolytic iron prepared at the Vitry metallurgical research station, under the direction of Professor G. Chaudron.

2—The electron diffraction study of oxide films has consistently shown, in the present work, the presence of Fe_3O_4 oxide although the authors admit that the oxide originally formed is FeO. Since the discussers' last publications on this subject, they have had the opportunity, in collaboration with J. Moreau, to make a similar study by electron diffraction. The reflection electron diffraction patterns on an iron specimen with nuclei show evidence for FeO. This difference perhaps might be the result of a faster cooling in their studies.

3—The authors have demonstrated clearly the reaction between superficial oxide and carbon in iron. However, it does not seem that this reaction alone can explain all the different aspects of the oxide according to the different crystalline orientations of the specimens.

It seems, in fact, that all these differences could be explained equally by orientation differences prior to oxide reduction by carbon or by mechanisms of coalescence or superficial reorganization of the oxide.

4—The authors attribute the lines of thermal etching to the presence of hydrogen in the metal, but it seems that they are more likely related to oxidation reaction under very low pressures. Similar aspects have been observed on silver, copper, or on certain alloys when heated in oxidizing atmospheres; in a subsequent heating in an inert gas or in hydrogen, these aspects generally disappear.

Some differences in the oxidation of Puron and Armco iron could be explained perhaps by the fact that Puron initially contains more oxygen than the quantity allowed by the oxygen solubility limit at 850°C. In particular, one part of the oxide in the electron micrograph of Fig. 8 could result from iron protoxide precipitation due to supersaturation during the cooling.

Earl A. Gulbransen, William R. McMillan, and **K. F. Andrew** *(authors' reply)*—The authors are very grate-

ful for the comments of Professor Bénard and M. Bardolle. They agree that the oxidation of metals under the conditions of low pressure and high temperature occurs by a discontinuous process. The authors would state that this discontinuous oxidation mechanism is probably true for a wide variety of oxidation conditions. The use of low pressure and high temperature oxidizing conditions makes possible a demonstration of the essential mechanism of oxidation.

In regard to the specific questions raised by Professor Bénard and M. Bardolle, the authors have the following comments to add:

1—They were not aware that pure electrolytic iron was used in the original work of Bardolle and Bénard.

2—The experimental apparatus used did not allow for rapid cooling of the oxidized specimens. The FeO, which was probably formed at the high temperature, transformed under the authors' conditions to Fe_2O_3 on cooling below 570°C.

3—The widely varying crystal habit of the oxide seen on the Armco iron specimens is due to both the effect of the original crystal orientation as well as to the subsequent carbon-oxide reaction. It is of interest to note that the oxide on certain crystal faces of the iron resists attack by carbon in the metal, while the oxide on other crystal faces is rapidly attacked. This suggests that the diffusion of carbon depends upon the direction in the crystal.

4—The authors think that the pretreatment of the specimen is important in determining the crystal habit of the oxide which is formed. The pretreatment in hydrogen at 850°C has been found to embrittle the metal and, in addition, to change the pattern of low pressure oxidation. It has been noted recently that vacuum annealing at 850°C gives a discontinuous oxidation pattern nearly random in nature in contrast to that observed after a hydrogen anneal.

5—The authors do not think that FeO is precipitated during cooling due to supersaturation of oxygen.

[14] J. Bardolle: *Journées Métallurgiques d'automne de la Société Française de Métallurgie.* (October 1953). To be published.
[15] J. Bardolle and J. Bénard: *Comptes Rendus* (1954) **239**, pp. 706-709.
[16] J. Moreau and J. Bénard: *Journal* Inst. of Metals (1954) **83**, pp. 87-93.

Warm Pressing of Beryllium Powder

by Norman P. Pinto

DISCUSSION, A. J. Shaler and W. P. Roe, Chairmen

K. G. Wikle *(The Brush Beryllium Co., Cleveland)*—Information on the powder metallurgy of beryllium is of great interest to the beryllium industry and Mr. Pinto is to be congratulated for accumulating data on a particular form of warm pressing that has not been extensively investigated heretofore.

To the best of present knowledge, the process of warm pressing as applied to beryllium powders was first developed by Sawyer and Dodds in 1947.[17] Since then, considerable development work has been carried out at The Brush Beryllium Co.[18, 19] to determine the technical and economic merits of this compaction technique. Based upon the results of these surveys in which taller compacts were consistently pressed to satisfactory densities without use of vacuum, the meaning of Pinto's strength values are seriously questioned. Also, any economic or property improvement of warm pressing at 450° to 800°C over the standard industrial technique of vacuum hot pressing beryllium powder at 1050° to 1150°C is questioned.

Beryllium compacting work in the so-called warm temperature range, or below recrystallization but above normal atmospheric temperature, revealed in the Brush data a temperature-compacting pressure (necessary for 1.85 g per cu cm density) curve as shown in Fig. 12. Such data was obtained using dies of 18-4-1 high speed tool steel from room temperature through 750°C and graphite at higher temperatures. All elevated temperature pressings were precompacted at room temperature with about 40 tsi to 70 to 75 pct of theoretical density. Pressure was maintained at elevated temperatures in the steel die for a time of about 15 sec, resulting in a compact 1¼ in. diam by 1.5 to 2 in. long. It is noted in Fig. 12 that about 50 tsi is required for complete densification at 600°C. This pressure compares to about 25 tsi reported by Pinto. The difference in the two pressures is so large that an explanation should be in order.

Generally, the major differences between the methods of attack were as follows:

1—A powder having an average diameter of 21 microns was used by Pinto, while powders of 12 to 16 microns average diameter were employed for the tests shown in Fig. 12.

2—The presence of a high vacuum during pressing vs a normal atmosphere is, of course, one of the main points of difference.

3—The side wall friction appears to be quite different in the two cases in that the work at Sylvania used compacts 0.3 in. in length while that at Brush used samples 1.5 to 2 in. long. Surfaces available for friction as well as differences in lubrication technique may have been influential.

The difference in the reported powder average diameters is believed to be a difference in measuring technique, this writer giving Fisher Sub-Sieve Sizer values and Pinto presenting Scott volumeter values. The powders in both cases were prepared in the same or identical attrition mills. Pinto reports getting the same warm-pressed densities with or without vacuum under identical time, pressure, and temperature conditions

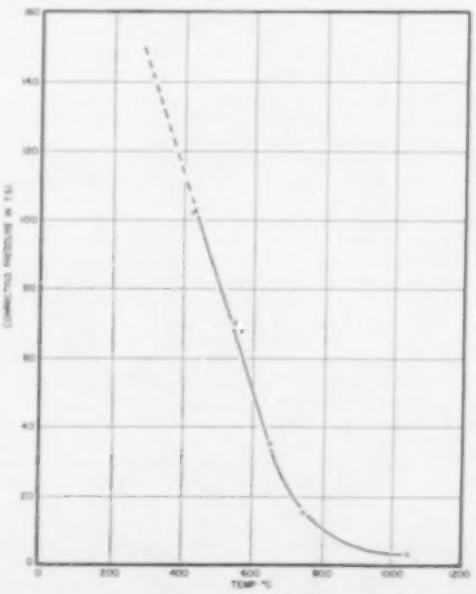

Fig. 12—Compacting pressure necessary to densify attritioned —200 mesh beryllium powder to theoretical density of 1.85 g per cu cm at various temperatures.

Table III. Mechanical Properties of Warm and Hot-Pressed Beryllium Compacts

Compact No.		Compacting Pressure, Tsi	Compacting Temperature, °C	Heat Treatment of Tensile Specimen	Ultimate Tensile Strength, 1000 Psi	Yield Strength, 1000 Psi	Pct Elongation	Hardness, R 15T	Density, G per Cu Cm
No. 5		100	425	None	30.3	—	0.2	67	1.845
No. 6		100	425	Vacuum sintered at 1125°C, annealed 800° for 20 min	40.5	43.4	1.3	78	1.846
No. 53		70	560	450°C for 20 min	46.3	—	0.9	92	1.847
No. 54		80	560	450°C for 20 min	38.1	—	0.5	83	1.845
No. 58		40	650	450°C for 20 min	40.1	—	0.6	91	1.863
No. 59		40	650	450°C for 20 min	58.0	—	0.0	92	1.870
No. 61		15	750	450°C for 20 min	51.8	—	0.0	90	1.849
Y-5694 *T**		1.5	1100	750°C for 20 min	51.9	39.0	3.3	—	1.845
Y-5694 *L*†		1.5	1100	750°C for 20 min	40.0	32.2	1.3	—	1.845
Y-4540 *VHP*‡ *T*† and *L*†		0.05	1050	750°C for 20 min	45.2	33.1	2.3	86	1.845
Y-5710 *VHP*‡ *T**		1.5	1100	750°C for 20 min	50.7	30.1	5.1	—	1.852
Y-5710 *VHP*‡ *L*†		1.5	1100	750°C for 20 min	39.5	26.5	1.8	—	1.852
Y-4522	*P***	*VHP*‡ and extruded 2¼ to 1½ in. diam at 425°C	1050	750°C for 20 min	85.3	51.0	6.8	82	1.851
Y-4522	*N*††	*VHP*‡ and extruded 2¼ to 1½ in. diam at 425°C	1050	750°C for 20 min	46.6	46.0	0.5	83	1.851
Y-5540	*P***	*VHP*‡ and extruded 4½ to ⅞ in. diam at 1950°F	1050	750°C for 20 min	101.0	—	14.3	84	1.845

* *T* is samples taken transverse to pressing direction.
† *L* is samples taken parallel to pressing direction.
‡ *VHP* stands for vacuum hot pressed (75 to 125 psi at 1050°C).
** *P* is samples taken parallel to extrusion direction.
†† *N* is samples taken normal to extrusion direction.

and thus the second point is not significant. Thus, the only explanation of greater consolidation reported by Pinto at equivalent pressures must be the shorter compact with which he worked. It is well known that short compacts can be pressed to density more easily than long ones.

Because of the longer length of compacts in warm pressing at Brush, conventional tensile data could be attained. Tensile and hardness data on −200 mesh powder compacted from 400° to 750°C at 15 to 100 tsi (Table III) are listed for comparison with Pinto's data. Properties of Brush's conventional hot-pressed beryllium, of warm (425°C) extruded rod, and of hot (1950°F) extruded rod are also shown.

In general, as stated by Pinto about the vacuum warm-pressing work, the as-pressed strength of dense compacts is about 115,000 psi, with hardness of 90 R_{15T}. Such compacts did not appear to have directional properties.

In the Brush material, the normal strength, based on a large number of samples, ranges between 30,000 and 100,000 with the greater strengths being obtained in directionally worked materials with extremely anisotropic mechanical properties. For warm pressing without vacuum at 550° to 600°C, at comparable times and temperatures, but with much longer samples at higher pressures, ultimate tensile strengths on the order of 58,000 psi were obtained with full density at 650°C or about one-half of the value reported as breaking strength by Pinto. Good agreement is shown with Pinto in the hardness values.

In view of the size of the samples used by Pinto, it appears that the "breaking strengths" reported were actually modulus of rupture values and not true strengths. The difference of 58,000 and 115,000 psi would, on this basis, be compatible, since the breaking pressure would be the same for the two methods. However, this point is open to question by the discusser. Also, it might be added that with commercial warm-pressing techniques, or in any technique wherein appreciable amounts of pressure are applied to beryllium, the mechanical properties of the resulting piece are generally anisotropic, being superior in the direction of flow; see Table III.

The Brush work shows further that the material pressed under the minimum sintering temperature for beryllium (about 750°C) does not have a strong intercrystalline bond. This is illustrated by the increase in tensile strength of the sintered sample No. 6 over the warm-pressed sample No. 5. The development of this bond is especially indicated on those samples which are vacuum hot pressed or hot worked above the recrystalline temperature. All of these specimens were low in hardness (80 to 84 R_{15T}) but exhibited tensile strengths greater than harder pieces pressed at 425° to 750°C.

Generally, in comparing the two warm-pressing methods, the discusser would like to sum up as follows:

1—It is difficult to believe that a hardness of R_{15T} in the 90's is indicative of tensile strength on the order of 110,000 to 120,000 psi compacted beryllium powder. The difference in strengths indicated between the two methods is probably that of difference in test method and interpretation. Actually, tensile strengths for the methods appear to be similar if the test results are interpreted properly.

2—There seems to be some advantage in the warm-pressing technique under vacuum. However, in view of the differences in size and operational techniques, the full extent of this advantage cannot be evaluated. The technical advantages of vacuum seem small in light of the heavy economic penalties involved.

3—Generally speaking, although the warm-pressing method is relatively old in beryllium powder compacting and has been employed in production, it has not become a process of extensive use. This is largely because of relatively brittle structure obtained by warm pressing. No evidence has been produced to indicate that vacuum warm pressing would change this situation. Generally, ductility with a strong intercrystalline bond can be obtained only by heating above the recrystallization point. For this reason, hot pressing, warm pressing-sintering, and hot working as well as warm working supersede the use, at least on a commercial basis, of the warm-pressing process alone.

Norman P. Pinto *(author's reply)*—The work at Brush represents an interesting addition to the data on the compacting of beryllium at elevated temperatures. Experience in hot pressing of powders indicates that the reasons why Brush required higher pressures to attain theoretical density are, in order of importance: 1—lubrication, 2—compact length/diameter ratio, and 3—atmosphere.

The selection and application of proper lubricants are of paramount importance in attaining high densities and optimum properties with any metal powder. In work at Sylvania, a thin graphite shell was em-

ployed to eliminate contact between the powder and the die, even though the length/diameter ratio was small; it was desirable to establish the ultimate densities attainable with given time-temperature combinations. Although the graphite-sleeve technique is not suitable to production applications, it does fix the ultimate density to which the results using the more practical lubricants may be compared. In determining the optimum conditions for hot pressing metal powders, Sylvania has found the development of suitable lubricants and proper methods for their application to be most critical. It is important that lubricants be characterized completely.[8] In determining the conditions adequate for obtaining optimum hot-pressed properties, it is usually simpler to establish the time-temperature combination, determined to a large extent by the die materials, heating medium, and the hot-pressing characteristics of the particular metal powder, than to establish the best lubricant and method of applying it. A definition of the proper lubricant should include statements as to its composition, porosity, thickness, thickness range, surface contour, etc., as well as the method by which it is applied, including the number of layers applied, temperature of lubricant and die at the time of application, lubricant carrier, solids concentration, purity, gas pressure, etc. It is assumed that Wikle's lubricant was applied to the die walls rather than to the powder; if this assumption is incorrect, the physical properties may have been altered by the residual admixed lubricant.

Widely divergent and misleading results may be reached by comparing densities obtained under identical conditions of time, temperature, and atmosphere but using different lubricants or the same lubricant applied in a different manner. In any statement of the properties of hot-pressed compacts, it is just as important to state the lubricating conditions as to state the other pertinent variables. It is the author's opinion, therefore, that the differences between Wikle's data and his at 600°C and 25 tsi, for example, is to be found in lubricant primarily but also in the difference in length/diameter ratio and in atmosphere and to a lesser extent in powder characteristics.

Work in the hot compacting of metal powders, including beryllium and aluminum,[11] emphasize the difference between compacting in air and in vacuo. Hot compacting in air is complicated by the oxidation of the metal and it is difficult to appraise the density of beryllium parts made from powder which had been exposed to high temperature air without a statement of its oxygen or oxide content, since beryllium powder, even in room temperature air, can pick up several percent of oxygen.[4] Wikle's data illustrate the contamination possible during high temperature pressing in air; the density of compact No. 89 (1.870 g per cu cm) corresponds to a concentration of 2.8 pct BeO if the metal is a mixture of beryllium and BeO. Again, the effects of small concentrations of contaminant may have a large effect on physical properties: compacts Nos. 58 and 59 were pressed under identical conditions and their ultimate tensile strengths vary considerably. The difference between respective densities corresponds to a difference in BeO of only 0.007 pct and there is a difference in ultimate tensile strength of 19,700, assuming, of course, the ultimate tensile strength data are averaged and not individual values. Sylvania studies on beryllium concentrated on vacuum pressing, and the author does not claim to be in a position to generalize about compacting in air; Brush's work apparently concentrated on air compacting.

In citing the data on strength and hardness, it was pointed out that, because of the small size of the compacts, it was necessary to use the simple beam test to compare the properties of hot-pressed compacts with those made by pressing and sintering. The sintered bars were carefully machined and ground to the same dimensions as the hot-pressed bars and the testing conditions were as nearly identical as possible. The conditions and method of test were outlined carefully so that the reader might not confuse the data with those obtained by the more conventional tensile tests. It was the size of the compacts which precluded the use of the standard tensile test. Obviously, strength data could not be obtained on bars cut parallel to the pressing direction because of the short height of the compact; however, hardness did not vary with the surface on which the reading was made.

Regarding the use of vacuum, industry in general in the past few years has acknowledged the advantages of vacuum processing certain materials and has accepted the increased costs as a necessary but minor disadvantage, far out-weighed by the advantages accrued. Vacuum melting, vacuum annealing, and vacuum sintering are being employed more and more widely not because of subtle improvements but because of important differences in physical properties, purity, reproducibility, yield, etc. Sylvania has been using vacuum processing on a commercial scale for over three years, and studies indicate that any penalties are offset by the gains. The general trend toward the utilization of special methods and techniques for the processing of special metals represents an attitude which will result in a more efficient utilization of the desirable properties of the new metals which are now being produced and of the older metals with excellent characteristics which have been developed recently.

The author would like to comment on the statements that "material pressed under the minimum sintering temperature (750°C) does not have a strong intercrystalline bond" and that "ductility with a strong intercrystalline bond can only be obtained by heating above the recrystallization point." In sintering a powder compact, the green compact has essentially point contact between particles, or at least contact over extremely small areas. Since there is no externally applied pressure forcing the particles together, the sintering or the densification occurs, due principally to the increased mobility of the atoms at the elevated temperature and by one or more of the methods of atom transfer. Conditions are entirely different in the case of elevated temperature pressing. Here the compacting pressure is applied when the particles are very ductile and have low strength; the particles are distorted and the voids are closed almost exclusively by the force of the externally applied pressure. As the particles become distorted, fresh clean unoxidized surfaces are exposed and establish bonds with the particles against which they are forced. One of the most important factors retarding interparticle bonding is the contamination of the surface of the particles, e.g., with oxide; this is particularly important at lower temperatures and, as the temperature is increased, the oxide particles on the surface layers tend to agglomerate, increasing further the area over which bonding may be effected and augmenting the bonding mentioned previously. It is known that metals may be cold welded by forcing pieces together so that the pieces are upset considerably and so that fresh clean surfaces come in contact; strong bonds may be effected even at room temperature with certain metals, e.g., copper. This type of bonding will be influenced to some extent by the atmosphere in which it is conducted, being improved by the use of vacuo. The author feels that the mechanisms by which bonding is effected during sintering and during low temperature or "cold" welding are substantially different.

The data presented by Wikle show a difference in ultimate tensile strength between compact Nos. 5 and 6 of 16,200 psi and a difference of 17,900 psi between two samples presumably prepared under identical conditions (compact Nos. 58 and 59). It would seem that the spread in tensile values characterized the variance associated with this particular series of experiments. Wikle has an interesting possibility here and it should be investigated more thoroughly, possibly on a statistical basis.

[8] H. Dodds and C. B. Sawyer: Patent Application SN 329,102 (Dec. 31, 1952).

[14] W. W. Beaver: Fabrication of Beryllium Powder Metallurgy. *Metal Progress* (1954) 65, No. 4, pp. 92-97; 166-173.
[15] W. W. Beaver and K. G. Wikle: Mechanical Properties of Beryllium Fabricated by Powder Metallurgy. Trans. AIME (1954) 200, pp. 559-573; JOURNAL OF METALS (May 1954).

[16] N. P. Pinto: Measurement of Lubricant Thickness on Powder Metallurgy Dies. *Lubrication Engineering* 10, p. 6.
[17] N. P. Pinto and G. P. Howland: *Hot Pressing of Aluminum Powders*. Presented at AIME Annual Meeting (February 1955).

The Influence of Carbon and Manganese on the Properties of Semikilled Hot Rolled Steel

by F. W. Boulger and R. H. Frazier

DISCUSSION, Howard Scott and Paul Gordon, Chairmen

A. B. Wilder *(National Tube Div., United States Steel Corp., Pittsburgh)*—The results reported by the authors are of particular interest to producers of pipe for large diameter gas pipelines. The chemical ranges and deoxidation practice described are commonly used in the production of welded pipe. In the manufacture of seamless pipe, usually an aluminum-killed steel is employed.

In the manufacture of high yield strength (52,000 psi minimum) large diameter line pipe, the material is frequently cold expanded. This cold working provides an increase in strength properties without a corresponding increase in chemical composition. An increase in carbon content, for example, would influence weldability.

The effect of cold working was not determined by the authors. In Table IX the chemical analysis is shown and in Table X the influence of cold working on the Charpy impact properties of semikilled steel is given. It will be observed the transition temperature (10 ft-lb level) was raised. A 2/3 size keyhole Charpy impact specimen was used. The material was aged at 450°F for 4 hr after cold working. The relationship of carbon and manganese to the transition temperature of cold-worked steel was not determined. The results reported in Tables IX and X were obtained by F. W. Crouch, National Tube Div., United States Steel Corp.

F. W. Boulger and **R. H. Frazier** *(authors' reply)*—Dr. Wilder's data on the effect of combined cold working and aging treatments on notched-bar properties of semikilled steels make a worthwhile addition to the paper. Although it is known that such treatments increase the likelihood of brittle fracture, very few quantitative data have been published. Many steels are cold worked during mill processing or in later fabrication. Since serious brittle fractures have occurred in structures containing such steels, research on the interrelated effects of composition, cold work, and aging on toughness seems desirable.

Table IX. Check Chemical Analysis

Heat	C	Mn	P	S
A	0.25	0.92	0.019	0.029
B	0.27	1.06	0.018	0.030
C	0.24	1.03	0.019	0.029
D	0.24	0.90	0.018	0.030
E	0.24	1.06	0.022	0.030

Table X. Impact Test Results, Average of Five Heats

Treatment	2/3 Size Charpy Keyhole Ft-Lb at Indicated Temperature, °F							
	75	50	25	0	−25	−50	−75	−100
As-rolled	19.7	18.6	17.9	16.5	14.0	11.9	9.3	2.6
Strained ½ pct, aged*	18.9	18.3	17.5	15.4	14.2	12.3	7.8	2.6
Strained 1 pct, aged	18.1	17.5	16.8	14.6	13.0	9.2	4.3	1.7
Strained 1½ pct, aged	18.3	17.0	15.7	14.8	11.6	7.7	1.7	1.3
Strained 2 pct, aged	17.2	16.5	15.4	13.1	10.1	4.3	1.4	1.4

* Aged at 450°F for 4 hr.

Temper Embrittlement of 5140 Steel

by S. H. Bush and C. A. Siebert

DISCUSSION, Howard Scott and Paul Gordon, Chairmen

S. R. Maloof *(Raytheon Manufacturing Co., Waltham, Mass.)*—The changes in the lattice parameter of ferrite following the embrittling treatments used by the authors are in complete accord with those noted by the writer in an earlier investigation.[6] However, the authors fail to make any mention of this study. Since the authors have shown a definite correlation between the lattice parameter of ferrite and the degree of temper brittleness as measured by the shift in transition temperature, any proposed mechanism of temper embrittlement must, as a consequence, be consistent with the changes observed in a_o. Do the authors have any thoughts on the subject?

Some investigators[6, 10] have favored the notion of segregation of various elements at the grain boundaries as the cause of temper brittleness; and one,[1] without any experimental support, had earlier proposed the mechanism of precipitation at the grain boundaries as the cause of temper brittleness. However, neither of these mechanisms would be expected to cause the changes in a_o observed. The maximum change in a_o observed (0.0012 kX units), although small, must result from a change occurring throughout the entire volume of each grain, as for example, the precipitation of a carbide phase or the diffusion of the alloying elements in ferrite into the carbide phase (cementite). If carbide precipitation per se is responsible for temper brittleness, it then becomes difficult to explain the dif-

ferent degrees of temper brittleness observed at the various temperatures investigated. Precipitation of carbide is detected in plain carbon as well as low alloy steels at temperatures generally lower than the temperature range where temper brittleness is observed. The authors have observed maximum embrittlement at 850°F after 3000 hr, very little at 750°F, and lesser amounts at 1050° and 1100°F.

While retaining the notion of carbide precipitation as the cause of temper brittleness, it is more reasonable to assume that a sufficient number of carbide particles of a critical size would be required to embrittle the steel. Maximum embrittlement would then occur at the temperature where the nucleation rate (N), according to the nucleation theory, is a maximum—the authors' 850°F temperature, for example.* At this temperature, the maximum number of precipitated particles would form. At temperatures below and above this temperature, the nucleation rate (N) being lower, fewer particles would be formed. Consequently, at temperatures lower than 850°F, an insufficient number of fine carbide particles would be formed such as to embrittle the steel. This may be the case at 750°F. At temperatures greater than 850°F, a smaller number of large particles would be formed and the steel should exhibit less embrittlement. Such is the case observed by the authors at 1050° and 1100°F. The return to toughness of a steel given a long-time temper at the embrittling temperature could be explained nicely by the agglomeration and growth of the precipitated particles. In the authors' Table I, a slight return to ductility of the steel is observed after 3000 hr at 950° and 1050°F. The return to toughness of the steel following heating to 1250°F for 1 hr after embrittling for 100 hr at 750° and 950°F also could be explained in a similar way. However, it must be assumed that partial resolution of carbide in ferrite occurred, since the lattice parameter of ferrite was shown to increase after this treatment.

On the other hand, the decrease in the lattice parameter of ferrite following temper embrittlement could be explained also by a diffusion of the alloying elements in ferrite into the carbide phase (cementite). Enrichment of cementite in alloy content has been observed by the writer and others.[10, 13] In this case, the brittleness would be associated with the existence of a carbide enriched in alloying elements. At higher tempering temperatures, the alloying elements would go progressively into solution, resulting in a disappearance of temper brittleness.[14] These and other phenomena observed during temper-brittle studies have yet to receive adequate explanations.

The writer firmly believes that more X-ray diffraction and electron microscope studies will be necessary before an exact explanation of temper brittleness is forthcoming.

* It is interesting to quote from the work of R. L. Rickett and F. C. Kristufek:[12] "Carbide particles precipitated from ferrite at relatively high temperatures (>1000°F) are fairly massive and occur in ferrite grain boundaries; those precipitated at lower temperatures are more numerous, smaller, and tend to form within the ferrite grains; precipitation appears to be most rapid at 800°F."

[8] S. B. Maloof: Some X-ray Diffraction and Electron Microscope Observations on Temper-Brittle Steels. *Trans.* ASM (1953) 44, pp. 264-274.

[9] D. McLean and L. Northcott: Micro-Examination and Electrode Potential Measurements of Temper-Brittle Steels. *Journal* Iron and Steel Inst. (1948) 158, pp. 169-177.

[10] B. C. Woodfine: Some Aspects of Temper-Brittleness. *Journal* Iron and Steel Inst. (1953) 173, pp. 240-255.

[12] R. L. Rickett and F. C. Kristufek: The Microstructure of Low Carbon Steel. *Trans.* ASM (1949) 41, pp. 1113-1141.

[13] F. Houdremont, W. Kock, and W. J. Wiester: On the Processes of Transformation in Cr-Mn Steels. *Archiv für das Eisenhüttenwesen* (1945) 18.

[14] F. Bowman: Partition of Molybdenum in Steels. *Trans.* ASM (1945) 35, p. 112.

[15] W. Bischof: Discussion of "Beitrag zur Frage der Anlassprodigkeit." *Archiv für das Eisenhüttenwesen* (1935) 8, p. 301.

Viscosity and Density of Liquid Lead-Tin and Antimony-Cadmium Alloys

by H. J. Fisher and A. Phillips

DISCUSSION, Howard Scott and Paul Gordon, Chairmen

Cyril Stanley Smith *(Institute for the Study of Metals, University of Chicago, Chicago)*—The almost discontinuous change in viscosity in the liquid above the eutectic now seems to be well established, although it is hard to explain theoretically. Have the authors compared the viscosity of melts made from pure components and never solidified with those that have been frozen and remelted? It is conceivable that an increase in viscosity could result from the presence of some solid impurity which forms easily in primary dendritic crystals and which cannot grow to a sufficient size in a eutectic.

H. J. Fisher and **A. Phillips** *(authors' reply)*—The interesting point raised by Dr. Smith regarding the comparison of the viscosity of alloys, which in their thermal history had never previously undergone a liquid-to-solid phase transformation with other alloys which had been previously frozen and remelted, was not investigated in the authors' work. Other work[16] on crystalline solids has indicated that phase changes can be initiated by foreign inclusions as well as by deviations from structural regularity, such as grain boundaries and dislocations. The presence of these structural irregularities may catalyze the nucleation and/or growth of new phases. In the case of frozen and remelted alloys, the influence of these factors on the viscosity-constitution relationship in the liquid state has never, to the authors' knowledge, been investigated and appears to merit study. The authors wish to thank Dr. Smith for bringing this to their attention.

[16] D. Turnbull: *Role of Structural Impurities in Phase Transformations.* (November 1954) Paper presented at the ASM Seminar on Imperfections.

On the Nucleation of Pearlite

by M. E. Nicholson

DISCUSSION, E. S. Machlin and J. K. Stanley, Chairmen

L. D. Jaffe *(Jet Propulsion Laboratory, California Institute of Technology, Pasadena, Calif.)*—The author's interesting speculations appear to depend almost entirely on the assumption that the rate of formation or nucleation of pearlite decreases with increasing carbon content. Unfortunately, this assumption is not in accord with experiment. The data of Sato,[17] of Lyman and Troiano,[18] of Blanchard, Parke, and Herzig,[19, 20] and of others[21] show that the pearlite reaction is accelerated by increase of carbon content.

Dr. Nicholson cites Digges' 1938 work as indicating otherwise; Digges[29] measured the cooling rate at which the first trace of nonmartensitic product appeared in Fe-C alloys. He referred to this product as "troostite," more recent evidence[30] indicates that under such conditions the nonmartensitic product would probably be what is now termed "bainite." Accordingly, Digges' data probably do not pertain to pearlite. Likewise, reference to original published data[29] for Dr. Nicholson's Fig. 2 does not substantiate his contention that the curves for beginning of the pearlite and of the proeutectoid ferrite reactions join tangentially.

M. E. Nicholson *(author's reply)*—Dr. Jaffe has stated that the mode of pearlite nucleation suggested in the paper depends upon the assumption that the rate of pearlite nucleation decreases with increasing carbon content. This is only half true. Based on the two-mode model, the rate of pearlite nucleation may decrease with increasing carbon content when pearlite is nucleated by ferrite-initiated sequence or it may increase with increasing carbon content when pearlite is nucleated by a cementite-initiated sequence. The former is the situation for plain carbon, low nickel, and low manganese steel. The latter is the case for such alloy steels as molybdenum, chromium, and tungsten steels. The references cited by Dr. Jaffe are for steels in the second class.

With regard to the reference to Dr. Digges, it should be pointed out that Dr. Digges described the first nonmartensitic product not only as nodular troostite, using the common contemporary terminology, but also as fine pearlite, using the terminology now in vogue. In a more recent work, Digges[29] confirmed his earlier work. He again found that in plain carbon steels, except for low carbon alloys in which ferrite formed first, the first nonmartensitic was fine pearlite. In these steels the critical quenching velocity descreased with increasing carbon content.

Dr. Jaffe indicates that the data used as the basis for Fig. 2 did not show the curves for the beginning of the pearlite and proeutectoid ferrite joining tangentially. The curves in the original reference and in Fig. 2 exhibit a rapidly decreasing curvature as the nose of the curve, where they join, is approached. Such curves quite conceivably may join tangentially. Actually whether or not they join tangentially is not pertinent. Much more to the point is the question whether these curves exhibit the relations shown in Fig. 1, where there is an abrupt change in direction as XA joins XC', or whether they exhibit those shown in Fig. 4 where no abrupt change occurs. The original curves, like those in Fig. 2, show no abrupt change where the proeutectoid ferrite curve joins the pearlite curve and therefore may be used as evidence to support the two-mode model of nucleation.

[29] T. Sato: On the Critical Points of Pure-Carbon Steels. *Technical Reports* Tohoku Imp. University (1929) 8, pp. 27-52.

[30] T. Lyman and A. R. Troiano: Influence of Carbon Content Upon the Transformations in a 3 Per Cent Chromium Steel. *Trans.* ASM (1946) 37, pp. 403-448.

[31] J. R. Blanchard, R. M. Parke, and A. J. Herzig: Effect of Molybdenum on the Isothermal Subcritical Transformation of Austenite in Low- and Medium-Carbon Steels. *Trans.* ASM (1941) 29, pp. 317-338.

[32] J. R. Blanchard, R. M. Parke, and A. J. Herzig: Effect of Molybdenum on the Isothermal Subcritical Transformation of Austenite in Eutectoid and Hypereutectoid Steels. *Trans.* ASM (1943) 31, pp. 849-876.

[33] *Atlas of Isothermal Transformation Diagrams.* (1951) pp. 97-100. Pittsburgh. U.S. Steel Corp.

[34] J. H. Hollomon and L. D. Jaffe: *Ferrous Metallurgical Design.* (1947) pp. 207-208. New York. John Wiley and Sons.

[35] *Atlas of Isothermal Transformation Diagrams.* (1951) pp. 44, 47-49. Pittsburgh. U.S. Steel Corp.

[36] T. G. Digges, C. R. Irish, and N. L. Carwile: Effect of Boron on the Hardenability of High-Purity Alloys and Commercial Steels. *Bulletin* National Bureau of Standards (1948) 41, pp. 545-574.

Stabilization of the Bainite Reaction

by R. F. Hehemann and A. R. Troiano

DISCUSSION, E. S. Machlin and J. K. Stanley, Chairmen

E. P. Klier and **Volker Weiss** *(Metallurgical Research Laboratories, Syracuse University, Syracuse, N. Y.)*—The strongest evidence of carbon enrichment of the austenite during bainite formation stems from tetragonality measurements on the martensite formed on quenching from the transformation temperature. Hehemann and Troiano state, "in steels containing 0.3 to 0.4 pct C . . . the [tetragonal] split indicative of a high carbon martensite has not been reported." The writers present Table II taken from the literature[38] in which the tetragonal split has been reported. Hehemann and Troiano further assert that "It should be noted, however, that no enrichment has been detected experimentally in high carbon steels."[1, 16, 18] Their attention is directed to Fig. 18 taken from Lyman and Troiano.[1] Of interest

Table II. Tetragonal Split in Steel, after Klier[38]

Steel	Transformation Temperature, Pct C	°C	°F	Time at Temperature, Sec	Structure
3 pct Cr	0.38	475	887	90	γ plus tetragonal split (?)
3 pct Cr	0.38	475	887	180	γ plus tetragonal split
3 pct Cr	0.38	475	887	23 hr	Tetragonal split plus (γ) ?
1 pct Cr, 0.40 pct Mo	0.42	515	959	90	γ plus tetragonal split
1 pct Cr	0.44	550	1022	120	Tetragonal split γ
1 pct Cr	0.44	515	959	45	plus tetragonal split
1 pct Cr	0.44	505	941	320	γ plus tetragonal split

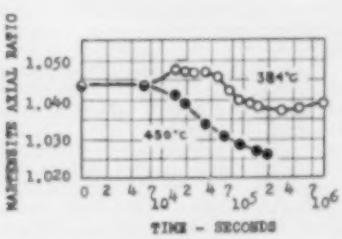

Fig. 18—Dependence of martensite axial ratio at 450° and 384°C during isothermal transformation in the 3 pct Cr steel.

is the martensite axial ratio curve obtained after transformation at 384°C for a 1 pct C, 3 pct Cr steel. There is unequivocal evidence here that carbon enrichment of the austenite has obtained.

After examining the present review and experimental program, the discussers find it desirable to reaffirm their belief that the mechanism of bainite formation proposed by Klier and Lyman[1] and by Klier[38] is essentially correct and is described in the following steps: 1—The diffusion of carbon in austenite to set up alternating regions of high and low carbon content. 2—The transformation of either region independently or both essentially in consort by a lattice shearing mechanism. In low carbon steels the low carbon regions, in general, precipitate; in high carbon steels all three possibilities may obtain. (The discussers refrain from calling the precipitation process a martensite reaction at the present time, as they consider this reaction now incompletely defined.) 3—The conditions described in items 1 and 2 depend on the temperature of transformation and, as this temperature is lowered, the extent of carbon diffusion is modified with the dif-

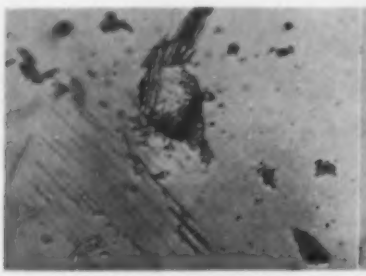

Fig. 19—1.5 pct Mo, 1.0 pct C steel, quenched from 1100° to 560°C for 5 min. Etched with nital. X500. Area reduced approximately 25 pct for reproduction.

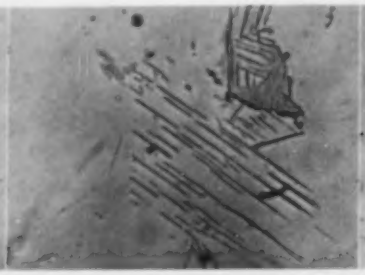

Fig. 20—1.5 pct Mo, 1.0 pct C steel, quenched from 1100° to 560°C for 5 min. Etched with nital, repolished, and etched with alkaline sodium picrate. X500. Area reduced approximately 25 pct for reproduction.

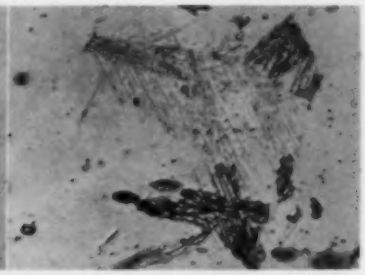

Fig. 21—1.5 pct Mo, 1.0 pct C steel, quenched from 1100° to 560°C for 5 min. Etched with nital. X500. Area reduced approximately 25 pct for reproduction.

ferential in carbon content between high and low carbon regions being reduced. Carbon movement, even if only from one location in the unit cell to another, is postulated for all bainite structures.

In postulating the foregoing mechanism of bainite formation, definite theoretical concepts have been the guide. Certain experimental data to which these concepts have guided the discussers will be outlined briefly.

Studies of bainite formation in high carbon steels have been completed mainly on slowly transforming steels. The micrographs Figs. 19 to 24 were obtained by D. E. Nulk[26] in a rapidly transforming steel containing 1 pct C and 1.5 pct Mo. In Figs. 19 and 20 carbon-rich regions are indicated in the austenite. These regions develop and grow while the high-low carbon complex remains coherent with the matrix austenite, Figs. 21 and 22. Finally the ferrite-carbide complex stands as a precipitated structure, Figs. 23 and 24. For this steel the carbide precipitated in the bainite range is not Fe_3C. Similar structures are possible in a somewhat different transformation sequence, Figs. 25 and 26. Here with reduction in transformation temperature, the normal bainitic structure is replaced by a lamellar structure which exists over a short temperature range only.

Over a span of about three years, many data relating to the stabilization effect of prior formation of "upper" bainite on the rate of formation of lower bainite were obtained. In these studies the discussers observed that even slight banding led to highly objectionable transformation characteristics on transforming at the lower temperatures. That this stabilization, however, might lead to increased hardenability was advanced by Cleveland[27] as responsible for the secondary hardness peak developed in 52100 steel. The potentialities of this process for developing worthwhile increases in hardenability escaped the discussers in their work.

The data for stepped transformation treatments in the bainite range are in agreement with the data of Lange and Mathieu,[25] Wever and Mathieu,[20] and with Hehemann and Troiano. Additional data of interest obtained by F. C. Wagner[28] are presented in Fig. 27. Here are reported three sets of transformation data in the bainite range after prior holding at 1200°F for 30, 300, and 500 sec, respectively. These holding times did not lead to the formation of pearlite. Of interest is the fact that holding for the long time has led to a virtual elimination of the upper bainite reaction, as indicated by the reduced dilatation after this treatment.

The fact that suitable holding at high subcritical temperatures may result in the suppression of upper bainite has led to an exploration of this behavior in 4340 steel. For the steel that has been studied at length, it has been possible in the standard Jominy bar to virtually eliminate the upper bainite reaction by replacement with the lower bainite reaction. A rather large program of studies of the properties of these structures has now been completed. The discussers hope to be able to publish the results in the near future.

R. F. Hehemann and **A. R. Troiano** *(authors' reply)*—The authors fear that this discussion will lead to some confusion on the part of the average reader. Much, but not all of this, can be dissipated on the basis of what constitutes bainite. This point is considered in detail in the text from which the discussers' Fig. 18 was taken.

Indeed, there is evidence of enrichment with a tetragonal split after substantial quantities of bainite have formed and sufficient time has elapsed after the end of reaction to allow diffusion. However, the authors cannot rationalize and have been unable to detect a tetragonal split under conditions comparable to those indicated in the discussers' table. To be sure, the authors' work was conducted on steels of different alloy content; however, the essential point is that only small amounts of bainite can form at temperatures near, but below, B_s.

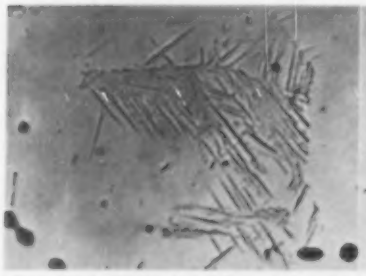

Fig. 22—1.5 pct Mo, 1.0 pct C steel, quenched from 1100° to 560°C for 5 min. Etched with nital, repolished, and etched with alkaline sodium picrate. X500. Area reduced approximately 25 pct for reproduction.

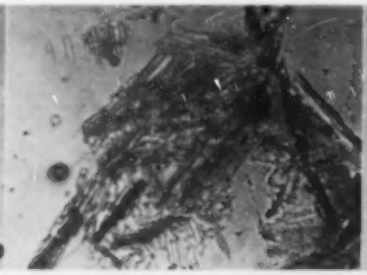

Fig. 23—1.5 pct Mo, 1.0 pct C steel, quenched from 1100° to 560°C for 5 min. Etched with nital. X500. Area reduced approximately 25 pct for reproduction.

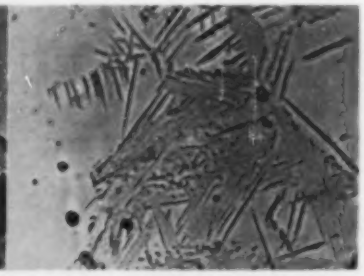

Fig. 24—1.5 pct Mo, 1.0 pct C steel, quenched from 1100° to 560°C for 5 min. Etched with nital, repolished, and etched with alkaline sodium picrate. X500. Area reduced approximately 25 pct for reproduction.

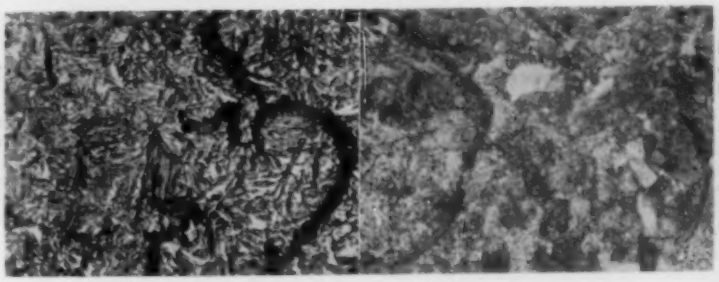

Fig. 25—Gray iron, quenched from 1600° to 750°F for 1½ hr. Note expected bainitic structure. Etched with nital. X500. Area reduced approximately 25 pct for reproduction.

Fig. 26—Gray iron, quenched from 1600° to 700°F for 3 hr. Note bainite structure having lamellar appearance. Etched with nital. X500. Area reduced approximately 25 pct for reproduction.

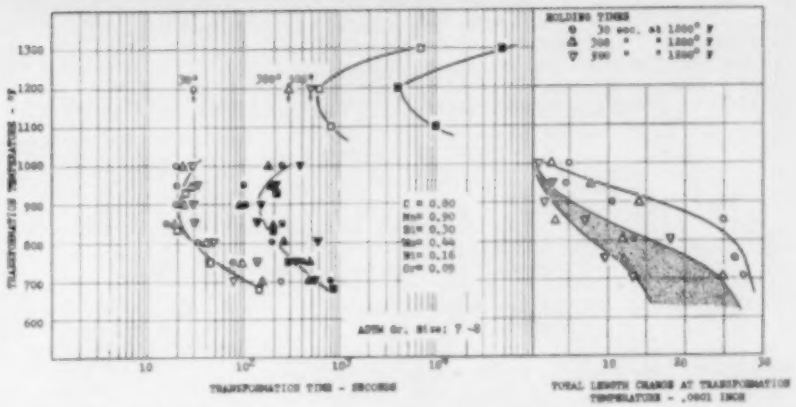
HOLDING TIMES
TRANSFORMATION TEMPERATURE - °F
TRANSFORMATION TIME - SECONDS
TOTAL LENGTH CHANGE AT TRANSFORMATION TEMPERATURE - .0001 INCH

Fig. 27—Isothermal transformation diagram in the bainite range after prior holding at 1200°F as indicated. Total dilatation is an approximate index of percentage of transformation.

Aside from the foregoing, a fundamental question is concerned with the role of carbon enrichment in controlling the reaction kinetics. Perhaps the most characteristic feature of the bainite reaction in alloy steels is its inability to transform all of the austenite at temperatures near B_s. Frequently, this has been attributed to carbon enrichment as the reaction proceeds. It is believed, however, that this enrichment is highly localized around each bainite plate. Thus, as explained in detail elsewhere,[29] such enrichment does not account for the temperature dependence of the extent of decomposition to bainite. Undoubtedly, the carbon movement producing this enrichment is of importance in specifying the form of the reaction curve.

[28] E. P. Klier: Discussion of ref. 5.
[29] E. P. Klier: Transformation of Austenite in a Steel Containing 3 Percent Chromium and 1 Percent Carbon. *Trans.* AIME (1945) 162, p. 186; METALS TECHNOLOGY (September 1945).
[30] Thesis work with E. P. Klier at Pennsylvania State University, completed before 1949.
[31] H. Lange and H. Mathieu: On the Progress of Austenite Decomposition in the Supercooled State in Iron-Nickel-Carbon Alloys. *Mitteilungen* Kaiser-Wilhelm-Institut Eisenforschung (1938) 20, p. 125.
[32] F. Wever and K. Mathieu: On the Transformation in Manganese Steels. *Mitteilungen* Kaiser-Wilhelm-Institut Eisenforschung (1940) 22, p. 9.

Some Characteristics of the Isothermal Martensitic Transformation

by C. H. Shih, B. L. Averbach, and Morris Cohen

DISCUSSION, E. S. Machlin and J. K. Stanley, Chairmen

R. E. Cech *(General Electric Co., Schenectady)*—The authors have not demonstrated a composition effect on the temperature of maximum isothermal nucleation frequency (T_n). The values of T_n obtained by Shih, Averbach, and Cohen and by Cech and Hollomon[6] can be considered in excellent agreement in view of the scatter attendant with the experimental measurements. The justification for the authors' conclusion thus rests upon the correctness of T_n for their alloy *B* and the one of Kurdjumov and Maksimova.[1, 2] Since isothermal nucleation of martensite was not measured in alloy *B* at any temperature, the T_n has not yet been determined. Therefore, it is presumptuous to assign a value for T_n in this alloy.

Table III. Comparison of Data in Which Martensite Occurred Primarily Isothermally

Investigator	Reference	Alloy	T_n
Shih, Averbach, and Cohen	Present paper	Fe-Ni-Mn	−140°C
Cech and Hollomon	6	Fe-Ni-Mn	−128°C
Kurdjumov and Maksimova	1	Fe-C-Mn	−130° to −140°C
Kurdjumov and Maksimova	1	Fe-C	−125°C*
Kurdjumov and Maksimova	2	Fe-Ni-Mn	−47°C*
Kulin and Speich	4	Fe-Cr-Ni	−28°C*

* T_n cannot be considered reliable, since one-fifth of the austenite was removed from the system by athermal transformation prior to determination of T_n.

The Kurdjumov-Maksimova alloy plotted is one which had an M_s of −17°C and formed as much as 17 pct martensite athermally on cooling to −47°C (T_n for this alloy). Since a large amount of austenite was removed from the system by athermal transformation above T_n, it is to be expected that T_n occurs at a higher temperature than it would in the absence of prior transformation.

If all the data in which martensite transformation occurred primarily isothermally are compared, a quite different result appears, Table III. It can be seen that in four out of six investigations, T_n was found to occur between −125° and −140°C.

C. H. Shih, B. L. Averbach, and **Morris Cohen** *(authors' reply)*—Mr. Cech has brought up several in-

teresting points. He has suggested that the presence of prior athermal martensite should raise T_m, the temperature for the maximum initial rate of isothermal martensite formation. In the experiments of Machlin and Cohen[7] on Fe-Ni alloys, the isothermal martensitic transformation was observed after prior cooling to liquid nitrogen and also on cooling directly to the reaction temperature. In the first instance, the amount of athermal martensite was greater, yet the value for T_m was lower (150°K) than for the other case (205°K). This trend is opposite to that proposed by the discusser, although the effects may be different when considering alloys with and without athermal martensite.

It is also interesting to note that T_m is observed to be about 50°C below the temperature at which the first isothermal martensite is detectable for each of the Fe-Ni-Mn alloys, Kurdjumov and Maksimova,[2] Cech and Hollomon,[4] and the authors' alloy *A*. This suggests that the entire isothermal transformation curve, and therefore T_m, changes with composition.

Kurdjumov and Maksimova do not state explicitly that their isothermal run was made with an initial martensite content of 17 pct. They used a "critical cooling rate" of 10°C per min, and report an "M_s" of −17°C on cooling at this rate. This is certainly not a rapid quench and the figure containing their rate data does not indicate how their specimens were actually cooled to the reaction temperature. It appears that some martensite was present at the start of the isothermal transformation, but the amount is indeterminate and could have easily corresponded to the accidental amounts prevailing in the Cech and Hollomon experiments.

Perhaps the point for alloy *B* in Fig. 6 should not have been plotted without further explanation. At liquid nitrogen temperature, martensite could only be formed in this alloy by plastic deformation. The M_s is thus below this temperature, and the authors assumed that T_m is also below this temperature. However, as Mr. Cech states, T_m was not determined and there is considerable uncertainty as to its magnitude.

Ordering Reaction of the Cu_4Pd Alloy

by A. H. Geisler and J. B. Newkirk

DISCUSSION, E. S. Machlin and J. K. Stanley, Chairmen

R. Smoluchowski *(Carnegie Institute of Technology, Pittsburgh)*—The discusser would like to comment on the authors' suggestion that the observed and calculated line intensities can be brought into better agreement with each other when errors, that is, deviations from the ideal ordered structure, are taken into account. It seems that this is a very interesting and fruitful procedure but perhaps it would be worthwhile to look into it in a somewhat greater detail by considering what kind of errors are particularly probable. For instance, a particular interchange of atoms of an ideal Cu_3Pd structure may lead to the formation of an area which locally looks like a Cu_4Pd structure. As a consequence, this particular type of error may be more probable than another kind of error which does not form a Cu_4Pd-like configuration. In that connection, it would be very worthwhile to find out whether the Cu_4Pd structure as observed by Jones and Sykes really exists.

B. Kiefer and **K. Schubert** *(Max Planck-Institut für Metallforschung, Stuttgart, Germany)*—The tetragonal distortion of the unit cell in Pd-Cu alloys between 81.5 and 71.0 atomic pct Cu is of special interest. Therefore, the discussers have made an investigation of this system.[10] Some of the results confirm those of Drs. Geisler and Newkirk. With regard to the structure, some different observations were made, the results of which were as follows:

The alloys show a tetragonal (body-centered) unit cell, the *a*-axes of which are the same as in the substructure, whereas the *c*-axis of the cell varies within the range of homogeneity. It is 18 times the *c*-axis of the substructure at 81.5 atomic pct Cu and 8 times at 75 atomic pct Cu. In the intermediate range, the reciprocal value of *c*-axis multiplication varies linearly with concentration. The precise structure is described in a short communication.[10]

J. B. Newkirk *(authors' reply)*—There is no doubt that certain types of interchange errors are more probable than others and a study of the relative probability of the different types may provide useful information concerning structural relationships between the various known ordered lattices. The relationship between the proposed Cu_3Pd structure and the Jones and Sykes Cu_4Pd structure is difficult to assess, since the atom placement in the ordered Cu_4Pd structure was not specified by Jones and Sykes.[1] They describe the cell only as one containing 36 atoms in which *A* equals 9.741Å (An internal inconsistency is here. They may have meant $A = 7.865$Å) and *C* equals 7.312Å. The complex array of faint superlattice lines did not yield to solution except to prove that the structure was not that of ordered Cu_4Au.

The long cell described by Kiefer and Schubert has not been checked. Such a shape is surprising but not impossible in the light of the known experimental support for the structurally similar CuAu II cell.

[10] K. Schubert, B. Kiefer, and M. Wilkens: *Ztsch. für Naturforschung* (1954) **9a**, p. 987.

Mechanism for the Origin of Recrystallization Nuclei

by John P. Nielsen

DISCUSSION, E. S. Machlin and J. K. Stanley, Chairmen

R. L. Fullman *(General Electric Co., Schenectady)*—The proposal that the large grain required as a nucleus for secondary recrystallization may arise as a result of two adjacent grains having very similar orientation appears quite plausible, and Professor Nielsen is to be congratulated for pointing out this extremely simple mechanism. In common with the older hypothesis that the large grains are those which nucleated earliest in primary recrystallization, the new theory would lead to a secondary preferred orientation identical to a minor component of the primary texture. Failure to observe this minor component does not invalidate either theory, since only an undetectably small fraction of the grains need be in the minor component orientation. The average grain diameter generally increases by a factor of at least ten during secondary recrystallization; hence, only one grain in 1000 of the primary grains need operate as a secondary recrystallization nucleus. Let *F* be the

ratio—number of adjacent grain pairs that are both close enough to a particular orientation to act as a single large grain: total number of grains. Then F is equal to the fraction f of grains that are sufficiently close to the specified orientation times the probability that a neighboring grain is also close enough to the specified orientation times ½ (since pairs, not individual grains, are being counted). The probability that a neighboring grain is close enough to the specified orientation is f times the average number Z of grains adjacent to a given grain. Hence

$$F = \frac{1}{2} f^2 Z. \qquad [1]$$

Z is probably of the order 12 to 14, so for $F = 0.001$, f is approximately 0.01. Thus a very sharp minor texture component, containing only 1 pct of the grains in the primary recrystallization structure, is sufficient to provide the required number of secondary recrystallization nuclei.

The nuclei could also be provided from a texture component that is stronger in magnitude but less sharp in orientation. Notice that f may be considered as a distribution function expressing the fraction of grains in various orientations of the primary texture. Similarly, F is proportional to the fraction of grain pairs in various orientations. If the nuclei for secondary recrystallization arise from these grain pairs or some selected group of them, the fraction of nuclei in various orientations is proportional to F, within the range of orientations permitted by any selective influences. Since F is proportional to f^2, the texture of these nuclei must be sharper in orientation than the minor texture component from which they arose.

If Eq. 1 were the only condition governing the abundance of nuclei in various orientations, the texture of the secondary nuclei would merely be a sharpened modification of the primary recrystallization texture. Professor Nielsen suggests (p. 1087) that one selective influence is that the boundary between the members of the grain pair must have low free energy *relative* to the boundaries between the pair and their neighbors, in order for the pair to act as a single grain in further growth. This condition limits the effectiveness of grain pairs with the orientation of major texture components, since the grains adjacent to such pairs usually are in orientations similar to the pair itself. Low mobility of boundaries between similarly oriented grains also would prevent grain pairs from major texture components from growing rapidly enough to provide an important contribution to the secondary texture.

On the other hand, the statement on p. 1087, based on the von Neumann equation,* that the driving force for growth of the grain pair increases with its misorientation relative to the matrix is incorrect. As was pointed out on p. 1086, this conclusion is the reverse of the relationship required by the author's equation. The discrepancy arises from application of the von Neumann equation to a situation that violates an assumption made in its derivation. In contrast to Professor Nielsen's statement that the interfacial free energy σ in von Neumann's equation "refers to the boundaries of the growing grain exclusively," it is assumed in the derivation of this equation that *all* boundaries have the *same* interfacial free energy. In order to examine the situation with an interfacial free energy σ_{om} for the boundaries between grain O and its neighbors and a different interfacial free energy σ_{mm} for the boundaries between the neighboring grains, it is necessary to derive a modification of the von Neumann equation.

It is assumed that all boundaries meet at equilibrium angles, and the boundaries have the shape of circular arcs. (It is *not* necessary to assume they are *equal* circular arcs, contrary to the statement on p. 1085.) The expression will be derived in terms of the rate of diffusion of a gas through the boundary walls, this rate being assumed to be proportional to the pressure difference Δp across each boundary, times the length of the boundary l_i, summed over all boundaries. (Calculations based on this analogue give identical results to more formal treatments involving the rate of change of free energy per unit volume swept by a boundary, and the boundary permeability K in the analogue calculation is identical to the boundary mobility in the more formal calculation.)

The pressure difference across each boundary between grain O and one of its neighbors is

$$\Delta p_i = \frac{\sigma_{om}}{r_i} \qquad [2]$$

where r_i is the radius of curvature of the ith boundary. The length of each boundary between grain O and one of its neighbors is

$$l_i = r_i \theta_i \qquad [3]$$

where θ_i is the central angle of the circular arc constituting the ith boundary. The rate of change of the grain's area A is equal to the rate of change of its gas content, or the sum of the net rate of gas influx over all boundaries.

$$\frac{dA}{dt} = \sum_i^n - K l_i \Delta p_i = -K \sum_i^n r_i \theta_i \cdot \frac{\sigma_{om}}{r_i} = -K \sigma_{om} \sum_i^n \theta_i. \qquad [4]$$

At each corner of grain O, two *om* boundaries meet at an interior angle ψ, such that

$$\sigma_{mm} = 2\sigma_{om} \cos \frac{\psi}{2}. \qquad [5]$$

If straight lines are drawn between adjacent corners of grain O, defining a polygon, the interior angles x_i of the polygon satisfy the relation

$$\sum_i^n x_i = \pi(n-2). \qquad [6]$$

The sum of the arc central angles $\Sigma\theta_i$ is equal to the difference $n\psi - \Sigma x_i$, so the rate of change of area is

$$\frac{dA}{dt} = K\sigma_{om}\left[\pi(n-2) - 2n \cos^{-1}\frac{\sigma_{om}}{2\sigma_{mm}}\right]. \qquad [7]$$

While Eq. 7 is quantitatively different from Professor Nielsen's equation (p. 1085), both require that the driving force for growth increases with decreasing misorientation of the O grain (i.e., decreasing σ_{om}), with increasing σ_{mm}, and with increasing n. The limiting condition for dA/dt to be just positive depends on n and the ratio $q = \sigma_{om}/\sigma_{mm}$ in the same way for both equations. This limiting condition is

$$\frac{1}{q} = 2 \cos \frac{\pi(n-2)}{2n}. \qquad [8]$$

Thus there are no qualitative discrepancies between the predictions of equations derived on the assumption of straight boundaries (Professor Nielsen's equations) and on the assumption of boundaries in the form of circular arcs (von Neumann equation and the modification derived here).

* A factor of 2 was omitted in the printed version of Professor Nielsen's equation. The driving force for growth should be

$$\sigma_{mm}\left[1 - 2q \cos \frac{\pi(n-2)}{2n}\right]$$

for the assumptions used in his analysis.

R. W. Cahn *(University of Birmingham, Birmingham, England)*—These comments will be restricted to the nature of primary recrystallization, examined in the light of Professor Nielsen's challenging theory. The writer feels quite sure he is on the right track concerning secondary recrystallization, but it is not as easy to be sure about the primary process.

The matter for which this theory does not, the discusser feels, adequately account is the role played by polygonization in relation to recrystallization. Professor Nielsen proposes that the creation of a "texture" through polygonization provides the condition for coalescence. He makes the further postulate that "geo-

metrical coalescences . . . must occur at regions where the texture has a sharp local deviation, such as where extensive inhomogeneous plastic flow has occurred . . ." This is indeed what the experimental evidence suggests; the discusser's theory of primary nucleation,[3] and the version of it published by Cottrell,[20] similarly view a polygonization process at sites of deviating orientation as the kingpin of the whole sequence.

It is necessary, however, to reconcile this view of the matter with the growing body of evidence which indicates that polygonization and recrystallization are competing, rather than casually connected, processes.

Guinier and Tennevin's[21] studies, by X-ray diffraction of high resolving power, of the fine structure of worked aluminum as a function of time of annealing, led them to characterize polygonization and recrystallization as competing processes. There was no indication that polygonization had to progress to a certain point before new grains were formed by recrystallization.

Lacombe and Berghezan[18] demonstrated that individual grains of various orientations in deformed metal, in which polygonization had progressed very far, often resisted absorption by a growing primary crystal.

More recently, Talbot, Beaulieu, and Chaudron[19] made the remarkable discovery that exceptionally pure iron could not be made to recrystallize after cold working, because it became polygonized so rapidly that the other competing process was forestalled. When the iron was contaminated with carbon and polygonization thereby retarded, recrystallization went ahead in the normal way and afterward the contamination could be removed again. If polygonization were to be regarded as a precursor to recrystallization, then any factor, such as purity, which favors the one should surely favor the other.

The cited experiments show that the *growth* of a newly created grain into a coarsely polygonized matrix is difficult or impossible. Since polygonization is also regarded, by Professor Nielsen and others, as being necessary for the *creation* of a new grain, it must be argued that polygonization is more rapid at the site of nucleation than elsewhere. More precisely, the breakdown into well defined subgrains is fastest where "the texture has a sharp local deviation." This is reasonable.

It is not obvious, however, why extensive polygonization should impede growth of a new grain. Perhaps the texture of subgrains is no longer sharp enough, so that the growing grain becomes apt to meet subgrains of like orientation to itself, which are known to present a barrier. (Just why a grain cannot grow into another grain of like orientation is again hard to understand.) In any case, this view will not explain the resistance to absorption of grains of unlike orientation to the growing one.

It is felt that there is a need to take into account the contained energy of cold work, which can be released either by polygonization or by recrystallization. The tendency in recent theories, including Professor Nielsen's, has been to view the whole complex of annealing processes as being determined exclusively by geometrical factors. This approach has paid handsome dividends in clarifying the driving forces of grain growth and secondary recrystallization. The discusser is not so sure that it suffices for interpreting primary recrystallization.

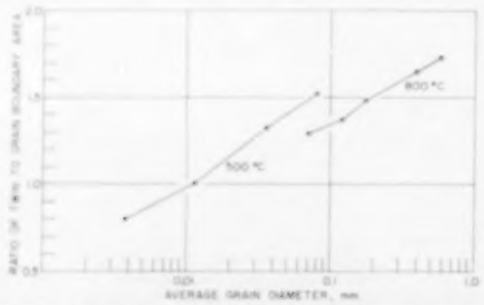

Fig. 8—Values for the ratio of twin boundary area to grain boundary area as a function of grain size for a series of samples of 65-35 brass cold worked 91 pct, recrystallized at 500°C, and then further annealed at 500° or 800°C.

Cyril Stanley Smith *(Institute for the Study of Metals, University of Chicago, Chicago)*—Dr. Nielsen's suggestions as to the origin of secondary recrystallization nuclei are most interesting. A somewhat similar mechanism was proposed in 1948[14] although the low energy boundaries were supposed to result from subgrain reorientation.

If it is assumed that the distribution of bubble shape in a two-dimensional froth stays constant with size, then the probability that the average two-dimensional bubble will make contact with a bubble that it has not hitherto encountered will be proportional to the fractional increase of its area. The total number of new contacts that an average grain will have encountered on growing from area A_1 to A_2 is, therefore, $N = \int_{A_1}^{A_2} p \frac{dA}{A}$. If p is independent of the area

$$N = p \int_{A_1}^{A_2} \frac{dA}{A} = p \ln \frac{A_2}{A_1}. \qquad [9]$$

This equation was derived by Dr. Ryoichi Kikuchi of the Institute for the Study of Metals. An evaluation of p in a random array should be possible, for it depends only on geometry and topology. The relation in three-dimensional bubble growth is precisely analogous.

Although the only bubbles that disappear are the triangular ones, the net effect of this disappearance is as if a hexagonal bubble had been removed. The sum, $\Sigma(n-6)P_n$ must always be effectively zero in a very large array. The local departures from a hexagonal array (either shortage or superfluity of sides) are, therefore, unaffected by the disappearance of grains, and an analysis of the spatial fluctuations of $(n-6)$ in an aggregate of small cells should permit a prediction of local bubble shape distribution at any larger size after growth. If this is combined with the relations of von Neumann,[4] the stable configuration that would not be changed on further growth should be computable.

To return to microcrystals; it should be noticed that the probability of forming a runaway grain by coalescence in a given volume decreases very rapidly with grain size, although the fraction of grains that are likely so to form stays constant. If the assumption of perpetual randomality can be maintained, then the process is actually a *normal* part of grain growth. The runaway grains will rapidly consume their neighbors and will continue to grow until they come in contact with others that have also been rapidly growing. The frequency with which they would occur in a random aggregate would depend on the orientation difference that can be tolerated on coalescence. In practice, of course, exact identity or twin formation would be infinitely rare, and such a wide variety of intermediate boundaries are possible that the effect could hardly be distinguished from simple froth growth due to size difference alone.

It is interesting to consider the role of these growth accidents in the formation of annealing twins. Burke[16] and Fullman and Fisher[22] have suggested that growth accidents can give rise to twin orientations by a *nucleation* process, which avoids the statistically improbable contact of grains in exactly twin orientations. The effective probability of producing a new twin on grain growth should then be proportional to the number of contacts with new grains and should follow Eq. 9 given previously. Support for this view is supplied by data recently obtained by Dr. Hsun Hu at the Institute for the Study of Metals. Fig. 8 shows his values for the ratio of twin boundary area to grain boundary area (proportional to the number of twins per grain if shape does not change) as a function of grain size for a series

of samples of 65-35 brass cold worked 91 pct, recrystallized at 500°C, and then further annealed at 500° or 800°C. At each temperature the number of twins increases lineally with Log D and, therefore, as Log A/A_o.

Since such a twin will be formed only in order to produce a lower energy boundary, it would be expected to increase the probability of forming runaway grains. In practice the very opposite is observed; materials that form annealing twins are *less* prone than others to form large grains by secondary recrystallization. Such grains are, indeed, unknown in brass or austenitic steels, yet they are easily produced in aluminum, ferritic steel, and most hexagonal metals. No explanation of this is offered.

Finally, it should be remembered when considering grain boundary migration that a boundary is not uniquely defined by the orientations involved. The boundary structure that corresponds to minimum energy can be changed by adding any number of vacancies and/or cancelling pairs of dislocations of opposite signs. If a boundary remains in the same location, it can relax to the equilibrium low energy form as a result of diffusion and escape of vacancies to the surface of the piece. If it is moving it cannot do this, particularly since motion itself will produce excess vacancies both from a decrease in area of the boundary or as a result of sweeping through imperfections or microporosity. Obviously grain boundaries reaching the surface of a piece can relax more easily and quickly achieve a low mobility configuration. Those boundaries distant from the surface will have a continued supply of vacancies as long as grain growth is occurring.

It is suggested that this is the principal cause of the slowing of grain growth as grains become larger or commensurate with the size of the specimen, as well as for the exasperating immobility of bicrystal boundaries under ordinary curvature forces. Diffusion to the surface of vacancies resulting from the solution of microporosity may be the reason for the formation of discontinuous surface grooves on annealing.

C. G. Dunn *(General Electric Co., Pittsfield, Mass.)*—Although the author points out reasons why "geometric coalescence" should not occur as readily in structures with severe (i.e., strong) textures as in ones with intermediate textures, he has wrongly stated, for the case of secondary recrystallization and the origin of secondary recrystallization nuclei, that the strong texture will increase the probability of two grains meeting with close orientation. The probability under question should apply to the nuclei, which are in deviating orientations from the matrix texture. It follows that this probability decreases with increase in sharpness of the matrix texture, since the number of grains in deviating orientation actually decreases.

A second error made in the paper involves the use of the von Neumann equation to a case involving texture. The von Neumann equation is based on one constant specific energy, but grain boundary energy is variable when a texture is present. Arguing from the von Neumann equation and a supposedly high driving energy, the author concludes that increasing σ in the boundary of the growing grain will increase the growth rate, but this implication is wrong in spite of the fact that growth rate of a secondary grain actually does increase. The energy for growth comes from the surrounding matrix—not from the energy in the boundary of the growing grain—and the driving energy actually decreases with increasing σ, since more energy is required to form the boundary of the enlarging grain. The reason for the increased growth rate is that mobility of atom movements increases with increasing σ and this more than offsets the loss in driving energy.

Finally regarding evidence supporting the mechanism proposed by Professor Nielsen—evidence, it should be said, for its occurrence late in the growth process—the discusser would like to cite a few observations obtained in the course of preparing single crystals of silicon iron. Some of these observations that have been published[11] show increased disorientation with growth distance, the disorientations being of the order of a degree or two.

Using special macro-etch techniques and suitable illumination, areas of different orientation can be delineated. Such areas show the positions of the start of growth of subgrains differing in orientation by a degree or two. Although delineated areas involving smaller disorientations are much harder to observe, the surprising thing is the low number seen in the 1° to 2° range. To date such subgrains or substructures have been observed in single crystals produced from polycrystalline materials using the strain-anneal method for two cases: 1—orientations favorable to growth, and 2—orientations unfavorable to good growth. Similar substructures also have been observed in secondary recrystallization.

Recently a different method of producing such substructures was noted. A cold-rolled single crystal was observed to recrystallize to another single crystal about 30° from the initial orientation, but having several areas of small disorientation. This case appears to involve interactions of polygonized subgrains and primaries formed in the early stages of recrystallization, but this phenomenon is still under study.

Further work is needed in these areas to clarify the picture, but it seems, in view of the rather low observed frequency of disorientations in the 1° to 2° range, that something in addition to the low σ boundary interaction effect proposed by Professor Nielsen may be involved.

John P. Nielsen *(author's reply)*—The problem of the density of geometrical coalescences in a given matrix and the texture of the resulting recrystallization grains is a difficult one to solve and Dr. Fullman's preliminary calculations are welcome contributions. In his Eq. 1, the quantity is difficult to evaluate. In a primary recrystallized structure before grain growth has progressed very far, a fraction of the grains present is already of the complex grain type, i.e., composed of subgrains, as a result of chance coalescences in the original system of contacts of recrystallization grains growing in the unrecrystallized matrix. Subsequent geometrical coalescences must come from new grain contacts other than with the immediate neighbors. Thus there are two series of coalescences. The first series probably obeys Eq. 1 and blends with normal grain growth following recrystallization. The second series probably obeys Eq. 1 in which it has a low but increasing value with grain growth, i.e., as new grain contacts increase. The second series probably consti-

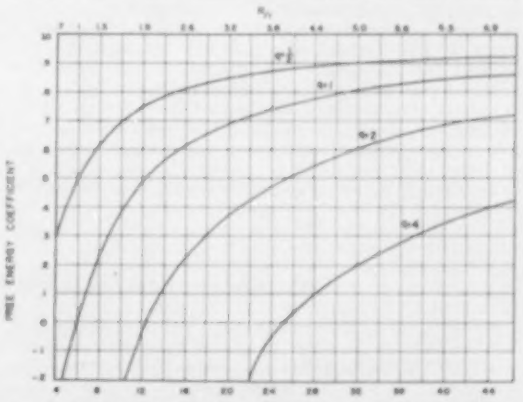

Fig. 9—Free energy coefficient plotted against number of sides, *n*, of the growing grain in a nongrowing idealized two-dimensional grain boundary matrix. *R* and *r* are the average radius vectors from the grain center to the vertices of the growing grain and the matrix grains, respectively, and *q* is the ratio σ_{om}/σ_{mm}, where *om* represents the average boundary of the 0 grain and *mm* the matrix grain boundaries.

tutes the nucleation of secondary grains, particularly if the normal grain growth after recrystallization has been retarded for some reason or other.

The author agrees with Dr. Fullman that there was an oversight on his part in concluding that the von Neumann equation cited is qualitatively opposed to his equation for the driving force of a complex grain. The author had overlooked the fact that the inward curvature of the growing grain would increase as σ_{gg} would increase relative to σ_{gm}. Fig. 9 shows how the driving energy coefficient (the bracketed portion of Dr. Fullman's Eq. 7 and of the equation given in the footnote of his discussion) increases with the relative size of the growing grain or its number of sides in a flat grain network for different q values. The author also appreciates that Dr. Fullman called his attention to the factor of 2 left out in one of the equations in the printed version.

Dr. Cahn takes issue, and rightly so, on the question of the applicability of the geometrical coalescence mechanism for the origin of *primary* recrystallization. The author is less sure of the matrix that exists surrounding the primary recrystallization nuclei than of the matrix surrounding secondary nuclei. However, the author wonders if his objection does not lack fortification. To be sure, polygonization in very pure metals can develop to such an extent that recrystallization does not take place. However, the precise analogy is had in secondary recrystallization. If grain growth is not retarded by a sharp texture, or by insoluble impurities in the grain boundaries, then normal grain growth overtakes any secondary recrystallization that tends to take place. In the author's view, polygonization always takes place before recrystallization on annealing a cold-worked metal, and recrystallization takes place at a later stage if, as is usually the case, the growth of the "polygons" is retarded, say, by foreign atoms or constituents lodged in the boundaries of the polygonized structure.

Dr. Smith presents some interesting and perhaps useful ideas in showing how foam cells should theoretically array themselves on growth in a fixed foam volume. Some observations might be made in this connection. As everyone is well aware, grain boundaries may vary immensely in their respective free energy values, and except for occasional punctures, foam cells do not coalesce. These two facts make grain boundary dynamics much more complex than the dynamics of foam structures. Incidentally, in liquid-liquid systems, e.g., oil globules in a suitable alcohol-water solution, coalescence is very common and the occurrence of "runaway" cells, as Dr. Smith would perhaps call them, appear to be quite analogous to the runaway grains that constitute secondary recrystallization. The author agrees that the mechanisms described for the origin and growth of the secondary grains are merely a part of normal behavior in boundary dynamics, but they are distinct from normal grain growth in which a macroscopic continuous grain growth washes out the discontinuous aspects of grain growth.

Regarding Dr. Smith's reference to twin formation on chance encounters of suitably oriented grains, it should be pointed out that in the paper the author had not intended to imply that coalescences are responsible for twins. Two grains on meeting might be approximately twin related and therefore they could coalesce geometrically because of the low energy of the new boundary formed. This, however, is not a twin boundary in the ordinary sense in which two parts of the twin are precisely twin related. The twin boundaries that are formed by nucleation as suggested by Fullman et al. are very low in energy to be sure, but since they do not come into being by the meeting of two normal size grains at a point, they are not part of a coalescence process. The fact that austenite and brass do not exhibit secondary recrystallization abundantly may be due to the general lowering of the grain boundary energy level on alloying and to the relatively small anisotropy of boundary energies in cubic metals (as against hexagonal metals). This still leaves the silicon iron behavior unexplained. Perhaps silicon has the unique property of raising the grain boundary energy level for α iron. The references to factors that affect grain energies other than orientation are indeed interesting and it is agreed that they must always be kept in mind in dealing with grain boundary dynamics.

Referring to Dr. Dunn's first paragraph, the author has not been able to locate the conflicting statements he refers to. The second paragraph refers to an error made in interpreting the von Neumann equation and which is also pointed out in Dr. Fullman's discussion.

The author is pleased that Dr. Dunn describes some evidence supporting the geometrical coalescence mechanism as probably having occurred in single crystal growth by the strain-anneal method. It is agreed that considerably more evidence will be needed before grain boundary interactions are fully understood. The mechanism proposed in the paper does not exclude other possible mechanisms for the origin of recrystallization. However, the author does feel that the high degree of nonequilibrium in grain boundary geometries that must occur when two grains of nearly identical orientation meet by chance must be of some primary significance in grain boundary interactions. Activation energies must play only a minor role, for they can contribute to no boundary migration if equilibrium, or low driving energy, exists.

[9] R. W. Cahn: A Theory of Recrystallization Nuclei. *Proceedings* Physical Soc., London (1950) **63A**, p. 323.
[10] A. H. Cottrell: *Dislocations and Plastic Flow in Crystals.* (1953) p. 192.
[11] A. Guinier and J. Tennevin: Researches on the Polygonization of Metals. *Progress in Metal Physics* (1952) **2**, p. 177.
[12] P. Lacombe and A. Berghezan: Orientation Relationship between Metal Crystals made by Recrystallization and Small Residual Grains. *Comptes Rendus* (1949) **228**, p. 93.
[13] J. Talbot, C. de Beaulieu, and G. Chaudron: The Inhibition, through Polygonization, of Recrystallization in Pure Iron. *Comptes Rendus* (1953) **236**, p. 818.
[14] *Journal* Inst. of Metals (1948) **74**, pp. 747-748.
[15] J. E. Burke: *Trans.* AIME (1950) **188**, pp. 1324-1328; JOURNAL OF METALS (November 1950).
[16] R. L. Fullman and J. C. Fisher: *Journal of Applied Physics* (1951) **22**, pp. 1350-1355.
[17] C. G. Dunn: Discussion. *Modern Research Techniques in Physical Metallurgy.* (1953) p. 184. Cleveland. ASM. Philadelphia Seminar (1952).

Some Observations on Grain Boundary Shearing During Creep

by Bernard Fazan, Oleg D. Sherby, and John E. Dorn

DISCUSSION, H. E. Howe and G. A. Timmons, Chairmen

R. W. Guard *(General Electric Co., Schenectady)*— The measurements on the contribution of grain boundary deformation processes to creep presented in this paper make an important contribution to the phenomenology of creep deformation. Of particular interest is the proposal that is given in the following equation

$$\epsilon_T = f_\epsilon(\theta) + f_{gb}(\theta). \qquad [5]$$

If the grain boundary shearing is strongly dependent on grain deformation as the authors suggest, the contribution to the strain would not be expected to be independent and additive as proposed in Eqs. 1 (of the paper) and 5.

Some measurements given by McLean[18] on grain boundary migration give a value of ΔH of 29,000 cal. Is this difference of 20 to 25 pct from the values the authors observe within experimental error?

It is mentioned that a great deal of scatter was observed in making measurements of k. Would the authors care to indicate a probable error in the value of k? Also, what proportion of the values of k used in the average were zero and what fraction negative, i.e., gave negative strain?

B. Fazan, O. D. Sherby, and **J. E. Dorn** *(authors' reply)*—The authors wish to thank Dr. Guard for his contributions to their paper. The apparent validity of Eq. 5, as revealed in the text of this paper, suggests that motion of dislocations as well as grain boundary shearing depends on the same ϕ parameter and therefore the same activation energy, namely, that for self-diffusion. Insofar as this might be correct, the two phenomena of grain deformation and grain boundary shearing are related and therefore to this extent interdependent. Additional suggestions of such correlations are revealed again in a recent paper by McLean[14] where it is shown that ϵ_p/ϵ_t is constant over primary creep. Since this ratio is constant, the additive relationship of Eq. 5 is possible.

Dr. Guard is apparently comparing the ΔH obtained for McLean's data on *grain boundary migration* with the ΔH the authors obtained by the uniquely dissimilar process of *grain boundary shearing*. These are two different mechanisms and grain boundary migration per se does not contribute to the creep strain except insofar as it might, on occasions, permit grain boundary shearing.

[13] D. McLean: Note on Boundary Migration during Creep. *Nature* (1953) No. 4372, p. 301.
[14] D. McLean: *Journal* Inst. of Metals (1954-1955) 83, preprint No. 1558.

Creep-Rupture Characteristics of Al-Mg Solid-Solution Alloys

by Arthur W. Mullendore and Nicholas J. Grant

DISCUSSION, H. E. Howe and G. A. Timmons, Chairmen

C. S. Roberts *(The Dow Chemical Co., Midland, Mich.)*—The results of this interesting work are similar in several respects to those which the discusser obtained in studying the creep of solid solutions of aluminum in magnesium. The importance of grain boundary deformation was also reaffirmed by this work. The accompanying micrographs (Figs. 17 and 18) show evidence of nonequilibrium boundary migration similar to that shown in Fig. 11b in the authors' paper. The alloys contained 2.0 and 6.2 pct Al, all of which was soluble at the test temperatures. The migration acts in conjunction with sliding in these cases as in the normal case. The Mg-2.0 pct Al alloy showed this behavior only occasionally, whereas the Mg-6.2 pct Al alloy showed it profusely.

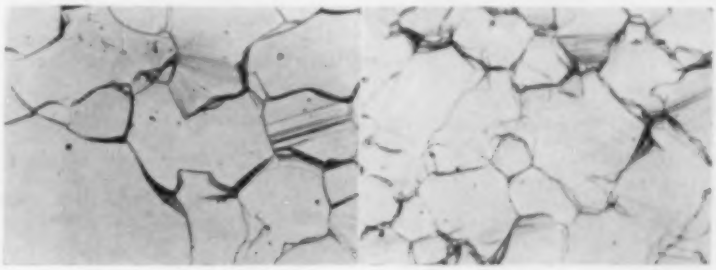

Fig. 17—Mg-2.0 pct Al alloy after 4.5 pct creep at 500°F and 1500 psi. The stress axis was vertical. X500. Area reduced approximately 35 pct for reproduction.

Fig. 18—Mg-6.2 pct Al alloy after 7.5 pct creep at 600°F and 4000 psi. The stress axis was vertical. X500. Area reduced approximately 35 pct for reproduction.

Creep Behavior of Magnesium-Cerium Alloys

by C. S. Roberts

DISCUSSION, H. E. Howe and G. A. Timmons, Chairmen

R. W. Guard *(General Electric Co., Schenectady)*—A detailed knowledge of the mechanisms by which alloying elements work their effects in simple systems is very valuable. This paper presents work on a system which has practical value as well. There are several questions about the results which might clarify certain of the results.

1—While realizing that it is necessary to use widely different creep stresses as the temperature is changed, how can the author be sure that the changes in curve shape attributed to temperature are not the result of using much lower stresses at the higher temperatures? If the tensile stress-strain properties of the same alloys were available, some light might be thrown on the behavior at low strains.

2—To what extent would changes in particle size and distribution account for the "tertiary" creep observed at lower temperatures?

3—Is there any other basis for postulating that propagation of nonbasal slip is a low energy process?

C. S. Roberts *(author's reply)*—The first question raised by Dr. Guard is certainly an important one. It is generally held that creep-curve shape is a function of both temperature and stress. Proof of the separate influence of stress in the range studied has not been attempted. However, the author does not wish to infer that the stress variable is insignificant. It certainly is important. The basis of the emphasis on the importance of temperature is the fact that, when overlap of the two variables did occur, curves at the same stress level but different temperatures had significantly different shapes.

In answer to the second question, it could be said that, because of the aging at 400°F, changes in precipitate size and distribution would be relatively unimportant at lower temperatures. However, at 500° and 600°F, concurrent continuation of the precipitation reaction may have some control on the deformation mechanisms observed.

At present the author is working on a model which promises to give a better basis than those already cited for the high energy requirement of initiation and low energy demand for continuation of nonbasal slip. However, it is not yet in sufficiently finished form for presentation.

Correlation Between Microstructure and Resistivity of Transforming Ti-Mn Alloys

by D. J. DeLazaro and D. W. Levinson

DISCUSSION, H. D. Kessler and Harold Margolin, Chairmen

Dean N. Williams *(Battelle Memorial Institute, Columbus, Ohio)*—The authors of this paper have shown that the $\beta/\alpha+\beta$ transformation of a β-stabilized titanium alloy can be followed quite successfully through the use of electrical resistance measurements. They are to be congratulated for the application of this method to the study of titanium alloys. It should prove to be a useful tool for those now engaged in studies of the transformation kinetics of titanium alloys using standard metallographic techniques.

Since their work will no doubt stimulate studies of other β-stabilized alloys using the resistance method, it might be well to point out at this time that the transformation rate variations found when comparing quenched and reheated material with isothermally transformed material are not unexpected. These variations are due to the nature of transformation and are not a result of the method of measurement.

The occurrence of a C-type *TTT* curve, such as that often observed in the $\beta/\alpha+\beta$ transformation in β-stabilized titanium alloys, is due to the inversely related rate-controlling factors of nuclei formation and particle growth. At high temperatures the reaction rate is controlled chiefly by the nucleation rate, since particle growth is quite rapid. The opposite is true at low temperatures where the retarded particle growth rate (slow diffusion rate) is the rate-controlling factor. The nose of the C curve occurs at the point where the nucleation rate and particle growth rate are ideally balanced.

Quenching to room temperature and reheating above the nose of the C curve has a marked accelerating effect on the transformation, since the nuclei formed during the quench are partially retained. Quenching to room temperature and reheating below the nose of the C curve has little effect on the transformation rate, however, since in this region the particle growth rate and not the number of available nuclei is the controlling factor.

The effectiveness of a water quench in increasing the available nuclei is readily apparent when comparing Fig. 6b (mistitled 6c) with Fig. 8a and Fig. 7c with Fig. 8b. The microstructures of the isothermally transformed samples show only a few fairly large α particles. The microstructures of the quenched and reheated samples, on the other hand, show an extensive precipitation of fine α particles.

Differences in the resistance-time curves of quenched and reheated material and isothermally annealed material were found in the 6 pct Mn alloy transformed below the nose of the C curve. These differences were no doubt due to the slowness of the lead-bath quench combined with the rapidity with which the 6 pct Mn alloy transforms at its critical temperature. The test results indicate that a large amount, if not all, of the transformation of the isothermally annealed material occurred during the quench to the isothermal annealing temperature.

F. R. Brotzen and **E. L. Harmon, Jr.** *(Rice Institute, Houston, and Case Institute of Technology, Cleveland, respectively)*—The authors' paper is a welcome addition to the growing fund of information on the isothermal transformation behavior of titanium-base alloys.

It is gratifying to note that the authors' electrical resistivity results are in close agreement with work conducted at Case Institute of Technology on the decomposition of metastable β in the Ti-V system. This investigation[4] revealed that the transition phase, ω, was the initial β decomposition product at relatively low temperatures in titanium alloys containing from 12.5 to 20 pct V. The formation of ω was accompanied by a decrease in electrical resistivity. Its disappearance and the simultaneous formation of α were associated with a further drop in resistivity.

Time-temperature-transformation diagrams determined by dilatometric and metallographic studies and X-ray diffraction revealed a typical C-shaped curve describing the beginning of α precipitation. In addition, a curve denoting the formation of ω was obtained at temperatures below about 430°C. Increasing vanadium content shifted the "nose" of this ω transformation curve to longer times. For those alloys in which ω could not be suppressed by rapid quenching, subsequent reheating formed additional ω at temperatures up to about 500°C and resulted in postponing the precipitation of equilibrium α at temperatures up to about 550°C.

In view of the discussers' results, the initial decrease in resistivity of the 6 pct Mn alloy when reheated to 500°C, Fig. 2 in the text, can be interpreted as due to the formation of ω.

At 400°C, each of the alloys, Figs. 2 and 3, appears to have formed ω in both the isothermally treated and the quenched and reheated conditions.

The absence of ω in the 10 pct Mn specimen reheated to 500°C implies that the ω transformation was delayed sufficiently to allow quenching and reheating without passing through the "nose" of the *TTT* curve. The close similarity in shape and form of the isothermally transformed and the quenched and reheated curves for the 400°C treatment confirms the tardiness of the ω reaction in this alloy.

Because the 6 pct Mn alloy appeared to form ω

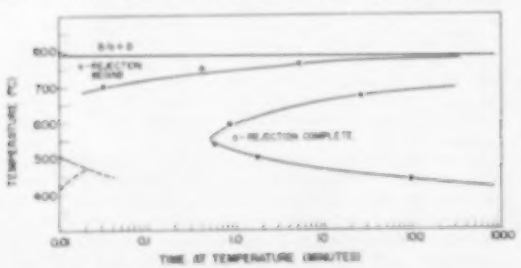

Fig. 9—*TTT* curve for Ti-6 pct Mn alloy.

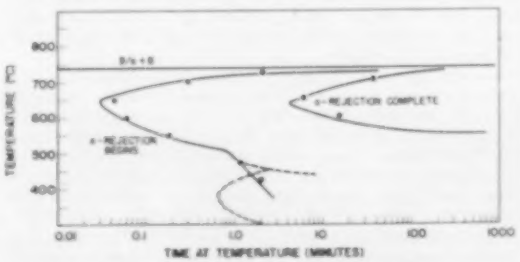

Fig. 10—*TTT* curve for Ti-10 pct Mn alloy.

upon reheating to 500°C but not upon direct quenching to that temperature, the minimum incubation time for ω transformation was probably extremely short. That is, ω must have formed during the quench and reheat treatment resulting in the formation of more ω at a temperature where it would never exist upon direct isothermal quenching. Another possibility which must not be neglected is that small amounts of α may have formed during the relatively slow isothermal quench to 500°C, preventing subsequent transformation to ω. The behavior of the 6 pct Mn alloy was similar to that observed in a 12.5 and a 15 pct V alloy.

Interpreting the authors' data in this manner would yield *TTT* diagrams which illustrate the beginning of the ω reaction in addition to describing the precipitation of α. The writers' concepts of these complete *TTT* diagrams are presented in Figs. 9 and 10.

D. J. DeLazaro and **D. W. Levinson** *(authors' reply)*—The points raised by Dr. Williams are well taken and are appropriate to the text of the paper. It is certainly of prime importance in any study of transformation kinetics to take cognizance of the nucleation which occurs during cooling. Attention may be drawn to the 500°C transformation curves for the Ti-6 pct Mn alloy (Fig. 6) in which the quench and reheat-type heat treatment produces a resistivity curve characteristic of the rejection of ω from β as shown in this discussion, and subsequently in a publication,[5] by Brotzen and Harmon. Since the isothermally transformed Ti-6 pct Mn alloy (Fig. 6) gives evidence of "normal" rejection of proeutectoid α from β, it is evident that the nuclei of ω produced during the quench to room temperature of the quenched and reheated sample grew at 500°C in preference to, or faster than, the nuclei of α. Since the plateaus in the resistivity curves of quenched and reheated samples were not observed for temperatures higher than 500°C, similarly it may be concluded that the ω nuclei must either transform too rapidly to be observed at temperatures higher than 500°C or, what is more likely, simply redissolve in β. There are less obvious indications of the same process operating for the Ti-10 pct Mn alloy (Fig. 3).

The interpretations shown in Figs. 9 and 10 of Brotzen and Harmon's discussion are certainly to be preferred and it is gratifying to find definitive work in this temperature range which verifies the authors' suspicions regarding the origin of the resistivity plateaus and the resulting irregularity in the *TTT* curve for the Ti-10 pct Mn alloy.

[5] F. R. Brotzen, E. L. Harmon, Jr., and A. R. Troiano: Decomposition of Beta Titanium. *Trans.* AIME (1955) 203, pp. 413-419; JOURNAL OF METALS (February 1955).

Mechanical Properties of Alpha Titanium as Affected by Structure and Composition

by R. I. Jaffee, F. C. Holden, and H. R. Ogden

DISCUSSION, H. D. Kessler and Harold Margolin, Chairmen

L. D. Jaffe *(Jet Propulsion Laboratory, California Institute of Technology, Pasadena, Calif.)*—Some of the microstructures shown in this paper may be clarified by considering the relation between the "acicular" and the "serrated" microstructures. If high purity titanium is cooled from the β field either rapidly or slowly, α presumably forms from the β as groups of parallel platelets of similar orientation. The etch used does not bring out the low angle boundaries between the platelets and so only their ends (high angle boundaries) etch. Each group of platelets then appears as a "serrated α grain," Fig. 2.

If aluminum is present, it does not have time to segregate during quenching, so the quenched structure of the Ti-Al alloys is "serrated," like unalloyed titanium, Fig. 4b. During slow cooling, however, there is time for some diffusion of aluminum to occur during the β-α transformation. This results in concentration differences between center and boundaries of the α platelets; the low rate of aluminum diffusion at lower temperatures prevents these differences from equalizing after β has disappeared. Because of these concentration differences, the boundaries between α platelets are attacked by the etch, giving an "acicular" appearance, Fig. 4c.

In Ti-N alloys, nitrogen probably diffuses fast enough to segregate to some extent during β-α transformation even on quenching, so platelet boundaries etch in quenched Ti-N alloys, giving a somewhat acicular microstructure, Fig. 6a. When these alloys are slow cooled, there is time after completion of the transformation for the segregated dissolved nitrogen to redistribute itself uniformly. The low angle boundaries then do not etch, giving a "serrated" appearance, Fig. 7a. (The slow cool here also permits the serrations to smooth.)

Hydrogen apparently behaves somewhat similarly to nitrogen, with the added feature that segregation of hydrogen to platelet boundaries leads to precipitation of hydride there, accentuating the acicularity and "basket weave" microstructure, as the authors point out.

Frank A. Crossley *(Armour Research Foundation, Chicago)*—The Ti-0.29 pct N alloy quenched from 1010°C is treated as though 1010°C placed it in the all β field. The preponderance of evidence argues that the 0.29 pct N alloy was not placed in the all β field by heating to 1010°C. The evidence is as follows:

1—The statement made by the authors that the β field was not bracketed for the Ti-0.29 pct N alloy; but as quenched from 1010°C, the structure was estimated to be over 95 pct β.

2—Work of Jaffee, Ogden, and Maykuth and work by Palty, Margolin, and Nielsen on the effect of nitrogen on the transformation of iodide titanium indicates that the 0.29 pct N alloy is in the α-β field at 1010°C.

3—Fig. 7d indicates that the alloy was still in the α-β field when quenched from 1010°C.

In the light of these evidences, it is considered that the fine grain size exhibited by the Ti-0.29 pct N alloy quenched from 1010°C is due to the inhibition to grain growth caused by the small amount of α present.

Relative to the explanation of yield point phenomenon in the Ti-N alloys as annealed in the α field and absence of it when the alloys are annealed in the α-β field, the authors state that, "If β heat treatments do not show the yield point, it follows that whatever was causing strain aging has already precipitated." What strain aging are the authors discussing? Yield point phenomenon is not identical to strain aging and it is not associated with precipitation. Yield point phenomenon results from segregation of solute atoms around dislocations. The use of the word "precipitation" is unwarranted in the context in which the authors use it.

Also there is no reason to suppose that an agent soluble in α is insoluble in β at temperatures in the vicinity of 1000°C. Nitrogen in the amounts present in the alloys under discussion certainly is, and other elements should be present to only a very small extent in these binary iodide titanium-base alloys. Furthermore, there is no reason to suppose that equiaxed α resulting from an anneal high in the α field will dissolve more of an agent than α resulting from β transformation on cooling.

A more likely explanation is the following: The α annealed Ti-N alloys are strengthened by the Suzuki

mechanism of solid-solution hardening applicable to close-packed metals. This mechanism relies upon the dissociation of dislocations in close-packed planes of face-centered-cubic and close-packed-hexagonal structures. This type of hardening does not occur in body-centered-cubic solid solutions. Since the establishment of conditions to give rise to Suzuki hardening is diffusion dependent, it is probable that Ti-N alloys heated to predominantly β structures do not show the yield point phenomenon, as there is not sufficient time during the cooling from β to the α phase field to establish the necessary conditions.

R. I. Jaffee, F. C. Holden, and **H. R. Ogden** *(authors' reply)*—The authors are grateful to Drs. Crossley and Jaffe for their fine discussions which add greatly to the interpretation of the experimental results.

Dr. Jaffe's explanation of relative acicularity caused by substitutional and interstitial solutes in the quenched and furnace-cooled α alloys appears to the authors to be entirely correct. Dr. Crossley also is correct in pointing out that, according to the presently accepted view, the yield point is not associated with precipitation, but with segregation of the solute atoms to preferred sites. His further discussion of the yield point in terms of the Suzuki mechanism is a valuable addition.

Dr. Crossley's discussion of the β grain size of the Ti-0.29 pct N alloy heat treated at 1010°C appears to be aimed at the conclusion that the β grain growth is faster when aluminum is present than when nitrogen is present. The authors agree that a small amount of α is remarkably effective in restricting β grain growth and that the Ti-0.29 pct N alloy, as shown in Fig. 6b, had a small amount of α phase present. The conclusion was not based on this result, but on the result found for the β-treated Ti-0.07 pct N alloy and observations on other interstitial alloys not described in the paper.

Note: On p. 1283, Fig. 1a and b were transposed. Fig. 1a is b and Fig. 1b is a. *Trans.* AIME (1954) **200**, pp. 1282-1290; JOURNAL OF METALS (November 1954).

Phase Transformations in Titanium-Rich Alloys of Iron and Titanium

by D. H. Polonis and J. Gordon Parr

DISCUSSION, H. D. Kessler and Harold Margolin, Chairmen

R. J. Van Thyne *(Armour Research Foundation, Chicago)*—The authors make several observations that are not in accord with the equilibrium relationships independently determined by several investigators. No doubt a portion of the differences may be attributed to contamination of powder samples used by the authors and they do admit to a degree of contamination. Hardening of as-cast unalloyed titanium is probably due to contamination rather than cooling rate.

The authors place the eutectoid temperature at 625°C using a Ti-12 atomic pct Fe alloy. The fact that this temperature is higher than the accepted one may be explained, as it is known that even slight amounts of contamination have pronounced effects on raising the eutectoid temperature. In the writer's work, no eutectoid decomposition was observed in samples annealed at 600°C for one month, and the eutectoid temperature was located between 575° and 600°C.[8] In the present work, α' was observed in alloys containing up to 12 atomic pct Fe. However, other investigators including the discusser, have found that 4 pct Fe fully retains the β phase. These differences are difficult to compromise.

The writer was unable to observe the reported phase Ti_2Fe in uncontaminated samples using X-ray and metallographic techniques. When the phase diagram studies were undertaken, it was thought that Ti_2Fe might form by a sluggish peritectic reaction. For this reason, an arc-melted 36 wt pct Fe alloy was very slowly cooled after remelting in a graphite crucible. The microstructure of this alloy did not show any peritectic wall around the primary TiFe as might be expected if the reported Ti_2Fe phase does exist. As the authors suggest in their paper, samples of small arc-cast ingots were annealed at 1000°C for several days. The phase Ti_2Fe was not observed. However, it has been demonstrated that the ternary phase Ti_4Fe_2O does exist.[9]

L. D. Jaffe *(Jet Propulsion Laboratory, California Institute of Technology, Pasadena, Calif.)*—The presence of α' in quenched alloys up to 12 pct Fe, and the absence of a hardness peak near 5 pct Fe, suggest that the authors were more successful than Worner in avoiding formation of β' during quenching. The lower oxygen content of the authors' alloys, and their probably higher cooling rate, would reduce the likelihood that hard β' would nucleate and grow.[11] Prevention of β' formation would avoid the accompanying depression of M_s[10] to below room temperature that probably occurred in Worner's work.

The authors' metallographic technique for determining M_s fails to take into account that remaining β may transform isothermally to α just as well below the M_s as above it. Since the technique provides no means of distinguishing martensite formed on cooling to the holding temperature from that formed subsequently on cooling to room temperature, it does not appear to be valid. The true M_s temperatures are probably much higher than those reported by the authors.

Appearance of the FeTi phase in less than an hour at 570°C in the alloys containing over 8 pct Fe is interesting. This relatively rapid formation of the intermediate phase in the Ti-Fe system is probably the cause of the rather poor toughness encountered in titanium-base alloys of commercial purity, which contain more than about 5 pct Fe, and suggests that the use of iron even in lower percentages may be undesirable in such materials.

D. H. Polonis and **J. Gordon Parr** *(authors' reply)*—The authors are intrigued that Dr. Van Thyne criticizes them for using contaminated specimens while he quotes the results he obtained by melting an alloy in a graphite crucible. It is certain that Ti_2Fe occurs as an equilibrium phase in Ti-Fe alloys, but so far ternary alloys with carbon have not been investigated. It is understood that work carried out at New York University confirms the authors' results. Of course, as Dr. Van Thyne points out, the authors do admit their alloys were contaminated, since some contamination is inevitable. Estimates of oxygen and nitrogen pickup are given in the paper, and these compare very favorably with figures given by other workers who publish such data.

The differences between the behavior of the authors' alloys and those of other workers is, as Dr. Jaffe suggests, probably due to the effect of specimen size and—they like to believe—also to the purity of the materials. Subsequent experiments[12] have shown the effects of specimen size to be appreciable. The authors think Dr. Jaffe is probably correct in suggesting that the technique for measuring M_s gives low results.

[11] L. D. Jaffe: Heat Treatment of Titanium Generalized in Terms of Beta Prime. *Trans.* AIME (1954) **200**, p. 210; JOURNAL OF METALS (February 1954).

[12] L. D. Jaffe: Heat Treatment and Alloying of Titanium. To be published in *Metal Progress*.

[13] D. H. Polonis and J. G. Parr: Martensite Formation in Powders and Lump Specimens of Ti-Fe Alloys. *Trans.* AIME (1955) **203**, p. 64; JOURNAL OF METALS (January 1955).

Appreciation is gratefully acknowledged to the following organizations whose support has helped to make possible AIME's extensive publications program of metallurgical research:

Allis-Chalmers Mfg. Co.
Aluminum Co. of America
American Iron & Steel Institute
American Metal Co. Ltd.
American Smelting & Refining Co.
American Zinc, Lead & Smelting Co.
Anaconda Copper Mining Co.
Bridgeport Brass Co.
Bunker Hill & Sullivan Mining & Concentrating Co.
Calumet & Hecla, Inc.
Cerro de Pasco Corp.
Climax Molybdenum Co.
Consolidated Coppermines Corp.
Consolidated Mining & Smelting Co. of Canada Ltd.
Copper Range Co.
Crane Co.
Cyprus Mines Corp.
Dow Chemical Co.
Electro Metallurgical Co., div. of Union Carbide & Carbon Corp.
Engineering Foundation
Freeport Sulphur Co.
General Electric Co.
Howe Sound Co.
Hudson Bay Mining & Smelting Co. Ltd.
International Nickel Co., Inc.
Kennecott Copper Corp.
Magma Copper Co.
Mallory-Sharon Titanium Corp.
Miami Copper Co.
Molybdenum Corp. of America
National Lead Co.
New Jersey Zinc Co.
Newmont Mining Corp.
Noranda Mines, Ltd.
Phelps Dodge Corp.
Raytheon Mfg. Co.
Rem-Cru Titanium Inc.
St. Joseph Lead Co.
Texas Gulf Sulphur Co.
Titanium Metals Corp. of America
U. S. Smelting, Refining & Mining Co.
Vanadium Corp. of America